Universitat de Lleida

# Geomorphic responses to natural and human disturbances in a mountain catchment at multiple temporal and spatial scales

Manel Llena Hernando

http://hdl.handle.net/10803/668358

**ADVERTIMENT**. L'accés als continguts d'aquesta tesi doctoral i la seva utilització ha de respectar els drets de la persona autora. Pot ser utilitzada per a consulta o estudi personal, així com en activitats o materials d'investigació i docència en els termes establerts a l'art. 32 del Text Refós de la Llei de Propietat Intel·lectual (RDL 1/1996). Per altres utilitzacions es requereix l'autorització prèvia i expressa de la persona autora. En qualsevol cas, en la utilització dels seus continguts caldrà indicar de forma clara el nom i cognoms de la persona autora i el títol de la tesi doctoral. No s'autoritza la seva reproducció o altres formes d'explotació efectuades amb finalitats de lucre ni la seva comunicació pública des d'un lloc aliè al servei TDX. Tampoc s'autoritza la presentació del seu contingut en una finestra o marc aliè a TDX (framing). Aquesta reserva de drets afecta tant als continguts de la tesi com als seus resums i índexs.

**ADVERTENCIA.** El acceso a los contenidos de esta tesis doctoral y su utilización debe respetar los derechos de la persona autora. Puede ser utilizada para consulta o estudio personal, así como en actividades o materiales de investigación y docencia en los términos establecidos en el art. 32 del Texto Refundido de la Ley de Propiedad Intelectual (RDL 1/1996). Para otros usos se requiere la autorización previa y expresa de la persona autora. En cualquier caso, en la utilización de sus contenidos se deberá indicar de forma clara el nombre y apellidos de la persona autora y el título de la tesis doctoral. No se autoriza su reproducción u otras formas de explotación efectuadas con fines lucrativos ni su comunicación pública desde un sitio ajeno al servicio TDR. Tampoco se autoriza la presentación de su contenido en una ventana o marco ajeno a TDR (framing). Esta reserva de derechos afecta tanto al contenido de la tesis como a sus resúmenes e índices.

**WARNING**. Access to the contents of this doctoral thesis and its use must respect the rights of the author. It can be used for reference or private study, as well as research and learning activities or materials in the terms established by the 32nd article of the Spanish Consolidated Copyright Act (RDL 1/1996). Express and previous authorization of the author is required for any other uses. In any case, when using its content, full name of the author and title of the thesis must be clearly indicated. Reproduction or other forms of for profit use or public communication from outside TDX service is not allowed. Presentation of its content in a window or frame external to TDX (framing) is not authorized either. These rights affect both the content of the thesis and its abstracts and indexes.

PhD Thesis

# GEOMORPHIC RESPONSES TO NATURAL AND HUMAN DISTURBANCES IN A MOUNTAIN CATCHMENT AT MULTIPLE TEMPORAL AND SPATIAL SCALES

Manel Llena Hernando

Universitat de Lleida

A thesis presented for the degree of Doctor at the University of Lleida

2019

Fluvial Dynamics Research Group
RIUS

Cover photo: Badlands of the Soto catchment during an intense rainfall episode,

November 2016.

Author: Manel Llena


# PHD THESIS

## GEOMORPHIC RESPONSES TO NATURAL AND HUMAN DISTURBANCES IN A MOUNTAIN CATCHMENT AT MULTIPLE TEMPORAL AND SPATIAL SCALES

Manel Llena Hernando

A thesis presented for the degree of Doctor at the University of Lleida

PhD program in Forest and Natural Environment Management

Supervisors

Damià Vericat

Mark W. Smith

September 2019

*Nothing can stop those who have the right mental attitude from achieving their goal.*

T. Jefferson

# AGRAÏMENTS

Han sigut quatre anys d'esforços i sacrificis, però també d'alegries i bons moments, fent que el balanç final hagi sigut sens dubte, positiu, tant des de el punt de vista professional i científic com personal. Si això ha sigut així és gràcies tota la gent que m'ha acompanyat durant aquest temps, als quals els hi vull donar les gràcies en aquestes breus línies.

En primer lloc vull donar-li les gràcies als meus directors, el Damià i el Mark, ja que sense ells dos no hagués pogut arribar fins aquí. Damià, no tinc paraules per agrair-te tot el temps i dedicació d'aquests anys. Vull donar-te les gràcies per formar-me com a científic, transmetent-me la teva passió per la geomorfologia, però sobretot per formar-me com a persona, transferint-me els valors primordials de la planificació, la constància i el sacrifici, però també els de l'amistat, l'alegria i la generositat. Mark, thank you very much for your very valuable help provided during this stage, especially during the last months. You have always been available to help with an immediate response, whether through Skype meetings, last minute corrections, field visits, or night beers.

Ramon, ja farà deu anys de les classes de geografia física que ens vas donar al rectorat. Gràcies a elles es va despertar en mi l'interès pels rius, el qual ha sigut la meva principal motivació per arribar fins aquí. Gràcies també per acollir-me dins de RIUS i per la confiança donada durant aquest temps.

Agradecer a José Antonio Martínez la oportunidad de introducirme en el mundo de la docencia. Han sido cinco cursos juntos en los cuales me he formado como docente y en los que me han servido para descubrir una vocación, cinco años de buenos recuerdos.

Grazie mille a la gente de l'Istitutto di Recerca per la Protezione Idrogeologica di Padova, in particolare Marco, Stefano, Lorenz, Giacomo e Sara. Grazie per avermi acolto nel vostro gruppo, per la proficua collaborazione durante i miei due stanze e soprattutto per i bei momenti trascorsi nella sala da moka, sul Dolomiti e gli spritzs della Yarda.

Also, I would like to thank Joe Wheaton and their "Ecomorphology and Topographic Analysis Laboratory" of the Utah State University for allowed me to do a research stay of three months with them, making me part of their group.

I would like to express my gratitude to the external reviewers of the thesis, Andrés Iroumé and Paolo Espa, for their valuable comments that improved the final version of the manuscript.

También agradecer a la Confederación Hidrográfica del Ebro (CHE) y Acciona su colaboración y suministro de datos. Del mismo modo, agradecer al Ministerio de Educación del Gobierno de España la financiación de los cuatro años de doctorado mediante un contrato de Formación de Profesor Universitario (FPU016/01687) así como el financiamiento de las estancias en centros de investigación en el extranjero mediante las Ayudas para Estancias Breves. Esta tesis se ha desarrollado en el contexto de dos proyectos de investigación estatales, MORPHSED (CGL2012-36394) y MORPHPEAK (CGL2016-78874-R), y uno internacional, Cost Action Connecteur (ES1306). També agrair el suport del Departament d'Economia i Coneixement de la Generalitat de Catalunya mitjançant el reconeixement del grup de Recerca en Dinàmica Fluvial com a grup consolidat (RIUS 2017 SGR 459).

Moltes gràcies al grup de recerca RIUS per ser com una gran família durant tot aquest temps. Agrair especialment a les companyes i companys del 5B per tantes i tantes hores compartides de riures i tés, tant durant la primera fase amb la Gemma, la María, l'Ester i el Álvaro, com la segona amb l'Antoni, la Fanny el Théo i la Meritxell. També agrair a l'Efrén tots els bons records compartits a camp i a Agrometeorologia. Gràcies a tota la gent del Departament de Medi Ambient i Ciències del Sòl pels bon moments compartits, especialment en aquests dinars que s'ajuntaven amb els sopars. També vull agrair la gran ajuda de la Clara durant tot aquest temps així com donar-li les gràcies a l'Asier per totes les bones estones passades.

Moltes gràcies a la meua família: Papa, Mama i Carla, però també als meus cosins, cosines, tietes, tiets i iaios, així com totes les bones amigues i amics de Baldellou, per fer del meu lloc un puesto de desconnexió, on realment soc jo mateix. Un especial record i gratitud per tots aquells que ja no hi son, particularment a la meua estimada iaia Pilar. Agradecer también a mi família de Altorricón el apoyo y cariño brindado durante todos estos años. Finalmente, quiero agradecer a mi compañera de vida, Amanda, toda la paciencia que has tenido que tener durante todo este tiempo, gracias por tus ánimos en momentos de bajón o nervios, gracias por tu apoyo y por estar siempre allí.

**A VOSALTRES, GRÀCIES!**

# Table of contents

ABSTRACT ..... **- 1 -**

**CHAPTER 1: Introduction ..... - 6 -**

1. GENERAL BACKGROUND AND RATIONALE ..... - 6 -

2. HYPOTHESIS, OBJECTIVES AND STRUCTURE OF THE THESIS ..... - 9 -

3. THE UPPER CINCA CATCHMENT ..... - 11 -

3.1. Location ..... - 11 -

3.2. Climate and hydrology ..... - 12 -

3.3. Land cover and human activities ..... - 13 -

4. REFERENCES ..... - 16 -

**CHAPTER 2: Fieldwork design and methods overview ..... - 22 -**

1. MULTI-SCALE APPROACH ..... - 22 -

2. METHODS OVERVIEW ..... - 23 -

2.1. Micro-catchment scale (CHAPTER 3) ..... - 23 -

2.2. Sub-catchment scale (CHAPTER 4) ..... - 47 -

2.3. Catchment scale (CHAPTER 5) ..... - 49 -

2.4. Reach scale (CHAPTER 6) ..... - 65 -

2.5. References not cited in the papers ..... - 89 -

**CHAPTER 3: Multi-temporal geomorphic processes signatures reshaping sub-humid Mediterranean badlands ..... - 92 -**

1. INTRODUCTION ..... - 93 -

2. STUDY SITE ..... - 94 -

3. METHODS ..... - 96 -

3.1. Field data collection and preparation ..... - 96 -

3.2. Data analyses ..... - 99 -

4. RESULTS ..... - 101 -

4.1. Quality assessment ..... - 101 -

4.2. Meteorological characterization of the periods ..... - 103 -

4.3. Topographic Changes ..... - 104 -

4.4. Geomorphic processes signatures ..... - 109 -

4.5. Statistical correlations between meteorological variables and geomorphic processes . - 112 -

5. DISCUSSION ..... - 113 -

5.1. The role of meteorological variables on geomorphic processes ..... - 113 -

5.2. The role of morphometry on geomorphic processes ..... - 114 -

5.3. The role of the temporal scale on depicting main geomorphic processes ..... - 116 -

5.4. Limitations and further work ..... - 117 -

6. CONCLUSIONS ..... - 118 -

7. ACKNOWLEDGEMENTS ..... - 119 -

8. REFERENCES ..... - 119 -

SUPPLEMENTARY MATERIALS: ..... - 124 -

**CHAPTER 4: Do badlands (always) control sediment yield? Evidence from small intermittent catchment ..... - 132 -**

1. INTRODUCTION ..... - 133 -

2. STUDY AREA ..... - 134 -

3. METHODS ..... - 135 -

3.1. Data acquisition and treatment ..... - 135 -

3.2. Data analysis ..... - 138 -

4. RESULTS ..... - 140 -

4.1. Temperature, rainfall and runoff ..... - 142 -

4.2. Sediment production from badlands ..... - 145 -

4.3. Catchment sediment yield ..... - 145 -

5. DISCUSSION ..... - 146 -

5.1. Pulses of water and sediment fluxes ..... - 146 -

5.2. The role of badlands and land cover on catchment sediment yield ..... - 149 -

5.3. Temporal dynamics of sediment transport ..... - 151 -

5.4. Sediment delivery and the role of the channel as sediment buffer ..... - 152 -

5.5. The sediment budget of the Soto catchment ..... - 154 -

6. CONCLUSIONS ..... - 155 -

7. ACKNOWLEDGMENTS ..... - 156 -

8. REFERENCES ..... - 156 -

9. SUPPLEMENTARY MATERIAL ..... - 163 -

**CHAPTER 5: The effects of land use and topographic changes on sediment connectivity in mountain catchments ..... - 168 -**

1. INTRODUCTION ..... - 169 -

2. STUDY AREA ..... - 171 -

3. METHODS ..... - 174 -

3.1 Data preparation ..... - 174 -

3.2 Scenarios of change ..... - 175 -

3.3. Assessment of changes in Sediment Connectivity associated with selected scenarios . - 177 -

4. RESULTS AND DISCUSSION ..... - 179 -

4.1 Changes in sediment connectivity driven by land cover changes (Scenario 1) ..... - 179 -

4.2 Changes in sediment connectivity by terracing (Scenario 2) ..... - 182 -

4.3 Changes in sediment connectivity driven by road construction (Scenario 3) ..... - 185 -

5. CONCLUSIONS ..... - 189 -

6. ACKNOWLEDGEMENTS ..... - 190 -

7. REFRENCES ..... - 190 -

**CHAPTER 6: Geomorphic responses to multi-scale disturbances in a mountain river: a century of observations ..... - 198 -**

1. INTRODUCTION ..... - 199 -

2. STUDY AREA ..... - 200 -

3. MATERIALS AND METHODS ..... - 201 -

3.1. Runoff and flood frequency and magnitude ..... - 201 -

3.2. Gravel mining and channel embankments ..... - 202 -
3.3. Aerial photos: orthomosaics, point clouds and land use maps ..... - 203 -
3.4. Digital Elevation Models (DEM), longitudinal profiles and topographic changes.. - 203 -
3.5. Geomorphic units and complexity of the channel pattern ..... - 204 -
3.6. Statistical analyses..... - 207 -
4. RESULTS AND DISCUSSION ..... - 207 -
4.1. Reach and catchment scale disturbances ..... - 207 -
4.1.1. Global changes ..... - 207 -
4.2. Process changes: water and sediment fluxes ..... - 210 -
4.3. Geomorphic responses ..... - 213 -
4.4. Synthesis..... - 223 -
6. CONCLUSIONS ..... - 226 -
7. ACKNOWLEDGMENTS ..... - 227 -
8. REFERENCES ..... - 227 -
9. SUPPLEMENTARY MATERIALS ..... - 236 -
3.3. Aerial photos: orthomosaics, point clouds and land use maps ..... - 236 -
**CHAPTER 7: Discussion and conclusions..... - 240 -**
1. GENERAL DISCUSSION ..... - 240 -
2. LIMITATIONS AND FUTURE WORK ..... - 245 -
3. KEY CONCLUSIONS ..... - 246 -
4. REFERENCES ..... - 247 -

**ABSTRACT:** This thesis focusses on the study of water and sediment transfer from sources to sinks at multiple temporal (from 5-min data to a century data sets) and spatial (from slope to catchment scales) scales and their implications for channel morphology in the Upper Cinca catchment, a mountain catchment located in the Southern Pyrenees. At the micro-catchment scale, our 5-year High Resolution Data Set of two contrasted badlands (around 0.3 ha each) reveal as rainfall control overland-surface flow processes while low temperatures have a significant relation with mass movement-based processes. Morphometry together with vegetation cover are key factors determining main geomorphic processes and associated topographic changes. Main observed geomorphic processes were *Cutting and Filling* and *Mass Wasting*. Although badlands may have an important role on sediment production, the 2-year sediment budget of the Soto catchment (10 $km^2$) indicates that badlands do not always control the export of sediments at the outlet of small intermittent mountain catchments. This is mainly due to the fluctuation of the functional connectivity of the channel network caused by the frequency and magnitude of water and sediment pulses during flashy floods. The channel drainage network acts as sediment source and sink and it is key to understand marked differences in the Sediment Delivery Ration. Land use and cover in many mountain catchments have been modified since the fifties of the $20^{th}$ century, having a direct effect on runoff and sediment production. Most of the area of the Upper Cinca catchment (1565 $km^2$) has undergone afforestation, which resulted in a decrease of structural sediment connectivity. Terracing affects connectivity much more than changes in land cover. Terraces generally reduce connectivity due to the establishment of flat areas between slopes and, contrarily, locally, may increase connectivity due the convergence produced by the structures or the collapse of terraces due to abandonment. Road construction, however, modify slope and the drainage network, which leads to changes in connectivity that could affect erosional processes in the neighbouring areas. Thus, water and sediment fluxes through the Upper Cinca are spatially and temporal dynamic and have been dramatically modified in the last century, with direct implications on channel morphology. Additionally, localised disturbances such as gravel mining, channel embankments and dams have also impacted on sedimentary dynamics, thus channel morphology. This situation led to a river metamorphosis, changing from a braided pattern to a more static channel towards a wandering pattern. We hypothesise that the lowermost 12-km reach of the Upper Cinca has reaching a new equilibrium imposed by catchment-scale changes of water and sediment fluxes caused by global changes, but also influenced by localised human-disturbances that modify channel geometry and morpho-sedimentary characteristics. Three phases were identified: before 1927, the reach remained in a quasi-equilibrium state imposed, mainly, by water and sediment supply during flood events. During the period 1927-2012 the river adjusted to the disequilibrium imposed by disturbances acting at different temporal and spatial scales, yielding two contrasted channel states. Finally, after 2012, we hypothesise that the river may be reaching again a new equilibrium, adjusting to the imposed water and sediment fluxes and the new channel configuration. This thesis presents some novel quantitative methods for the study of sediment production and transfer between the different compartments of fluvial catchments. The main transversal novelty in all the methods used in each chapter lies in the high resolution of the data obtained. This comprehensive analysis aids at understanding the functioning of the river system and their evolution based on multiple-scale disturbances, which can help to support integrated watershed management practices or plans.

**Key words:** Upper River Cinca, badlands, geomorphic processes, morphometry, meteorology, MaGPiE algorithm, pulses, Sediment Delivery Ratio, flow intermittency, sediment connectivity, land use changes, geomorphic changes, morphology, gravel mining, floods, fluvial metamorphosis.

**RESUM:** Aquesta tesis es centra en l'estudi de la transferència d'aigua i sediments des de les àrees font de sediments fins les zones de sedimentació a múltiples escales temporals (des de dades amb una freqüència de cinc minuts fins informació de tot un segle) i espacials (des de vessants fins a conques), i les seves implicacions en la morfologia de la llera de la conca de l'Alt Cinca, una conca de muntanya localitzada al vessant sud dels Pirineus. A escala de micro-conca, les dades d'alta resolució obtingudes durant 5 anys en dos *badlands* contrastats (0.3 ha cadascun) revelen com la pluja controla els processos erosius associats a l'escolament superficial, m'entre que les baixes temperatures tenen una relació significativa amb els processos de moviments en massa. La morfometria d'aquestes superfícies, conjuntament amb la cobertura vegetal són factors clau que determinen els principals processos geomorfològics i els associats canvis topogràfics. Els principals processos observats han estat seqüències d'Erosió i Sedimentació (*Cutting and Filling*) i Moviments Gravitacionals (*Mass Wasting*). Tot i que els *badlands* tenen un paper important en la producció de sediments, el balanç de sediments de la conca del riu Soto (10 $km^2$) indica que aquestes superfícies no sempre controlen l'exportació de sediments a la sortida de petites conques de muntanya amb caràcter intermitent. Aquest fet és degut a la fluctuació de la connectivitat funcional de la xarxa de drenatge causada per la freqüència i magnitud dels polsos d'aigua i sediments durant crescudes sobtades o *flashy*. La xarxa de drenatge actua com a font i zona d'emmagatzematge de sediments i es clau per entendre les marcades diferències que hi ha en la proporció del sediment que s'exporta en relació a la producció o també anomenat *Sediment Delivery Ratio*. Els canvis en els usos de sòl en moltes conques de muntanya constatats des de els anys 50 del segle XX tenen un efecte directe en la generació d'escolament (quantitat i magnitud) i en la producció de sediments. La majoria de la superfície de la conca de l'Alt Cinca (1565 $km^2$) ha sofert aforestació, que ha resultat en una reducció de la connectivitat sedimentaria estructural. La construcció de terrasses afecta la connectivitat molt més que els canvis en la coberta del sòl. Les terrasses generalment redueixen la connectivitat degut a l'establiment de zones planes entre mig de zones en pendent. Contràriament, a una escala més local, les terrasses poden incrementar la connectivitat degut a la convergència de flux produïda per les pròpies estructures, o per la caiguda d'aquestes degut a l'abandonament. La construcció de carreteres modifica el pendent i la xarxa de drenatge, fet que comportarà canvis en la connectivitat estructural, que a la vegada poden afectar els processos erosius en les zones veïnes. Així, els fluxos d'aigua i sediments a la conca de l'Alt Cinca han estat àmpliament modificats durant l'últim segle, amb implicacions directes en la forma de la llera. A més a més, impactes locals derivats de les extraccions d'àrids, construcció d'esculleres i embasaments també han condicionat la dinàmica sedimentaria d'aquest riu, amb un impacte directe sobre la morfologia. Aquesta situació ha generat una metamorfosis de la morfologia del riu en la part baixa de l'Alt Cinca (12 km), canviant d'un patró trenat, molt dinàmic, a un patró més estable amb una tendència cap a canal únic. Els resultats obtinguts indiquen que el tram d'estudi està assolint un nou equilibri morfo-sedimentari imposat pels canvis en els fluxos d'aigua i sediments ocorreguts en el darrer segle, incloent les pertorbacions antròpiques que han modificat la geometria del canal i les característiques morfològiques de la llera. S'han observat un total de tres fases en la seva evolució: abans de l'any 1927, el tram d'estudi es trobava en una situació de quasi-equilibri majoritàriament condicionada per les riuades. Entre l'any 1927 i 2012 el riu s'ha ajustat a les diferents pertorbacions que ha tingut a múltiples escales temporals i espacials. Aquest ajust s'ha portat a terme mitjançant dos canvis contrastats en les característiques morfològiques. Finalment, després de l'any 2012, els resultats indiquen que el riu pot haver assolit de nou un nou equilibri, ajustant-se als fluxos d'aigua i sediment imposats i a la nova configuració del canal. Aquesta tesis presenta innovadors mètodes quantitatius per a l'estudi de la producció de sediments i la transferència entre els diferents compartiments de les conques fluvials. La principal novetat en la majoria dels capítols de la tesis recau en l'elevada resolució, de les dades obtingudes, tant temporal com espacial. Els resultats obtinguts en aquesta tesi permeten entendre millor el funcionament dels sistemes fluvials i la seva evolució, aspectes claus per donar suport en la millora i gestió de conques hidrogràfiques de muntanya.

**Paraules clau:** Riu Alt Cinca, *badlands*, processos geomorfològics, morfometria, meteorologia, algoritme MaGPiE, polsos, *Sediment Delivery Ratio,* flux intermitent, connectivitat sedimentària, canvis dels usos de sòl, canvis geomorfològics, morfologia, extraccions d'àrids, crescudes, metamorfosis fluvial.

**RESUMEN:** Esta tesis se centra en el estudio de la transferencia de agua y sedimentos desde las áreas fuente de sedimentos hasta las áreas de sedimentación a múltiples escales temporales (desde datos con una frecuencia de cinco minutos hasta información de un siglo) y espaciales (desde laderas hasta cuencas), y sus implicaciones en la morfología del cauce en la Cuenca del Alto Cinca (vertiente sur de los Pirineos). A escala de micro-cuenca, los datos de alta resolución obtenidos durante 5 años en dos *badlands* contrastados (0.3 ha cada uno) revelan como la lluvia controla los procesos erosivos asociados a la escorrentía superficial, mientras que las bajas temperaturas tienen una relación significativa con los procesos de movimientos en masa. La morfometría de estas superficies, conjuntamente con la cobertura vegetal, son factores clave que determinan los principales procesos geomorfológicos y los cambios topográficos asociados. Los principales procesos observados han sido secuencias de Erosión y Sedimentación (*Cutting and Filling*) y Movimientos Gravitacionales (*Mass Wasting*). Pese a que los *badlands* tienen un papel importante en la producción de sedimentos, el balance de sedimentos de la cuenca del rio Soto (10 $km^2$) indica que estas superficies no siempre controlan la exportación de sedimentos a la salida de pequeñas cuencas de montaña con carácter intermitente. Esto principalmente se debe a la fluctuación de la conectividad funcional de la red de drenaje causada por la frecuencia y magnitud de los pulsos de agua y sedimentos durante las crecidas súbitas o *flashy*. La red de drenaje actúa como fuente y zona de almacenamiento de sedimentos, y es clave para entender las marcadas diferencias que hay en la proporción de sedimento que se exporta en relación a la producción o *Sediment Delivery Ratio*. Los cambios en los usos del suelo en muchas cuencas de montaña constatados desde los años 50 del siglo XX tienen un efecto directo en la generación de escorrentía (cantidad y magnitud) y en la producción de sedimentos. La mayoría de la superficie de la cuenca del Alto Cinca (1565 $km^2$) ha sufrido forestación, que ha resultado en una reducción de la conectividad sedimentaria estructural. La construcción de terrazas afecta la conectividad mucho más que los cambios en la cobertura del suelo. A una escala más local, las terrazas pueden incrementar la conectividad debido a la convergencia de flujo producida por las propias estructuras, o por la caída de estas debido a su abandono. La construcción de carreteras modifica la pendiente y la red de drenaje, hecho que comporta cambios en la conectividad estructural, que a su vez pueden afectar a los procesos erosivos en las zonas vecinas. Así, los flujos de agua y sedimento en la cuenca del Alto Cinca han estado ampliamente modificados durante el último siglo, con implicaciones directas en la morfología del canal. Además, impactos locales derivados de las extracciones de áridos, construcción de escolleras y embalses también han condicionado la dinámica sedimentaria de este río, con un impacto directo sobre la morfología. Esta situación ha generado una metamorfosis de la morfología del río en la parte baja del Alto Cinca (12 km), cambiando de un patrón trenzado, muy dinámico, a un patrón más estable con una tendencia hacia el canal único. Los resultados obtenidos indican que el tramo de estudio está alcanzando un nuevo equilibrio morfo-sedimentario impuesto por los cambios en los flujos de agua y sedimentos ocurridos durante el último siglo, incluyendo las perturbaciones antrópicas que han modificado la geometría del canal y las características morfológicas del cauce. Se han observado un total de tres fases en su evolución: antes de 1927, el tramo de estudio se encontraba en una situación de casi-equilibrio, mayoritariamente controlada por las crecidas. Entre el año 1927 y 2012 el río se ha ajustado a las diferentes perturbaciones que ha tenido a múltiples escalas temporales y espaciales. Este ajuste se ha llevado a cabo mediante dos cambios contrastados en las características morfológicas. Finalmente, después del año 2012, los resultados indican que el río puede haber alcanzado un nuevo equilibrio, ajustándose a los flujos de agua y sedimento impuestos y la nueva configuración del canal. Esta tesis presenta innovadores métodos cuantitativos para el estudio de la producción de sedimentos y la transferencia entre los diferentes compartimentos de las cuencas fluviales. La principal novedad en la mayoría de los capítulos de la tesis recae en la elevada resolución de los datos obtenidos, tanto temporal como espacial. Los resultados obtenidos en esta tesis permiten entender mejor el funcionamiento de los sistemas fluviales y su evolución, aspectos clave para dar soporte y apoyo en la mejoría y gestión de cuencas hidrográficas de montaña.

**Palabras clave:** Río Alto Cinca, *badlands*, procesos geomorfológicos, morfometría, meteorología, algoritmo MaGPiE, pulsos, *Sediment Delivery Ratio,* flujo intermitente, conectividad sedimentaria, cambios de los usos de suelo, cambios geomorfológicos, morfología, extracciones de áridos, crecidas, metamorfosis fluvial.

# CHAPTER 1

## INTRODUCTION

# CHAPTER 1: Introduction

## 1. GENERAL BACKGROUND AND RATIONALE

Rivers are dynamic systems transferring water and sediments (Schumm, 1977). Although sediments are eroded, transported and deposited through the entire catchment, the dominance of each process varies spatially and temporally defining different landscape compartments (Fryris and Brierley, 2013). This variability depends on the dynamic equilibrium between driving and resisting forces. In general, sediment acts as a resisting force while water flow acts as impelling force. An excess of flow or a reduction of the sediment load yields to erosion and incision, whereas an excess of sediment or reduction of flows tilt the balance towards deposition and channel aggradation (Lane, 1995). In this way, the balance between these processes will determine the morphology of river channels and the associated instream habitats (Kondolf, 1997). According to Wohl (2017 and 2019), river form and processes can be most effectively understood if explicit attention is given to the connectivity within river reaches and between the reach and the catchment, and the geomorphic context, defined by the catchment settings (e.g. geometry, location within a global context) and disturbances (i.e. natural or human-induced).

Connectivity can be defined as the potential for a specific particle to move through the compartments of a system at different temporal scales (Hooke, 2003; Braken and Croke, 2007; Fryirs, 2013; Heckman et al., 2018). Therefore, connectivity is not static and varies over time and space due to the interaction between landscape properties (i.e. structural connectivity), and the magnitude of water and sediment fluxes (i.e. functional connectivity), that will ultimately determine the frequency, distribution and magnitude of erosional and sedimentation processes (Bracken et al., 2015). The examination of (dis)connectivity patterns permits analysis of river sensitivity. River sensitivity can be described as the possibility, probability and propensity for change along a river course, and the ability of the system to recover from any given disturbance dictated by the operation of fluxes (water, sediment and vegetation) that occur at the catchment scale (Harvey, 2001; Fryirs, 2017).

According to Schumm (1973), a disturbance refers to a situation yielded by any factor that affects to the threshold condition of a river system, in the way that this system will be sensitive to change it lies close to a threshold. Disturbances may alter the dynamic equilibrium state of a river system, which infers a balance between processes and forms (Nanson and Huang, 2018; Thoms et al., 2018). Disturbances could be due to both natural (e.g. flood, tectonic events) and human (e.g. dam construction, gravel mining) factors. Lake (2000) described three typologies of disturbances depending on their intensity and duration: (i) pulse, (ii) press and (iii) ramp. The posterior recovery after each disturbance will be different in each category and would imply a new equilibrium. In this way, pulse disturbances refer to low frequency events with low duration and high magnitude (e.g. flood), that have a punctual effect and typically a relatively rapid recovery; although, in some cases extreme events may produce a lasting effect. Press disturbances have a longer duration and may directly affect larger areas (e.g. gravel mining), so their recovery is slower. Finally, in ramp disturbances, perturbations increase in a constant way over time and space (e.g. decrease of sediment and water flows due to increase of forest cover), and the system does not recover to the previous state; rather it becomes adjusted to a new state. Related to that, Schumm (1969) introduced the term 'river metamorphosis' to describe a complete transformation of river system as a consequence of changes in water and sediment yield associated with high intensity disturbances, usually related with direct or indirect human impacts.

The response of the river channels to each type of disturbance will be different (Fryirs, 2017) depending, among other factors, on the morpho-sedimentary conditions before the disturbance (i.e. how close to a threshold the system is) and the degree of connectivity (i.e. how coupled the system is). In coupled catchments, the effects of a given disturbance are often conveyed efficiently through the landscape. In contrast, responses to disturbances are inefficiently propagated through decoupled landscapes, as barriers or buffers inhibit conveyance of water and sediment, absorbing or damping the impacts of these (Fryris and Brierley 2013). The segregation of these disturbances is limited because of the feedbacks between disturbances and the associated adjustments and the variability in the time required for the river to adjust to a new state after a given disturbance. The response to a given disturbance is not immediate. According to Petts and Gurnell (2005), system responses to disturbance events are composed by three phases: (a) Reaction phase, which refers to the time required to the river to react to a given disturbance; and (b) Relaxation phase, referring to the time taken for the system to attain a new dynamic equilibrium through a sequence of transient states. The new regime state can be either similar to the previous state or different, based on the new imposed water and sediment flux conditions. Within the relaxation phase the authors identified the (c) Adjustment phase, which refers explicitly to the time that river requires adapting to the new conditions, from one to another regime state. Various forms of adjustment can occur depending on the sensitivity of the system to disturbance and the time between disturbance events. Thus, disturbance events modify water and sediment transfer at different temporal and spatial scales. Channel form is considered to be in equilibrium when the imposed water and sediment fluxes do not cause a net change (i.e. Lane, 1955; Richards, 1982; Church, 2006). Any alteration caused to these conditions (e.g. increase/decrease of sediment supply) will generate an adjustment of channel's morphology to the new situation; ultimately, a new equilibrium or regime state will be reached. Additional to natural-induced disturbances, rivers are subjected to human-induced disturbances which may modify water and sediment fluxes such as those caused by damming (e.g. Williams and Wolman, 1984; Kondolf, 1997; Vericat and Batalla, 2006). Additionally, other more localised disturbances such as instream gravel mining, embankment and rip-rapping (e.g. Kondolf, 1994; Rinaldi et al., 2005) may also have a direct impact on channel geometry and bed structure. These will ultimately have an effect on flow hydraulics, competence and physical habitat availability (e.g. Brown et al., 1998; Béjar et al., 2018).

During the last decades there has been a growing interest in the assessment of the relative contribution of climate change and forest growth on the vulnerability of water resources and impacts on sediment transport in Mediterranean regions (e.g. García-Ruiz et al., 1996; López-Moreno et al., 2014; Buendia et al., 2015; Buendia et al., 2016a). In general, these studies pointed out that due to afforestation mainly caused by the rural abandonment in mountain Mediterranean areas during the 20$^{th}$ century, and due to the decreasing trends for the precipitation caused by climate change, there was a clear decrease of runoff and sediment yield. Reforestation implies an increase in rainfall interception (e.g. Gallart et al., 1997; Llorens et al., 1997) and a reduction in the generation of direct runoff. This, combined with the replacement of cereal crops by dense scrub on steep slopes, has led to more moderate hydrological responses, accompanied by a clear decrease in sediment supply. Contrarily, Mediterranean regions represent one of the areas with the greatest presence of badlands (Clotet et al., 1987; Torri et al., 1994) due to their geology and marked climatic seasonal contrast (i.e. temperature, rainfall). Badlands are described as dissected landscapes with little or no vegetation cover, usually subjected to high erosion rates, representing the main source of fine sediments in some catchments (Yair et al., 1980; Gallart et al., 2002). Better understanding of main geomorphic processes re-shaping badlands, together with their relation with meteorological variables and morphometric characteristics, is key to understand cycles of sediment production and their

transfer downstream, which allows to better undertanding of the sediment Dynamics and the sediment budget at catchment scale.

Mediterranean catchments are frequently highly regulated. In the case of Spain, as reviewed by Batalla (2003), there are around 1200 large dams, representing nearly the 2.5% of the total number of dams in the world. Mediterranean rivers are thus highly variable in flow and sediment load (e.g. Conacher and Sala, 1998), naturally and human-driven. This sediment, in turn, is responsible for the loss of reservoir storage capacity due to siltation (e.g. Batalla, 2003; Martínez-Casasnovas and Poch, 1998; Valero-Garcés et al., 1999; Navas et al., 2009; Batalla and Vericat, 2011). Additionally, dams interrupt the continuity of sediment transfer downstream (see the example in the lower River Ebro –NE Iberian Peninsula- in Vericat and Batalla, 2006) and may alter flow and flood regimes (see the example in the whole Ebro catchment in Batalla et al., 2002). These disturbances will eventually have a direct impact on channel degradation processes such as channel incision and/or bed armouring (see the cycles reported in Vericat et al., 2006 for the lower Ebro).

Thus, understanding the relationship between catchment runoff and sediment yield, changes in water and sediment connectivity, and downstream implications at multiple temporal and spatial scales is considered fundamental for developing sustainable river basin management plans. From the applied or management point of view, there are several studies trying to understand processes and drivers operating at different landscape compartments. Mekonmen et al. (2015) presented an extensive review of studies that have assessed soil conservation efforts and their sediment trapping efficiency to prevent soil erosion off-site effects. They concluded that the spatial location of the measures is a key factor to disconnect landscape units from each other; decreasing runoff and sediment transport and, consequently, reducing downstream flooding and sedimentation problems. In the case of mountain streams, Marchi et al. (2019) recently observed that, overall effects of channel control works (e.g. check dams) on sediment connectivity consist of an alteration of the sediment cascade with a decrease in the efficiency of sediment transfer through channels, contributing to decouple or disconnect alluvial fans from the upslope catchment. Moving downstream to the channel network, there are several studies that have used historical analysis (i.e. multi-temporal) of geomorphic changes to support reach-scale management strategies (e.g. Ziliani and Surian, 2016; Heckman et al., 2017; Mould and Fryirs, 2019). Specifically, Ziliani and Surian (2016) analyzed historical channel adjustment of the lower river Tagliamento (Italy) during the last two centuries in order to assess a conceptual model of channel evolution for the period 2012-2035 based on historical analysis and numerical modelling. They suggest that, in future the river will reach a new equilibrium state, controlled mainly by the imposed flow regime and the established vegetation, concluding that the no intervention is the best possible river plan strategy due to its trend. More recently, Heckman et al. (2017) used a multi-temporal and multi-spatial approach in a dammed river of the German Alps in order to diagnose the effects of the disturbance caused by a dam construction and to analyze the evolution of artificially inserted or injected sediment in the river channel through topographic changes analysis. They observed that, injected sediment was entrained during floods of different return periods (magnitude) depending on the position of these deposits in relation to the channel.

Within this context, in general, this thesis is focussed on the study of water and sediment transfer from source to sinks at multiple temporal (from 5-min data to a century data sets) and spatial scales (from slope to catchment scale) and their implications for channel morphology. First, the thesis analyses sediment production in two highly erodible micro-catchments during a period of 5 years with the objective to infer in the main geomorphic processes controlling

sediment production and transfer in headwaters (Chapter 3). Secondly, water and sediment yield from a 10 $km^2$ catchment during two consecutive contrasted hydrological years are analysed in relation to sediment production in order to study the role of highly erodible landscapes in supplying sediments, the importance of the channel acting as sediment source and sink, and their temporal variability (Chapter 4). Thirdly, the thesis analyses changes in structural sediment connectivity in the last 60 years in relation to land abandonment and afforestation (Chapter 5). Finally, linked to all of these, geomorphic responses to multi-scale disturbances in a 12 km channel reach during the last century are analysed (Chapter 6). The thesis is focused in the Upper Cinca catchment, a mountain catchment located in the Southern Pyrenees (see full description in the following section). The Upper Cinca offers a perfect scenario to study all these aspects, relationships and interrelations because, among others, it offers a wide range of sub-basins that have notable differences in terms of sediment production, land cover and disturbances. This comprehensive analysis aids at understanding the functioning of the river system, which can help to support integrated watershed management practices or plans.

## 2. HYPOTHESIS, OBJECTIVES AND STRUCTURE OF THE THESIS

The overall aim of this thesis is to assess the geomorphic responses to natural and human disturbances in a mountain catchment at multiple temporal and spatial scales. The following hypotheses are tested in the thesis:

**H1**. Weathering and erosion in badlands are determined by different geomorphic processes acting at multiple temporal and spatial scales, being controlled or conditioned by meteorological and morphometric variables.

**H2**. Badlands are not controlling the entire sediment yield in small catchments with intermittent streams; the channel network may act as sediment source or sink, changing through time.

**H3**. Land use (and cover) changes together with the associated topographic changes modify sediment connectivity in mountain catchments having a direct implication in the amount of sediments being potentially transferred to river channels.

**H4**. Multi-scale disturbances in mountain river catchments have led to river metamorphosis in less than a century; channel planform have been simplified its braided complexity to a more static configuration, towards a wandering pattern.

In order to response these hypotheses, the specific objectives of the thesis are to:

**O1**. Quantify the importance of geomorphic processes in re-shaping badlands and exporting sediment downstream and their relationships with meteorological and morphometric variables.

**O2**. Study the relationships between sediment production and sediment yield in a small mountain catchment patched by badlands and drained by intermittent streams at multiple temporal scales.

**O3**. Analyse catchment scale effects of land use changes and associated topographic changes on structural sediment connectivity.

**O4**. Analyse geomorphic responses multi-scale disturbances during the last century in a mountain river reach.

These objectives set the framework for how the thesis is structured (Figure 3) and they also form the focal points for individual chapters (Chapters 3 to 6). In this way, the main objectives of the thesis are addressed in each results-focused chapter. Each of these chapters correspond to a scientific paper already published or submitted, except for Chapter 4, which is collected in paper format but not submitted at the moment this document was finalised. Following the regulation of the University of Lleida (i.e. Article 28 of the Normativa acadèmica de doctorat de la Universitat de Lleida), which specifies the requirements of the Thesis based on article format, each of the focal chapters (Chapters 3 to 6) can be considered as a self-contained unit with an introduction section outlining the specific research context and objectives, the full details of the methods used, the results and discussion. The present Chapter 1 represents a general introduction of the Thesis. Chapter 2 provides a general overview of the methods used for the respective focal chapters, including three scientific papers dealing with specific methods developed in the thesis. The final chapter (Chapter 7) is a synthesis that integrates the results from each of the individual chapters/papers, presenting a comprehensive short discussion that subsequently allows general conclusions do be drawn in relation to each of the objectives of the work (Figure 3).

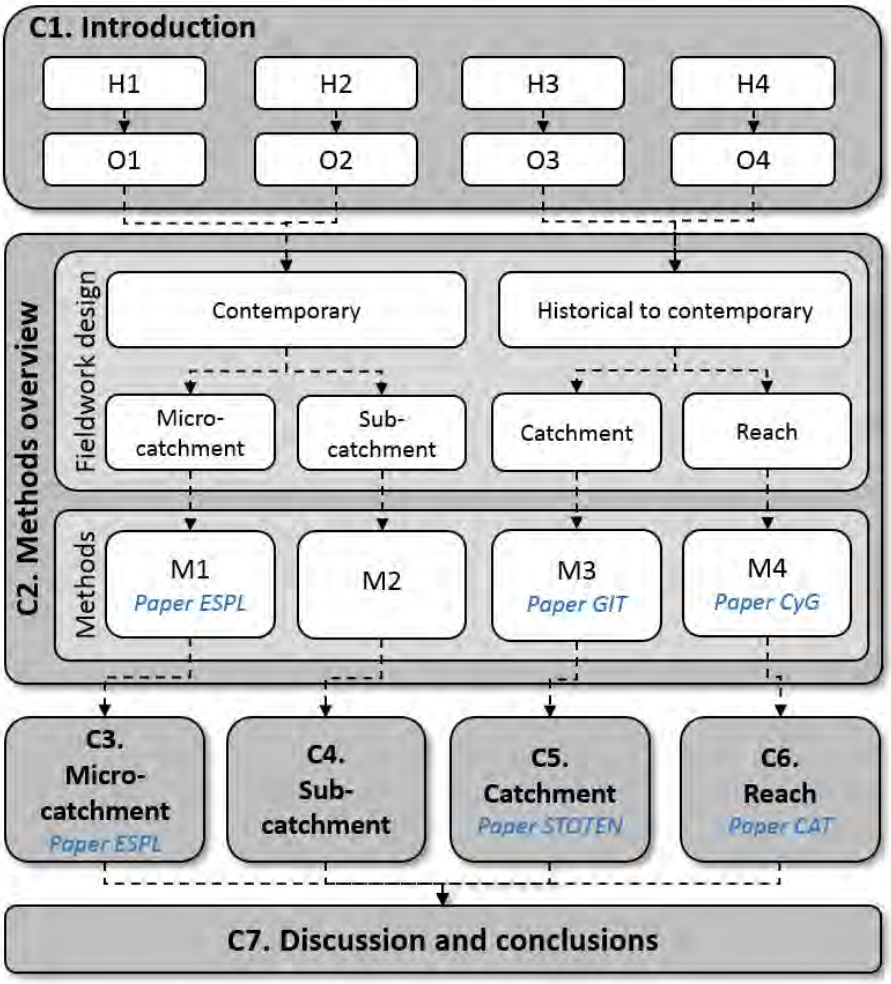


**Figure 3**. General structure of the Thesis with the different Chapters (i.e. C) covering each one of the main objectives (i.e. O), associated methods (i.e. M) at different spatial and temporal scales, and the Journals where the papers have been submitted, accepted and/or published in each case (i.e. *ESPL = Earth Surface Processes and Landfroms; GIT = Rendiconti Online Società Geologica Italiana; CyG = Cuaternario y Geomorfología; STOTEN = Science of the Total Environment; CAT = Catena*. Note that the specific status of each paper, together with the rank of each journal is provided in the corresponding chapter.

## 3. THE UPPER CINCA CATCHMENT

### 3.1. Location

The Upper Cinca catchment is located in the headwaters of the river Cinca catchment (8300 $km^2$), in the centre of the south face of the Pyrenees (NE Iberian Peninsula; Figure 1A). The upper catchment, which drains to the Mediano Reservoir (435 $hm^3$, finalised in 1974), covers a total area of 1565 $km^2$ and is composed by two sub-catchments: the Ara (715 $km^2$) and Cinca (850 $km^2$). The elevation ranges from 522 m a.s.l. at the outlet to 3375 m a.s.l. on the Posets Peak at the headwaters (Figure 1B). The catchment presents a moderate mean slope (i.e. around 20º or 36%). Overall, the magnitude of the slope is positively correlated with altitude, i.e. high values are observed in the high parts of the catchment (Figure 2A). Slope decreases towards the valley bottoms of the main rivers, where the valleys open out and slopes reach the lowest values (i.e. <10 º). Morphologically, the lower parts of those reaches are highly dynamic with multiple active channels, different typologies of bars and vegetation cover. Both the Ara and Cinca rivers present a stream order value of 3 (Strahler, 1952) in a 1:700000 scale (Figure 2B).

In terms geology, there are three main distinct lithological units arranged in a N-S axis (Ríos et al., 1979): (a) the axial Pyrenees, in the northern part, made up of the oldest reliefs with metamorphic (e.g. shales, schists and marbles) and igneous (e.g. granites, granodiorites) rocks. (b) The internal mountain ranges, a large over-thrusting fold of Cretaceous and Paleogene sediments, composed mainly of limestone (e.g. Perdido-Cotiella, highest limestone massifs of Europe), sandstones and conglomerates. This mountain range was formed during the Alpine orogeny, and was greatly affected by most active stages of quaternary glaciation. (c) The middle depression, which occupies the centre and the lowest parts of the basin (>50% of the catchment area), being composed by softer sedimentary materials (e.g. marls, sandstones) giving a relatively smooth relief. These softer materials provide large amount of fine sediment to the secondary channels, which drain in the lower parts of the Ara and Cinca reaches (e.g. the Soto sub-catchment), but also directly to the Mediano reservoir (e.g. de la Nata sub-catchments) in the lower areas (Figure 2C). These materials have been already proven to be the main source of fine sediments in counterpart catchments such as the Ésera and Isábena (e.g. López-Tarazón et al., 2012; Piqué et al., 2014; Lobera et al., 2015; Buendia et al., 2016b).

Although the Upper Cinca catchment is the general study area, as will be stated in Chapter 2, each of the central Chapters of the thesis will be focused in a different spatial scale (Figure 1). Because the specific details of each study area are extensively explained in each of the chapters, this section only provides a general idea of the locations of the different specific study areas. In this way (i) Chapter 3 is focused on the study of two micro-catchments developed on badlands (i.e. around 0.5 ha each), located in the Soto sub-catchment in the lower part of the Upper Cinca catchment (Figure 1E). (ii) Chapter 4 is dedicated to the entire Soto sub-catchment (i.e. around 10 $km^2$), which drains to the lower part of the River Cinca that immediately drains to the Mediano reservoir in the true left bank side of the River Cinca (Figure 1D). (iii) Chapter 5 analyses the entire Upper Cinca catchment (1565 $km^2$) through four different sub-catchments (from 7 $km^2$ to 16 $km^2$) being representative of the main land uses of the overall catchment (Figure 1B). Finally, (iv) Chapter 6 is focused on the lower part of the River Cinca, a 12 km long river reach, being affected by the transfer (and changes) of water and sediment through the entire catchment (Figure 1C).

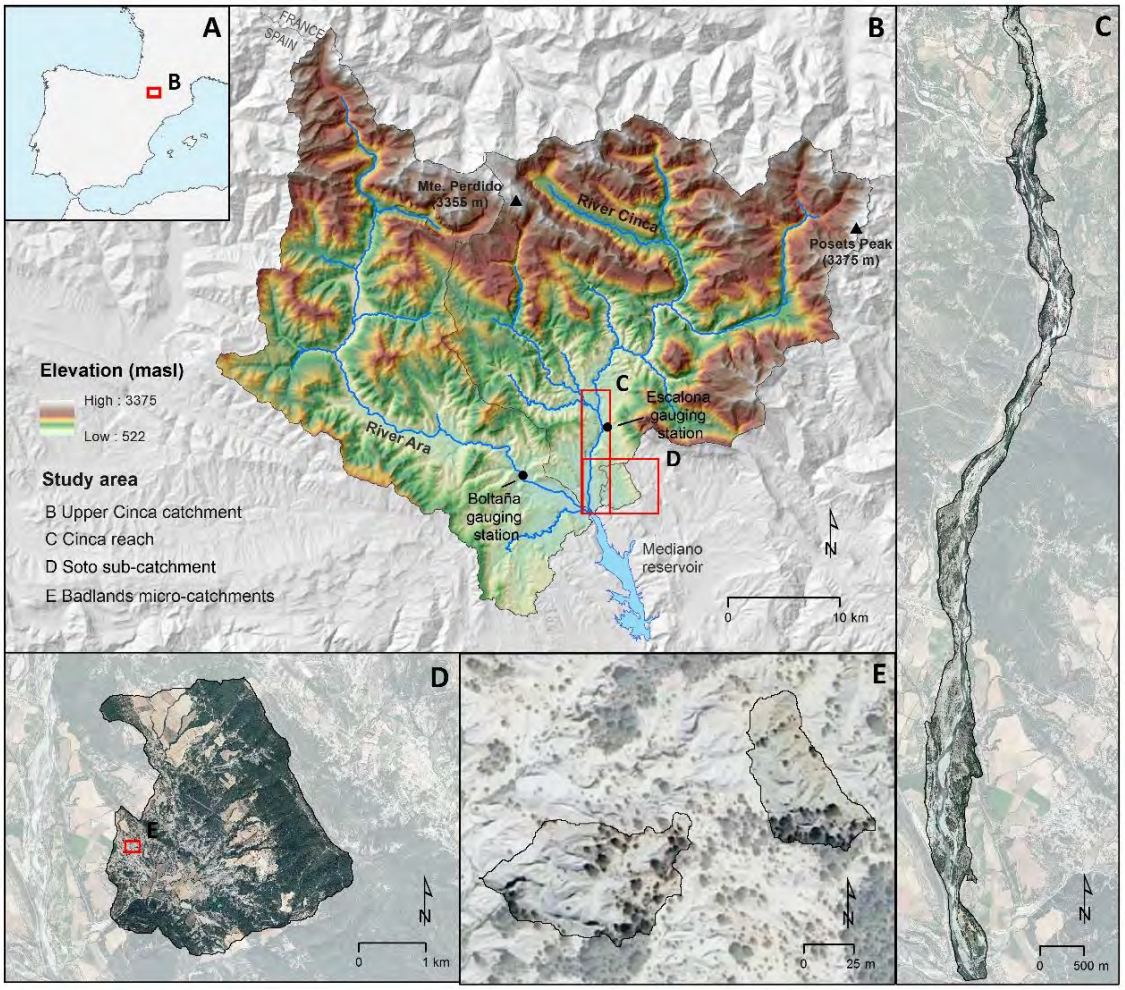


**Figure 1**. **A.** Location of the Upper Cinca catchment within the Iberian Peninsula. **B.** The Upper Cinca Catchment (spatial scale analysed in Chapter 5). **C.** The 12 km long river reach of the Upper Cinca being the focus of the analyses presented in Chapter 6. **D.** The Soto sub-catchment corresponding to the study area of Chapter 4. **E.** The two experimental micro-catchments in badlands corresponding to the study area of Chapter 3. See specific details of each study are in the corresponding chapters.

## 3.2. Climate and hydrology

The climate of the Upper Cinca catchment has strong latitudinal contrasts. The Mediterranean continental climatic domain causes a warm and dry climate in the southern zone, while in the northern part the prevalence of mountain domain yields a cooler and more humid climate (Rubio, 1995). Between these two marked latitudinal climatic domains, there is also a longitudinal gradient between a Mediterranean-Oceanic transition climate (west of the basin) and a humid sub-Mediterranean climate (east of the basin). In order to characterize the spatial variability of the key variables, the annual average temperature and precipitation values in two meteorological stations located in two contrasted climatic domains are presented below. Data recorded for the period 1981-2018 in the (a) Góriz (north of the basin; Figures 2E and 2F) and (b) Aínsa (south of the basin; Figures 2E and 2F) stations were used (stations property of the Spanish Meteorological Agency; the data was provided by the Aragon Statistics Institute in May 2019). Mean annual temperature varies between 5 °C in the north (i.e. Góriz) to 13 °C in the valley bottom (i.e. Aínsa, Figure 2E). In both stations maximum mean daily values are registered in July and August (i.e. around 23 ºC in Aínsa and 13 ºC in Góriz), while minimum values are

registered during December and January (i.e. around 4 ºC in Aínsa and -2 ºC in Góriz). Both areas show a similar pattern in terms of the monthly distribution of daily maximum and minimum rainfall. Maximum values are registered during the equinoxes and minimum are during solstices. In spite of this, there is a strong latitudinal gradient, the north zone presenting a much greater rainfall than the south (Figure 2F). The annual average precipitation in Aínsa station is 755 mm, with maximum monthly values of 80 mm in May and September, and minimum monthly values of 33 and 41 mm are observed in February and March, respectively. For the Góriz station, the annual average precipitation is 1730 mm, with maximum monthly values of 213 and 203 mm measured in October and November, and minimum monthly values of 84 and 101 mm registered in February and March, respectively.

Hydrologically, the catchment is characterized by a rain-snowy regime with large intra-annual variability with high variations in flow. There is a seasonal variation in the occurrence of floods, which typically occur in spring due to snowmelt and, especially, in the late summer and autumn as a consequence of localized thunderstorms. Minimum flows occur in summer and winter but the river never dries up (Béjar, 2018). In the case of the River Cinca, the mean annual discharge at the Escalona gauging station (operated by the Ebro Water Authority, CHE; the data were provided by the Automatic Hydrologic Information System –SAIH- of the -CHE in May 2019) for the period 1959-2015 is 27 $m^3/s$, while the annual mean runoff is 789 $hm^3$ (note that this station is located 8 km upstream from Mediano reservoir; Figure 1). Annual floods are around 250 $m^3/s$ and high magnitude floods (i.e. floods with a recurrence interval of 10 years) exceed 530 $m^3/s$. In the case of the River Ara, the mean annual discharge at the Bolataña gauging station (operated by the CHE; the data was provided by SAIH-CHE in May 2019) for the period 1951-2015 is 17 $m^3/s$, while the annual mean runoff is around 500 $hm^3$. Annual floods are around 180 $m^3/s$ and high magnitude floods (i.e. floods with a recurrence interval of 10 years) exceed 390 $m^3/s$ (note that this station is located 7 km upstream from Mediano reservoir; Figure 1) Further analysis of hydrological trends and magnitude of floods are fully performed in Chapter 6.

## 3.3. Land cover and human activities

During the 20$^{th}$ century, the Upper Cinca catchment and the majority of the Mediterranean mountain areas suffered important changes in land use, mainly due to the changes of the economic model and the consequent abandonment of rural areas, which among other aspects caused an important reforestation process (see examples in the Pyrenees in García-Ruiz et al., 1996; and in the Alps in Tasser et al., 2007). Reforestation implies an increase in interception and a reduction in the generation of direct runoff, at least for rainfall events of medium and high frequency (e.g. Llorens et al., 1997; Gallart et al., 1997). This, combined with the replacement of cereal crops by dense scrub on steep slopes, has led to more moderate hydrological responses, accompanied by a clear decrease in sediment yield (e.g. García-Ruiz and Ortigosa, 1988; García-Ruiz et al., 1996; López-Moreno et al., 2014; Buendia et al., 2016). The deficit of sediment makes an adjustment in the riverbed causing a series of changes in its channel morphology that can be reinforced with additional localised human disturbances such as gravel mining or more structural disturbances such as damming. These situations can lead to a change from braided patterns (with domain channels and bars in the horizontal plane of the channel) to single channel patterns (wandering to meandering platforms), dominated by incision and stabilization of sedimentary bars (e.g. Begueria et al., 2006). The most dominant land use cover (in terms of extension) in the Upper Cinca catchment is forest (i.e. 52 %), followed by shrubs and pastures (i.e. 28%), bare areas (i.e. 15%; %; e.g. bare rocks, badlands, river bars, glaciers and snow), and agricultural fields (i.e. 4 %; data extracted from the 2018 CORINE Land Cover map 1:100000

spatial scale; Figure 2D). The rest of the catchment (i.e. <1%) is comprised of other marginal land cover or uses (e.g. water bodies, artificial surfaces; Figure 2D). Forest in the lower part of the catchment (i.e. up to 800 m a.s.l.) is dominated by pines (*Pinus nigra salzmanii)* and oaks (*Quercus humilis* and *Quercus subpyrenaica)*. The vegetation between 800 and 1800 m a.s.l. is characterised by *Fagus sylvatica, Abies alba* and *Pinus sylvestris*. Forest in the upper part of the catchment (i.e. 2200 m a.s.l.) is dominated by *Pinus uncinata* and *Betula pendula*. Pastures can only survive the climatic conditions up to 2200 m a.s.l. (where predominant genus is *Festuca sp.*; Béjar, 2018; Figure 2D).

The Upper Cinca catchment has been heavily regulated since 1923. The main objective of this regulation has been hydropower generation, as with many such mountain rivers. Specifically, 4 small dams impounding 4.65 $hm^3$ and 58 km of canals and diversions were constructed (Galán, 2012) in the Upper Cinca. The study reach is subjected to daily rapid flow fluctuations (hydropeaks; maximum flows around 25 $m^3/s$) caused by hydropower generation. Water is managed by the Laspuña Dam, a dam located 7 km upstream of the upstream end of the study reach of Chapter 6 (Figure 1C), built in 1965 with a capacity of 0.35 $hm^3$. This dam has a wicked gates that impound low flows for transfer through the network of canals; however, they are open during floods facilitating the continuity of the flow and sediment transport. Therefore, the lowermost part of the Upper Cinca is subjected to two contrasted daily flow regimes: (i) a low flow regime given by environmental flows released from Laspuña Dam that affects the first 2 km of the study reach, and (ii) the hydropeaking-based regime affecting the lowest 10 km of the study reach. The Ara catchment, however, is not regulated, being a unique not hydrologically-disturbed mountain catchment in the southern Pyrenees. Downstream of the study catchment, the Mediano reservoir (435 $hm^3$, built in1974), caused some impacts upstream. Among other effects, this reservoir alters the longitudinal profile of the river changing the local base level, a fact that causes some loss of competence, resulting in a significant increase in sedimentation just upstream of the reservoir (Rubio, 1995) in both the Ara and Cinca rivers and its confluence (Figure 1).

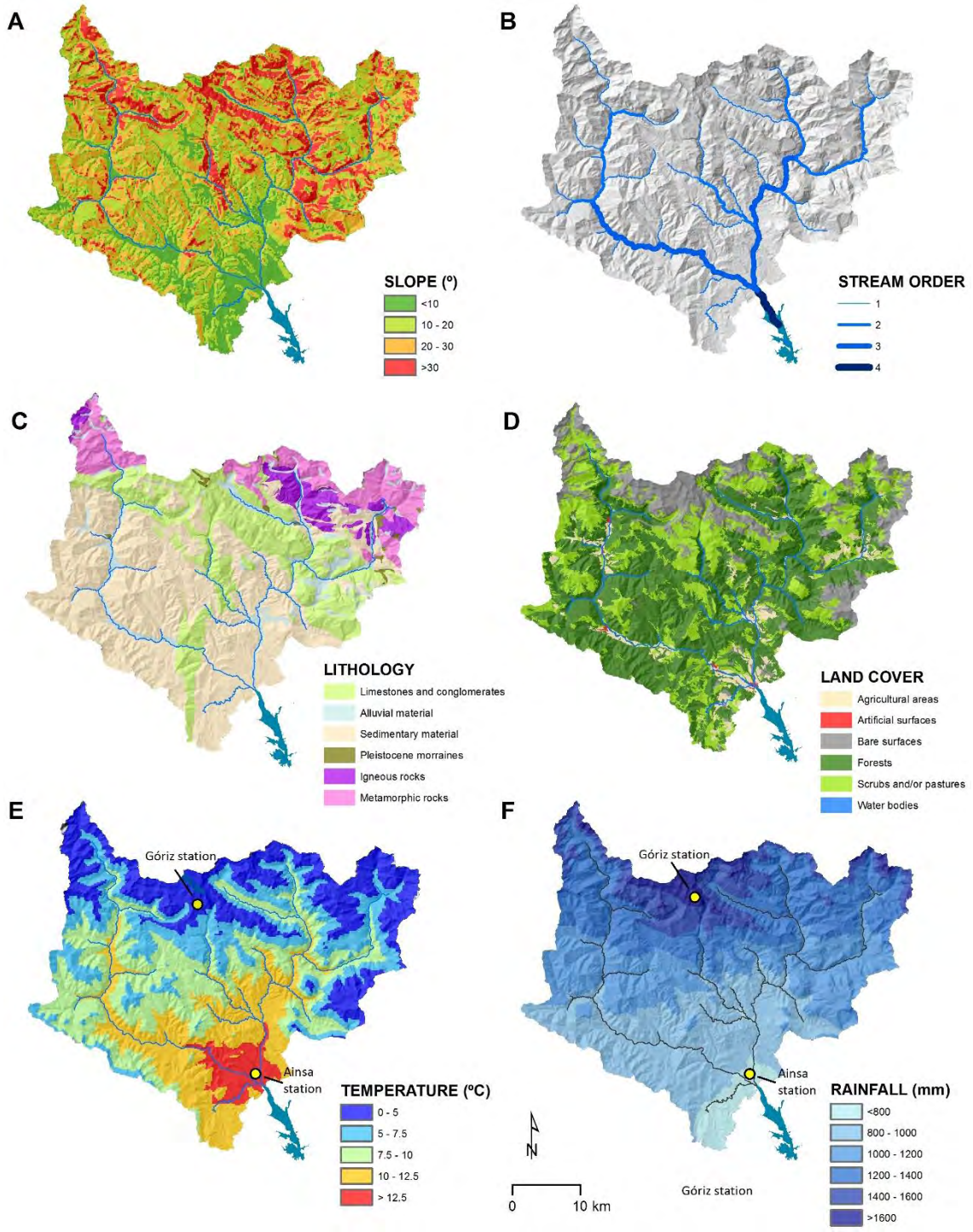


**Figure 2**. Physical context of the Upper Cinca catchment including both the Cinca and Ara sub-catchments: **A.** Slope (in degrees) calculated from a Digital Elevation Model (DEM) of 200 m of spatial resolution (data source: Spanish National Centre of Geographic Information, CNIG). **B.** Stream order calculated by the Strahler (1952) from a DEM of 200 m resolution at 1:700000 spatial scale. **C.** Main lithological units (data source: *Instituto Geológico y Minero de España* and *Bureau de Recherches Gèoligiques et Minières*, 2009). **D.** Land cover map (data source: CORINE, European Environment Agency, 2018). **E.** Mean annual temperature and **F.** mean annual precipitation for the period 1981-2018 (data source: Spanish Meteorological Agency). Note that the location of the Góriz and Ainsa weather stations are indicated as reference (see text for the specific discussion of the data in these two stations).

After the extraordinary flood registered in 1982 (recurrence interval larger than 100 years) the Ebro Water Authorities (CHE) together with local governments decided to construct lateral embankments and rip-raps, especially in the lower parts of both the Ara and Cinca rivers. These two locations were characterised by areas where both rivers increase their active width considerably, with a clear and active floodplain. The objective of the construction of these channel-infrastructures was to prevent lateral bank erosion, preserving floodplains for agricultural and other human related uses and to reduce the possible damages caused by future floods (Hernández, 1991; Rubio, 1994). As discussed in Chapter 6, these constructions had a direct effect on channel geometry, decreasing sinuosity significantly, concentrating flows (thereby increasing flow velocity and competence), and decreasing lateral connectivity. Additionally to these effects, the Upper Cinca catchment has a long history of in-channel gravel mining which, as discussed again in Chapter 6, has modified the morpho-sedimentary equilibrium of the upper Cinca over the last decades. Currently, instream gravel mining works are only approved in the background of projects aimed at improving channel conditions with the objective to prevent, for instance, channel erosion and flooding (e.g. works to stabilize channel embankments).

## 4. REFERENCES

Aragon Statistics Institute. 2019. Clima/Datos climatológicos. Gobierno de Aragón. Zaragoza. Accessed on May 2019. Available online: http://www.aragon.es/DepartamentosOrganismosPublicos/Institutos/InstitutoAragonesEstadistica/AreasTematicas/14_Medio_Ambiente_Y_Energia/ci.05_Clima_Datos_climatologicos.detalleDepartamento?channelSelected=ea9fa856c66de310VgnVCM2000002f551bacRCRDT.

Automatic Hydrologic Information System of the Ebro river Basin, 2019. *Historical data*. The Ebro River Basin Authority. Zaragoza. Accesed on May 2019. Available online: http://www.saihebro.com/saihebro/index.php?url=/historicos/peticion.

Batalla RJ. 2003. Sediment dèficit in rivers caused by dams and instream gravel mining. A review with examples from NE Spain. *Cuaternario y Geomorfología* 17(3-4): 79-91.

Batalla RJ, Vericat D. 2011. An appraisal of the contemporary sediment yield in the Ebro Basin. *Journal of Soils and Sediments* 11: 1070-1081.

Beguería S, López-Moreno JI, Lorente A, Seeger M, García-Ruiz JM. 2006. Assessing the effect of climate oscillations and land-use changes on streamflow in the central Spanish Pyrenees. *Ambio* 32:283–283.

Béjar M. 2018. Interactions between sediment transport, physical habitat and benthic communities in a mountainous river affected by natural and human disturbances PhD Thesis, Universitat de Lleida, Departament de Medi Ambient i Ciències del Sòl. 216 pp.

Béjar M, Vericat D, Batalla R, Gibbins CN. 2018. Variation in flow and suspended sediment ransport in a montane river affected by hydropeaking and instream mining. *Geomorphology* 310: 69-83.

Braken LJ, Croke J. 2007. The concept of hydrological connectivity and its contribution to understanding runoff-dominated geomorphic systems. *Hydrological Processes* 21: 1749–1763.

Braken, LJ, Tumbull L, Wainwright J, Bogaart P. 2015. Sediment connectivity: a framework for understanding sediment transfer at multiple scales. *Earth Surface Processes and Landforms* 40: 177–188.

Brown AV, Lyttle MM, Brown KB. 1998. Impacts of Gravel Mining on Gravel Bed Streams. *Transactions of the American Fisheries Society* 127: 979-994.

Buendia C, Batalla RJ, Sabater S, Palau A, Marcé R. 2015. Runoff trends driven by climate and afforestation in a Pyrenean basin. *Land Degradation and Development* 27: 823-838.

Buendia C, Bussi G, Tuset J, Vericat D, Sabater S, Palau A, Batalla RJ. 2016a. Effects of afforestation on runoff and sediment load in an upland Mediterranean catchment. *Science of Total Environment* 540: 144-157.

Buendia C, Vericat D, Batalla RJ, Gibbins CN. 2016b. Temporal dynamics of sediment transport and transient in-channel storage in a highly erodible catchment. *Land Degradation and Development* 27: 1045-1063.

Church M. 2006. Bed Material Transport and the Morphology of Alluvial River Channels. *Annual Review of Earth and Planetary Sciences* 34: 325-354.

Clotet N, Gallart F, Sala M. 1987. Los badlands: características, interés teórico, dinámica y tasas de erosión. *Notes de Geografía Física* 15-16: 28-37.

Conacher AJ, Sala M. 1998. *Land degradation in Mediterranean environments of the world. Nature, extent, causes and solutions*. John Wiley and Sons, Chichester, 491 pp.

European Environment Agency. 2018. CORINE Land Cover. Scale: 1:100,000. Accessed on January 2019. Available online: https://www.eea.europa.eu/data-and-maps/data/corine-land-cover-accounting-layers

Fryirs KA. 2013. (Dis)Connectivity in catchment sediment cascades: a fresh look at the sediment delivery problem. *Earth Surface Processes Landforms* 38: 30–46.

Fryirs KA. 2017. River sensivity: a lost foundation concept in fluvial geomorphology. *Earth Surface Processes and Landforms* 42: 55-70.

Fryris KA, Brierley GJ. 2013. *Geomorphic analysis of river system: an approach to reading the landscape*. Chischester: John Wiley and Sons. 360 pp.

Galán F. 2012. *Centrales hidroeléctricas y presas del Alto Aragón*. Fundación ESTEYCO. Madrid. 177 pp.

Gallart F, Llorens P, Latron J, Rabadà D. 1997. Hydrological functioning of Mediterranean mountain basins in Vallcebre, Catalonia: Some challenges for hydrological modeling. *Hydrological Processes* 11: 1263-1272.

Gallart F, Solé A, Puigdefàbregas J, Lázaro R. 2002. Badland Systems in the Mediterranean. In: Dryland Rivers: Hydrology and Geomorphology of Semi-arid Channels. Bull LJ, Kirkby MJ (Eds.). John Wiley & Sons, Ltd. 299-326.

García-Ruiz JM, Ortigosa LM. 1988. Algunos efectos geomorfológicos de las repoblaciones forestales. Cambios en la dinámica del cauce en pequeñas cuencas del Pirineo Central español. *Cuaternario y Geomorfología* 2 (1-4): 33-41.

García-Ruiz JM, Lasanta T, Ruiz-Flano P, Ortigosa L, White S, González C, Martí C. 1996. Land-use changes and sustainable development in mountain areas: a case study in the Spanish Pyrenees. *Landscape Ecology* 11: 267-277.

Harvey AM. 2001. Coupling between hillslopes and channels in upland fluvial systems: implications for landscape sensitivity, illustrated from the Howgill Fells, northwest England. *Catena* 42, 225–250.

Heckman T, Haas F, Abel J, Rimböck A, Becht M. 2017. Feeding the hungry river: Fluvial morphodynamics and the entrainment of artificially inserted sediment at the dammed river Isar, Eastern Alps, Germany. *Geomorphology* 291: 128-142.

Heckmann T, Cavalli M, Cerdan O, Foerster S, Javaux M, Lode E, Smetanová A, Vericat D, Brardinoni F. 2018. Indices of sediment connectivity: opportunities, challenges and limitations. *Earth Sciences Review* 187: 77–108.

Hernández S. 1991. Geomorfología del área de confluencia de los ríos Cinca y Ara (prov. de Huesca). University of Zaragoza. Spain. 311 pp.

Hooke J. 2003. Coarse sediment connectivity in river cannel systems: a conceptual framework and methodology. *Geomorphology* 56: 79-94.

Kondolf GM. 1994. Geomorphic and environmental effects of instream gravel mining. *Landscape and urban Planning* 28: 225-243.

Kondolf GM. 1997. Hungry Water: Effects of Dams and Gravel Mining. *Environmental Management* 21: 533–551.

Instituto Geológico y Minero de España and Bureau de Recherches Gèoligiques et Minières. 2009. Mapa Geológico de Pirineros. Scale: 1:400,000. Madrid. Accessed on January 2019. Available online: http://info.igme.es/cartografiadigital/geologica/mapa.aspx?parent=../tematica/tematicossingulares.aspx&Id=14.

Lake PS. 2000. Disturbance, patchiness, and diversity in streams. *Freshwater Science* 19(4): 573-592.

Lane EW. 1955. The importance of fluvial morphology in hydraulic engineering. *J. Hydraul. Div. ASCE*. 81: 1–17.

Lane SN, Richards KS, Chandler JH. 1995. Morphological Estimation of the Time-Integrated Bed Load Transport Rate. *Water Resources Research* 31(3), 761–772.

Llorens P, Poch RM, Latron J, Gallart F. 1997. Rainfall interception by a Pinus sylvestris forest patch overgrown in a Mediterranean mountainous abandoned area. Monitoring design and results down to the event scale. *Journal of Hydrology*. 199: 331-345.

Lobera G, Batalla RJ, Vericat D, López-Tarazón JA, Tena A. 2015. Sediment transport in two mediterranean regulated rivers. Science of the Total Environment. *Science of the Total Environment* 540: 101-113.

López-Moreno JI, Zabalza J, Vicente-Serrano SM, Revuelto J, Gilaberte M, Azorin-Molina C, Morán-Tejeda E, García-Ruiz JM, Tague C. 2014. Impact of climate and land use change on water availability and reservoir management: Scenarios in the Upper Aragón River, Spanish Pyrenees. *Science of the Total Environment* 493: 1222-1231.

López-Tarazón JA, Batalla RJ, Vericat D, Francke T. 2012. The sediment budget of a highly dynamic mesoscale catchment: the river Isábena. *Geomorphology* 138: 15–28.

Marchi L, Comiti F, Crema S, Cavalli M. 2019. Channel control works and sediment connectivity in the European Alps. *Science of the Total Environment* 668: 389-399.

Martínez-Casasnovas JA, Poch RM. 1998. Estado de conservación de los suelos d ela cuenca del embalse Joaquín Costa. *Limnética* 14: 83-91.

Mekonmen M, Keestra SD, Stroosnijder L, Baartman EM, Maroulis J. 2015. Soil conservation through sediment trapping: a review. *Land Degradation and Development* 26: 544-556.

Mould S, Fryirs K. 2019. Contextualising the trajectory of geomorphic river recovery with environmental history to support river management. *Applied Geography* 94: 130-146.

Nanson GC, Huang HQ. 2018. A philosophy of rivers: Equilibrium states, channel evolution, teleomatic change and least action principle. *Geomorphology* 302: 3-19

Navas A, Valero-Garcés B, Gaspar L, Machín J. 2009. Reconstructing the history of sediment accumulation in the Yesa reservoir: an approach for management of mountain reservoirs. *Lake and Reservoir Management* 25(1): 15-27.

Petts GE, Gurnell AM. 2005. Dams and geomorphology: Research progress and future directions. *Geomorphology* 71 (1–2): 27-47.

Richards, K. 1982. *Rivers: form and process in alluvial channels*. Blackburn Press. London. 361 pp.

Ríos LM, Beltrán FJ, Lanaja JM, Marín FJ. 1979. Contribución a la geología de la Zona Axial Pirenaica, valles del Cinca y Ésera, provincia de Huesca. Acta Geológica Hispánica. Homenaje a Lluis Solé i Sabarís. 14: 271-279.

Rinaldi M, Wyzga B, Surian N. 2005. Sediment mining in alluvial channels: Physical effects and management perspectives. *River Research and Applications* 21(7): 805–828.

Rubio V. 1995. Dinámica Fluvial Del Rio Ara (Pirineo Aragonés). PhD Thesis, Universidad Autónoma de Madrid, Departamento de Geografía. 815.

Schumm SA. 1969. River metamorphosis. *Journal Hydraulics Division of American Society of Civil Engineering* 1: 255-273.

Schumm, S.A., 1973. Geomorphic thresholds and complex response of drainage systems. In: Morisawa M (Ed.) Fluvial Geomorphology. Binghampon Publications in Geomorphology. 299-309 pp.Schumm, SA. 1977. *The fluvial system*. John Wiley and Sons, New York. 338 pp.

Strahler, A. 1952. Dynamic Basis of Geomorphology. *Geological Society of America Bulletin* 63: 923-938.

Tasser E, Walde J, Tappeiner U, Teutsch A, Noggler W. 2007. Land-use changes and natural reforestation in the Eastern Central Alps. *Agriculture Ecosystems and Environment* 118: 115-129.

Thoms MC, Piégay H, Parsons M. 2018. What do you mean, 'resilient geomorphic systems'?. *Geomorphology* 305: 8-19.

Torri D, Colica A, Rockwell D. 1994. Preliminary study of the erosion mechanisms in a biancana badland (Tuscany, Italy). *Catena* 23: 281-294.

Valero-Garcés BL, Navas A, Machín J, Walling D. Sediment sources and siltation in mountain reservoirs: a case study from the Central Spanish Pyrenees. *Geomorphology* 28(1-2): 23-41.

Wohl E. 2017. Connectivity in rivers. *Progress in Physical Geography* 41: 345–362.

Wohl E. 2019. Geomorphic context in rivers. *Progress in Physical Geography* 42(6): 841–857.

Williams GP, Wolman MG. 1984. *Downstream Effrects of Dams on Alluvial Rivers*, US Geological Survey Profesional Paper. 90 pp.

Yair A, Lavee H, Bryan RB, Adar E. 1980. Runoff and erosion processes and rates in the Zin Valley badlands, Northern Negev, Israel. *Earth Surface Processes* 5: 205-225.

Ziliani L, Surian N. 2016. Reconstructing temporal changes and prediction of channel evolution in a large Alpine river: the Tagliamento river, Italy. *Aquatic Sciences* 78: 83-94.

# CHAPTER 2

## FIELDWORK DESIGN AND METHODS OVERVIEW

# CHAPTER 2: Fieldwork design and methods overview

As outlined in Figure 3 in Chapter 1 (Introduction), a multi-spatial and multi-temporal approach was designed and implemented in order to address the specific objectives of the Thesis. In the following chapter a general overview of the multi-scale approach in relation to the different chapters and objectives of the thesis, followed by a summary of the methods linked to each spatial scale are provided. It is noting that this section also includes a total of three research papers, two of which are already published and one accepted subject to major revisions. A full description of the status of these papers and the details of the journals including their impact factors are provided at the beginning of each paper. Finally, although a general summary of the methods is provided here, each of the focal chapters (Chapters 3 to 6) are considered as a self-contained unit with full details of the methods used, independently to the general overview provided in this chapter.

## 1. MULTI-SCALE APPROACH

Figure 1 shows the different spatial and temporal scales addressed in the thesis, their interrelations and their links to the focal chapters of the thesis. Four interrelated spatial scales are included in the thesis (Figure 1). Chapter 3 is focused on the micro-catchment scale (i.e. 0.5 ha), analysing topographic changes in badlands over a period of five years and infers the main geomorphic process re-shaping these highly erodible landscapes and producing sediment. The temporal scale addressed in this chapter is considered representative of the present conditions. Chapter 4 analyses water and sediment yield in a small intermittent stream sub-catchment (i.e. 10 $km^2$) during two consecutive years (present conditions, Figure 1) in relation to the dynamics observed in the micro-catchments presented in Chapter 3 (i.e. a nested approach). Chapter 5 is based on the catchment scale (the entire Upper Cinca, 1565 $km^2$), integrating the other spatial scales, but in this case analysing changes in land use and sediment connectivity from the past to the present. Finally, Chapter 6 is focused on a 12 km river reach (i.e. reach scale), analysing almost a century of data to evaluate the geomorphic responses due to different natural and human disturbances the entire catchment has suffered in the last century. Therefore, although it is evident that the spatial scale analysed in Chapter 6 is smaller than Chapter 5, dynamics in this reach are clearly affected by the imposed catchment-scale water and sediment fluxes, together with localised disturbances in the channel such as instream gravel mining or the construction of embankments and rip-rapping (Figure 1).

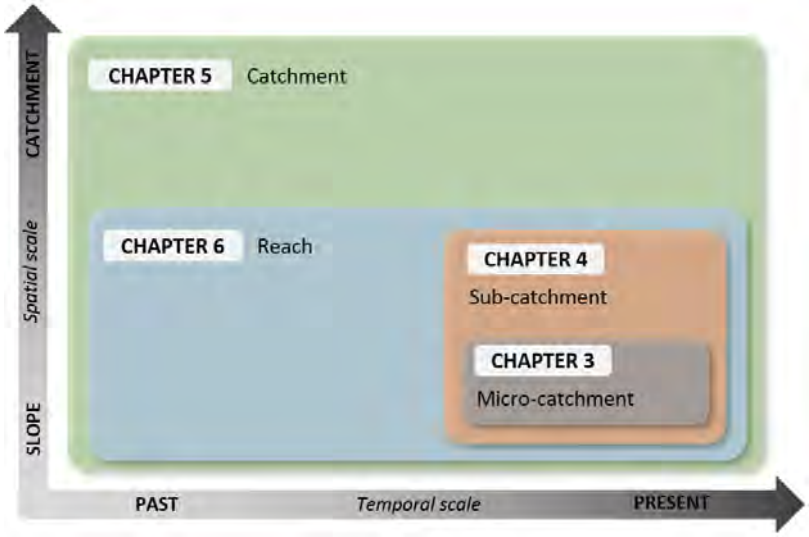


**Figure 1.** Spatial and temporal scales integration for each one of the Chapters of the thesis.

# 2. METHODS OVERVIEW

In this section we provide (a) a general overview of the methods and (b) three scientific papers presenting the methodology applied in the focal chapters 3, 5 and 6. These papers presented a more thorough and robust evaluation of the method applied in the focal chapters and this is the reason they have included in this section. In the following sections we will present an overview of the methods based on each spatial scale, corresponding to each of the focal chapters of the thesis. We would like to remark that all focal chapters (Chapters 3 to 6) are considered as a self-contained unit with full details of the methods used, independently to the overview provided here.

## 2.1. Micro-catchment scale (CHAPTER 3)

### 2.1.1. Introduction and general overview

The main objective of Chapter 3 is to quantify the importance of geomorphic processes in re-shaping badlands (i.e. topographic changes) and producing/exporting sediment (i.e. net changes) downstream, and the relationship between these and meteorological and morphometric variables. As shown in Figure 2, the general workflow applied in this chapter is composed by three interrelated tasks: A. Data acquisition, B. Post-processing, and C. Data preparation and results. **A. Data acquisition.** Two types of data were obtained: (i) meteorological data from a rain gauge and temperature sensor; and (ii) topographic data by the application of Structure from Motion (SfM) and Terrestrial Laser Scanning (TLS). Ground Control Points (i.e. GCPs) and Check Points (i.e. data for validation) were taken by a Total Station (i.e. TPS). **B. Post-processing.** Both SfM and TLS datasets were post-processed accordingly. Correspondent point clouds were geographically and geometrically corrected by means of the GCPs. Point clouds were filtered and regularized in order to remove outliers and points not correspondent to ground surface (e.g. vegetation), and homogenise the point clouds through regular cells and posterior conversion to Triangulated Irregular Networks (i.e. TIN). **C. Data preparation and results.** TINs were transformed into Digital Elevation Models (i.e. DEM) at 5 cm resolution in order to: (i) obtain landform descriptors (i.e. Concentrated Runoff Index, Roughness and Slope); and (ii) estimate topographic changes by DEMs of Differencing (i.e. DoD). After that, both groups of data were used as an input for the Mapping Geomorphic Processes in the Environment (i.e. MaGPiE) algorithm, which permits identification of geomorphic process signatures in badlands from changes in form. Finally, DoDs were segmentated based on each geomorphic process signature identified, and the correlation between processes and meteorological variables was analysed.

Part of this entire workflow presented in Figure 2, specifically that related to the MaGPiE algorithm, is detailed explained in a scientific paper submitted, accepted subjected to major revisions, reviewed, and re-submitted to the *Earth Surface and Processes* journal (see section 2.1.2 for the entire paper and further details about the status of the paper).

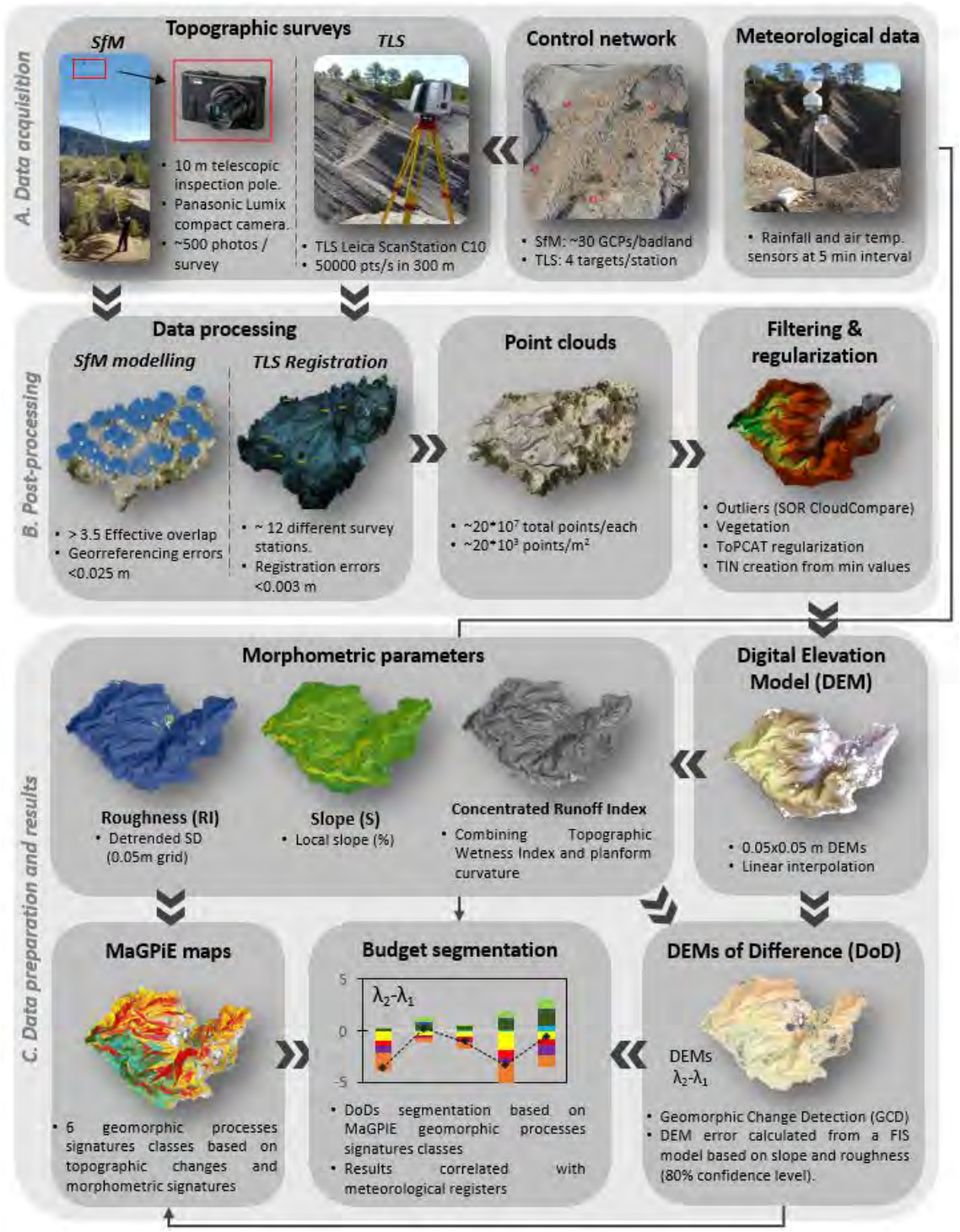


**Figure 2**. Summary of the methodological workflow followed to quantify multi-temporal geomorphic processes in badlands (Chapter 3).

## 2.1.2. Inferring geomorphic processes signatures in badlands from the measurement of changes in form

This section contains the following scientific paper submitted (27/03/2019), accepted subject to major revisions (19/06/2019), reviewed, and re-submitted (14/08/2019) in the journal *Earth Surface Processes and Landforms.* JCR-SCI Impact Factor (2018): 3.598. Category: Earth-Surface Processes; 1st Quartile. Next section correspond to the resubmitted version of the manuscript.

Llena M, Vericat D, Smith MW, Wheaton J. 2019. Inferring geomorphic processes signatures in badlands from the measurement of changes in form. *Earth Surface Processes and Landforms*. (Accepted).

**ABSTRACT:** High Resolution Topography data sets have improved the spatial and temporal scales at which we are able to investigate the landscape through the analysis of landform attributes and the computation of topographic changes. Yet, to date, there have been only limited attempts to infer key geomorphic processes in terms of contributions to shaping the landscape. Highly erodible landscapes such as badlands provide an ideal demonstration of such an approach owing to the rapid changes observed over a relatively short time frame. In this technical note we present the Mapping Geomorphic Processes in the Environment (MaGPiE): a new algorithm that allows mapping of geomorphic processes signatures through analysis of repeat High Resolution Topography data sets. The method is demonstrated in an experimental badland located in the Southern Central Pyrenees. MaGPiE is a GIS-based algorithm that uses as input: (a) landform attributes (i.e. Slope, Roughness and Concentrated Runoff Index) extracted from Digital Elevation Models (DEM), and (b) a map of topographic changes (DEM of Difference, DoD). Initial results demonstrate that MaGPiE allows the magnitude and the spatial distribution of the main geomorphic processes reshaping badlands to be inferred for the first time.

**KEYWORDS**: *Geomorphic processes signatures, badlands, Structure from Motion, Topographic Changes, Mapping Geomorphic Processes in the Environment algorithm (MaGPiE).*

## INTRODUCTION

The proliferation of High Resolution Topography data sets, driven by the development of new surveying platforms (e.g. Unmanned Aerial Vehicles, UAVs), sensors (e.g. High Resolution Multispectral Cameras) and algorithms (e.g. Structure from Motion photogrammetry, SfM) has permitted quantification of topographic changes at unprecedented spatial resolutions over a wide range of temporal and spatial scales (see, for example, reviews in Passalacqua et al., 2015; Smith et al., 2015; Tarolli, 2014; Vericat et al., 2017). SfM-based topography has reduced substantially the cost involved in surveying. SfM may provide data sets at equivalent resolution and precision than other more-expensive surveying methods such as Terrestrial Laser Scanning (e.g. Carrivick and Smith, 2018; Smith and Vericat 2015; Westoby et al., 2012). Additionally, depending on the platform used to acquire the photographs, SfM allows large spatial scales to be surveyed in a short time, allowing the reconstruction of landscape topography at temporal scales that were difficult to reach before. High-frequency surveying has the potential to describe short-term controls on geomorphologic changes and more accurate analysis of processes (e.g. Cucchiaro et al., 2019; Williams et al., 2018). Therefore, we are now capable of acquiring detailed facsimiles of the landscape before and after disturbances, quantifying changes in form and, from these, we may infer the main reshaping geomorphic processes.

Badlands are described as highly dissected landscapes with steep hillslopes in soft rock outcrops or unconsolidated sediments and regolith, with little or no vegetation, being useless for agriculture (Gallart et al., 2002; Yair et al., 1980). Badlands are highly erodible with rapid erosion rates and high sediment yields (Bryan and Yair, 1982; Clotet et al., 1987) that make disproportionately large contributions to catchment scale sediment budgets (e.g. López-Tarazón et al., 2012; Nadal-Romero and Regüés, 2010) with potential negative effects on the downstream channel network (e.g. clogging, Buendía et al., 2013; Piqué et al., 2014) and infrastructure (e.g. reservoir siltation; Baade et al., 2012; Martínez-Casasnovas and Poch, 1998; Mueller et al., 2010). In general, surface features result from the interaction between highly erodible materials (soft or unconsolidated) with multiple geomorphological processes acting at different temporal and spatial scales (Moreno-de las Heras and Gallart, 2018; Nadal-Romero and García-Ruiz, 2018). The main factors controlling badland development are lithology, rainfall, temperature, vegetation cover, human activities and the degree of connectivity, that is directly related to main landform attributes such as topography and roughness (Clarke and Rendell, 2010; Faulkner, 2008). Ultimately, geomorphic processes in such environments are determined by the interactions of these factors.

Topographic changes in badlands are generally estimated from sparse observations across relatively small scales (e.g. erosion pins in Barnes et al., 2016; Benito et al., 1992; Sirvent et al., 1997; experimental plots in Nadal-Romero et al., 2007; Regüés et al., 1995). High Resolution Topography offers the opportunity of examining topographic changes in a spatially-distributed way at multiple temporal and spatial scales. During the last decade several authors have used these data sets to monitor topographic changes in badlands (e.g. Ferrer et al., 2017; Nadal-Romero et al., 2015; Neugirg et al., 2016; Nobajas et al., 2017; Smith and Vericat, 2015; Stöcker et al., 2015; Vericat et al., 2014). Although these studies have greatly improved the quantification of rates of erosion or deposition and sediment yields, to our knowledge there has yet to be an attempt to further interrogate the rich data sets and quantify the magnitude and spatial distribution of the changes in form in relation to main geomorphic processes. There is a knowledge gap related to mapping geomorphic processes signatures in a quantified manner to determine their spatial and temporal variability. Such maps will help to infer the magnitude of the main geomorphic processes controlling sediment export, landscape changes and evolution, and would help to prioritise and target catchment management practices aimed at reducing

sediment yields. In this methodological note, we present the Mapping Geomorphic Processes in the Environment (MaGPiE) algorithm: MaGPiE facilitates the quantitative mapping of main geomorphic processes signatures through analysis of repeat SfM-based High Resolution Topography data sets. We first present the MaGPiE algorithm followed by its application in an experimental badland landscape in the Southern Central Pyrenees.

## THE MaGPiE ALGORITHM

MaGPiE is a GIS-based algorithm that uses as input: (i) landform attributes extracted from Digital Elevation Models (DEM), and (ii) a map of topographic changes obtained via DEM of Difference (DoD). Therefore, DEMs before and after changes in form are required. In general, main geomorphic processes signatures are first identified, together with their main characteristics in terms of both spatial extent and the magnitude and sign of the topographic changes associated with these. The inputs are then combined to provide the signatures that infer each process. Finally, a decision tree algorithm is applied to map the geomorphic processes on a cell-by-cell basis. The complete MaGPiE workflow is presented in Figure 3 and explained below.

**Step 1. Identification of Main Geomorphic Processes Signatures.** We have combined a literature search and field observations to identify and classify the most relevant geomorphic process signatures that can be observed in badlands, the focus of this MaGPiE demonstration. A similar exercise would be needed to apply the MaGPiE algorithm in other geomorphologic landscapes in which main processes may differ to those identified here. In the case of sub-humid badlands, dominant geomorphic processes were divided into two main groups: (a) weathering-based processes and (b) erosional-based processes. Erosional processes are split between overland-flow and mass movement driven processes (following Barnes et al., 2016; Bryan and Yair, 1982; Clotet et al., 1987; Gallart et al., 2002; Huggett, 2011; Nadal-Romero and Regües, 2010; Nadal-Romero and García-Ruiz, 2018; Moreno-de las Heras and Gallart, 2018). Despite this classification, badlands are complex landscapes in which the interaction between (i.e. overlapping) geomorphic processes is often present (e.g. Vergari et al., 2019). In our case we have considered overlapping processes those that cannot be classified as any of the other identified. We are aware that the overlapping processes class may also include other processes not identified as the main geomorphic processes signatures.

Table 1 shows the main badland geomorphic processes that are possible to be inferred from their signatures based on landform attributes and changes in form. The table also presents the main drivers and some references in which these specific processes are described. In that way, a total of 6 specific geomorphic processes were identified: (1) *Sheet Washing*; (2) *Rilling and Gullying*; (3) *Cutting and Filling*; (4) *Mass Wasting* (5) *Regolith Cohesion Loss*; and (6) *Overlapping Processes*.

It is worth mentioning that sub-surface geomorphic processes (i.e. pipping) were not taken into account here because these are not acting in Eocene marls such as the ones observed in the experimental badlands. Even so, changes in form associated with these processes may be dominant in other environments (e.g. Faulkner, 2018; Gutiérrez et al., 1997), requiring consideration in the identification of main geomorphic processes signatures in such environments.

**Table 1**. Key geomorphic processes in badlands in relation to the main drivers and according to previous literature and field observations.

| Geomorphic process | Description | Main drivers | References |
|---|---|---|---|
| **Sheet Washing** | Uniform erosion of soil in thin superficial layers. | Laminar surface runoff (overland flow) and rainsplash | Gallart et al., 2002; Nadal-Romero and García-Ruiz, 2018 |
| **Rilling and Gullying** | Shallow channels cut into hillside soil or soft rock outcrops. Smaller incised channels are considered rills while larger channels are known as gullies | Concentrated surface runoff (overland flow) | Clotet et al., 1987; Moreno-de las Heras and Gallart, 2018 |
| **Cutting and Filling** | Fluvial processes that take place in the main channel bottom with relatively low slope and higher section width in comparison with the rest of the drainage network. | Concentrated surface runoff (overland flow) | Clotet et al., 1987; Gallart et al., 2002 |
| **Mass Wasting** | Caused by regolith slope mass movements (falling) produced after its destabilization | Freeze-thaw (winter), wetting-drying cycles and rainsplash | Barnes et al., 2016; Nadal-Romero and Regües 2010 |
| **Regolith Cohesion Loss** | Surface raising caused by the fracture or expansion of the superficial regolith | Freeze-thaw (winter) and wetting-drying cycles | Barnes et al., 2016; Nadal-Romero and Regües 2010 |
| **Overlapping Processes** | Geomorphic processes that interact/overlap and it is not possible to infer from the signatures based on landform attributes and changes in form | Interaction of different drivers | Vergari et al., 2019 |

### Step 2. Preparing Inputs: landform attributes & topographic changes

Following Wheaton et al. (2013), we consider a geomorphic process signature arise when a distinct main process leads to a consistent landform change, being also characterised by specific landform attributes. A total of three landform attributes (Slope, Roughness and a new developed Concentrated Runoff Index) extracted from the second (or 'new') DEM are used alongside the DoD to define key signatures of each geomorphic process.

The local Slope was selected as an input because is considered one of the main parameters that determine (slope) stability, and consequently, triggering mass movements (Bishop and Morgenstern, 1960; Morgenstern and Price, 1965). In the same way, Slope is also a main factor determining the distribution of erosional landforms associated with concentrated-fluxes (e.g. rills, gullies, channels; Gallart et al., 2002). Usually, the erosional stream landform size is negatively correlated with the slope and positively correlated with the upslope catchment area. Thus, Slope was used to differentiate between the processes that took place in steep areas (e.g. erosion caused by *Mass Wasting* and by *Rilling and Gullying*) and those occurring in relatively flat areas (e.g. *Regolith Cohesion Loss*, *Sheet Washing*). Slope is defined here as the maximum rate of change in elevation from each cell to its neighbours.

Several authors (e.g. Gallart et al., 2002; Regüés and Torri, 2002; Römkens et al., 2001) reported that Roughness is one of the main landform attributes that determines erosion and a range of geomorphic processes. Roughness values help to discern between deposition in main channels caused by in-channel processes (i.e. *Filling*) and deposition caused by lateral *Mass Wasting*, with the latter exhibiting higher roughness values (based on field observations; see some examples in figures of section 3.3). Roughness is defined as the mean of the detrended standard deviation of the elevations within regular grid cells (see specific details in section 3).

The Topographic Wetness Index (TWI), a quantification of the topographic control on hydrological processes, is considered as a proxy of the concentrated surface water fluxes (Ali et al., 2014; Beven and Kirkby, 1979). Although the relation between slope and upslope area on which TWI is based has been used to discern between concentrated (i.e. channel) and diffuse

(i.e. slope) processes (e.g. Roering et al., 2001; Vergari et al., 2019; Willgoose et al., 1991), it assumes a fully connected hydrological system. Badlands, however, can present different degrees of disconnectivity. In order to overcome this limitation, we have developed the Concentrated Runoff Index (CRI), a landform attribute based on a modification of the TWI. The CRI takes into account not just the magnitude of the TWI but also the Planform Curvature (PC). We assume that concave surfaces reflect more locally connected areas than convex areas. The CRI was calculated by means of the expression TWI+(PC×-1); where the TWI was computed as $\ln(A/\tan\beta)$, A is referred to the upslope area of a given cell ($m^2$), and β is the local gradient (in degrees). PC represents the normalised (from -1 to 1) planform curvature value obtained from the most recent DEM. The values were normalized by this range in order to not dominated the signal and only affect in those cases in which the TWI was very close to the threshold between concentrated and diffuse. Normalised PC values are multiplied by -1 in order to invert the sign of concave and convex surfaces. In that way, concave surfaces will be positive while convex surfaces will be negative, having an additive and subtractive weight on the TWI. The CRI was used to distinguish between overland flow processes caused by concentrated runoff (e.g. rills, gullies and channels, from small to big size), and those caused by diffuse runoff (e.g. *Sheet Washing*).

Finally, topographic changes were obtained by the comparison of the DEMs between surveys (the DoD). The old DEM is subtracted from the new DEM, where negative values indicate surface lowering or erosion and positive values indicate surface raising or deposition. It is important to note that negative and positive DoD values do not imply always erosion and sedimentation. For instance, in the case of the *Regolith Cohesion Loss*, the elevation of the surface increases when the old and the new DEMs are compared, but this is not related to any depositional process occurred during the study period. In this case physical weathering controls the expansion of the regolith (e.g. so-called '*popcorn'* features) in relation to climate and geological conditions (e.g. Gallart et al., 2002; Kasanin-Grubin, 2013; Nadal-Romero and Regüés, 2010). The DoD is calculated using the Geomorphic Change Detection (GCD) extension for ArcMap (available at http://gcd.joewheaton.org/; see Wheaton et al., 2010) which has the advantage of incorporating uncertainty analysis based on minimum Level of Detection (minLoD), propagated errors or probabilistic thresholding.

**Step 3. Defining the combination of landform attributes and topographic changes for each Geomorphic Process signature.**

An expert-map of the main geomorphic processes signatures is first elaborated examining (i) topography; (ii) orthomotomosaics; and (iii) oblique photographs taken from a trail camera. The 90% of the mapped processes signatures are used to (a) establish the thresholds of the classes of each attribute and DoD, and (b) to define the signatures (i.e. combination of classes) of each geomorphic process. The remaining 10% of the processes mapped in the field are used for validation of the classification.

Each landform attribute is divided in two classes: high and low in case of roughness and slope; or diffuse flow and concentrated flow in case of the Concentrated Runoff Index. DoD values are divided into four classes: high lowering, low lowering, low raising and high raising. The thresholds of each class and their combinations are based on the distribution of the values of the landform attributes and DoD per each geomorphic process. In the case of the landform attributes, the median value of each attribute was calculated across the whole DEM. These values will determine the class boundaries. In order to assign each geomorphic process signature to a class, the median value of the same attribute for cells classified into each geomorphic process is then compared with the class ranges and categorised accordingly (see example in

Figure 3). In case of the thresholds for the DoD values, 0 defines the division between surface lowering and raising classes, while the 90$^{th}$ and 10$^{th}$ percentiles of the DoD values define the thresholds between high and low raising and lowering, respectively. Again, once the thresholds were established, the median DoD values in each process were analysed to classify each process. The expert-map identification of thresholds and combinations of attributes and DoD classes has been chosen to decrease the subjectivity and to allow a validation of the results. The class boundaries and combinations identified for each geomorphic process are now described below.

In the case of Slope, two classes were defined: High Slopes (>45°) and Medium to Low Slopes (<45°). The selected threshold of 45° allows us to: (i) identify steep areas in which mass movements can be observed (e.g. *Mass Wasting*); and (ii) discern between concentrated runoff processes in rills and gullies (i.e. *Rilling and Gullying*) and those observed in the main channel (i.e. *Cutting and Filling*). These thresholds are agreement with Zhang et al. (2017) who identified the slope gradient of 47% to be the threshold value of increasing runoff and associated soil loss.

Roughness was grouped in two classes: High Roughness (>0.03 m) and Low Roughness (<0.03 m). In particular, regolith deposits coming from mass movements (e.g. *Mass Wasting*) tend to have a higher roughness than the values observed in deposits coming from overland-flow processes (e.g. *Sheet Washing, Cutting and Filling*). Gallart et al. (2002) described that in steep badlands hillslopes, unestablished regolith mass may fall towards the valley bottom with a consequent coarser roughness than the regolith transported by the channel system.

CRI was divided in two groups, a value of 1 was selected as a threshold between Diffuse flow (CRI<1) and Concentrated Flow (CRI>1), being the later mainly attributed to *Rilling and Gulling* and *Cutting and Filling* processes. Recently, Jancewicz et al. (2019), stated that the thresholding of TWI from the mean value plus standard deviation helps to recognize pathways of water and possible sediment transfer (i.e. concentrated flow). Similarly, here we have used the curvature to modify the results provided by the TWI when values are very close to the threshold between concentred and diffuse flows.

Finally, the DoD was grouped into four classes: High Lowering (<-0.15 m), Low Lowering (-0.15 – 0 m), Low Raising (0 – 0.07 m) and High Raising (>0.07 m). These values are in agreement with the average values of topographic changes observed in sub-humid badlands developed on marls for similar study periods (i.e. less than one year; Clarke and Rendell, 2010; James et al., 2017; Mathys et al., 1996; Nadal-Romero and Regüés, 2010; Smith and Vericat, 2015; Vericat et al., 2014). However, it is worth mentioning that the thresholds between these classes will depend on the considered time span and require what re-evaluation if the survey interval is altered.

The combination of these classes provides a unique signature or combination per each process. The inset table in Figure 3 shows the combined signatures of each process. For instance, the signature that defines surface lowering caused by *Rilling and Gullying* is: High Slope, High or Low values of Roughness, Concentrated Flow (High CRI) and either High or Low surface lowering. Therefore, a pixel that has all these inputs will be characterised as lowering potentially caused by *Rilling and Gullying.* It is worth to mention that in our case we have considered *Overlapping Processes* those yielding a distinct signature to the other identified processes.

Finally, the accuracy of the classes was estimated by a confusion matrix calculated following the method described by Chuvieco (2016). In this way, the 10% of the expert-mapped processes are used as training areas. These areas are compared with the MaGPiE results to assess the percentage agreement between observed and MaGPiE-based process as a measure of the accuracy of the classification. The results of the confusion matrix also allow to identify which processes were most reliable and which were more confused based in the classification results.

**Step 4. Mapping Geomorphic Processes Signatures**

Once the thresholds of the classes of all inputs were defined, the classified rasters were combined in a multiband raster: a single data set in which each pixel has associated the different combinations of the input data sets. The signatures of each process were then considered to classify the multiband raster. In order to automate the processes and repeat it in subsequent analyses, a supervised Maximum Likehood Image Classification was performed. First, a training sample for each process is created and a signature file for the whole training samples was saved. This signature file can be considered valid for mapping geomorphic processes in badlands based on the specific mentioned processes signatures, and the thresholds defined per each class of the input data sets.

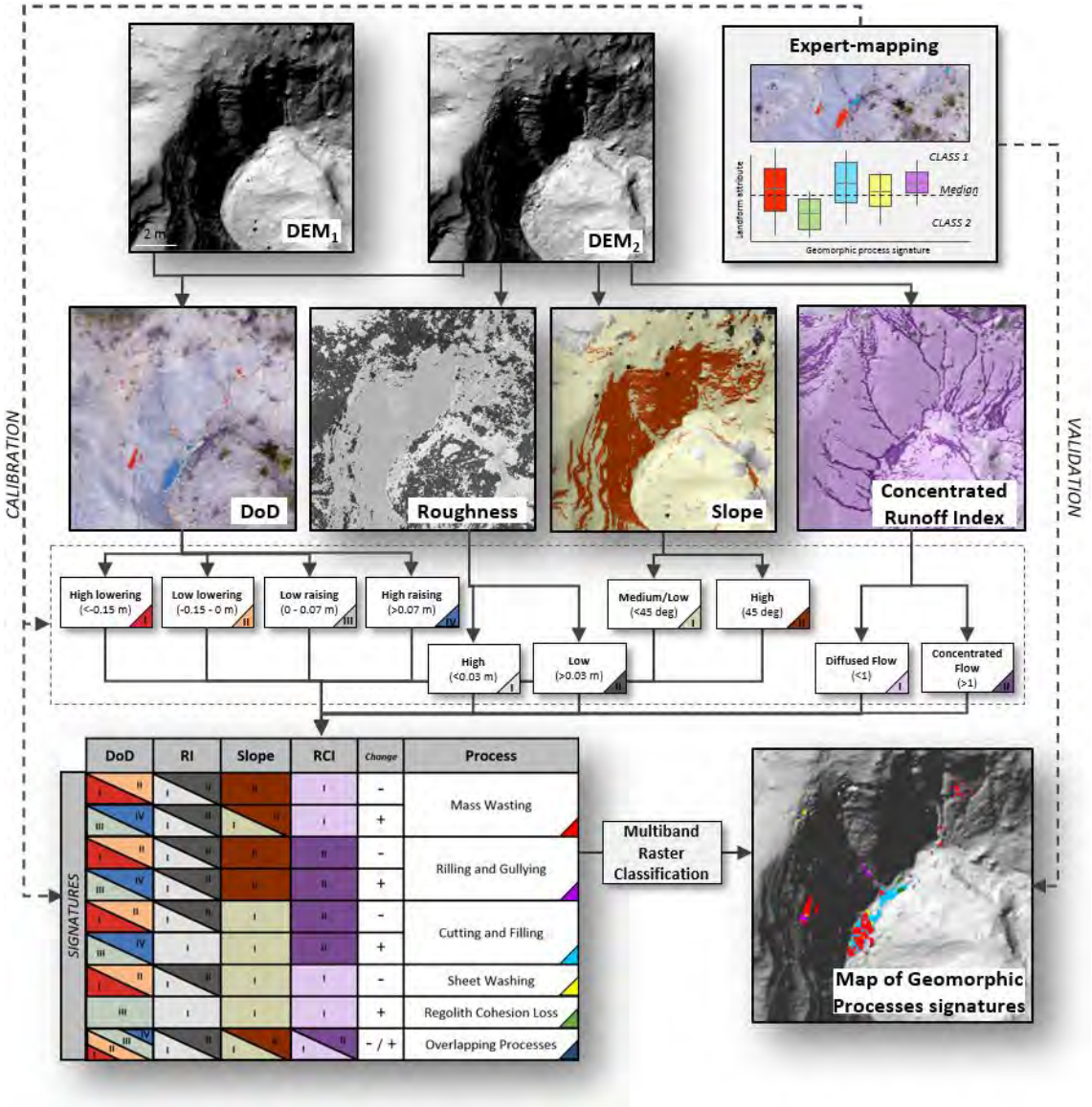


**Figure 3**. The MaGPiE GIS-based decision tree algorithm used to obtain Maps of Geomorphic Processes Signatures in sub-humid badlands. Note that the algorithm was developed to map the signatures of the main processes observed in sub-humid Badlands but it can be modified according to other landscapes as discussed in the text. *Overlapping Processes* are considered those yielding a distinct signature to the other identified processes, being not able to be classified.

## MAPPING AND QUANTIFYING GEOMORPHIC PROCESSES IN BADLANDS

### Study area

The study area is located in an experimental badland (0.05 km$^2$) located in the Soto catchment (10 km$^2$; Figure 4A and 4B). The Soto is a small tributary of the Upper River Cinca (8275 km$^2$, Central Pyrenees, Ebro Catchment, Iberian Peninsula). The main land covers of the catchment are forest (56%), badlands (26%), and field crops (18% surface). The badlands are located at an average altitude of 600 m.a.s.l. and the slope gradient can be more than 15 m with steep slopes and high degree of dissection (Figure 4A and 4B). The badlands are composed by a sequence of Eocene marls with different degrees of compactness with some few layers of sandstones. Therefore, erosional processes are hypothesised to be highly complex and spatially variable (Smith and Vericat, 2015; Figure 4B). The experimental badland in this study is described further in Smith and Vericat (2015) and at https://sites.google.com/site/badlandscan/. Specifically, the badland has a low vegetation cover (i.e. <20%), composed by isolated shrubs (e.g. *Buxus sempervirens*) on steep slopes and small groups of relatively young trees (e.g. *Pinus halepensis*) on low slopes (Figure 4A). The site has a continental climate with an annual rainfall around 700 mm. Maximum rainfall is observed during spring and autumn (e.g. maximum intensities around 47 mm h$^{-1}$ were registered for the period 1981-2018). The average temperature is 11°C, while temperatures below freezing are often observed in winter. Figure 4B indicates some representative examples of signatures attributed to the main geomorphic processes reshaping the experimental badland.

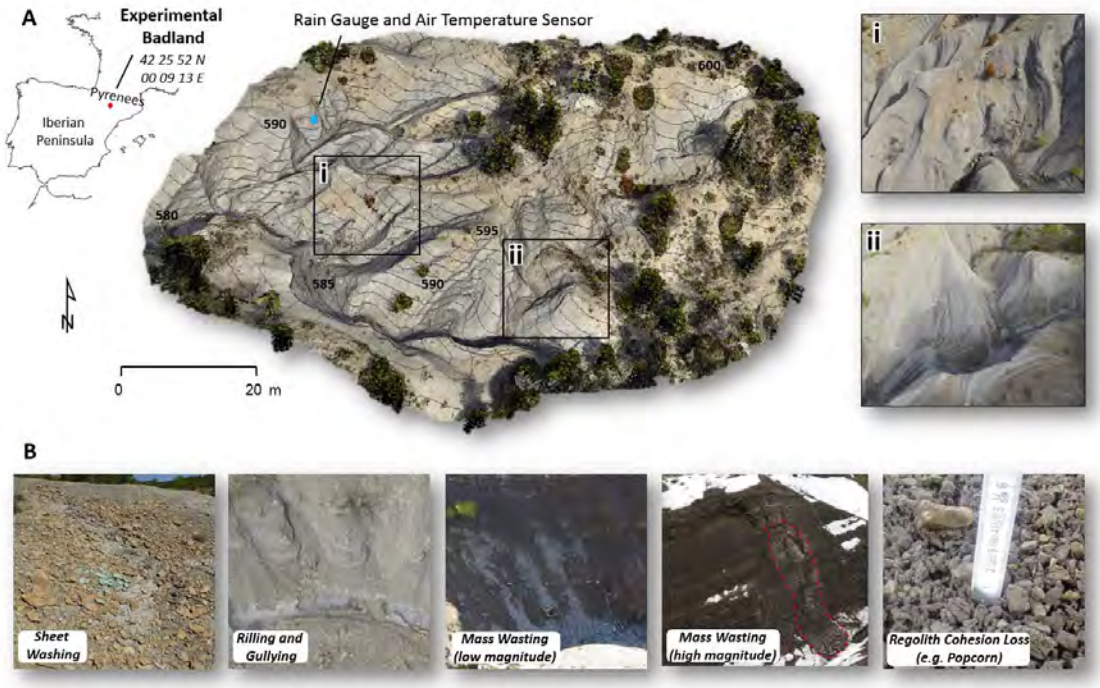


**Figure 4**. **A.** Location of the Experimental Badland (red dot) and Photo-rendered point cloud of the targeted Badland with 2 close up photo views (i and ii). Note that contour lines with an equidistance of 1 m are also shown on it. The blue dot indicates the location of both the Rain Gauge and Temperature Sensor. **B.** Examples of the signatures of main geomorphic processes observed in the experimental badland.

## Data

Rainfall was measured continuously by a Campbell ARG100 tipping bucket rain gauge, while air temperature was registered by means a Campbell Temperature Probe-109 (see location in Figure 4B). Both were recorded in the same a datalogger (Campbell CR200X) at a 5-minute interval.

Topographic data sets were obtained through Structure from Motion photogrammetry (SfM). Two field campaigns were performed: June 19$^{th}$ (S1) and December 7$^{th}$ 2016 (S2). Around 650 pictures per campaign were taken using a Panasonic Lumix DMC-TZ60 compact camera (focal length 4 mm which is a 35-mm equivalent of 25 mm; 10 Mpx) mounted on a 10 m telescopic inspection pole. SfM processing was implemented using standard workflows within Agisoft Photoscan Professional 1.3.4. Dense point clouds with an average point density of around $5x10^4$ obs $m^{-2}$ (i.e. 5 obs $cm^{-2}$) were obtained. Georeferencing and scaling were performed by a secondary control network of 30 Ground Control Points (GCPs) surveyed with a Leica TPS1200 Total Station (TS). The TS was set up based on a primary control network of four (fixed) benchmarks. The coordinates in each benchmark were obtained by means of a Leica Viva GS15 GNSS system and RINEX data from 3 reference stations.

3D data quality after post-processing was 0.006 m on average. Reported errors in terms of scaling and georeferencing were 0.0185 m (2.298 pixels) and 0.0222 m (1.195 pixels) for the S1 and S2 surveys, respectively. In terms of quality assessment, an independent validation dataset of 270 (S1) and 256 (S2) Check Points (ChPs) were obtained with the TS. The corresponding differences between SfM-derived point clouds and the ChPs were calculated by the M3C2 plugin (Lague et al., 2013) implemented in the open source software CloudCompare 2.6.2. Results indicated a Mean Absolute Error (i.e. MAE) of 0.0187 m (S1) and 0.0157 m (S2), and a Standard Deviation of the errors of 0.0261 m (S1) and 0.0214 m (S2).

Point clouds were filtered to remove outliers and vegetation. Outliers were filtered by means the Statistical Outlier Filter (SOR) of Cloud Compare 2.6.2 (Girardeau-Montaut, 2016), meanwhile the points located in vegetated areas were removed using the results of the supervised image classification. The open-source Topographic Point Cloud Analysis Toolkit (ToPCAT; Brasington et al., 2012; Rychkov et al., 2012) was then used to regularize the point cloud. A 0.05 x 0.05 m grid was selected taking into account the magnitude of the study area topographic changes and the size of the small geomorphic features (e.g. rills). Observations within each grid were analysed and a series of statistics of these were calculated (e.g. maximum, mean and minimum elevations and detrended standard deviation of elevations). The minimum elevation within each grid was used to represent the ground elevation within each cell. A Triangular Irregular Network or TIN was calculated based on these observations for each survey. Finally, a 0.05 m resolution DEM was computed from each TIN. The most recent DEM or $DEM_{S2}$ was used to calculate the landform attributes: (i) Slope, (ii) Roughness, and (iii) Concentrated Runoff Index (all inputs of MaGPiE). Following Brasington et al. (2012), Smith and Vericat (2015) and Vericat et al. (2014), roughness was calculated using the detrended standard deviation of the elevations in each grid.

The DEMs for the two periods ($DEM_{S2}$-$DEM_{S1}$) were compared (DoD) to assess the topographic changes during the study period. The MAE of each data set was considered to represent the DEM error and the minLoD was calculated by the propagation of both $DEM_{S1}$ and $DEM_{S2}$ errors. Therefore, those DoD cells with absolute values below the minLoD were considered uncertain and not used in the computation of topographic changes (i.e. thresholded DoD).

For MaGPiE, the thresholds of each attribute class and the combinations between attributes and DoD classes were based on an expert-map of processes (see classes presented in the inset table

of Figure 3). The processes identified in the field occupied an area of 20 $m^2$. 90% of this area was used as a training area while 10% was used to validate the classification. Processes in this area were compared with the MaGPiE classification in order to assess the percentage of agreement between observed and MaGPiE-based process, being considered as a proxy of the accuracy of the classification.

All rasters were combined in a multiband raster data set and classified. The classification was performed based on the signatures associated with each process. The map of geomorphic processes signatures (i.e. integer type raster) was transformed to a feature class (polygons). Finally, the DoD was segregated based on each geomorphic process (feature class) through the GCD ArcMap-based extension. This last step allows identification of the vertical and volumetric changes associated with each process.

## Results

The study period (142 days) was characterised by a total rainfall of 355 mm distributed in 12.5 rainy days with an average intensity of 2.17 mm $h^{-1}$, and a maximum of 20.4 mm $h^{-1}$. The mean temperature was 18.2 °C, with 13 days in which the temperature reached values below 0°C with an average value of -1.4 °C and a minimum value of -4.2 °C for these days.

The thresholded DoD indicates that the majority of the area was subjected to a change below the minLoD (i.e. uncertain topographic change). Only the 8% of the total study area presents changes above the minLoD. The spatial variability of these changes is revealed as surface lowering or erosional processes are mainly located in high slope areas, in the highest flat areas and in the main channels (76% of total area with detectable change, see Figure 5A). Conversely, surface raising or deposition is mainly located in west-facing slopes and in main channels (24 % of the total area with detectable change; Figure 5A). In terms of vertical changes, areas showing erosion have an average change of -0.06 m, while areas subjected to surface raising yield an average difference of 0.07 m (Figure 5A). Finally, the net change during the study period was -5.7 $m^3$ with -9.9 $m^3$ of erosion and 4.1 $m^3$ of surface raising or deposition (69% and 31% of the total volumetric changes respectively, Figure 5A).

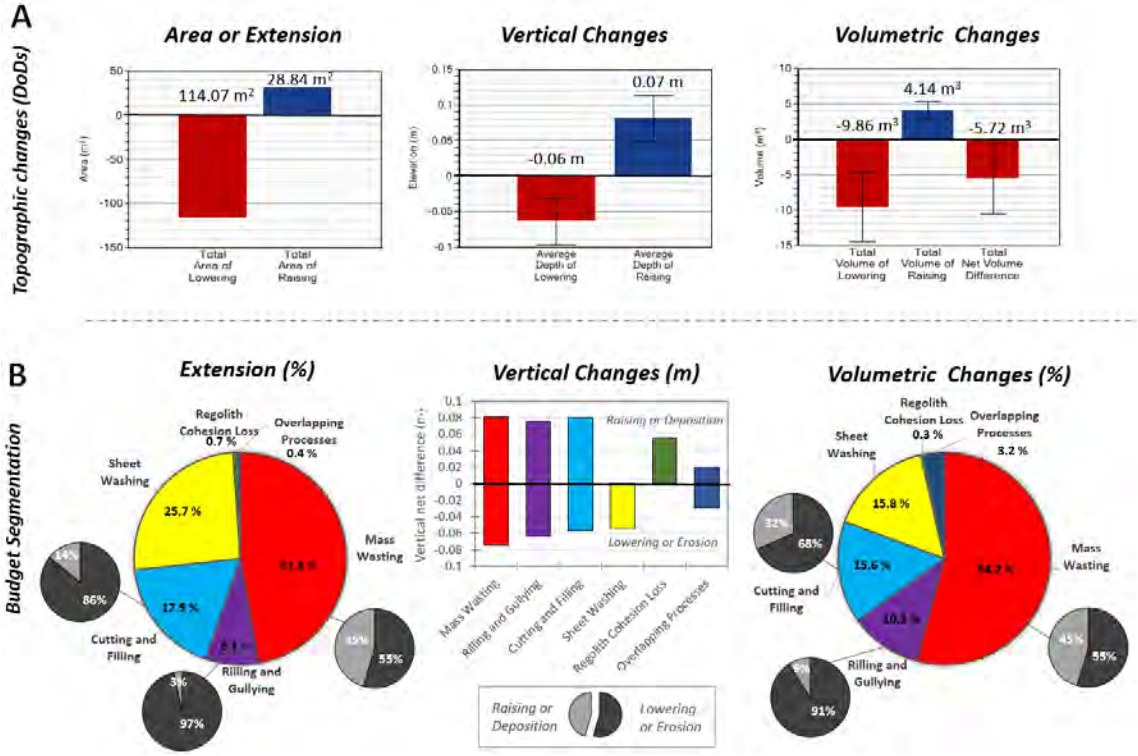


**Figure 5**. **A.** Topographic changes in the Experimental Badland for the period July 2016 (S1) to December 2016 (S2) expressed in terms of areal extent ($m^2$), vertical (m) and volumetric ($m^3$) changes. Note that the coloured bars represent the average values and the error bars show the possible variation (+/-) related to the propagated error. Average values are also presented above each bar. **B.** DoD segregation results of experiencing changes areas based on mapped geomorphic processes: areal extension of each process (%), mean vertical differences (m), and volumetric differences expressed in percentage (%).

The percentage of agreement between observed and MaGPiE-based process was around 75%, being the *Regolith Cohesion Loss* and deposition caused by *Rilling and Gullying* the more reliable signatures (i.e. 90% of agreement) and the erosion caused by *Mass wasting* the more confused signature (i.e. 60% of agreement). Figure 5B represents the DoD segregation results indicating the extension, and the vertical and volumetric changes associated to each process, while Figure 6 shows the map of main geomorphic processes signatures reshaping the form of the experimental badland during the study period. Results indicate that the majority of the processes are concentrated in steep slopes, selected flat areas, and in the main channels.

*Mass Wasting* features, located mainly in the steepest north-facing slopes (Figure 6D), are the main geomorphic process signatures observed during the study period, both in terms of extension (54.2% of the total area with significant change) and volumetric change (47.3% of the total volumetric change; Figure 5B). These observations are in agreement with the results of Gallart et al. (2002) and Ciccacci et al. (2008), who explained that the main source of the sediments transferred from the hillslopes to channel networks in badlands developed on cohesive marls and claystones in mountain areas is via regolith falling. This gravitational process is mainly triggered by gelivation together with overlapping rainfall-driven processes (e.g. Nadal-Romero and Regüés, 2010). Regolith that was previously weathered by freeze-thaw and soil moisture changes is mobilized from steep slopes to the bottom of the main channels (see example D in Figure 6), or to small accumulation zones located at the base of the slopes near the main channel (C in Figure 6). The magnitude of these erosional processes in slopes is

generally low and is likely to be below the minLoD and thus not mapped. It is important to recognise that the omission of such low magnitude yet spatially extensive processes would bias the sediment yield estimates. The magnitude of deposition caused by *Mass Wasting* is larger, mainly due to both the accumulation of materials in small areas and the decrease in the density of the regolith after its fracture (D in Figure 6; Nadal-Romero et al., 2007). In both cases, 55% of the *Mass Wasting* geomorphic process signatures correspond to lowering or erosion while te 45% correspond to raising or deposition changes.

The second geomorphic process signature in terms of magnitude was *Sheet Washing* (25.7% of total surface and 15.8% of volumetric changes; Figure 5B). This process is mainly caused by laminar flows and rainfall drops (rainsplash) in less steep but highly exposed slopes (Figure 6B). The magnitude of *Sheet Washing* in terms of volumetric change is lower than in terms of extension (i.e. 9.9% less) due to the fact that the associated vertical changes were very low (i.e. -0.05 m on average, the process signature associated with the second-smallest vertical negative change; see B in Figure 6).

*Cutting and Filling* signatures were observed over 17.9% of the surface (Figure 5B) and represented the 15.6% of total volumetric change (A in Figure 6), while *Rilling and Gullying* were observed over the 8.1% of the surface of change, representing a similar volumetric change (i.e. 10.9%). Both processes are mainly caused by concentrated surface flows (runoff) but with the principal difference is that *Rilling and Gullying* was observed in steep slopes perpendicular to main channels (A in Figure 6), while *Cutting and Filling* occurred in the main channel bottoms (C in Figure 6). In terms of extension, both geomorphic processes signatures presented a negative change (i.e. lowering or erosion) in more than the 85% of the surface. Finally, the signatures process that yielded the lowest magnitudes were *Regolith Cohesion Loss* (0.7% of surface and 0.3% of volumetric change with <0.05 m of surface raising on average) and the rest of combinations being considered the result of *Overlapping Processes* (0.4% of surface and 3.2% of volumetric change with 0.02 m of surface raising and -0.3 of surface lowering, on average). The low values of *Regolith Cohesion Loss* are attributed to the fact that, although freeze-thaw is considered one of the main weathering process in these landscapes, the study period was not sufficiently long to yield significant changes (i.e. only 13 days with T<0°C). Similar observations were made in Barnes et al. (2016) and Tsutsumi and Fujita (2016).

In summary, the main processes in the study badlands were both erosional and depositional processes associated to *Mass Wasting* (55% erosion and 45% deposition) and *Sheet Washing* (16% of the total volumetric change). *Cutting and Filling* (15.6%) and *Rilling and Gullying* (10.9%) were also evident processes presenting higher erosion than deposition values. These represent the key processes controlling badland evolution in the Soto catchment, yielding erosive landscapes with highly dissected shapes and high drainage densities (as observed e.g. Howard, 2009; Moreno-de las Heras and Gallart, 2018).

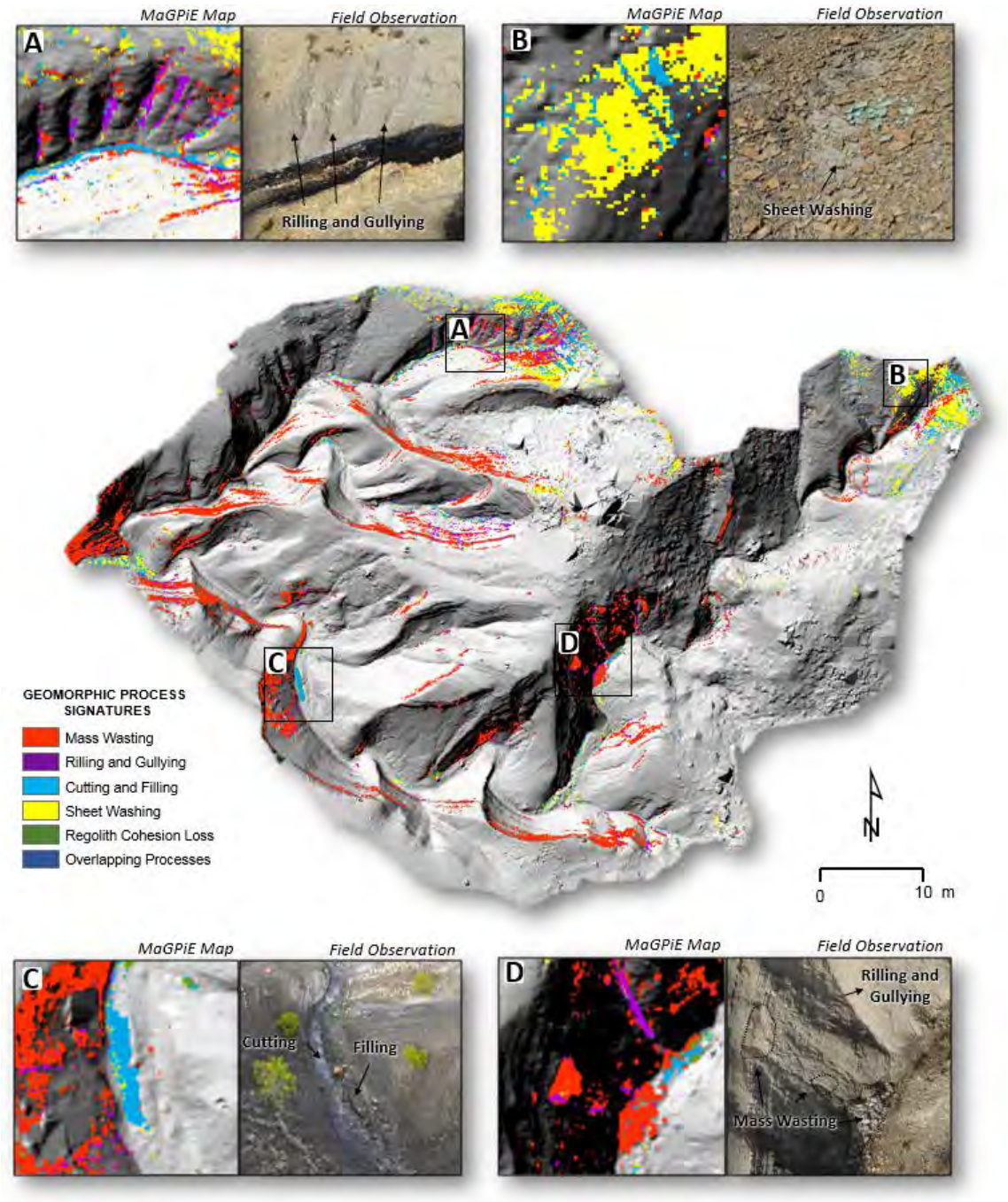


**Figure 6**. Map of geomorphic processes in the experimental badland for the period July 2016 (S1) to December 2016 (S2) with selected examples of field observations of processes in close agreement with the MaGPiE outputs (A-D). Note that the extension of the Field Observation did not fully match with the extent of the MaGPiE Map zoom due to it corresponds to oblique photography taken form the ground.

## LINKING PROCESSES, SEDIMENT SOURCES AND SINKS

Several studies have tried to infer on geomorphic processes by combining landform analysis through remote sensing but at coarser resolutions than the reported here (e.g. Bartsch et al., 2002; Gude et al., 2002; Haas et al., 2016). In all cases, the most challenging task has been to establish relationships between processes and the trajectory and movement of sediment in time and space. Within this context, Sidle et al. (2019) established that hydrological and sediment connectivity is a key aspect for the parameterization of process-based models. According to Heckman et al. (2018), hydrological and sediment connectivity can be defined as the degree to which a system facilitates the transfer of water and sediment through itself, through coupling relationships between its components. The degree of connectivity in a given landscape is not static and varies over time and space due to the interaction between the external forcing (mainly precipitation and temperature), landscape properties (i.e. structural connectivity), and the magnitude of the water and sediment fluxes (i.e. functional connectivity), that will ultimately determine the frequency, distribution and magnitude of geomorphic processes (Bracken et al., 2015; Harvey, 2001; Wohl et al., 2018). Cavalli et al. (2013) developed a raster-based Index of Connectivity (IC) that quantitatively assesses the spatial distribution of structural sediment connectivity, the potential of a landscape to be connected according to its attributes; while Heckmann and Vericat (2018) presented a method to infer on the functional sediment connectivity by the computing of spatially distributed Sediment Delivery Ratios (SDR). Therefore, the approach presented here can be used to map main geomorphic process signatures and link these to the degree of connectivity to infer on source to sink trajectories at multiple spatial and temporal scales.

Figure 7 shows two examples on how the connections between geomorphic processes signatures and structural and functional sediment connectivity can be further investigated. On one hand, the maps of geomorphic process signatures allow the classification of main processes acting during a given period of time (Figure 7A), while the IC maps represent the potential of a landscape to be connected in a given time (Figure 7B). A first look at the differences between both maps indicates a positive relation between IC and *Mass Wasting* and *Rilling and Gullying* processes (i.e. located in highly connected areas), while *Sheet Washing* processes are negatively related to the IC (i.e. located in disconnected areas). Lu et al. (2019) found a spatial correlation between the IC and geomorphic processes caused by overland flow, but did not find a consistent relationship with mass wasting processes. On the other hand, SDR maps (Figure 7C) permit the transfer of sediments through the landscape to be inferred alongside sediment pathways between eroding areas (i.e. source) and depositional areas (i.e. sink) and their link to main geomorphic processes triggering the flux.

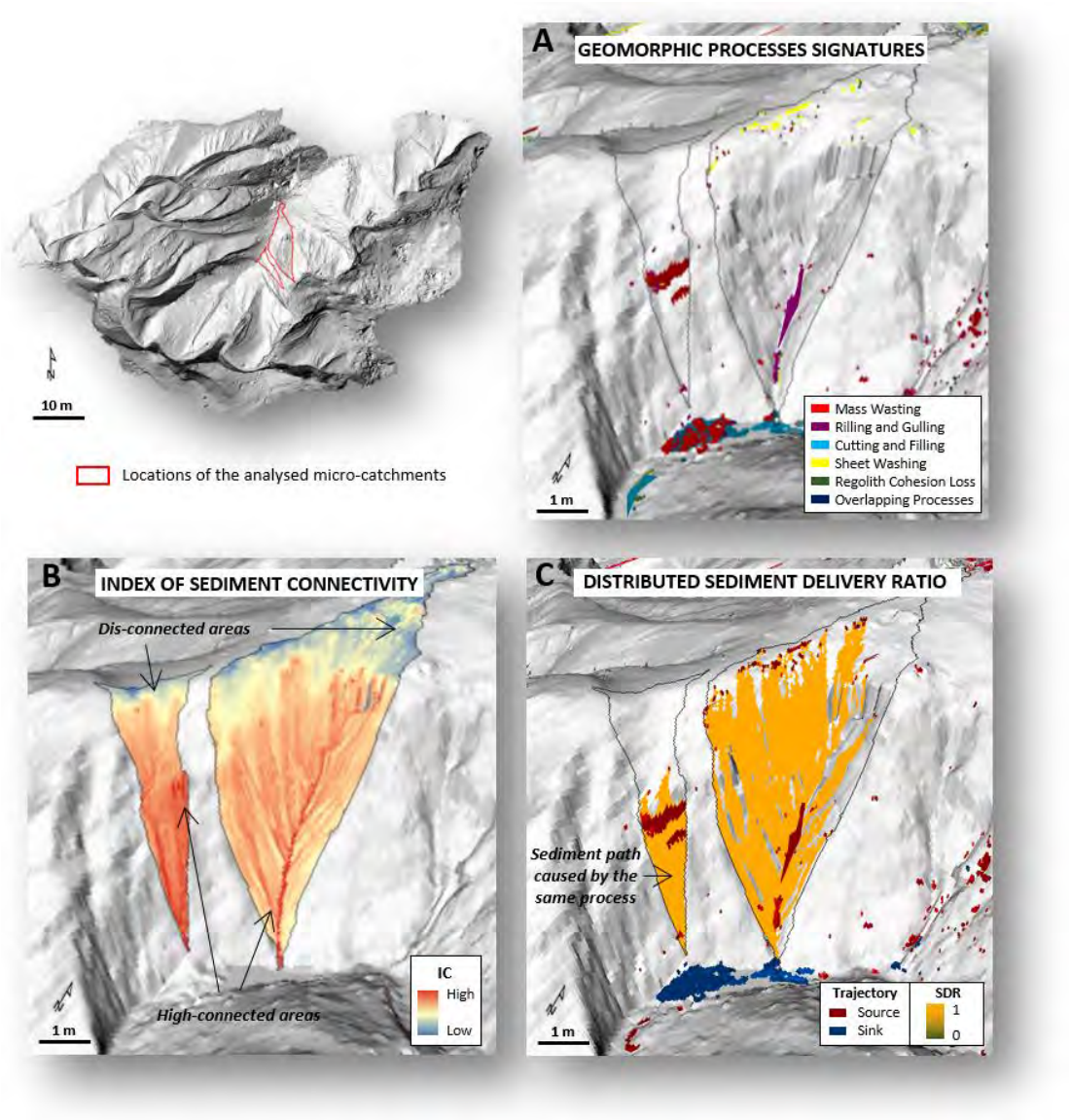


**Figure 7**. Inferring the connections between Geomorphic Processes Signatures and structural and functional sediment connectivity for two representative micro-catchments of the study badlands. **B.** Geomorphic Processes Signatures map obtained from the application of the MaGPiE algorithm. **C.** Map of Index of Sediment Connectivity (IC) developed by Cavalli et al. (2013). **D.** Spatial Distributed Sediment Delivery Ratio (SDR) computed by the method presented by Heckmann and Vericat (2018). Note that the erosion and deposition features are also shown as indicative of source and sink of sediment trajectories respectively.

## LIMITATIONS AND CONCLUDING REMARKS

MaGPiE is based on landform attributes and topographic changes obtained from high resolution DEMs. The quality or accuracy of the map will be directly related to the resolution and precision of the DEMs. In the same way, uncertainties in the DoDs will have a direct effect, especially in landscapes like the experimental badland or during short temporal scales, in which the magnitude of observed changes may be in the range of the minLoD. In our case study, we assessed DoD uncertainty by the propagation of two uniform errors extracted from an independent network of Check Points. Although our method is widely used in the literature (e.g.

Brasington et al., 2000; Lane et al., 2003; Milan et al., 2011; Wheaton et al., 2010), Anderson (2018) has recently demonstrated that net changes estimated from repeat high density observations may be affected by correlated or fully systematic errors and uncorrelated or random errors. Other more complex or complete approaches can be also applied for the assessment of uncertainties as for instance probabilistic thresholding through Fuzzy Inference Systems (e.g. Bangen et al., 2016; Wheaton et al., 2010). In the same way, more recently, James et al. (2017) presented an approach (developed in the same experimental badland) to establish spatially variable precision maps for SfM-based surveys that enables a confidence-bounded quantification of topographic changes. In complex topography like the study area, direct 3D point cloud comparison (e.g. Lague et al., 2013) is particularly recommended.

Although the selection of the thresholds for the classes of the inputs and the different signatures or combinations were based on an expert-map-based procedure there remains a degree of uncertainty at this stage. A more objective identification of the thresholds and process signatures would be possible using Machine Learning Software such as Weka (Witten et al., 2011). Smith and Warburton (2018) previously demonstrated this machine-learning approach to select the best roughness metrics for classifying peat surfaces. In the case of MaGPiE, field observations can be used to create a training data set containing each of the main geomorphic processes which can be then used to establish the best combinations of inputs (i.e. signatures) to classify the processes.

In this technical note we have presented MaGPiE: a new algorithm that permits the mapping of geomorphic processes signatures in the landscape through the analyses of repeat High Resolution Topography data sets. The method is demonstrated in an experimental badland using DEMs obtained 142 days apart. Our results indicate that MaGPiE not only allows the main geomorphic processes to be inferred, but also the evaluation of the role of each process driving the extent, vertical and volumetric changes. Through segregation of observed topographic changes the link between changes in form and geomorphic processes can be elucidated alongside evaluation of their contributions to catchment sediment yields in relation to meteorological drivers at multiple spatial and temporal scales, altogether helping in understanding landscape evolution.

## Acknowledgments

This research was carried out within the framework of two research projects funded by the Spanish Ministry of Economy and Competitiveness and the European FEDER funds: MORPHSED (CGL2012-36394) and MORPHPEAK (CGL2016-78874-R). The first author has a grant funded by the Ministry of Education, Culture and Sports, Spain (FPU016/01687). The second author is a Serra Húnter Fellow at the University of Lleida. The first and second authors are part of the Fluvial Dynamics Research Group-RIUS, a Consolidated Group recognized by the Generalitat de Catalunya (2017 SGR 459645). We also acknowledge the support of the CERCA Program of the Generalitat de Catalunya. Finally, we also thank the British Society for Geomorphology to support the long-term geomorphological monitoring program in the experimental badland that started in 2013; and the members of the Fluvial Dynamics Research Group for their assistance during the field work campaigns. We thank all comments and suggestions received from two anonymous referees and from the associate editor and the editor in chief of Earth Surface Processes and Landforms. All their comments have helped to clarify and improve this technical note.

## REFERENCES

Ali G, Birkel C, Tetzlaff D, Soulsby C, McDonnell JJ, and Tarolli P. 2014. A comparison of wetness indices for the prediction of observed connected saturated areas under contrasting conditions. *Earth Surface Processes and Landforms* 39: 399-413.

Anderson SW. 2018. Uncertainty in quantitative analyses of topographic change: error propagation and the role of thresholding. *Earth Surface Processes and Landforms* 44: 1015-1033.

Baade J, Franz S, Reichel A. 2012. Reservoir siltation and sediment yield in the Kruger National Park, South Africa: a first assessment. *Land Degradation and Development* 23: 586–600.

Bangen S, Hensleigh J, McHugh P, Wheaton J. 2016. Error modelling of DEMs from topographic surveys of rivers using fuzzy inference systems. *Water Resources Research* 52: 1176–1193.

Barnes N, Luffman I, Nandi A. 2016. Gully erosion and freeze-thaw processes in clay-rich soils, northeast Tennessee, USA. *GeoResJ* 9-12: 67-76.

Bartsch A, Gude M, Jonasson C, Scherer D. 2002. Identification of geomorphic process units in Kiirkevagge, northern Sweden, by remote sensing and digital terrain analysis. Geografiska Annaler 84(3-4): 171-178.

Benito G, Gutiérrez M, Sancho C. 1992. Erosion Rates in Badland Areas of the Central Ebro Basin (NE-Spain). *Catena* 19: 269-286.

Beven KJ and Kirkby MJ. 1979. A physically based, variable contributing area model of basin hydrology. *Hydrological Sciences Journal* 24(1): 43-69.

Bishop A and Morgenstern N. 1960. Stability coefficients for earth slopes. *Geotechnique* 10: 129–150.

Braken LJ, Tumbull L, Wainwright J, Bogaart P. 2015. Sediment connectivity: a framework for understanding sediment transfer at multiple scales. *Earth Surface Processes and Landforms* 40: 177–188.

Brasington J, Rumsby B, McVey R, 2000. Monitoring and Modelling Morphological Change in a Braided Gravel-Bed River Using High Resolution GPS-Based Survey. *Earth Surface Processes and Landforms* 25: 973-990.

Brasington J, Vericat D, Rychkov I. 2012. Modelling river bed morphology, roughness, and surface sedimentology using high resolution terrestrial laser scanning. *Water Resources Research*. 48: 1-18.

Bryan R, Yair A. 1982. Perspectives on studies of badland geomorphology. In: *Badland Geomorphology and Piping*, Bryan RB, Yair A (Eds.). Geobooks: Norwich; 1–12.

Buendia C, Gibbins CN, Vericat D, Batalla RJ. 2013. Reach and catchment-scale influences on invertebrate assemblages in a river with naturally high fine sediment loads. *Limnology and Ecological Management of Inland Waters* 43: 362–370.

Carrivick JL, Smith MW. 2018. Fluvial and aquatic applications of Structure from Motion photogrammetry and unmanned aerial vehicle/drone technology. *WIREs Water* 1-17.

Cavalli M, Trevisani S, Comiti F, Marchi L. 2013. Geomorphometric assessment of spatial sediment connectivity in small Alpine catchments. *Geomorphology* 188: 31–41.

Chuvieco E. 2016. *Fundamentals of Satellite Remote Sensing: An Environmental Approach*. Second edition. Taylor and Francis, USA. 468 pp.

Ciccacci S, Galiamo MC, Roma MA, Salvatore MC. 2008. Morphological analysis and erosion rate evaluation in badlands of Radicofani area (Southern Tuscany, Italy). *Catena* 74: 87–97.

Clarke ML, Rendell HM. 2010. Climate-driven decrease in erosion in extant Mediterranean badlands. *Earth Surface Processes and Landforms* 35: 1281-1288.

Clotet N, Gallart F, Sala M. 1987. Los badlands: características, interés teórico, dinámica y tasas de erosión. *Notes de Geografía Física* 15-16: 28-37.

Cucchiaro S, Cavalli M, Vericat D, Crema S, Llena M, Beinat A, Marchi L, Cazorzi F. 2019. Geomorphic effectiveness of check dams in a debris-flow catchment using multi-temporal topographic surveys. *Catena* 174: 73-83.

Cossart E, Viel V, Lissak C, Reulier R, Fressard M, Delahaye D. 2018. How might sediment connectivity change in space and time? *Land Degradation and Development* 29: 2595–2613.

Faulkner H. 2008. Connectivity as a crucial determinant of badland morphology and evolution. *Geomorphology* 100: 91-103.

Faulkner H. 2018. The Role of Piping in the Development of Badlands. In: *Badland Dynamics in the Context of Global Change*. Nadal-Romero E, Martínez-Murillo JF, Kuhn NJ. (Eds.). Elsevier, Amsterdam. 217-253.

Ferrer V, Errea P, Alonso E, Gómez-Guitierrez A, Nadal-Romero E. 2017. A Multiscale Approach to asses Geomorphological Processes in a semiarid badland area (Ebro Depression, Spain). *Cuadernos de Investigación geográfica* 43: 41-62.

Gallart F, Solé A, Puigdefàbregas J, Lázaro R. 2002. Badland Systems in the Mediterranean. In: *Dryland Rivers: Hydrology and Geomorphology of Semi-arid Channels*. Bull LJ, Kirkby MJ (Eds.). John Wiley & Sons, Ltd. 299-326.

Girardeau-Montaut D. 2019. CloudCompare - Open Source Project. http://www.danielgm.net/cc/ (accessed 01 February 2019).

Gude M, Daut G, Dietrich S, Mäusbacher R, Jonasson C, Bartsch A, Scherer D. 2002. Towards an integration of process measurements, archive analysis and modelling in geomorphology – the Kärkevagge experimental site, Abisko area, northern Sweden. Geografiska Annaler 84(3–4): 205–212.

Gutiérrez M, Sancho C, Benito G, Sirvent J, Desir G. 1997 Quantitative study of piping processes in badland áreas of the Ebro Basin, NE Spain. *Geomorphology* 20: 237-253.

Jancewicz K, Migon P, Kasprzak M. 2019. Connectivity patterns in contrasting types of tablelands sandstone relief revealed by Topographic Wetness Index. *Science of Total Environment* 656: 1046-1062.

Harvey, A.M., 2001. Coupling between hillslopes and channels in upland fluvial systems: implications for landscape sensitivity, illustrated from the Howgill Fells, northwest England. *Catena* 42: 225–250.

Haas F, Hilger L, Neugirg F, Umstädter K, Breitung C, Fischer P, Hilger P, Heckman T, Dusik J, Kaiser A, Schmidt J, Della Seta M, Rosenkranz R, Becht M. 2016. Quantification and analysis of geomorphic processes on a recultivated iron ore mine on the Italian island of Elba using long-

term ground-based lidar and photogrammetric SfM data by a UAV. *Natural Hazards and Earth System Sciences* 16: 1269-1288.

Heckmann, T, Vericat D. 2018. Computing spatially distributed sediment delivery ratios: inferring functional sediment connectivity from repeat high-resolution digital elevation models. *Earth Surface Processes and Landforms*. 43: 1547–1554.

Howard AD. 2009. Badlands and gullying. In: *Geomorphology of Desert Environments*. Parsons AJ, Abrahams AD. (Eds.). Springer, Berlin. 265–299.

Huggett RJ. 2011. *Fundamentals of Geomorphology*, 3rd edition. Routledge, New York. 533 pp.

James MR, Robson S, Smith, MW. 2017. 3-D uncertainty-based topographic change detection with structure-from-motion photogrammetry: precision maps for ground control and directly georeferenced surveys. *Earth Surface Processes and Landforms* 42: 1769–1788.

Jancewicz K, Migon P, Kasprzak M. 2019. Connectivity patterns in contrasting types of tableland sandstone relief revealed by TopographicWetness Index. *Science of the Total Environment* 656: 1046-1062.

Kasanin-Grubin M. 2013. Clay mineralogy as a crucial factor in badlands hillslope processes. *Catena* 106: 54–67.

Lane SN, Westaway RM, Hicks M. 2003. Estimation of erosion and deposition volumes in a large, gravel bed, braided river using synoptic remote sensing. *Earth Surface Processes and Landforms* 28: 249-271.

López-Tarazón JA, Batalla RJ, Vericat D, Francke T. 2012. The sediment budget of a highly dynamic mesoscale catchment: the river Isábena. *Geomorphology* 138: 15–28.

Lague D, Brodu N, Leroux J. 2013. Accurate 3D comparison of complex topography with terrestrial laser scanner: Application to the Rangitikei canyon (N-Z). *ISPRS Journal of Photogrammetry and Remote Sensing* 82: 10-26.

Lu X, Li Y, Washington-Allen RA, Li Y. 2019. Structural and sedimentological connectivity on a rilled hillslope. *Science of Total Environment* 655: 1479-1494.

Martínez-Casasnovas JA, Poch RM. 1998. Estado de conservación de los suelos d ela cuenca del embalse Joaquín Costa. *Limnética* 14: 83-91.

Mathys N, Brochot S, Meunier M. 1996. Erosion of the Terres Noires (Black Earth) in the southern French Alps : A contribution to an assessment of mean annual values (Draix experimental catchment areas). *Revue de géographie alpine* 84 (2): 17-27.

Milan DJ, Heritage GL, Large ARG, Fuller IC. 2011. Filtering spatial error from DEMs: Implications for morphological change estimation. *Geomorphology* 125: 160–171.

Moreno-de las Heras M, Gallart F. 2018. The Origin of Badlands. In: *Badland Dynamics in the Context of Global Change*. Nadal-Romero E, Martínez-Murillo JF, Kuhn NJ. (Eds.). Elsevier, Amsterdam. 27-59.

Morgenstern N. 1965. The analysis of the stability of general slip surfaces. *Geotechnique* 15(1): 79–93.

Mueller EN, Güntner A, Francke T, Mamede G. 2010. Modelling sediment export, retention and reservoir sedimentation in drylands with the WASA-SED model. *Geoscientific Model Development* 3: 275-291.

Nadal-Romero E, Regüés D, Martí-Bono C, Serrano-Muela P. 2007. Badland dynamics in the Central Pyrenees: temporal and spatial patterns of weathering processes. *Earth Surface Processes and Landforms* 32: 888-904.

Nadal-Romero E, García-Ruiz JM. 2018. Rethinking Spatial and Temporal Variability of Erosion in Badlands. In: *Badland Dynamics in the Context of Global Change*. Nadal-Romero E, Martínez-Murillo JF, Kuhn NJ. (Eds.). Elsevier, Amsterdam. 217-253.

Nadal-Romero E, Regüés D. 2010. Geomorphological dynamics of sub-humid mountain badland areas: weathering, hydrological and suspended sediment transport processes. A case of study in the Araguás catchment (Central Pyrenees), and implications for altered hydro-climatic regimes. *Progress in Physical Geography* 34 (3): 123–150.

Nadal-Romero E, Revuelto J, Errea P, López-Moreno JI. 2015. The application of terrestrial laser scanner and SfM photogrammetry in measuring erosion and deposition processes in two opposite slopes in a humid badlands area (central Spanish Pyrenees). *SOIL* 1, 561–573.

Neugirg F, Stark M, Kaiser A, Vlacilova M, Della Seta M, Vergari F, Schmidt J, Becht M, Haas F. 2016. Erosion processes in calanchi in the Upper Orcia Valley, Southern Tuscany, Italy based on multitemporal high-resolution terrestrial LiDAR and UAV surveys. *Geomorphology* 269: 8–22.

Nobajas A, Waller RI, Robinson ZP, Sangonzalo R. 2017. Too much of a good thing? the role of detailed UAV imagery in characterizing large-scale badland drainage characteristics in South-Eastern Spain. *International Journal of Remote Sensing* 38: 2845-2860.

Passalacqua P, Belmont P, Staley DM, Simley JD, Arrowsmith JR, Bode CA, Crosby C, DeLong SB, Glenn NF, Kelly SA, Lague D, Sangireddy H, Schaffrath K, Tarboton DG, Wasklewicz T, Wheaton JM. 2015. Analyzing high resolution topography for advancing the understanding of mass and energy transfer through landscapes: a review. *Earth-Science Reviews* 148: 174-193.

Piqué G, López-Tarazón JA, Batalla RJ. 2014. Variability of in-channel sediment storage in a river draining highly erodible areas (the Isábena, Ebro basin). *Journal Soils Sediments* 12: 2031-2044.

Regüés D, Pardini G, Gallart F. 1995. Regolith behaviour and physical weathering of clayey mudrock as dependent on seasonal weather conditions in a badland area at Vallcebre, Eastern Pyrenees. *Catena* 25: 199-212.

Regüés D, Guàrdia R, Gallart F. 2000. Geomorphic agents versus vegetation spreading as causes of badland occurrence in a Mediterranean subhumid mountainous area. *Catena* 40(2): 173–187.

Regüés D, Torri D. 2002. Efecto de la energía cinética de la lluvia sobre la dinámica de las propiedades físicas y el encostramiento en un suelo arcilloso sin vegetación. *Cuaternario y Geomorfología* 16: 57–71.

Roering JJ, Kirchner JW, Dietrich WE. 2001. Hillslope evolution by nonlinear, slope-dependent transport: steady-state morphology and equilibrium adjustment timescales. *Journal of Geophysical Research* 106: 16499–16513.

Römkens MJM, Helming K. Prasad SN. 2002. Soil erosion under different rainfall intensities, surface roughness, and soil water regimes. *Catena* 46(2-3): 103-123.

Rychkov I, Brasington J, Vericat D. 2012. Computational and methodological aspects of terrestrial surface analysis based on point clouds. *Computers & Geosciences* 42: 64-70.

Sidle RC, Jarihani B, Kaka SI, Koci J, Al-Shaibani A. 2019. Hydrogeomorphic processes affecting dryland gully erosion: Implications for modelling. *Progress in Physical Geography* 43(1): 46-64.

Sirvent J, Desir G, Gutierrez M, Sancho C, Benito G. 1997. Erosion rates in badland areas recorded by collectors, erosion pins and profi lometer techniques (Ebro Basin, NE-Spain). *Geomorphology* 18: 61–75.

Smith, MW, Carrivick, JL, and Quincey, DJ 2015. Structure from Motion photogrammetry in physical geography. *Progress in Physical Geography* 40(2): 247-275.

Smith MW, Vericat D. 2015. From experimental plots to experimental landscapes: topography, erosion and deposition in sub-humid badlands from Structure-from-motion photogrammetry. *Earth Surface Processes and Landforms* 40: 1656-1671.

Smith MW, Warburton J. 2018. Microtopography of bare peat: a conceptual model and objective classification from high-resolution topographic survey data. *Earth Surface Processes and Landforms* 43: 1557-1574.

Stöcker C, Eltner A, Karrasch P. 2015. Measuring gullies by synergetic application of UAV and close range photogrammetry — a case study from Andalusia, Spain. *Catena* 132: 1–11.

Tarolli, P. 2014. High-resolution topography for understanding Earth surface processes: opportunities and challenges. *Geomorphology* 216: 295–312.

Torri D, Calzolari C, Rodolfi G. 2000. Badlands in changing environments: An introduction. *Catena* 40: 119–125.

Tsutsumi D, Fujita M. 2016. Field observations, experiments, and modeling of sediment production from freeze and thaw action on a bare, weathered granite slope in a temperate region of Japan. *Geomorphology* 267: 37-47.

Vergari F, Troiani F, Faulkner H, Del Monte M, Della Seta M, Ciccacci S, Fredi P. 2019. The use of the slope-area function to analyse process domains in complex badland landscapes. *Earth Surface Processes and Landforms* 44: 273-286.

Vericat D, Smith MW, Brasington J. 2014. Patterns of topographic change in sub-humid badlands determined by high resolution multi-temporal topographic surveys. *Catena* 120: 164–176.

Vericat D, Wheaton J, Brasington J. 2017. Revisiting the Morphological Approach: Opportunities and Challenges with Repeat High-Resolution Topography. In: *Gravel-Bed Rivers: Processes and Disasters*. Tsutsumi DT, Laronne JB. (Eds.). Wiley, 121-158.

Westoby MJ, Brasington J, Glasser NF. 2012. 'Structure-from-motion' photogrammetry: a low-cost, effective tool for geoscience applications. *Geomorphology* 179: 300–314.

Wheaton JM, Brasington J, Darby SE, Kaspark A, Sear D, Vericat D. 2013. Morphodynamic signatures of braiding mechanisms as expressed through change in sediment storage in a gravel-bed river. *Journal of Geophysical Research: Earth Surface* 118: 759-779.

Wheaton JM, Brasington J, Darby SE, Sear DA. 2010. Accounting for uncertainty in DEMs from repeat topographic surveys: improved sediment budgets. *Earth Surface Processes and Landforms* 35(2): 136–156.

Wohl E, Brierley G, Cadol D, Coulthard TJ, Covino T, Fryirs KA, Grant G, Hilton RG, Lane SN, Magilligan FJ, Meitzen KM, Passalacqua P, Poeppl RE, Rathburn SL, Sklar LS. 2018. Connectivity

as an emergent property of geomorphic systems. *Earth Surface Processes and Landform* 44:4-26

Willgoose GR, Bras RL, Rodriguez-Iturbe I. 1991. A coupled channel network growth and hillslope evolution model. *Water Resources Research* 27: 1671–1702.

Williams JG, Rosser NJ, Hardy RJ, Brain MJ, Afana AA. 2018. Optimising 4-D surface change detection: an approach for capturing rockfall magnitude-frequency. *Earth Surface Dynamics* 6: 101–119.

Witten IH, Frank E, Hall MA. 2011. *Data Mining: Practical Machine Learning Tools and Techniques*, 3rd edn. Burlington USA: Morgan Kaufmann.

Yair A, Lavee H, Bryan RB, Adar E. 1980. Runoff and erosion processes and rates in the Zin Valley badlands, Northern Negev, Israel. *Earth Surface Processes* 5: 205-225.

Zhang FB, Yang MY, Li BB, Li ZB, Shi WY. 2017. Effects of slope gradient on hydro-erosional processes on an aeolian sand-covered loess slope under simulated rainfall. *Journal of Hydrology* 553: 447-456.

## 2.2. Sub-catchment scale (CHAPTER 4)

### 2.2.1. Introduction and general overview

The main objective of Chapter 4 is to study the contribution of highly erodible surfaces draining badlands to the sediment yield of a small intermittent catchment and their relationships with meteorological variables. Therefore, methods developed in this section are focused on analysing water and sediment yield, and rainfall and air temperature at multiple temporal scales. The methodological design also includes data obtained in Chapter 3 in relation to sediment production from the two badlands and meteorological variables. Three interrelated tasks compose the general workflow (Figure 8): A. Data acquisition, B. Post-processing, and C. Data preparation and results. **A. Data acquisition.** Different data types were acquired: (i) Rainfall was characterized by data provided by a meteorological station with a rainfall gauge, which also measures air temperature. (ii) Sediment production was measured in the two experimental badlands by the estimation of erosion rates from the comparison of repeat high resolution topographic surveys performed by Structure from Motion (SfM) (see section 2.1; results of Chapter 3). (iii) Sediment fluxes at the outlet of the catchment were estimated by continuous water turbidity measures and samples collected by a water stage sampler (designed and built following the initial model developed by Schick (1967). Runoff was estimated by continuous water stage measures and by applying the specific formulations for the rectangular weir (surveyed by means of SfM to extract the specific geometry of the weir in the station). **B. Post-processing.** In order to estimate sediment production for all the catchment, measured erosion rates in the experimental badlands were extrapolated for all the badland surface of the catchment. Sediment production for the other land uses (i.e. forest and land crops) was extracted from the literature. Turbidity records were converted to suspended sediment fluxes using the calibration performed by means of measured suspended sediment concentrations obtained from water samples. In the same way, out of range periods were characterized by water samples taken by the stage water sampler. Water stage was converted to a discharge using a specifically derived open rectangular channel formula (h/Q relation) using the geometry obtained by the topographic survey explained in the step A. **C. Data preparation and results.** From the combination of sediment concentration and flow it was possible to estimate the water and sediment yield at the catchment outlet. A sediment budget for the different study periods was developed via comparison between sediment yield and production. Hydrologic analyses were performed examining runoff and rainfall data. From this, it was possible to infer in the role of sediment production in badlands in relation to the total sediment yield. Finally, meteorological, runoff, sediment production and sediment transport variables were correlated in order to analyse the effect of pulses in the transfer of water and sediment, and infer in the role of drainage network as a sediment storage (sink) and source.

This methodology was not presented in any specific technical paper; however full detailsare provided in Chapter 4 itself.

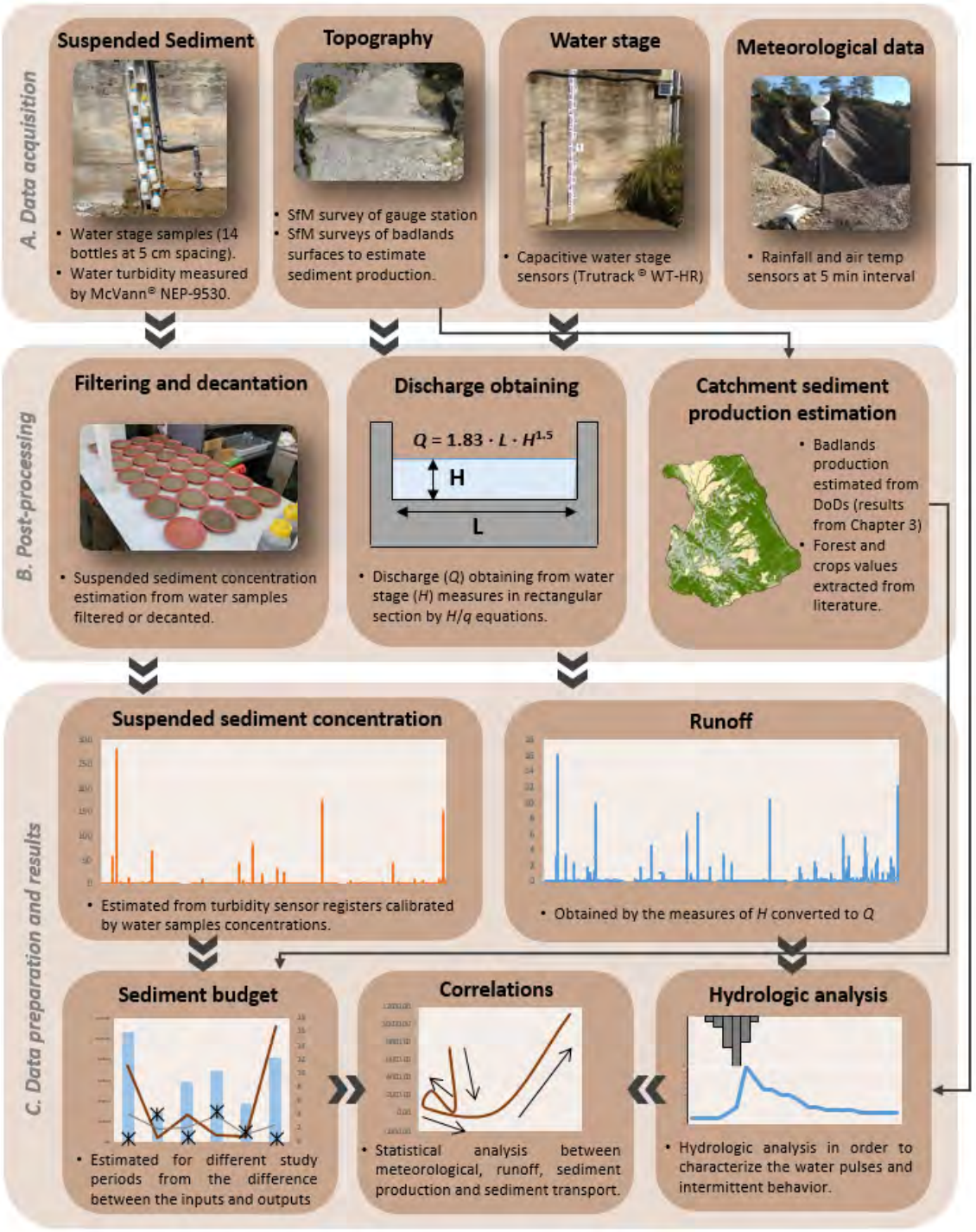


**Figure 8**. Summary of the methodological workflow followed to study the role of high erodible surfaces draining badlands on the sediment yield of a small intermittent catchment (Chapter 4).

## 2.3. Catchment scale (CHAPTER 5)

### 2.3.1. Introduction and general overview

The main objective of Chapter 5 is to analyse catchment scale effects of land use changes and associated topographic changes on structural sediment connectivity. Three interrelated tasks compose the general workflow (Figure 9): A. Data acquisition, B. Post-processing, and C. Data preparation and results. **A. Data acquisition.** Multi-temporal aerial photographs were processed by SfM photogrammetry in order to obtain orthomosaics and point clouds. Scaling and georreferencing was performed by the establishment of a ground control network (i.e. GCPs) homogeneously distributed throughout the catchment. **B. Post-processing.** Land use maps were obtained from the orthomosaics for each of the study periods by means of a supervised image classification. Point clouds were filtered, co-registrated, regularized and finally converted to DEMs. **C. Data preparation and results.** Maps of Sediment Connectivity Index (IC) per each period were obtained by the combination of DEMs and weighting factor maps, which were calibrated by land use maps based on Manning's roughness coefficient. The IC developed by Borselli et al. (2008) and further modified by Cavalli et al. (2013) was specifically calculated. By the comparison of the IC maps obtained before and after changes on the landscape (cover or topography), it was possible to assess the impact of these disturbances on structural sediment connectivity.

Part of this entire workflow (Figure 9), specifically the section explaining how to obtain catchment-scale point clouds and orthomosaics by means of SfM applied to historical photos is detailed explained in a scientific paper published in the *Rendiconti Online della Società Geologica Italiana* journal (see section 2.3.2 for further information about this paper).

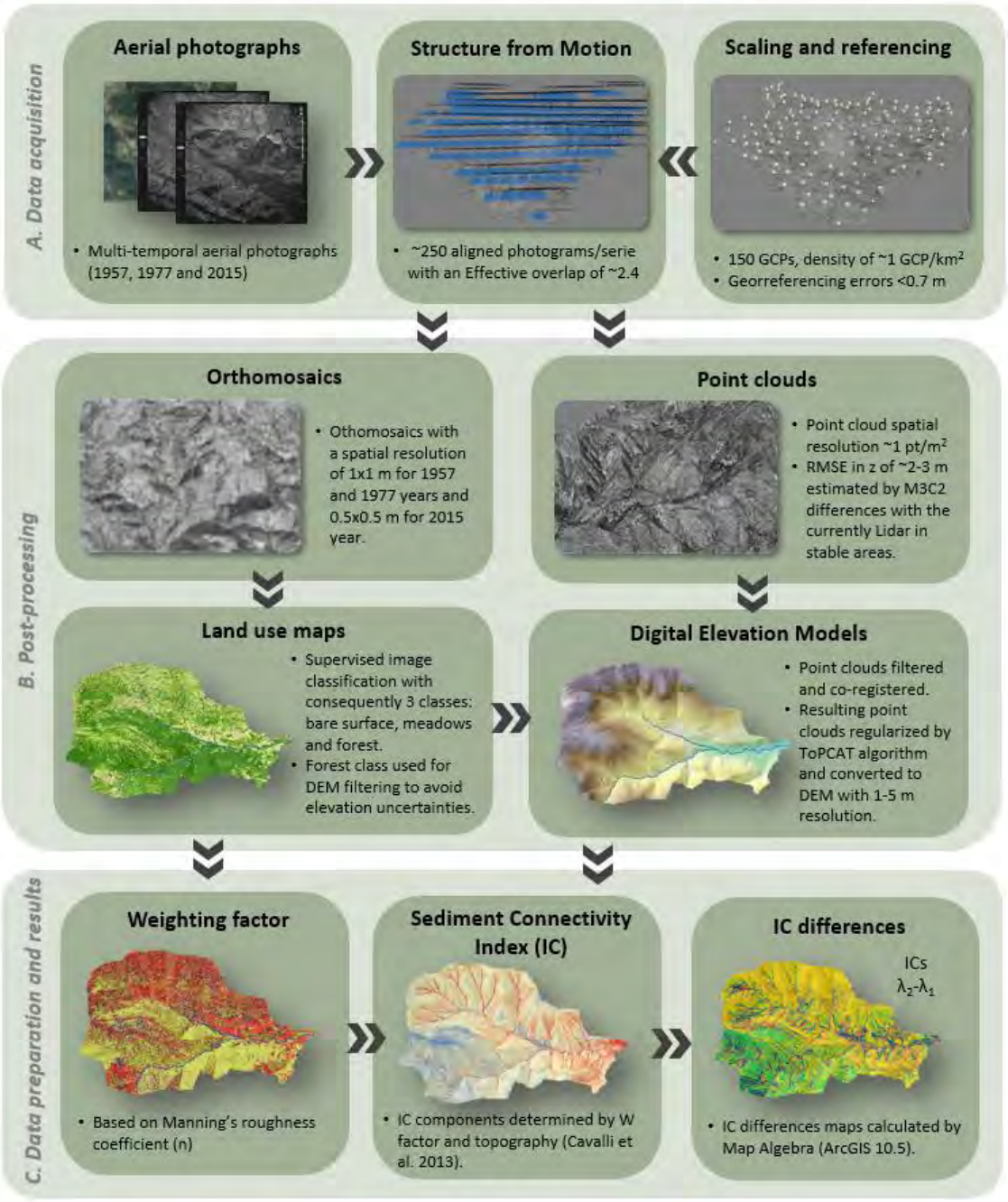


**Figure 9**. Summary of the methodological workflow followed to analyse the effects of land use and topographic changes on sediment connectivity (Chapter 5).

-

### 2.3.2. Assessing historical landscape changes by SfM-photogrammetry

This section contains the following accepted and already published paper in the journal *Rendiconti Online Società Geologica Italiana.* SJR Impact Factor (2018): 0.395. Category: Geology; 3rd Quartile.

Llena M, Cavalli M, Vericat D, Crema S. 2018. Assessing landscape changes associated to anthropic disturbances by means of the application of Structure from Motion photogrammetry using historical aerial imagery. *Rendiconti Online Società Geologica Italiana* 46: 74-81.

**ABSTRACT:** In this paper we present a methodological workflow to obtain planimetric and topographic data from historical aerial photos using photogrammetric methods through Structure from Motion (SfM) and Multi-View Stereo (MVS) algorithms. This methodology is applied in two case studies located in the Upper Cinca River catchment (Southern Pyrenees). These sites have suffered a series of direct anthropogenic disturbances that have modified landscape topography. Specifically, topographic changes associated with the construction of a road and the extraction of materials from a pit quarry have been analysed. The resultant products extracted by the application of SfM-MVS are orthomosaics with a root mean square error (RMSE) between 0.5 and 1 m, and points clouds (topography) with a RMSE between 1 and 2 m. The topography before and after each of the impacts was compared with the objective to analyse the changes attributed to these disturbances. A simple minimum Level of Detection (minLoD) was estimated based on the RMSEs in order to distinguish potential real changes from those due to the noise ascribable to the uncertainty of the topographic data sets. The significance of both impacts is relevant in terms of topographic changes (from -20 to +15 m). The dominant topographic change (in extension) in the case of the road construction (51% of the surface) is extraction (i.e. erosion). In the case of the pit quarry, the dominant process is deposition (i.e. sedimentation; 27% of the area). The extension below the minLoD is around the 23% and 48%, respectively, indicating that the magnitude of the changes is substantially higher in the case of the road construction. In both cases the net volume is negative (-913,710 and -16,197 $m^3$ in the case of the road and the quarry, respectively), that show the differences in terms of the extension of the processes and their magnitude in each case study. Finally, both impacts had a direct effect on landscape morphometry (e.g. changes in the slope and flow direction). The developed approach provides an opportunity to analysed and quantify landscape changes that may help to improve our understanding of the long-term evolution of the transfer of water and sediment through landscapes.

**KEYWORDS**: *aerial photographs, Structure from Motion, land use changes, topographic changes, road construction, open-pit quarry.*

## INTRODUCTION

Landscapes evolve through time owing to geological and climatic processes, such as erosion and transfer of water and sediments from hillslopes to channel networks. This transfer is also conditioned by landscape properties (e.g. soil roughness, vegetation, aspect, etc.). Land use changes, such as the abandonment of agricultural activities together with reforestation, affect surface runoff, erosion and sediment transfer at multiple spatial scales (Gallart & Llorens, 2004; Garcia-Ruiz, 2010). The replacement of cereal crops on steep slopes by dense shrubs leads to a moderate decrease in hydrological and sedimentary responses (Beguería et al., 2006; López-Moreno et al., 2009). Likewise, localized impacts such as the construction of infrastructures (e.g. roads) or the extraction of materials from open-pit quarries may have a noticeable impact also ahead from the disturbance location. Although the impacts of these disturbances are very localized (space and time), their effects can modify heavily topography and connectivity, disturbing the fluxes of water and sediment, and, potentially triggering a series of hydrological and geomorphological adjustments upstream and downwards the disturbed zone (Chen et al., 2015; Jones et al., 2000; Tague & Band, 2001).

To assess the impact of these disturbances on runoff and sediment connectivity it is necessary to compare the situation of the study site before and after the impact. In the case of land use changes, there are many free available spatial datasets at reasonable resolutions to reconstruct the characteristics after the disturbance (i.e. contemporary period). Information to reconstruct the landscape proprieties and characteristics before the disturbance (i.e. historic period) is instead very limited. The use of planimetric analysis or maps from historical aerial photos (Cerovski-Darriau & Roering, 2016; Gordon & Meentemeyer, 2006) is quite common in literature. Even so, historical topographic data are rare to obtain, a fact that limits the study of geomorphological changes, especially in the cases where the impacts of disturbances have prompted topographic changes.

Within this context, current advances in computer vision and photogrammetry have allowed the development of a novel, fast and cheap methodology based on classic photogrammetric techniques, the Structure-from-Motion and Multi View Stereo algorithms (SfM-MVS). SfM-MVS allows to obtain planimetric (i.e. orthomosaics) and topographic (i.e. point clouds) information from multiple photos with different orientation or points of view (see more details in Micheletti et al., 2015a; Smith et al., 2016; Westoby et al. 2012). From the geomorphological point of view, this methodological approach offers a wide range of possibilities to study changes in landscape properties and topography through time (e.g. Carrivick et al., 2016).

In this paper, we present a simple workflow to obtain spatial data (i.e. orthomosaics and point clouds) by means of applying SfM-MVS algorithms to historical aerial photos. The workflow is applied to two contrasted case studies in the Upper Cinca River catchment (Southern Pyrenees) with the objective to analyze the potential of this methodology to quantify the impact of two localized anthropic landscape disturbances: (1) a road construction in a mountain area and (2) the hard rock extraction in an open pit quarry. Several authors have recently used this approach to study topographical changes in fluvial geomorphology (e.g. Bakker and Lane, 2017), glacial geomorphology (e.g. Mertes et al., 2017; Midgley & Tonkin, 2017), big landslides or rockfalls (e.g. Dugonjic et al., 2016; Warrick et al., 2017), and volcanology (e.g. Gomez, 2014). In the particular case of the River Cinca, Llena et al. (2018) have recently presented part of this workflow but focused to the study of topographic changes in fluvial corridors suffering incision and sedimentation due to a combination of human impacts such as gravel mining and channel embankment and floods.

## STUDY AREA

The Upper Cinca River catchment is located in the north east of the Iberian Peninsula (Southern Pyrenees), within the Ebro River basin (Figure 10), covering an area of approximately 1550 km2. This catchment is composed of the Ara river sub-catchment to the west (715 km2) and Cinca river sub-catchment to the east (850 km2; Figure 10A). Like most of the mountain basins in the Pyrenees, it has suffered important anthropic disturbances that have affected its sedimentary dynamics, especially since the second half of the 20th century when land uses went through important modifications (Beguería et al., 2006; García-Ruíz et al., 2010). Additionally, other localized disturbances have also modified the transfer of water and sediments through the catchment. For instance, gravel mining and channel embankments have a direct impact on river corridors, while the construction of large infrastructures such as roads, or the extraction of sediments in open pit quarries modified the topography of hillslopes with a direct impact on sediment connectivity (Chen et al., 2015; Jones et al., 2000; Tague & Band, 2001). Within this context, the first case study we present in this paper aim at evaluating the topographic changes associated with the construction of a road in the middle part of the Ara River sub-catchment (Figure 10A & B) during the beginning of the 20th century. The road has a length of 5 km and an average width of 20 m. Its construction induced important changes on the hillslopes and the movement of large amounts of material modifying the natural drainage network (Figure 10B). The second case study is focused on an open-pit quarry located in the lower part of Upper Cinca River sub-catchment (Figure 10A & C), covering a surface area of 3.5 ha (Figure 10C). We aim to evaluate the amount of sediments removed during the period 2003-2015.

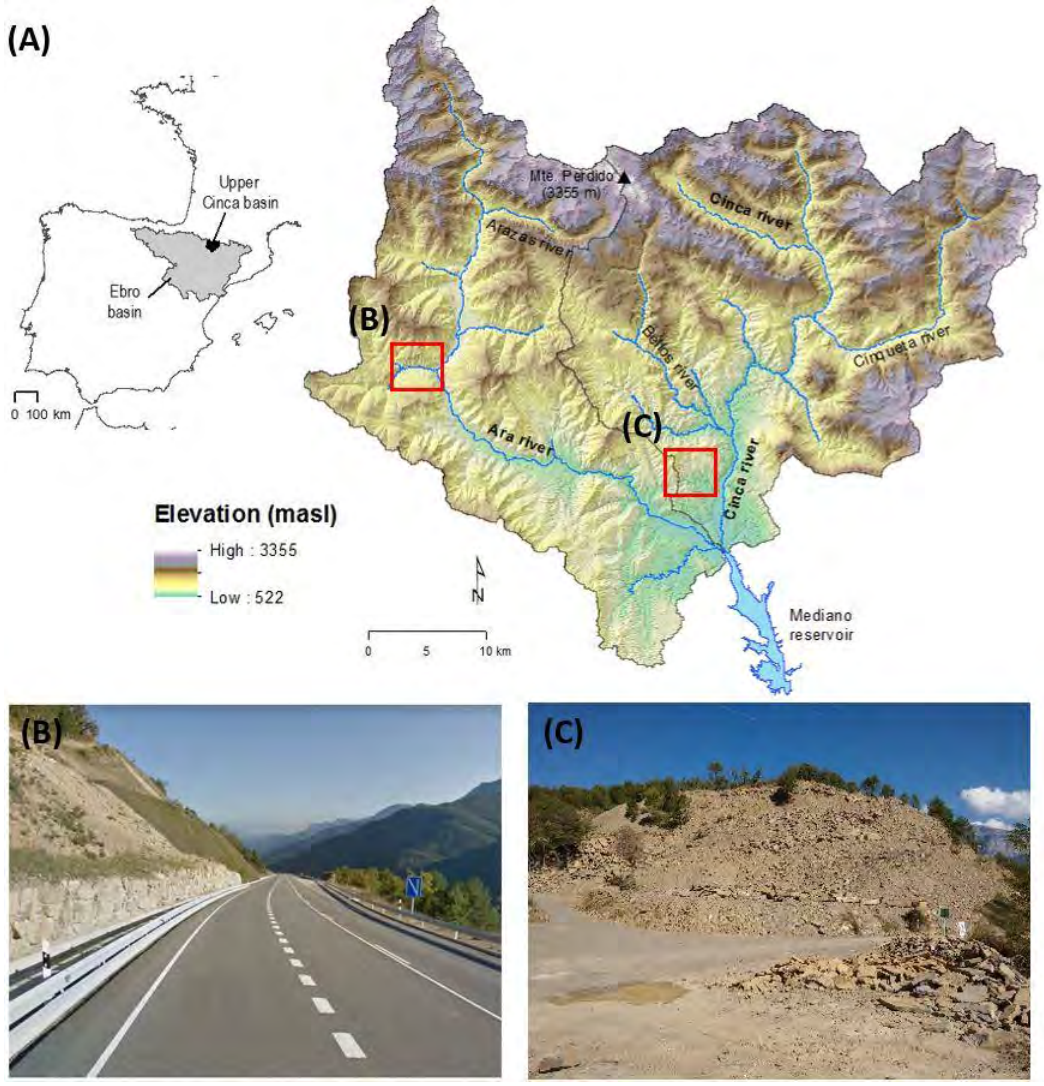


**Figure 10**. **A.** Upper Cinca River Basin within the context of the Iberian Peninsula and location of the case studies. **B.** View of the road construction case study. (C) View of the open pit quarry case study.

## METHODS

Figure 11 shows the methodological workflow that has been designed and applied. Part of this approach has been recently presented by Llena et al. (2018) but focused on the study of topographic changes in river channels, which seeks a different objective with respect to the one presented here. This workflow consists of four main blocks that are explained in the following sections.

### Historical aerial photographs

The selection of the aerial photos is based on their availability related to the periods to compare. Two sets of photographs were selected for each of the two case studies. In the case study of the road construction, we selected the historical aerial photographs of the year 1977 (considered

pre-impact) and 2012 (post-impact). In the case study of the open pit quarry, were selected photographs of the year 2003 (pre-impact) and 2015 (post-impact). All the aerial photo imagery was freely obtained from the Spanish National Center of Geographic Information (CNIG). To improve the photogrammetric process, the photograms were corrected adjusting the contrast and image exposure using the software Adobe Photoshop Lightroom© 6.6.1.

*Ground Control Points*

The selection of the Ground Control Points (GCPs) is a key task, based on the location of coincident points from the photographs in potentially unchanged locations (e.g. road crossings, field boundaries, low constructions). The coordinates of these points need to be extracted. This step represents a source of uncertainty for historical photographs since it relies on the choice of the points in the area that should have remained unchanged between the photo acquisition and the periods when he GCPs are extracted. It is important to avoid the selection of GCPs in elements with complex or irregular geometries since these irregularities may decrease the accuracy of the GCPs and may introduce significant errors in the final point cloud. In the case study of the road construction, 10 GCPs were obtained, while in the quarry case study 8 GCPs were selected. In both cases, the GCP network had an approximate density of 1 GCP per 0.8 km2. The coordinates of the GCPs (x, y) were extracted from the 2012 official orthomosaic (PNOA CNIG). The geographic coordinate system used in both cases was UTM ETRS 1989 Zone 31. The elevation information (z) of the GCPs was obtained from the 2010 LiDAR survey (CNIG), which is characterized by a point cloud density of 0.5 pts / m2 and an accuracy of ± 0.2 m. To validate GCPs remained static, a series of field surveys were carried out using a RTK Leica VIVA® GS15 GPS (with 3D data quality values smaller than 0.05 m). The heights of 39% of the total of GCPs were surveyed. Errors (i.e., RMSE) at elevation were located at 0.6 m RMSE.

## Photogrammetric process

*Structure from Motion (SfM) implementation*

The images were photogrammetrically processed using Agisoft Photoscan Professional 1.2.2 software. The first step was to import and align the photographs; the software searches for common elements visible in several photographs from different points of view and identifies their correspondence. Then, the 3D geometry of the scene was estimated, both the coordinates of the common points found, the position of the cameras (i.e. extrinsic calibration) and the internal parameters of the cameras (i.e. intrinsic calibration; Ullman, 1979). For more details, the reader can refer to the works by Carrivick et al. (2016), Micheletti et al. (2015a) and Smith et al. (2016).

The use of historical aerial photographs presented some issues that may affect data accuracy and precision: a) the overlap between photographs; and b) the quality of the image (Bakker and Lane 2017, Micheletti et al., 2015b). At least two photographs are necessary to identify common features. However, a minimum of three photographs is recommended to validate the point geometrically, since its reliability increases if the point is identified using a larger number of photographs (i.e. greater overlap between photographs). As for the image quality of the photographs, it determined the texture, which facilitates the identification of common features. In historical photographs, the quality of the image is often compromised during the digitalization or scanning process, which is not always done with enough resolution or care, leading to the loss of image quality (e.g. blurred areas, presence of artifacts), and a consequent increase of errors

in the alignment process. These two limiting factors can generate important errors and, consequently, a previous evaluation is required.

*Scaling and georeferencing*

The georeferencing and scaling process consists of the geometric and geographic correction of the sparse point cloud by locating the GCPs established in Section 2 of the workflow. In the case of Agisoft Photoscan Professional 1.2.2, the georeferencing is performed by a linear model obtained from 7 transformation parameters: 3 translation parameters; 3 of rotation and 1 of scale. The software also allows to automatically calibrate the cameras to minimize the errors associated with the distortions caused mainly by the lens. It is an automated process that improves significantly the quality of the results. In the particular case of the Upper Cinca River, the georeferencing errors (RMSE) for all the models of the two study cases were less than 1 m. This leads to consider the georeferencing process satisfactory taking into account that the errors associated with this process in historical aerial photographs are usually between 2 and 5 meters (e.g. Arnaud et al., 2015; Comiti et al., 2011; Surian et al., 2009).

*Dense point cloud*

Once the sparse point cloud is georeferenced in a known coordinate system, the following step is to apply different algorithms (e.g. Multi View Stereo; MVS) to increase the density of the point cloud by at least two orders of magnitude. There are several types of MVS algorithms (Seitz et al., 2006; Smith et al., 2016). Agisoft Photoscan Professional uses a combination of methods based on pair-wise depth map computation (i.e. Smooth and Height-field methods) and a method based on a multi-view approach (i.e. Fast method; Semyonov, 2011).

*Orthorectification*

The last step in the photogrammetric workflow is the orthorectification process. Through this process, a single orthomosaic is obtained and this is corrected geographically and geometrically thanks to the spatial information provided in the preliminary steps. In this process, a color correction is also performed in the boundary zones between photographs by homogenizing the histograms of the adjacent pairs. In the case of Upper Cinca River, the resolution of the selected pixel size was 1 m for all the generated orthomosaics. This resolution was selected because the maximum possible resolutions for each time series (i.e. 0.6 - 0.9 m) were homogenized in one resolution (i.e. 1 m), which was sufficient to represent both study areas with enough detail.

## Post-processing

The derived data products (i.e. point clouds and orthomosaics) need to be post-processed in order to extract reliable information based on the objective of the analysis. Post-processing was based on five main steps: (1) Co-registration; (2) Error analysis; (3) Image classification; (4) Regularization of the point clouds; and (5) DEM preparation and comparison.

*Co-registration*

The errors of the georeferencing process of the point cloud are relatively low (RMSE less than 1 m). Even so, there are areas (mainly those farthest from GCPs) that can present larger errors,

especially in historic aerial photos characterized by poor image quality. In order to minimize the errors associated with this fact, a co-registration of each point cloud with another reference point cloud was performed. In this study, the reference cloud was the available LiDAR (2010, form the CNIG) and the process was carried out using the tool Fine Registration (ICP) included in the software Cloud Compare 2.6.2.

*Error analysis*

In order to analyze the error of the points clouds obtained after the co-registration, the point clouds on stable zones (i.e. rocky outcrops without vegetation cover) were compared to the reference cloud (2010 LiDAR, CNIG), considering the later as the real surface. In our case studies, the comparison of the point clouds was carried out by the M3C2 plugin included in the software Cloud Compare 2.6.2 (Lague et al., 2013). In all cases, the differences in elevation in those areas were below 2 m, with a mean value of 1.7 m and a standard deviation of 0.3 m.

*Image classification*

A supervised image classification of the orthomosaics for each of the study times was carried out in order to identify those elements that may need a specific treatment. For instance, vegetation does not represent the ground surface and, therefore may increase the errors when topography is compared in these zones. Once the image is classified, the polygons of this specific class (e.g. vegetation) may be used to mask the results and avoid comparisons or analyses in those areas that we know are not accurate or uncertain (e.g. vegetation, buildings, water) and focus the study in those areas of interest.

*Regularization of the point clouds*

The results of the image classification can be also used to remove point clouds in undesired areas that may affect the generation of the DEMs (i.e. filtering). Once the point clouds were filtered, point clouds were regularized by using geostatistics techniques. For this purpose, the ToPCAT algorithm was used (Brasington et al., 2012). ToPCAT is implemented in ArcGIS 10.3 through Geomorphic Change Detection extension (GCD, available at http://gcd.joewheaton.org/; Wheaton et al., 2010). This algorithm allowed defining a regular grid of analysis (the length was defined by the user). All points in each cell were sorted and a series of elevation statistics calculated. Between this, the mean elevation value in each cell is obtained, a value that can be used as an estimate of the ground elevation. For more details see the work by Brasington et al. (2012).

*DEM preparation and comparison*

ToPCAT was run on a regular grid of 5 x 5 m in the case study of the road construction, and 2 x 2 m in the case of the quarry. These resolutions were set based on the extension and magnitude of the impacts in relation to the errors reported above. The mean elevation of the points in each cell was considered an estimate of the ground elevation. These points were interpolated to create the DEMs. Interpolation was performed by means of the natural Neighbor method implemented in ArcGIS 10.3.

Once the DEMs were obtained for each of the periods, their corresponding differences were calculated. The old one DEM (pre) was subtracted from the new one, and a DEMs of Difference (DoD) was obtained. Additionally, a minimum Level of Detection (minLod) was set in order to

distinguish those cells in which the topographic change might be uncertain from those considered real (i.e. DoD > minLoD). A simple minLod of 2 m was considered in our case studies based on the previously calculated errors. The estimation of the minLoD can be done in multiple ways that are determined by the available information to perform more complex uncertainty analyses. In this study, we followed the simplest option (a single minLoD) but more complex analyses can be also performed as reported by Wheaton et al. (2010). The thresholded DoDs represented the vertical changes on the DEMs for those cells in which the magnitude of the change was higher than the minLoD.

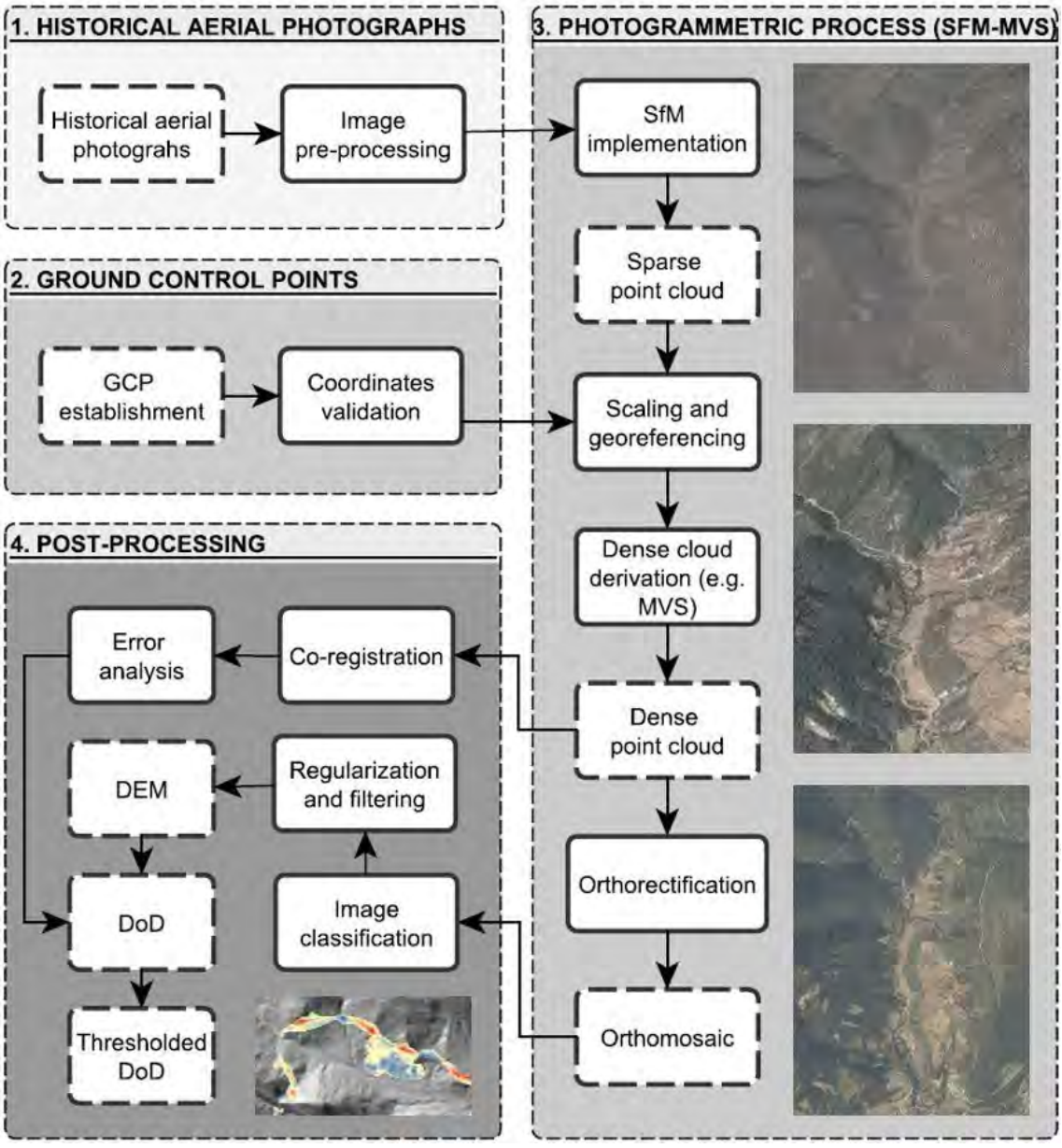


**Figure 11**. Workflow for obtaining orthomosaics and topographic information from aerial photographs: Dashed polygons correspond to the data inputs and outputs while the solid polygons represent procedures.

## RESULTS

Figure 12 and 13 show the two orthomosaics and 3D models (pre and post-impact) together with the thresholded DoD for the road construction and quarry study cases respectively.

### Road construction

The works carried out for the construction of the road implied relatively high magnitude topographic changes along the road (Figure 12). Note that sediment extraction and deposition were used instead of erosion and sedimentation since all topographic differences reported in this study are human-based. This terminology was chosen to make sure these processes are not interpreted to be the result of natural disturbances associated to, for instance, overland flows or floods. The mean sediment extraction during the period 1977-2012 was around -7.5 m, while the average deposition was around 5.8 m. The 51% of the total affected area showed sediment extraction, being the dominant process, owing to the works driven during the road construction. The 25% of the area showed deposition while the remaining cells (23%) had values lower than the minLoD. The average net change in elevation was -2.4 m. Taking into account the distribution and the sign of the changes, these are mainly due to the excavation of material in the slopes (i.e. extraction) and to the infilling in depressions or deep channels (i.e. deposition; Figure 12). On the basis of the DoD, 1,489,507 m3 of material was extracted from the study area during the execution of the works, while 575,996 m3 of material was deposited. In terms of total balance, there was a net sediment extraction of -913,710 m3 of material. The total net balance without taking into account the minLoD was -917,668 m3, which only represented 0.4% of change. Therefore, the uncertainty of the DEMs propagated to the DoD was very low with respect to the magnitude of the occurred changes and this uncertainty did not limit the application of the workflow used in this study.

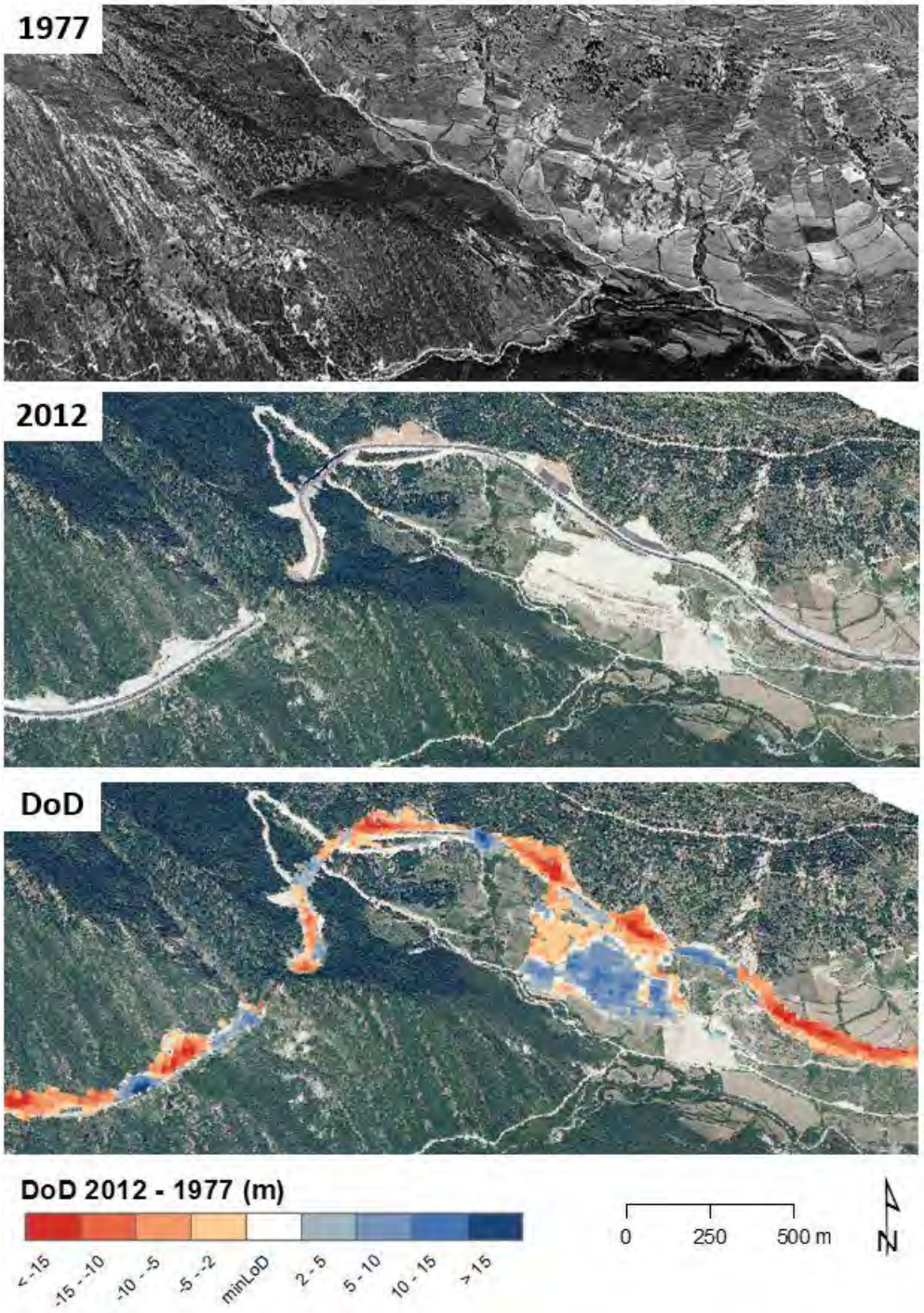


**Figure 12**. Road Construction Case Study. Orthomosaics of the years 1977 and 2012 (upper and center of the figure). Thresholded DoD (bottom) calculated from the difference between the 1977 and 2012 DEMs with the 2012 orthomosaic as background. Note that the maps are presented as a 3D view.

### Pit quarry

Topographic changes associated with the extraction of materials in the pit quarry were evident and spatially concentrated (Figure 13). Areas that showed sediment extraction (greater than 10 m in some places) corresponded to slopes where rocks were extracted, while deposition areas correspond to the edges in which the extracted materials that had a low commercial interest (i.e. debris) were deposited. The 24% of the total area showed extraction, while deposition was observed in 27%. The remaining 48% represented cells below the minLoD. The mean sediment extraction during the period 2003-2015 was around -24.5 m, while the average deposition was around 15.9 m. The average change in elevation was -1.1 m. The topographic changes resulted in a total sediment extraction of 61,814 m3 and a deposition of 45,617 m3, yielding a net balance of -16,197 m3. In this case, the total topographic changes, without taking into account the minLoD, represented an increase of 31% of the net balance (-11,201 m3). These results were explained because changes in the surroundings of the pit were relatively of low magnitude, in the range of the minLoD (48% of the compared surfaces were below the minLoD). Therefore, this case study showed that special attention needs to be given to studies with expected changes in a similar order of the errors on the derived data products.

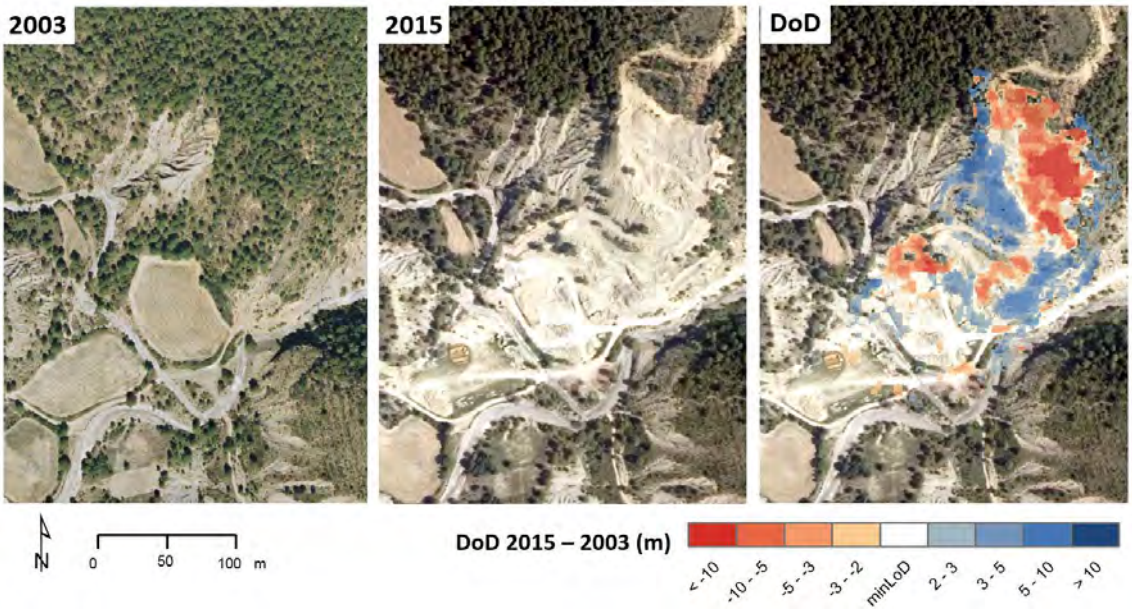


**Figure 13**. Open pit quarry case study. Orthomosaic of the years 2003 and 2015 (left and right). Thresholded DoD calculated from the difference between the 2003 and 2015 DEMs with the 2015 orthomosaic as background.

## FINAL CONSIDERATIONS AND CONCLUSIONS

In this article, we have presented and applied a methodology of great interest for the extraction of geomorphological information from historical aerial photographs at multiple temporal and spatial scales. The methodology was applied in two case studies located in the Upper Cinca River Catchment (Southern Pyrenees, Iberian Peninsula). Two different anthropogenic disturbances were analyzed with the objective to quantify the topographic changes associated with them. The significance of both impacts was relevant in terms of topographic changes (from –20 m to +15 m). The dominant topographic change (in extension) was related to sediment extraction in

the case of the road construction (51% of the surface), and deposition in the case of the pit quarry (27% of the area). The extension below the minLoD (data considered uncertain) was around 23% and 48% of the total study areas, respectively. These differences indicated that the magnitude of the changes was substantially higher in the case of the road construction. Even so, in both cases the net volume was negative, -913,710 and -16,197 m3 in the road and the quarry, respectively. Therefore, the differences between extension and volumetric changes indicated the role of the magnitude of both sediment extraction and deposition on the net changes. Three main conclusions can be drawn as:

1. The application of SfM-MVS to historical photos allows the acquisition of orthomosaics with relatively low errors when compared to standard methods.

2. The accuracy of the point clouds is heavily influenced by the characteristics of the photos (including the overlap) and by the quality of the Ground Control Points.

3. The magnitude of the processes to be analyzed or quantified determines the limits of the application of this workflow, in the sense that the magnitude of these processes must be higher than the propagated error of the topographic models or DEMs that are compared.

## Acknowledgments

This research was carried out within the framework of two research projects funded by the Spanish Ministry of Economy and Competitiveness: MORPHSED (CGL2012-36394) and MORPHPEAK (CGL2016-78874-R). The first author has a grant funded by the Spanish Ministry of Education Culture and Sports (FPU016/01687), while the third author is beneficiary of a Ramón y Cajal Grant of the Spanish Ministry of Economy, Industry, and Competitiveness (RYC-2010-06264). This manuscript has benefited from the work carried out during a Short Term Scientific Mission funded by the EU Cost Action Connecteur (ES1306: Connecting European Connectivity Research). Both authors are part of the Fluvial Dynamics Research Group-RIUS, which is a Consolidated Group recognized by the Generalitat de Catalunya (2014 SGR 645). Is appreciated the CERCA Program of the Generalitat de Catalunya. We thank all comments and suggestions received by two anonymous referees that have helped to improve the final version of the manuscript.

## REFERENCES

Arnaud F, Piégay H, Schmitt L, Rollet AJ, Ferrier V, Béal D. 2015. Historical geomorphic analysis (1932–2011) of a by-passed river reach in process-based restoration perspectives: The Old Rhine downstream of the Kembs diversion dam (France, Germany). *Geomorphology* 236: 163–177.

Bakker M, Lane SN. 2017. Archival photogrammetric analysis of river-floodplain systems using Structure from Motion (SfM) methods. *Earth Surface Processes and Landforms* 42: 1274–1286.

Begueria S, López-Moreno JI, Gómez-Villar A, Rubio V, Lana-Renault N, García-Ruiz JM. 2006 Fluvial adjustments to soil erosion and plant cover changes in the Central Spanish Pyrenees. *Swedish Society for Antropology and Geography* 88: 177–186.

Brasington J, Vericat D, Rychkov I. 2012. Modeling river bed morphology, roughness, and surface sedimentology using high resolution terrestrial laser scanning. *Water Resources Research* 48: 1-18.

Carrivick JL, Smith MW, Quincey DJ. 2016. *Structure from Motion in the Geosciences*. Wiley-Blackwell, 208 pp.

Cerovski-Darriau C, Roering JJ. 2016. Influence of anthropogenic land-use change on hillslope erosion in the Waipaoa River Basin, New Zealand. *Earth Surface Processes and Landforms* 41: 2167–2176.

Chen J, Li K, Chang KJ, Sofia G, Tarolli P. 2015. Open-pit mining geomorphic feature characterisation. *International Journal of Applied Earth Observation and Geoinformation* 42: 76–86.

Comiti F, Da Canal M, Surian N, Mao L, Picco L, Lenzi MA. 2011. Channel adjustments and vegetation cover dynamics in a large gravel bed river over the last 200 years. *Geomorphology* 125: 147–159.

Dugonjic S, Perani J, Ru I, Arbanas Ž. 2016. Analysis of a historical landslide in the Rječina River Valley, Croatia. *Geoenvironmental Disasters* 3: 1-9.

Gallart F, Llorens P. 2004. Observations on land cover changes and water resources in the headwaters of the Ebro catchment, Iberian Peninsula. *Physical Chemical Earth* 29: 769–773.

Garcia-Ruiz JM. 2010. The effects of land uses on soil erosion in Spain: a review. *Catena* 81: 1-11.

Gomez C. 2014. Digital photogrammetry and GIS-based analysis of the bio-geomorphological evolution of Sakurajima Volcano, diachronic analysis from 1947 to 2006. *Journal of Volcanology and Geothermal Research* 280: 1–13.

Gordon E, Meentemeyer RK. 2006. Effects of dam operation and land use on stream channel morphology and riparian vegetation. *Geomorphology* 82: 412–429.

Jones JA, Swanson FJ, Wemple BC, Snyder KU. 2000. Effects of roads on hydrology, geomorphology, and disturbance patches in stream Networks. *Conservation Biology* 14: 76–85.

Lague D, Brodu N, Leroux J. 2013. Accurate 3D comparison of complex topography with terrestrial laser scanner : Application to the Rangitikei canyon (NZ). *ISPRS Journal of Photogrammetry and Remote Sensing*. 82: 10–26.

Llena M, Vericat D, Martínez-Casasnovas JA. 2018. Apliación de algoritmos Structure from Motion (SfM) para el análisis histórico de cambios en la geomorfología fluvial. Cuaternatio y Geomorfología 32(1-2): 53-73.

López-Moreno JI, Begueria S, Valero-Garcés BL, García-Ruíz JM. 2009. Intensidad de las avenidas y aterramiento de embalses en el Pirineo Central español. *Ería Revista Cuatrimestral de Geografía* 61: 159–167.

Mertes JR, Gulley JD, Benn DI, Thompson SS, Nicholson LI. 2017. Using structure-from-motion to create glacier DEMs and orthoimagery from historical terrestrial and oblique aerial imagery. *Earth Surface Processes and Landforms* 42: 2350-2364.

Micheletti N, Chandler JH, Lane SN. 2015a. Structure from Motion (SfM) Photogrammetry. Photogrammetric heritage. *British Society for Geomorphology: Geomorphological Techniques* 2: 1–12.

Micheletti N, Lane SN, Chandler JH. 2015b. Application of Archival Aerial Photogrammetry to Quantify Climate Forcing of Alpine Landscapes. *The Photogrammetric Record* 30: 143-165.

Midgley NG, Tonkin TN. 2017. Geomorphology Reconstruction of former glacier surface topography from archive oblique aerial images. *Geomorphology* 282: 18–26.

Seitz SM, Diebel J, Scharstein D, Szeliski R. 2006. A Comparison and Evaluation of Multi-View Stereo Reconstruction Algorithms. *IEEE Computer Society Conference* 1: 519–528.

Semyonov D. 2011. Algorithms used in Photoscan [Msg 2]. Retrieved 3 May 2011. Message posted to www.agisoft.ru/forum/index.php?topic=89.0.

Surian N, Rinaldi M. 2003. Morphological response to river engineering and management in alluvial channels in Italy. *Geomorphology* 50: 307–326.

Smith MW, Carrivick JL, Quincey DJ. 2016. Structure from motion photogrammetry in physical geography. *Progress in Physical Geography* 40: 247–275.

Tague C, Band L. 2001. Simulating the impact of road construction and forest harvesting on hydrologic response. *Earth Surface Processes and Landforms* 151: 135–151.

Ullman S. 1979. *The interpretation of structure from motion*. The Royal Society, London. 203, 405–442.

Warrick JA, Ritchie AC, Adelman G, Adelman K, Limber W, Warrick JA, Limber PW. 2017. New techniques to measure cliff change from historical oblique aerial photographs and Structure-from-Motion Photogrammetry. *Journal of Coastal Research* 33: 39–55.

Westoby MJ, Brasington J, Glasser NF, Hambrey MJ, Reynolds JM. 2012. "Structure-from-Motion" photogrammetry: A low-cost, effective tool for geoscience applications. *Geomorphology* 179, 300–314.

Wheaton JM, Brasington J, Darby SE, Sear D. 2010. Accounting for Uncertainty in DEMs from Repeat Topographic Surveys: Improved Sediment Budgets. *Earth Surface Processes and Landforms* 35: 136-156.

## 2.4. Reach scale (CHAPTER 6)

### 2.4.1. Introduction and general overview

The objective of Chapter 6 is to analyse geomorphic responses in relation to natural and human disturbances during the last century in a mountain river reach. Methods developed in this section are based on the application of SfM photogrammetry to historical aerial photographs to extract multi-temporal spatial information (point clouds and orthomosaics), and subconsequent geomorphic information, of a 12 km long river reach. Three interrelated tasks compose the general workflow (Figure 14): A. Data acquisition, B. Post-processing, and C. Data preparation and results. **A. Data acquisition.** Geomorphic changes were characterized by multi-temporal aerial photographs processed by SfM photogrammetry in order to obtain orthomosaics and point clouds. The main direct channel disturbances analysed were floods, instream gravel mining (i.e. from data from the CHE) and land land use changes (i.e. from orthomosaics). **B. Post-processing.** DEMs from each study period were developed and DoDs computed. Additionally, two types of information were extracted from orthomosaics: (i) land use maps of the entire catchment (related to Chapter 5), and (ii) morphological maps showing the location an extension of main morphological units together with vegetation. Both maps were used to analyse changes through time and infer the magnitude of afforestation and geomorphic changes within the study period. **C. Data preparation and results.** Geomorphic responses and main disturbances were integrated in order to analyse statistical correlations between them, together with potential trends and breakpoints in these trends.

Part of this entire workflow (Figure 14), specifically the section explaining how to obtain point clouds and orthomosaics by application of SfM to historical photos for analysis of geomorphic changes at the reach scale, is fully explained in a scientific paper published in the *Cuaternario y Geomorphología* journal (see section 2.4.2 for further information about this paper; published in Spanish). It is also worth noting that part of this workflow is the same as the described in Chapter 5 (see section 2.3).

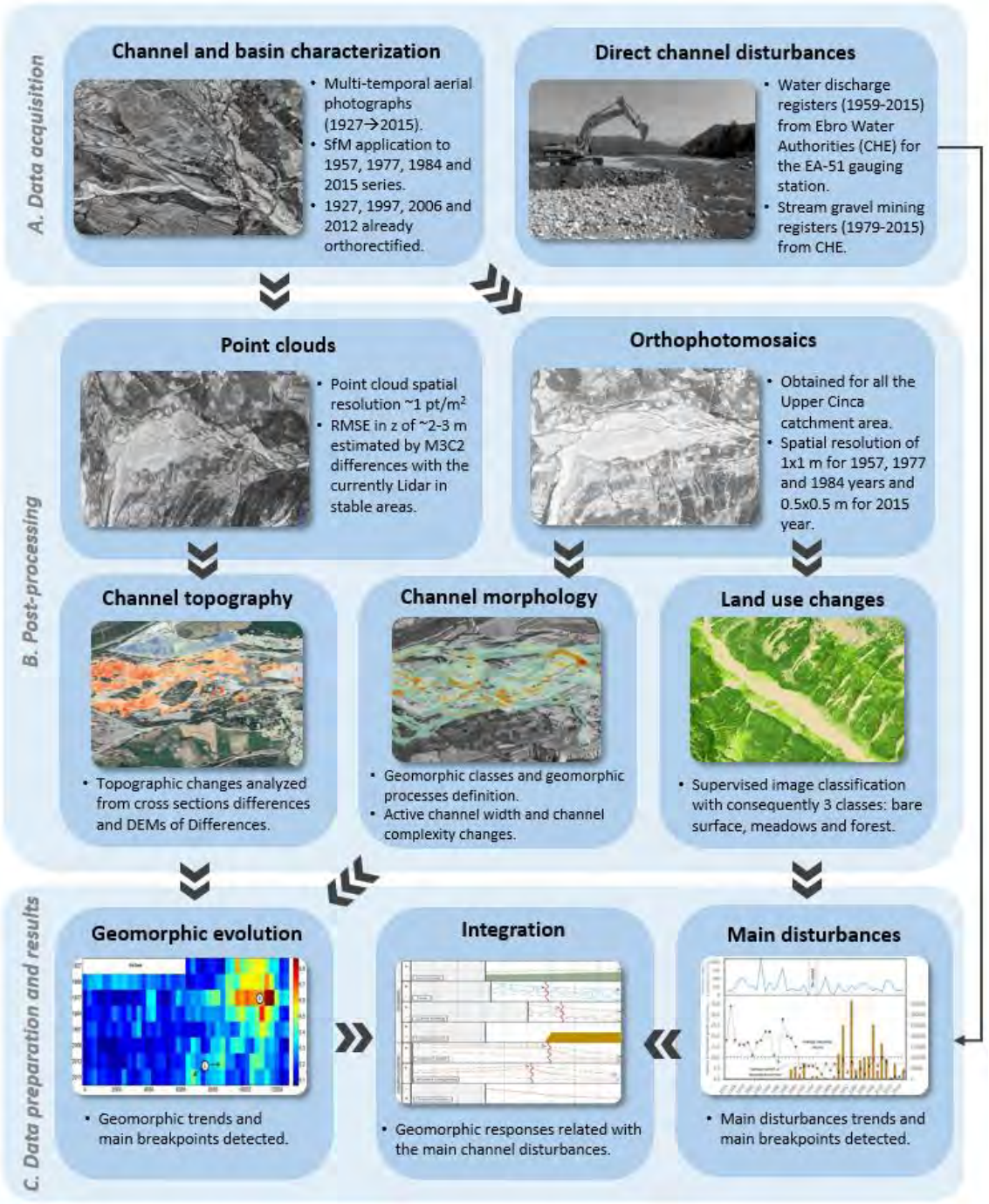


**Figure 14**. Summary of methodological workflow followed to analyse the geomorphic responses to natural and human disturbances in a mountain river at a reach scale (i.e. Chapter 6).

### 2.4.2. Study of historical fluvial geomorphic changes by SfM photogrammetry

This section contains the following accepted and already published paper in the journal *Cuaternario y Geomorfología.* SJR Impact Factor (2018): 0.270. Category: Earth Surface Processes; 3rd Quartile.

Llena M, Vericat D, Martínez-Casasnovas JA. 2018. Aplicación de algoritmos Structure from Motion (SfM) para el análisis histórico de cambios en la geomorfología fluvial. *Cuaternario y Geomorfología* 32(1-2): 53-73.

**ABSTRACT:** This work presents the workflow used to obtain spatial information to analyze geomorphological changes in the upper reach of the Cinca River (Southern Pyrenees) during the 1927-2015 period. The final products after application of the SfM-MVS methodology are orthomosaics with a root mean square error (RMSE) of 0.5-1 m, and point clouds with an RMSE of 1-2 m. The results of the study indicate that the study reach has suffered a clear reduction of the active channel width (i.e. 52%) with a high incision processes associated (e.g. >5m in some points), and a simplification in the channel pattern (i.e. reduction of the braiding index and changes from a multi-channel pattern to a single-channel one). These processes are directly influenced by the anthropogenic impacts associated with in-channel gravel mining and the associated impacts related to channel embankment (reach scale, localized impacts), and also influenced by the impacts on the production and transfer of sediment (catchment scale) due to land use changes since the 50s of the 20th century.

The methodology presented in this paper is very useful for the diagnosis of the morphosedimentary state of river systems. In the particular case of the Alto Cinca River, the results are of great interest for the improvement of the understanding of the cause-effect relationships in the morphosedimentary dynamics observed for the period 1927-2015. This improvement can help modify basin management plans through a more comprehensive view of contemporary processes.

**KEYWORDS**: *SfM-MVS; historical geomorphological analysis; fluvial dynamics.*

## INTRODUCCIÓN

El estudio evolutivo de la morfología fluvial ha sido tradicionalmente analizado mediante el análisis de los cambios en el cauce y en la llanura de inundación entre dos o más periodos temporales a partir de la interpretación de fotografías aéreas o mediante la repetición de observaciones topográficas. De manera general, son dos los tipos de análisis para este estudio: (a) el análisis planimétrico; y (b) el análisis altimétrico o topográfico (e.g. Vericat et al., 2017; Vericat y Batalla, 2016).

El análisis planimétrico por medio de la interpretación de mapas históricos y fotografías aéreas (e.g Batalla et al., 2006; Calle et al., 2017; Comiti et al., 2011; Ibisate et al., 2013; Sanchis-Ibor et al., 2017; Surian et al., 2009) permite la delimitación y caracterización de la geometría de unidades morfológicas. De esta forma, mediante la comparación de cartografía de sucesivos años, se puede observar la evolución morfológica en planta (e.g. cambios en la extensión de las unidades, variación de la anchura activa, frecuencia de canales), así como determinar las áreas en las que los procesos dominantes durante el período de estudio han sido de erosión o sedimentación (e.g. la desaparición de una barra indica que el proceso dominante entre el período analizado es erosivo). Existen varias incertezas y errores asociados a este tipo de análisis, como son por ejemplo los errores de georreferenciación (e.g. Vericat et al., 2009). La magnitud de estos errores está influenciada por el proceso de georreferenciación y la posterior creación del mosaico que se lleva a cabo mediante Sistemas de Información Geográfica (SIG). De la misma forma, la resolución de los datos también condiciona la calidad de los resultados, especialmente en los casos de las fotografías y mapas históricos en los que suele ser baja. El punto fuerte de esta metodología es que permite el estudio de la evolución morfológica para un amplio periodo temporal debido a la elevada disponibilidad de fotogramas y mapas históricos. Por el contrario, una de las limitaciones de esta metodología recae en la frecuencia en la que se dispone de sucesivos fotogramas o mapas, lo que significa que los cambios observados son el resultado del total de los procesos ocurridos entre períodos y, al incrementar la escala temporal, se integra la dinámica asociada a múltiples episodios competentes.

Dentro del análisis altimétrico o topográfico, la obtención de secciones topográficas permite caracterizar la geometría del cauce y evaluar los cambios topográficos entre periodos mediante la comparación de los perfiles de cada sección. Este método se limita a escalas de tramo (centenares de metros), y mediante la interpolación (i.e. propagación de los resultados entre secciones) se pueden obtener cambios volumétricos para el conjunto del tramo analizado. La baja densidad de observaciones hace que la fiabilidad y representatividad de las zonas interpoladas fuera de las propias secciones sea relativamente baja (Lane et al., 1994). Se trata de un método común hasta principios de siglo XXI debido a la limitación de las técnicas de adquisición de datos topográficos. Actualmente sigue siendo utilizado por algunos autores, sobre todo en trabajos donde el objetivo es el análisis histórico (e.g. Arnaud et al., 2015; Comiti et al., 2011; Moretto et al., 2014; Surian et al., 2009). Los avances en los campos de la geomática y la teledetección desde finales de los años 90 y principios del siglo XXI (ver la Figura 1 en Brasington et al., 2012 y en Passalacqua et al., 2015) ha permitido la obtención de información topográfica de elevada resolución. Esta información es fundamental para la creación de Modelos Digitales del Terreno (MDT) de tramos fluviales (e.g. Brasington et al., 2012; Williams, 2012; Williams et al., 2013). Así pues, los MDT permiten una representación continua de la superficie, simplificada por medio de celdas regulares, y de distinta tipología a la disponible a partir de secciones topográficas. Del mismo modo, la comparación entre MDT o DoD (DoD del inglés DEMs of Difference) permite observar la evolución topográfica, pudiendo localizar y cuantificar los procesos de erosión y sedimentación que hayan tenido lugar en un tramo determinado (Brasington et al., 2000; Lane et al., 1996; Vericat et al., 2017; Wheaton et al., 2010).

En la actualidad, los avances en el post-proceso de imágenes aéreas (e.g. nuevos algoritmos, mejoras computacionales) han permitido desarrollar una novedosa, rápida y económica metodología basada en técnicas de fotogrametría clásica. Los algoritmos Structure from Motion y Multi View Stereo (SfM-MVS) permiten la identificación espacial de puntos comunes en diferentes fotografías, habitualmente más de tres. A partir de estos puntos se orientan y localizan las cámaras y, posteriormente, se obtiene una nube de puntos (i.e. información topográfica) en tres dimensiones, así como ortomosaicos rectificados geométrica y geográficamente (i.e. información planimétrica; ver más detalles del método en Carrivick et al., 2016; Micheletti et al., 2015a; Smith et al., 2016; Ullman, 1979). Los algoritmos SfM-MVS no requieren información interna de las cámaras (e.g. lentes) ni datos de orientación ni ubicación 3D de las mismas para la reconstrucción de la escena (Westoby et al., 2012). Aun así, el establecimiento de una red de puntos de control topográficos permite el registro de la información a un Sistema de Coordenadas Geográfico (georreferenciación) para la comparación de la información o la integración con datos ya disponibles y registrados. Además, esta técnica es, junto con las técnicas de láser terrestre, la que mayor versatilidad ofrece para garantizar altas densidades de información de elevada resolución a escalas espaciales amplias (e.g. Smith y Vericat, 2015).

Desde el punto de vista del análisis histórico, este enfoque metodológico ofrece un amplio abanico de posibilidades para el estudio geomorfológico. Por un lado, a partir de fotografías aéreas con cierto solape es posible extraer atributos topográficos relativos de las zonas a las cuales representan, los cuales tendrán una resolución directamente dependiente de la resolución y solape de las fotografías, y de los puntos de control desde los cuales se registre la información para obtener valores relativos a un Sistema de Coordenadas determinado. Por otro lado, los ortomosaicos permiten el estudio planimétrico de unidades de interés y su evolución. En este contexto, este artículo presenta un flujo de trabajo para la obtención de información topográfica y ortomosaicos a partir de SfM-MVS aplicada a fotografías aéreas históricas para el análisis morfológico de cauces fluviales. La metodología se aplica en un tramo de 13 km del Alto Cinca (aguas arriba del municipio de Aínsa, Huesca; Pirineo Central) durante el periodo de tiempo comprendido entre los años 1927 y 2015. Mediante la aplicación de esta metodología es posible realizar un diagnóstico del estado morfológico de la zona de estudio para cada una de las series temporales, así como los procesos y cambios geomorfológicos sucedidos entre dichas series. Es importante remarcar que, en el caso particular de la cuenca del Alto Cinca, parte de este enfoque metodológico ha sido presentado por Llena et al. (2018). Este trabajo se centra en análisis de cambios topográficos a causa de la construcción de una carretera en una ladera y la extracción de piedra de una cantera a cielo abierto, teniendo en cuenta el análisis y la propagación de errores de los correspondientes modelos, lo cual busca un objetivo distinto con respecto al presente artículo.

## ÁREA DE ESTUDIO

La cuenca del Alto Cinca ocupa una superficie de 848 $km^2$ y está localizada en la cabecera del río Cinca, dentro de la cuenca del Ebro. El tramo de estudio se sitúa en la parte baja de la cuenca y abarca 13 km de río entre el municipio de Escalona y el embalse de Mediano, en las inmediaciones del municipio de Aínsa (Huesca). En este tramo se reduce claramente la pendiente respecto al tramo de aguas arriba, comportándose como una zona receptora de todo el sedimento procedente de las cabeceras. Se trata de un tramo muy dinámico, con múltiples canales, barras sedimentarias de distinta tipología y con distintos niveles de vegetación. El promedio de la anchura del canal activo está entorno a los 200 m, mientras que la profundidad media con caudales medios es de 0,3 m. La granulometría superficial va desde arenas a grandes

bloques (i.e. 0,5 a 2000 mm), con una mediana del tamaño de los sedimentos superficiales de alrededor de los 64 mm (ver más detalles de la zona de estudio en Béjar et al., 2017 y Béjar et al., 2018). El tramo de estudio ha sufrido importantes impactos antrópicos que han afectado directa o indirectamente la geomorfología del lecho fluvial, especialmente a partir de la segunda mitad de siglo XX. Impactos que van desde los cambios en los usos del suelo y el abandono rural, los cuales han tenido un efecto importante sobre la transferencia de agua y sedimentos (e.g. Beguería et al., 2006; García-Ruíz et al., 1996), hasta impactos directos en el cauce como son las extracciones de áridos y la construcción de escolleras, especialmente a partir de los años 1980 del siglo XX. Así, se trata de un tramo en el que la morfología fluvial del cauce ha cambiado substancialmente, especialmente a partir de los años 1950-1960 del siglo XX (Figura 15B), lo que permite un contexto muy propicio para la aplicación y evaluación de la metodología que se presenta en este trabajo.

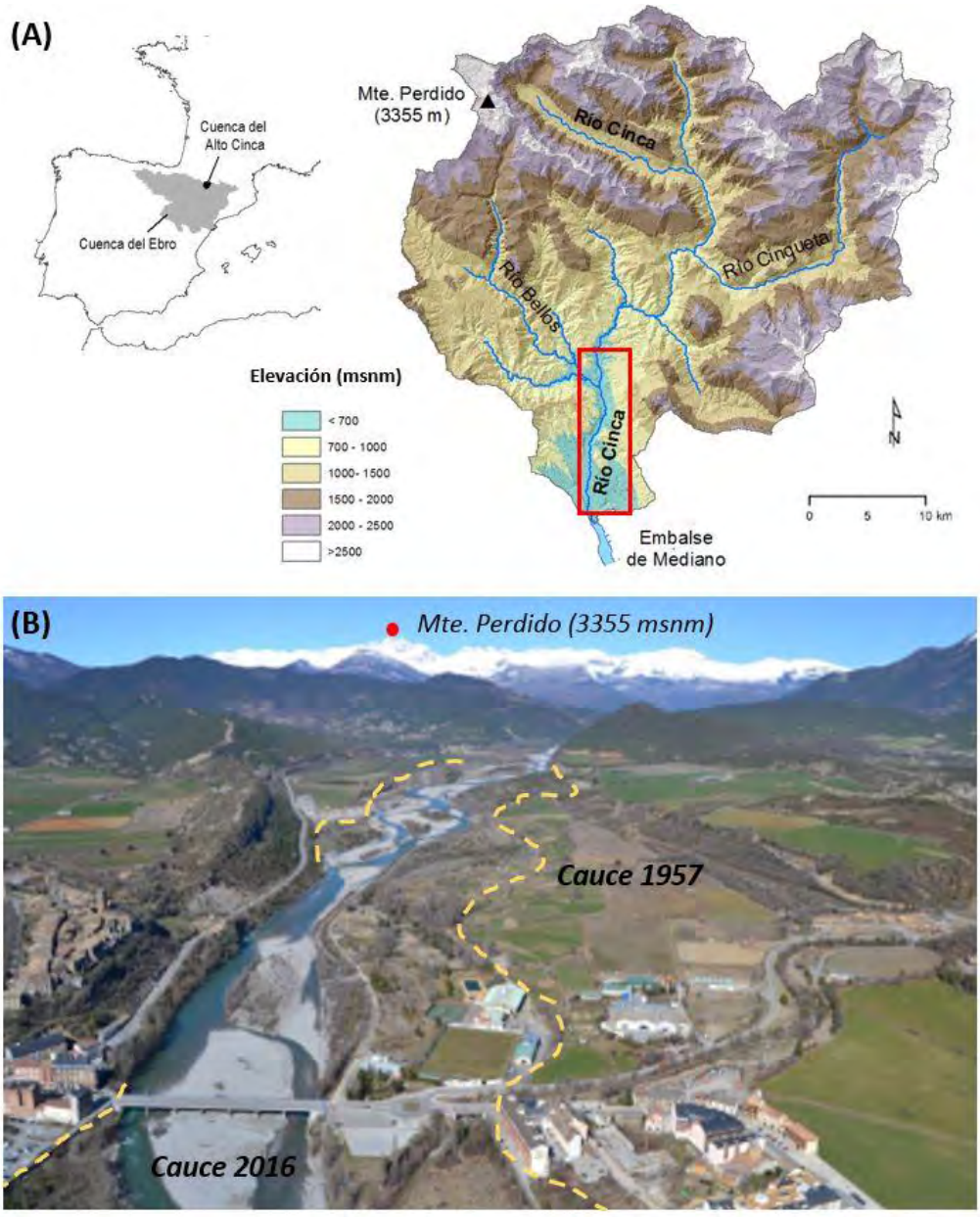


**Figura 15**. **A.** Localización del área de estudio dentro del contexto de la Península Ibérica y Cuenca del Alto Cinca. **B.** Imagen del tramo bajo de la zona de estudio con los límites aproximados del cauce activo en 1957 y 2016 respectivamente.

## METODOLOGÍA

El flujo metodológico que se ha llevado a cabo en el presente artículo se presenta en forma de diagrama esquemático en la Figura 16. La metodología consta de 5 bloques. Los apartados descritos a continuación corresponden a la explicación detallada de cada uno de los bloques del diagrama. Con el objetivo de optimizar el espacio y la representatividad de las figuras, el tramo que aparece cartografiado en las figuras corresponde a la parte baja del tramo de estudio (i.e. 3 km), el cual es representativo de los procesos y cambios geomorfológicos que ha tenido el conjunto del tramo de estudio (i.e. 13 km).

### Fotografías aéreas históricas

La selección de los fotogramas y los periodos temporales de análisis viene determinada por su disponibilidad, el grado de solape, la calidad y la resolución de los mismos. De este modo, en el caso particular del Alto Cinca y para el periodo de estudio comprendido entre el año 1927 y 2015, se analizaron las siguientes series temporales: 1927, 1957, 1977, 1984, 1997, 2006, 2012 y 2015. De estas, se pudieron obtener fotografías aéreas con solape de las series de los años 1957, 1977, 1984 y 2015, mientras que para el resto de las series solo se pudo obtener ortomosaicos ya ortorectificados (años 1997, 2006 y 2012) y fotoplanos sin referencia espacial ni solape (año 1927), los cuales fueron georreferenciados mediante un SIG (ArcGIS 10.3). Así, para estas últimas series no se extrajo información topográfica, obteniendo solo información morfológica en planta. En cuanto a las fuentes de información, todas las series fotográficas históricas fueron adquiridas del Centro Nacional de Información Geográfica (CNIG) a excepción de a) los fotoplanos de 1927 que pertenecen a la Confederación Hidrográfica del Ebro (CHE); b) la serie de 1957 que se obtuvo del Centro Cartográfico y Fotográfico del Ejército del Aire (CECAF); y c) la serie de 1997 que se obtuvo del Centro de Información Territorial de Aragón (CINTA). Debido a que el formato original de los fotogramas históricos es el analógico, para poder procesarlos mediante algoritmos SfM-MVS, las imágenes se escanearon mediante un escáner fotogramétrico de alta resolución (1200 dpi) y se transformaron en un formato de imagen digital (i.e. TIF). El escaneo y envío de los fotogramas se realizó por parte de los organismos con titularidad de los fotogramas (Tabla 1).

La única serie temporal que no se obtuvo por medio de estas fuentes fue la del año 2015, la cual se tomó como serie contemporánea de referencia. Esta fue facilitada por el Grupo de Investigación de Dinámica Fluvial de la Universidad de Lleida (RIUS). Estas fotografías forman parte del proyecto de investigación MorphSed dentro del cual se enmarca el presente artículo (ver referencia en los agradecimientos). Los fotogramas se tomaron con un vuelo bajo (máx. 200 m de altura) realizado con un autogiro biplaza tripulado. El resultado fue un ortomosaico de alta resolución (0,1 m), así como información topográfica de elevada densidad con errores medios cuadráticos (i.e. RMSE de sus siglas en inglés Root Mean Square Error) por debajo de los 0,05 m (ver más detalles en Vericat et al., 2016).

Una vez obtenidas las fotografías, el siguiente paso consistió en el pre-proceso de las mismas para facilitar y mejorar el proceso fotogramétrico. En primer lugar, se realizó una corrección de la imagen mediante el ajuste del contraste y exposición con el software Adobe Photoshop Lightroom© 6.6.1. En segundo lugar, mediante la herramienta de enmascaramiento del propio software SfM (i.e. Agisoft Photoscan Profesional 1.2.2 en el presente estudio), se eliminaron los marcos de los fotogramas en los cuales sale reflejada cierta información técnica (e.g. marcas fiduciarias, altura de vuelo, focal cámara), así como otros elementos que pudieran provocar distorsiones en el proceso fotogramétrico (e.g. partes aeroplano, zonas borrosas).

**Puntos de control de terreno (GCP)**

El primer paso para realizar la georreferenciación consiste en la creación y establecimiento de una red homogénea de puntos de control (i.e. GCPs; de sus siglas en inglés Ground Control Points) alrededor del tramo de estudio. Existen varios autores que ofrecen diferentes pautas para establecer el número y la distribución de los GCPs para la obtención de mosaicos a partir de fotografías aéreas de distinta resolución con el objetivo de evaluar los cambios geomorfológicos en cauces fluviales (e.g. Hughes et al., 2006; Leys y Werrity, 1999; Muñoz-Narciso et al., 2014; Vericat et al., 2009). Leys y Werrity (1999) o Muñoz-Narciso et al. (2014) señalan que la manera de minimizar los errores de georreferenciación recae en la localización de los GCPs con un patrón perimetral sobre una amplia distribución. Este criterio es apropiado en fotografías aéreas que tienen relativamente poco error, ya sea debido a zonas de poco relieve o fotografías con una alta resolución. En cambio, Hughes et al. (2006) indica que se consigue un menor error de georreferenciación mediante la concentración de GCPs cerca de las áreas de interés. En el caso del presente trabajo, se tuvo en cuenta una combinación de ambos criterios, intentando tener una densidad de GCPs constante en todo el tramo. Se debe remarcar que se tiene una fuerte dependencia del hecho que existieran GCPs identificables en el máximo número de series posibles para que estos sean válidos para todas (i.e. puntos en los que la topografía no se haya modificado).

En el caso particular del Alto Cinca, la elección de los puntos de control se basó en la localización de puntos identificables desde las fotografías en zonas que potencialmente no hayan variado de posición (i.e. x, y, z) a lo largo del tiempo (e.g. cruces de caminos, lindes de campos, construcciones bajas). Es importante evitar la selección de puntos de control en elementos volumétricos o con una geometría irregular puesto que esto podría producir errores importantes en la cota de la nube de puntos final. Para la identificación de estos puntos de control se eligió como referencia el ortomosaico del año 2012 del PNOA (Plan Nacional de Ortofotografía Aérea) así como la consulta de las fotografías aéreas de las series fotográficas de los años 1927, 1957, 1977 y 1984. Se digitalizaron un total de 95 GCPs en el tramo de estudio, con una densidad aproximada de 2 GCP $km^{-1}$. Para evaluar la sensibilidad de los errores a la densidad de la red de control, se redujo alrededor del 50% el número de puntos iniciales (45 puntos). Esta reducción supuso un incremento del error del modelo resultante de 0,6 m a 2 m. Todo ello indica, tal y como ya se ha discutido en diversos estudios ya expuestos (e.g. Hughes et al., 2006; Leys y Werrity, 1999; Muñoz-Narciso et al., 2014; Vericat et al., 2009), la necesidad de tener en cuenta la distribución de los puntos de control y su densidad para reducir las fuentes de incertidumbre en el post-proceso y así reducir los errores a valores que se adapten al objeto de estudio.

Tal y como se ha introducido, las coordenadas planimétricas (x, y) de los GCPs se extrajeron del ortomosaico del año 2012 del PNOA, la cual utiliza el sistema de coordenadas UTM ETRS 1989 Huso 31. Por otro lado, la información de la cota o elevación (z) se extrajo del levantamiento LIDAR del CNIG del año 2010, el cual tiene una densidad de 0,5 puntos $m^{-2}$ y precisión de <0,2 m (RMSE de la coordenada z). Para validar esta información se realizaron mediciones en campo mediante un GPS diferencial Leica VIVA® GS15 con corrección RTK que permite obtener información topográfica (x, y, z) con errores inferiores a los 0,05 m (errores 3d, integración de las tres coordenadas). Se tomaron las cotas de 35 del total de puntos fijos localizados (i.e. 32 % de los GCP). Los errores (i.e. RMSE) en cota se situaron en 0,6 m RMSE. Este ejercicio permite concluir que se dispone de una red de control con errores aceptables teniendo en cuenta: que los errores asociados al proceso de georreferenciación de fotografías aéreas históricas suelen estar entre los 2 y los 5 metros (e.g. Arnaud et al., 2015; Clerici et al., 2015; Comiti et al., 2011; Surian et al., 2009); y la precisión del LIDAR utilizado para extraer la elevación o cota de los GCPs. Pese a ello, se debe señalar que existe mucha incertidumbre asociada al hecho de suponer que

estas alturas son iguales en todas las series temporales, puesto que, pese a tratarse de puntos considerados fijos o estables, en los que es difícil que se produzcan variaciones topográficas, los resultados indican que existe una considerable incertidumbre asociada (i.e. 0,6 m). De este modo, para la elaboración de modelos con la máxima rigurosidad, lo óptimo sería disponer de coordenadas (x, y, z) tomadas en campo para cada una de los periodos de análisis, información difícil de obtener cuando se realizan estudios evolutivos en los que existen series temporales muy amplias.

**Proceso fotogramétrico**

*Aplicación de Structure from Motion (SfM)*

Las imágenes fueron post-procesadas fotogramétricamente mediante el software Agisoft Photoscan Profesional 1.2.2. El primer paso consiste en la importación y alineamiento de las fotografías. En este proceso, el software busca elementos comunes visibles en varias fotografías desde diferentes puntos de vista e identifica su correspondencia. Posteriormente, mediante una serie de algoritmos se estima la geometría en 3D de la escena, tanto las coordenadas de los puntos comunes encontrados, como la posición de las cámaras (i.e. calibración extrínseca) y los parámetros internos de la cámara (i.e. calibración intrínseca; Ullman, 1979). Así pues, se genera una primera nube de puntos de baja densidad dentro de un sistema de coordenadas local. Cabe destacar que en la actualidad existen ya algunos trabajos que describen de manera detalla la metodología SfM con aplicaciones sobre el estudio geomorfológico. En este artículo tan solo proporcionamos información general de este proceso (ver más detalles e.g. Carrivick et al., 2016; Micheletti et al., 2015a; Smith et al., 2016).

Cuando se trabaja con fotogramas históricos, existen dos factores determinantes que condicionan la calidad final de los productos: a) el solape entre fotogramas y b) la calidad de los mismos (Micheletti et al., 2015b; Bakker y Lane 2016). Para identificar un elemento común es necesario un mínimo de dos fotogramas, pero se recomienda un mínimo de 3 para validar geométricamente dicho punto, puesto que la fiabilidad de éste aumenta cuando sea identificado desde un mayor número de fotografías (i.e. mayor solape entre fotogramas). En el caso de los fotogramas históricos del presente artículo (i.e. 1957, 1977 y 1984), esto supone un importante limitante puesto que casi el 80 % de los puntos de la nube de baja densidad solo es visto desde 2 fotogramas, existiendo muchos vacíos (sin datos) en el área de estudio debido a la inexistencia de solape. En cuanto a la calidad de la imagen del fotograma, ésta determina la textura del mismo, que es la que facilita la identificación de elementos comunes. En fotogramas históricos, la calidad de la imagen se ve afectada en muchas ocasiones en el proceso de escaneado, el cual no siempre se hace con la resolución o cuidados necesarios, lo que propicia la pérdida de calidad de las imágenes (e.g. zonas borrosas, presencia de artefactos) y un consecuente incremento de errores en el proceso de alineación. Estos dos factores limitantes pueden generar errores importantes y en algunos casos, en zonas en la que la calidad de la imagen es baja se observa en la nube de puntos una especie de superficie abultada de hasta ± 2 m.

Este hecho condiciona el tipo de análisis que se haga de las nubes de puntos históricas, limitando el estudio de cambios topográficos a casos donde los errores de cota en las nubes de puntos superan la magnitud del cambio observado. Por otro lado, en los casos que se aplica SfM-MVS sobre fotogramas históricos, existe otra posible fuente de error importante. Se trata de vuelos que se planificaron con criterios basados en la fotogrametría clásica, por lo que la geometría de la toma vertical y los ejes paralelos pueden dar lugar a importantes errores sistemáticos no lineales tipo “domo” (e.g. Wackrow y Chandler, 2008; Eltner y Schneider, 2015).

*Georreferenciación*

La corrección geométrica o georreferenciación de la imagen es una transformación que implica cambiar de posición y escala de los pixeles de una imagen original, para dotarla de coordenadas reales (Chuvieco, 1995). La georreferenciación de la nube de puntos requiere las tres coordenadas espaciales (x, y, z) de distintos puntos de control (GCPs). En el caso de Agisoft Photoscan Profesional 1.2.2, la georreferenciación se realiza mediante un modelo lineal obtenido a partir de 7 parámetros de transformación: 3 parámetros de translación; 3 de rotación y 1 de escala. Por otro lado, el software permite calibrar las cámaras de manera automática para minimizar los errores asociados a las distorsiones ocasionadas mayoritariamente por la lente. Se trata de un proceso automatizado que mejora substancialmente la calidad de los resultados. Adicionalmente, es posible realizar una optimización de la georreferenciación que se basa, de manera general, en la minimización de la suma de errores de georreferenciación a partir de la modificación reiterativa de la posición estimada para todas las cámaras. Estos pasos permiten una reducción substancial de los errores de georreferenciación. En el caso de este trabajo, mediante este proceso, los errores (i.e. RMSE) se redujeron un orden de magnitud, de un promedio de 30-50 m a 3-5 m.

Una vez realizada la optimización se analizan los errores asociados a cada uno de los GCPs en relación a su posición espacial dentro del modelo georreferenciado. Antes de aceptar la georreferenciación se deben eliminar aquellos GCPs con errores muy elevados (i.e. valores atípicos). Además, en el presente estudio, también se eliminaron los GCPs que presentaban errores que se consideraron superiores al umbral de aceptación en función a la resolución de la información. El umbral de aceptación en el presente estudio fue de 1 m (i.e. 1,7 veces el RMSE de la validación de campo de los GCPs, ver sección 3.2). Una vez eliminados estos GCPs, se comprobó la validez de dicha modificación mediante la actualización del proceso de georreferenciación. Este proceso permite disminuir la magnitud de los errores de georreferenciación. En el caso particular del alto Cinca los errores (RMSE) de georreferenciación para los modelos de las series de 1957, 1977 y 1984 fueron de 0,72, 0,62 y 0,66 m respectivamente, un 80% inferiores a los errores iniciales, eliminando menos de un 5 % del total de los GCPs (i.e. valores atípicos).

*Obtención de nubes densas de puntos*

Una vez obtenida la nube de puntos de baja densidad georreferenciada dentro de un sistema de coordenadas conocido, el siguiente paso consiste en la aplicación de distintos algoritmos (e.g. *Multi View Stereo*; MVS) para incrementar la densidad de la nube de puntos al menos dos órdenes de magnitud. Existen varios tipos de algoritmos MVS (Seitz et al., 2006; Smith et al., 2016). Agisoft Photoscan Profesional 1.2.2 usa una combinación de métodos basados en el cálculo del mapa de profundidad por pares (i.e. *Smooth* y *Height-field*) y un método basado en un enfoque de múltiples vistas (i.e. *Fast method; Semyonov, 2011*). Si se está interesado en los algoritmos específicos de cálculo sería necesario una revisión detallada de la versión y los métodos de cálculo (revisión más allá del objetivo del presente estudio).

*Ortorectificación y obtención de ortomosaicos*

El último paso en el flujo de trabajo fotogramétrico consiste en el proceso de ortorectificación. Mediante este proceso se obtiene una única fotografía corregida geográfica y geométricamente gracias a la información espacial que aporta la nube de puntos georreferenciada. En este proceso se realiza una corrección del color en las zonas de límite entre fotogramas mediante

homogeneización de los histogramas de las fotografías colindantes. En el caso del Alto Cinca, la resolución del tamaño de pixel seleccionada fue de 1 m para todos los ortomosaicos producidos.

**Post-procesado**

Los productos (i.e. nubes de puntos y ortomosaicos) obtenidos a partir de esta metodología son post-procesados con el fin de mejorar la interpretación y análisis de la información producida. El post-proceso de la información resultante se basa en cuatro procedimientos: (1) Co-registro; (2) Clasificación supervisada de las imágenes; (3) Regularización de la información; y (4) Obtención de los MDTs.

(1) Pese a que los errores en el proceso de georreferenciación de la nube de puntos son relativamente bajos, existen zonas (principalmente las más alejadas de los GCPs) que pueden sufrir errores de posicionamiento y orientación superiores, especialmente en nubes de puntos extraídas de fotogramas históricos con baja calidad de la imagen. Con el objetivo de minimizar los errores asociados a este hecho, es recomendable aplicar el co-registro de cada una de las nubes de puntos históricas con la nube de puntos de referencia (LIDAR del año 2010). Este proceso permite reajustar la nube de puntos obtenida a partir de zonas comunes entre esta y una de referencia. Estas zonas deben cumplir el requisito de que no se hayan desplazado (i.e. x, y, z) entre los períodos de estudio. En el caso de este estudio se utilizó el software CloudCompare 2.6.2 para la realización de dicho proceso. Posteriormente, se compararon las nubes de puntos obtenidas y la del LIDAR de zonas estables (i.e. afloramientos rocosos sin cobertura vegetal). Este análisis permite estimar el error de las nubes de puntos obtenidas una vez realizado el co-registro de la información. En el caso del Alto Cinca, la comparación de las nubes de punto se realizó mediante el algoritmo M3C2, incluido en el software libre CloudCompare 2.6.2, el cual permite realizar una comparación entre nubes de puntos teniendo en cuenta irregularidades topográficas y la rugosidad de la superficie, así como introducir un valor mínimo de detección para tener en cuenta las incertidumbres en los cálculos de diferencia (Lague et al., 2013). En todos los casos se obtuvieron diferencias en cota inferiores a los 2 m, siendo inferior a los 0,5 m en el caso de la nube de puntos de 1957.

(2) Se recomienda realizar la clasificación supervisada de los ortomosaicos de cada una de las series de estudio con el fin de eliminar los puntos de las diferentes nubes de puntos que estuvieran dentro de las zonas clasificadas como vegetación o agua, y de esta manera eliminar la incertidumbre de cota asociada a estos.

(3) Una vez filtradas las nubes de puntos, el siguiente paso consiste en la regularización de las nubes de puntos mediante técnicas de geoestadística. Para ello se utilizó el algoritmo ToPCAT de libre distribución desarrollado por Brasington et al., (2012) e implementado en ArcGIS 10.3 a través de Geomorphic Change Detection (GCD, disponible en http://gcd.joewheaton.org/; ver más detalles metodológicos del GDC en Wheaton et al., 2010). ToPCAT permite definir una malla regular de análisis que se superpone a la nube de puntos y, para cada conjunto de datos ubicados en cada una de las celdas de la malla calcula una serie de estadísticos: (a) el número total de observaciones (n); (b) el valor mínimo de elevación ($z_{min}$) y su posición exacta en el espacio (i.e. x, y); (c) el valor máximo de elevación ($z_{max}$) y su posición exacta (i.e. x, y); (d) la elevación media ($z_{mean}$) dentro de la celda; (e) la desviación estándar de los valores de elevación en cada celda; y (f) la desviación estándar de las elevaciones (ver más detalles en Brasington et al., 2012).

(4) En el caso del Alto Cinca, la variable seleccionada de los resultados de ToPCAT para la elaboración de los MDTs fue el valor medio de cada celda. En cuanto a la resolución, teniendo en cuenta la resolución y errores en el proceso y el objetivo del estudio, se seleccionó un tamaño

de celda de análisis de 5 m. El método seleccionado para la creación de los MDTs de cada uno de los periodos de estudio fue la interpolación mediante el método de Vecino natural en ArcGIS 10.3.

**Obtención de resultados: Análisis morfológico (planta) y topográfico (cota)**

Desde el punto de vista del análisis morfológico en planta, a partir de los ortomosaicos y mapas de clases obtenidos a partir de las clasificaciones supervisadas de éstos, se puede realizar una primera clasificación y cartografía de las unidades morfológicas del cauce del río en cada una de las series de estudio. Entendiendo como unidad morfológica las diferentes tipologías de estructuras sedimentarias presentes en el tramo de estudio (barras sedimentarias; e.g. Church y Jones 1982). En la Figura 17A se puede observar un ejemplo de las unidades identificadas y cartografiadas en este trabajo. A partir de la caracterización morfológica realizada para cada una de las series de estudio se analiza la evolución de la geomorfológica del cauce lo largo de todo el periodo. En el caso específico del Alto Cinca, las variables que se tuvieron en cuenta para ello son: anchura activa del cauce, índices de multiplicidad de canales y matrices de cambio morfológico. El análisis de la anchura activa a lo largo de todo del tramo de estudio se puede realizar mediante la observación de la amplitud de una serie de secciones transversales comunes para todas las series, con una separación regular entre sección (longitudinalmente). En el caso de este artículo la separación fue de 300 m (Figura 18A). Los índices de multiplicidad permiten cuantificar el grado de complejidad morfológica para un momento determinado, observando su evolución a lo largo del tiempo mediante la comparación entre series (Figura 18B). Los índices seleccionados en el presente artículo fueron: el índice de número de canales de Hong y Davies (1979); el índice de sinuosidad según Mosley (1981) y el índice de barras sedimentarias según Germanoski y Schumm (1993). Cabe destacar que muchos de estos índices, así como la anchura activa, son dependientes del caudal que circula en el momento de la toma de las fotografías y su interpretación se tiene que realizar teniendo en cuenta este hecho. Finalmente, el análisis de los cambios de las unidades morfológicas a lo largo del periodo de estudio se hizo a través de la combinación analítica de series temporales (matrices de cambio; Figura 17B). Este análisis se basa en la intersección de capas entre distintos periodos, tanto consecutivos como no consecutivos, y el cálculo de cambios que se atribuyen a cada pixel de análisis. Por ejemplo, si un determinado pixel se encuentra en el año 1957 en una zona categorizada como barra sedimentaria y en el año 2012 ha pasado a canal de aguas bajas, consideraremos que ha sufrido un proceso de erosión. Por otro lado, si sucede lo contrario, y este pixel pasa de canal de aguas bajas a barra sedimentaria se considerará que se ha producido un proceso de sedimentación (Figura 17B).

Mientras que el análisis morfológico en planta tiene como objetivo el estudio de cambios geomorfológicos planimétricos, el análisis altimétrico o topográfico en cota tiene como objetivo del estudio de los cambios topográficos del cauce activo. El análisis topográfico se realizó mediante la comparación de modelos de superficies (2D) o MDTs con cálculos básicos de álgebra de mapas disponible en todos los softwares de SIG (Figura 19). Es importante remarcar las limitaciones de estos cálculos asociadas a la exactitud de las nubes de puntos obtenidas (información topográfica), los posibles errores asociados a la interpolación para obtener los MDTs, y la superficie ocupada por el cauce activo mojado y la vegetación. En ambos casos no es posible obtener información topográfica del terreno e influenciará a los cálculos correspondientes.

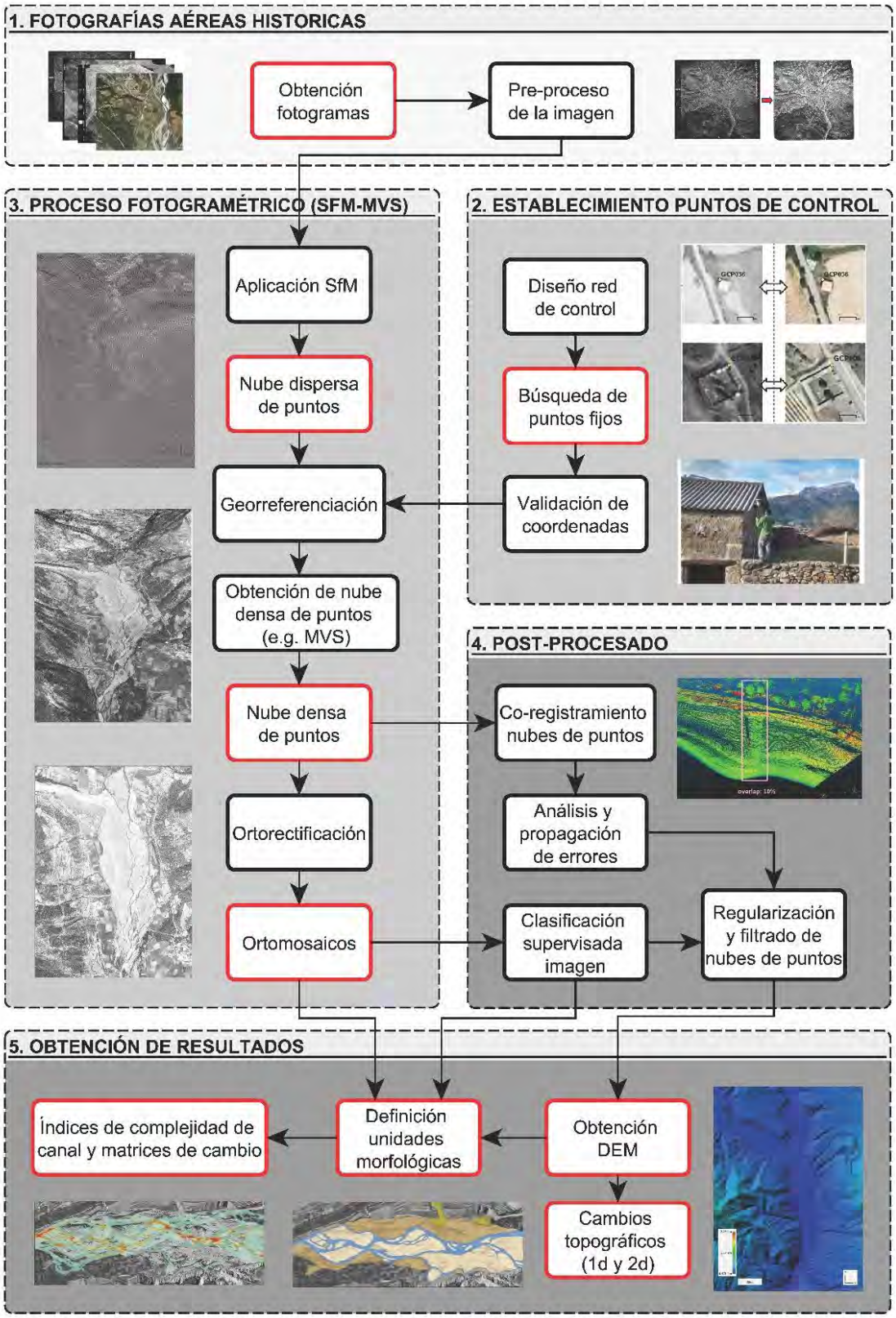


**Figura 16**. Flujo de trabajo para la obtención de ortomosaicos e información topográfica a partir de fotografías aéreas: **1.** Obtención de fotografías aéreas históricas; **2.** Establecimiento puntos de control; **3.** Proceso fotogramétrico (SfM-MVS); **4.** Post-procesado de los productos; y **5.** Obtención de resultados. Los cuadros rojos corresponden a los inputs y outputs mientras que los negros corresponden a procesos.

## RESULTADOS: EVOLUCIÓN MORFOLÓGICA DEL ALTO CINCA

A partir de los cambios morfológicos en planta se observó cierta tendencia a la reducción de las barras centrales, mientras que las barras laterales se mantuvieron más o menos estables (Figura 17A). El resto de tipologías de barras no siguió ningún patrón evolutivo a lo largo del tiempo, a excepción de las barras de confluencia o de tributario, las cuales siguieron un patrón claramente decreciente. Esta reducción del tamaño de este tipo de acumulaciones pudo ser debida a la disminución del aporte sedimentario de los tributarios laterales, causado probablemente por la combinación de múltiples factores como la reducción de las tasas de erosión por los cambios de los usos del suelo y el aumento de la cubierta vegetal, la desconexión sedimentaria de estos tributarios respecto al cauce principal debido al confinamiento lateral causado por la construcción de escolleras, o el déficit de sedimentos asociado a las extracciones de áridos y los posibles cambios en la capacidad de transporte del río debido a la concentración del flujo asociado a la reducción de la anchura activa del cauce por las escolleras (Figura 18A).

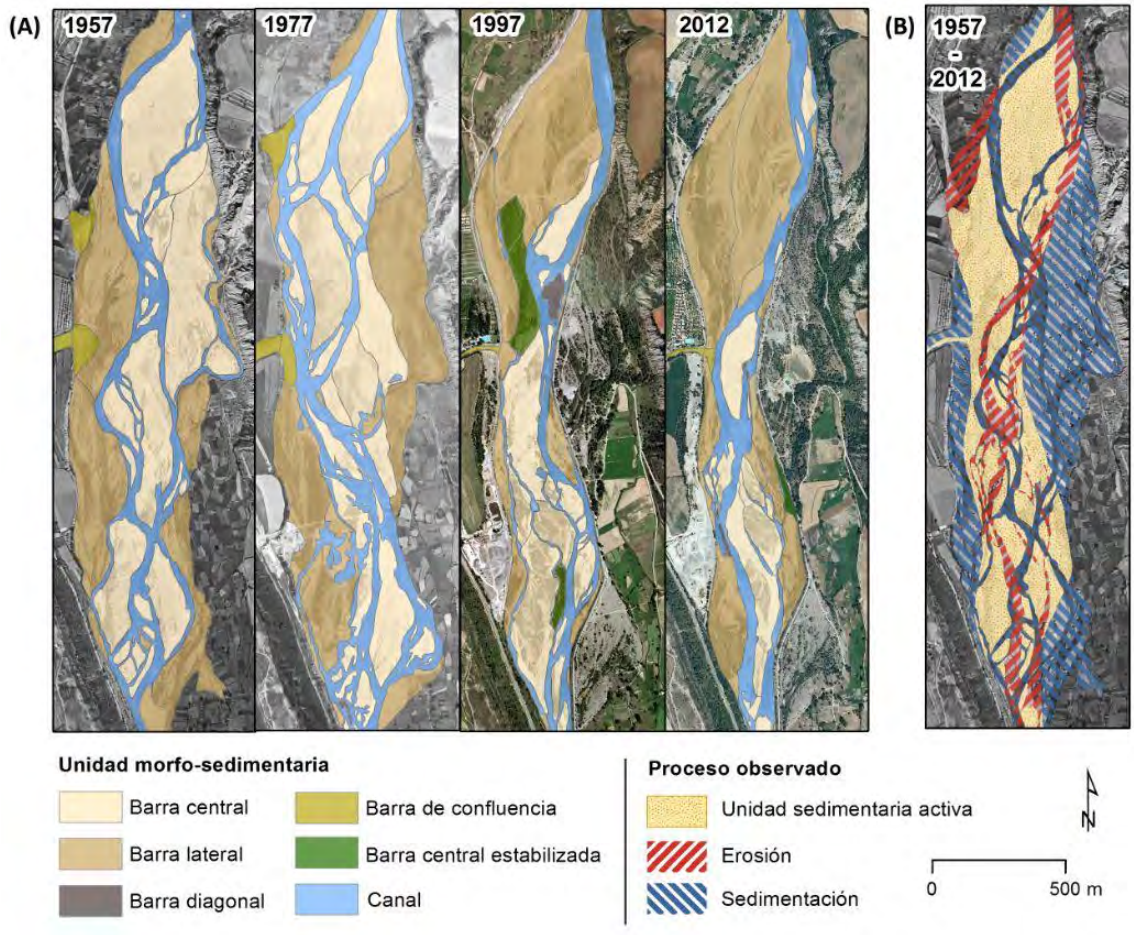


**Figura 17**. **A.** Secuencia de la distribución y tipología de las unidades sedimentarias en el tramo representativo de la zona de estudio para las series temporales de los años 1957, 1977, 1997 y 2012. **B.** Distribución espacial de los procesos morfosedimentarios sucedidos entre los años 1957 y 2012; obtenidos a partir de la combinación analítica de series temporales (matrices de cambio).

La reducción en la anchura activa del cauce fue uno de los principales procesos observados en el tramo de estudio, llegando en algunos puntos como el tramo final en las proximidades del km 10 aguas abajo del inicio de la sección de estudio, a reducirse casi 400 m (Figura 18A). Esta reducción fue debida principalmente a la construcción de escolleras durante los años 1980. Por otro lado, la Figura 17B muestra un mapa de calor del Índice de Complejidad del Cauce (ICC). El ICC corresponde al promedio normalizado del índice de canal, índice de sinuosidad e índice de barras. Esta única variable permite analizar la variabilidad espacial y temporal de la complejidad morfológica del cauce entre el periodo comprendido entre 1927-2015. Tal y como se ha dicho, este estudio se ha hecho a partir de un mapa o digamma de calor en el cual se presentan los valores más elevados de ICC con colores cálidos y los más bajos con colores fríos. En este caso el mapa de calor muestra la evolución del ICC en el tiempo (i.e. eje y, representado por las series estudiadas) y en el espacio (i.e. eje de las x, distancia aguas abajo des del inicio del tramo de estudio de la sección analizada). Tal y como se observa en la Figura 18B, existe una clara reducción del valor del ICC (i.e. reducción dela complejidad; valores azules en el mapa de calor). Aun así, existen ciertas zonas en las cuales la reducción de la complejidad fue de mayor magnitud y muy concentrada en un período temporal determinado. De manera específica, en el tramo bajo del tramo de estudio detallado de este artículo (10 km aguas abajo del punto inicial de estudio) se aprecia un primer periodo con una elevada complejidad (i.e. dinámica) atribuida principalmente al régimen de crecidas (i.e. valores rojos en el mapa de calor). A partir del año 1977 se observa una reducción de la complejidad muy notable. Esta disminución fue debida a la importante reducción de la anchura activa en esta área asociada a la construcción de escolleras. La reducción de la anchura a su vez conlleva asociado un proceso de incisión del cauce (mayor competencia del flujo), el cual se ve agravado por las extracciones de gravas realizadas en él. Este proceso queda comprobado si se analizan los cambios topográficos sucedidos entre el periodo 1957-2015. En la zona de cauce activo actual se pueden observar incisiones generalizadas que pueden llegar hasta los 5-7 m en algunos puntos (i en la Figura 19), mientras que en las zonas del cauce desconectadas por la construcción de las escolleras se observan importantes procesos de sedimentación (ii en la Figura 19). Por otro lado, el establecimiento de una planta de áridos también ha provocado cambios topográficos notables en la llanura de inundación que pueden ser cuantificados a partir de la comparación de MDTs de distintos periodos (iii en la Figura 19).

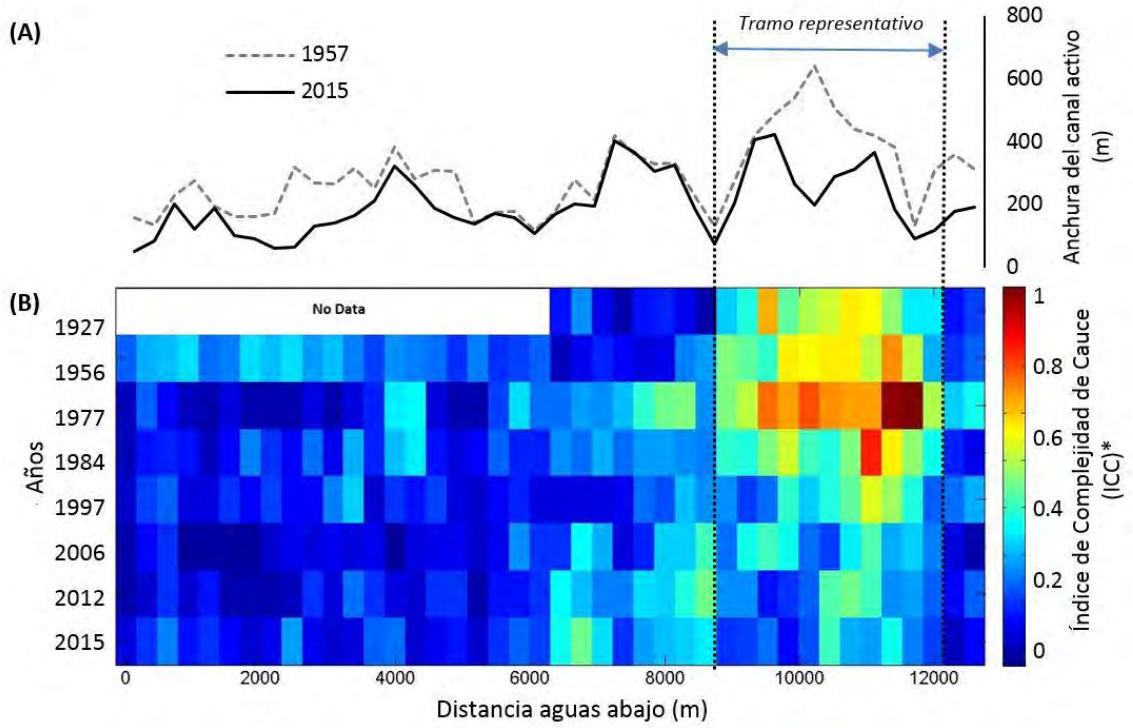


**Figura 18**. Resumen de los cambios morfológicos en planta en el tramo Alto del río Cinca. **A.** Evolución de la anchura activa para todo el tramo de estudio entre los años 1957 y 2015. **B.** Mapa de calor del índice de multiplicidad para las diferentes series temporales. *El Índice de Complejidad de Cauce (ICC) ha sido calculado a partir del promedio de los índices de canal, sinuosidad y barra previamente normalizados para cada una de las secciones.

Por último, una simple cartografía del cauce activo para distintos períodos temporales (e.g. Figura 19C) permite estudiar cuales son los impactos de infraestructuras hidráulicas sobre la conectividad lateral. En el caso del tramo Alto del río Cica, se puede observar que no solo hay una reducción de la complejidad morfológica del cauce a distintos niveles, sino que también existe un impacto directo sobre la conectividad lateral debida a la construcción de escolleras, aislando parte de la llanura de inundación. Esta síntesis de resultados muestra cómo la metodología que se presenta en este trabajo es de gran utilidad para el diagnóstico del estado morfo-sedimentario de sistemas fluviales. En el caso particular del Alto Cinca, los resultados son de gran interés para la mejora de la comprensión de las relaciones causa-efecto en la dinámica morfo-sedimentaria observada para el período 1927-2015 (Llena et al., en revisión). Esta mejora puede ayudar a modificar los planes de gestión de cuenca mediante una visión más integral de los procesos contemporáneos.

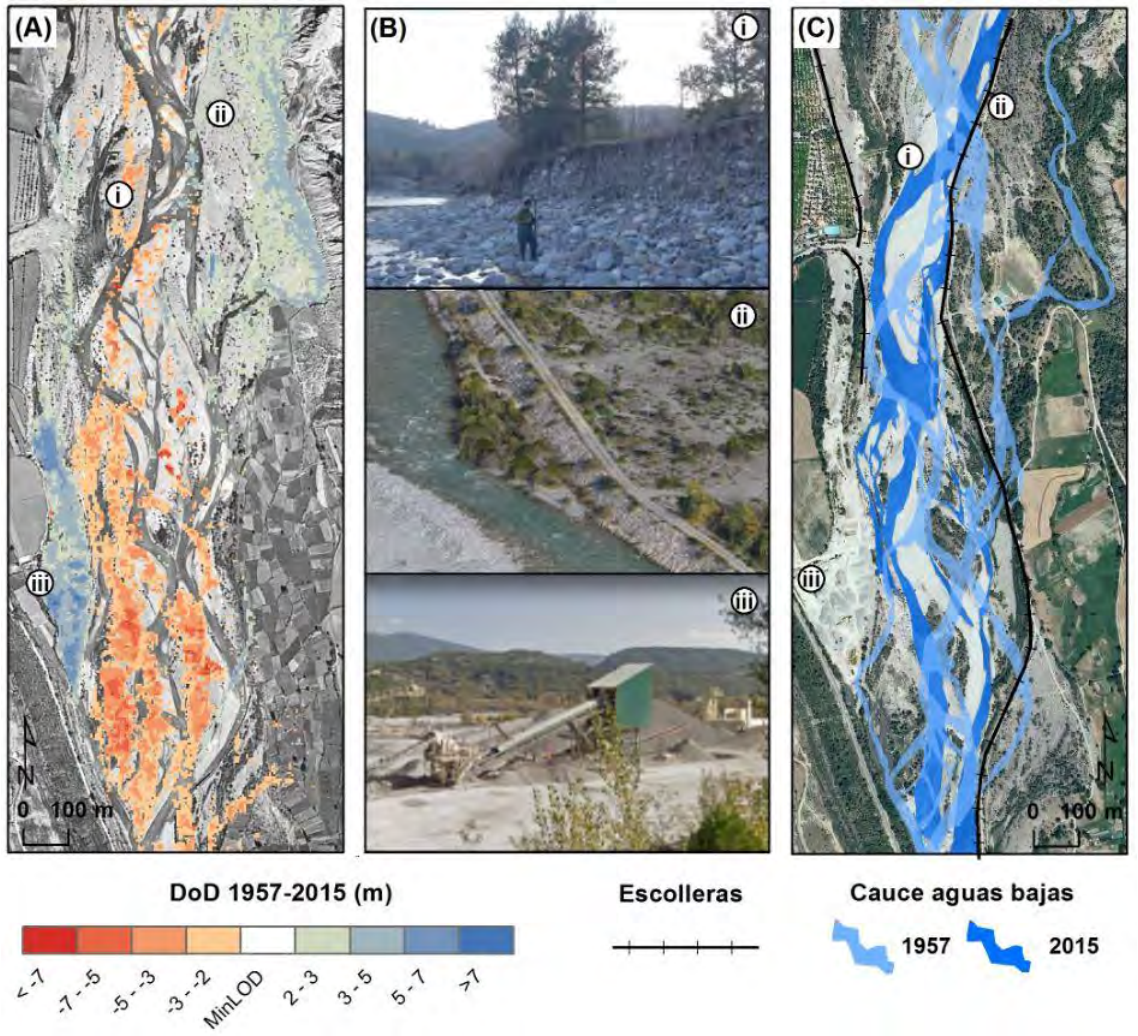


**Figura 19.** Cambios geomorfológicos en cota en el tramo bajo de la zona de estudio: **A.** Modelo de cambios topográficos (DoD) calculado a partir de las diferencias de los MDTs de los años 1957 y 2015 (se muestra la ortomosaico del año 1957 como referencia). Los valores negativos indican erosión, mientras que los positivos sedimentación. Cabe destacar que aquellos cambios entre ± 2 m se han considerado inciertos, por debajo del nivel mínimos de detección, lo que significa que no se han representado en el mapa de cambios obtenido. **B.** Evidencias observadas en campo de los cambios topográficos analizados. **C.** Situación de los cauces de aguas bajas para los años 1957 y 2015 y localización de las escolleras construidas en los años 1980 (ortomosaico año 2015). El tramo que se presenta en la figura consiste en el tramo que se indica como tramo de detalle en el mapa de calor de la figura 17C.

## DISCUSIÓN Y CONCLUSIONES

El estudio de cambios geomorfológicos históricos en sistemas fluviales se ha realizado tradicionalmente desde el punto de vista del análisis planimétrico (e.g. Arnaud et al., 2015; Comiti et al., 2011; Downs et al., 2013; Latapie et al., 2014). Este hecho limita de manera importante la interpretación de procesos geomorfológicos, puesto que no se tienen en cuenta las variaciones en cota debidas a los cambios topográficos. Una de las opciones ha sido la utilización de secciones topográficas (e.g. Arnaud et al., 2015; Comiti et al., 2011; Moretto et al., 2014; Surian et al., 2009), aunque en muchas ocasiones, la baja densidad dificulta la interpretación delos procesos. Frente a ello, la aplicación de fotogrametría digital basada en algoritmos Structure from Motion – Multi View Stereo se presenta como una metodología de

gran aplicabilidad e interés para la obtención de información geomorfológica (e.g. Carrivick et al., 2016; Micheletti et al., 2015b; Smith et al., 2016; Westoby et al., 2012), tanto a nivel planimétrico como topográfico.

En los últimos años se han realizado numerosos estudios en los que se aplica SfM para la obtención de información geomorfológica histórica, siempre en casos donde los cambios morfológicos son de una elevada magnitud: geomorfología glacial (e.g. Mertes et al., 2017; Midgley y Tonkin, 2017); geomorfología vulcanológica (e.g. Gomez 2014; Gomez et al. 2015; Ishiguro et al., 2016), o el estudio de grandes deslizamientos y desprendimientos (e.g. Dugonjic et al., 2016; Warrick et al., 2017). En cambio, existen pocos trabajos que traten sobre la aplicación de SfM en el campo de la geomorfología fluvial (se considera el trabajo de Bakker y Lane, 2016 como uno de los únicos). Esto es debido principalmente a que los cambios topográficos son de una magnitud relativamente baja, lo que dificulta su detección con la metodología SfM histórica. De este modo, en sistemas fluviales, es importante seguir un flujo de trabajo riguroso, en el cual se traten de minimizar cada uno de los errores asociados al proceso fotogramétrico. Tal y como se ha visto, en el análisis SfM de fotogramas históricos los errores vienen determinados principalmente por a) las características de los propios fotogramas y b) el establecimiento y calidad de la red de control.

Los fotogramas históricos suelen tener un bajo grado de solapamiento, lo que supone una menor redundancia de imágenes en la identificación de elementos comunes, propiciando la reducción de la estimación geométrica de los mismos. Por otro lado, la calidad de la imagen de los fotogramas históricos no suele ser la óptima (e.g. mal estado de conservación de los fotogramas originales, errores en el proceso de escaneo) lo que provoca, entre otras cosas, la reducción de la resolución original, con una consecuente modificación de la textura. Según Bakker y Lane (2016) la modificación de la textura es una de las principales limitantes de la densidad de la nube de puntos, puesto que determina la identificación de elementos comunes entre fotogramas. Mertes et al. (2017) proponen realizar una corrección de la imagen mediante el ajuste del contraste y exposición para la mejora de la calidad y textura de la imagen, proceso que también se ha hecho en el presente estudio. Por otro lado, tal y como se ha demostrado en este trabajo, el co-registro de las nubes de puntos producidas previo a su análisis puede evitar los errores asociados al posicionamiento de los puntos lejanos a los GCPs del modelo. Este proceso fue aplicado también por Bakker y Lane (2016) obteniendo en algunos casos mejoras del error medio en cota de 0,4 m.

La red de control es uno de los elementos críticos que condicionará la precisión y exactitud de los resultados (e.g. Mertes et al., 2017; Midgley y Tonkin, 2017). El establecimiento de puntos de control precisos para fotografías históricas es crítico puesto que en muy pocos casos (i.e. Gomez, 2014) se dispone de medidas directas. En el resto de casos se utilizan coordenadas actuales en puntos que potencialmente no hayan variado sus coordenadas (x, y, z). En el caso de los errores planimétricos de georreferenciación (x, y), estos suelen ser menores a 1 m, muchas veces aceptables para la cartografía en planta de unidades morfológica de interés. En cambio, la incertidumbre asociada a la estimación de la cota (z) es frecuentemente más elevada, lo que dificulta algunos estudios cuando los procesos esperados son del orden del error obtenido.

En este trabajo se ha desarrollado y aplicado una metodología de gran interés para la extracción de información geomorfológica (i.e. planimétrica y altimétrica) a partir de fotografías aéreas históricas a múltiples escalas temporales y espaciales. La metodología se ha aplicado al tramo Alto del río Cinca (Pirineo Aragonés), un tramo de elevada complejidad morfo-sedimentaria que ha sufrido importantes cambios geomorfológicos durante la segunda mitad del siglo XX debido

a perturbaciones, tanto naturales (e.g. crecidas) como antrópicas (e.g. extracción de gravas). La puesta a punto de esta metodología indica que:

1) es posible obtener información en planta e información topográfica a partir de la restitución fotogramétrica digital mediante algoritmos SfM de fotografías aéreas históricas;
2) los errores planimétricos asociados a los ortomosaicos producidos mediante esta técnica (i.e. RMSE 0,5 m) pueden ser menores que los que se producen mediante otras técnicas convencionales de georreferenciación;
3) los errores de cota asociados a las nubes de puntos (i.e. RMSE +/- 2m) han permitido analizar el impacto en la geomorfología fluvial de las perturbaciones antrópicas sucedidas en el tramo de estudio durante el periodo histórico analizado; y
4) la calidad de los productos finales, especialmente las nubes de puntos 3D, está muy condicionada por la calidad y resolución de los fotogramas, el grado de solapamiento entre estos, así como de la disponibilidad y calidad de los puntos de control o GCPs. Es muy importante tener en cuenta estos aspectos para producir un producto que sea válido para el análisis geomorfológico histórico, siempre teniendo en cuenta el objeto de estudio y su magnitud.

La metodología que se presenta en este trabajo es de gran utilidad para el diagnóstico del estado morfo-sedimentario de sistemas fluviales, en especial de sistemas modificados como el caso del Alto Cinca. Este diagnóstico puede ser determinante para entender la dinámica contemporánea asociada a zonas críticas que requieren trabajos de adecuación del cauce para la solución de problemas puntuales de erosión lateral o inundación. Del mismo modo, estos estudios sirven como base sólida a la hora de hacer estimaciones sobre la topografía del lecho en reconstrucciones de crecidas históricas, las cuales son de gran interés para analizar la recurrencia de crecidas de gran magnitud.

**Agradecimientos**
El estudio se ha beneficiado de la metodología de análisis de datos desarrollada en los proyectos MORPHSED (CGL2012-36394) y MORPHPEAK (CGL2016-78874-R), financiados por el Ministerio de Economía y Competitividad y Fondos Europeos FEDER. La página web del proyecto MORPHSED presenta más información de éste: www.morphsed.es. El trabajo se ha beneficiado de comentarios y discusiones surgidas en distintas reuniones de la EU-COST-Action Connecteur (ES1306). El primer autor tiene un contrato doctoral FPU (FPU014/01687), mientras que el segundo autor está contratado mediante el programa Ramón y Cajal (RYC-2010-06264) del Programa Nacional de Contratación e Incorporación de Recursos Humanos de Investigación. Ambos autores forman parte del Grupo de Investigación de Dinámica Fluvial –RIUS es Grupo Consolidado reconocido por la Generalitat de Catalunya (2014 SGR 645). Se agradece el *CERCA Programme* de la Generalitat de Catalunya. Se agradece a la Confederación Hidrográfica del Ebro la disponibilidad en su archivo cartográfico online de los fotoplanos históricos del año 1927. También agradecer toda la ayuda de los miembros del grupo de investigación RIUS, así como los comentarios del editor y de dos revisores anónimos que han mejorado la calidad este trabajo.

**BIBLIOGRAFÍA**

Arnaud F, Piégay H, Schmitt L, Rollet AJ, Ferrier V, Béal D. 2015. Historical geomorphic analysis (1932–2011) of a by-passed river reach in process-based restoration perspectives: The Old Rhine downstream of the Kembs diversion dam (France, Germany). *Geomorphology* 236: 163–177.

Bakker M, Lane SN. 2017. Archival photogrammetric analysis of river-floodplain systems using Structure from Motion (SfM) methods. *Earth Surface Processes and Landforms* 42: 1274–1286.

Batalla RJ, Vericat D, Martínez T. 2006. River-channel changes downstream from dams in the lower Ebro River. *Zeitschrift für Geomorphologie* 143: 1-14.

Begueria S, López-Moreno JI, Gómez-Villar A, Rubio V, Lana-Renault N, García-Ruiz JM. 2006 Fluvial adjustments to soil erosion and plant cover changes in the Central Spanish Pyrenees. *Swedish Society for Antropology and Geography* 88: 177–186.

Béjar M, Gibbins CN, Vericat D, Batalla RJ. 2017. Effects of suspended sediment transport on invertebrate drift. *River Research and Applications* 33: 1655-1666.

Béjar M, Vericat D, Nogales I, Gallart F, Batalla RJ. 2018. Efectos de las extracciones de áridos sobre el transporte de sedimentos en suspensión en ríos de montaña (alto río Cinca, Pirineo Central). *Cuadernos de Investigación Geográfica* 44: 641-658.

Brasington J, Rumsby BT, Mcvey RA. 2000. Monitoring and modelling morphological change in a braided gravel-bed river using high resolution GPS-based survey. *Earth Surface Processes and Landforms* 25: 973-990.

Brasington J, Vericat D, Rychkov I. 2012. Modeling river bed morphology, roughness, and surface sedimentology using high resolution terrestrial laser scanning. *Water Resources Research* 48: 1-18.

Calle M, Alho P, Benito G. 2017. Channel dynamics and geomorphic resilience in an ephemeral Mediterranean river affected by gravel mining. *Geomorphology* 285: 333-346.

Carrivick JL, Smith MW, Quincey DJ. 2016. *Structure from Motion in the Geosciences*, Wiley-Blackwell, 208 pp.

Church M, Jones D. 1982. Chanel bars in gravel bed rivers. In: *Gravel bed rivers* (R.D. Hey, J.C. Bayhurst, C. R. Thorne eds.), Wiley, 291-324 PP.

Chuvieco E. 1995. *Fundamentos de teledetección espacial*. Ed. Rialp, Madrid, 453 pp.

Clerici A, Perego S, Chelli A, Tellini C. 2015. Morphological changes of the floodplain reach of the Taro River (Northern Italy) in the last two centuries. *Journal of Hydrology* 527: 1106–1122.

Comiti F, Da Canal M, Surian N, Mao L, Picco L, Lenzi MA. 2011. Channel adjustments and vegetation cover dynamics in a large gravel bed river over the last 200 years. Geomorphology 125: 147–159.

Downs PW, Dusterhoff SR, Sears WA. 2013. Reach-scale channel sensitivity to multiple human activities and natural events: Lower Santa Clara River, California, USA. *Geomorphology* 189: 121–134.

Dugonjic S, Perani J, Ru I, Arbanas Ž. 2016. Analysis of a historical landslide in the Rječina River Valley, Croatia. *Geoenvironmental Disasters* 3: 1-9.

Eltner A, Schneider D. 2015. Analysis of different methods for 3d reconstruction of natural surfaces from parallel-axes UAV images. *The Photogrammetric Record* 30(151): 279–299.

Garcia-Ruiz JM, Lasanta T, Ruiz-Flano P, Ortigosa L, White S, Gonzalez C, Martí C. 1996. Land-use changes and sustainable development in mountain areas: a case study in the Spanish Pyrenees. *Landscape Ecology* 11: 267–277.

Germanoski D, Schumm SA. 1993. Changes in braided river morphology resulting from aggradation and degradation. *Journal of Geology* 101: 451–466.

Gomez C. 2014. Digital photogrammetry and GIS-based analysis of the bio-geomorphological evolution of Sakurajima Volcano, diachronic analysis from 1947 to 2006. *Journal of Volcanology and Geothermal Research* 280: 1–13.

Gomez C, Hayakawa Y, Obanawa H. 2015. A study of Japanese Landscapes using Structure from Motion Derived DSMs and DEMs based on Historical Aerial Photographs: New Opportunities for Vegetation Monitoring and Diachronic Geomorphology. *Geomorphology* 242: 11-20.

Hong LB, Davies TRH. 1979. A study of stream braiding. *Geological Society of America* 90: 1839–1859.

Hughes ML, McDowell PF, Marcus WA. 2006. Accuracy assessment of georectified aerial photographs: Implications for measuring lateral channel movement in a GIS. *Geomorphology* 74: 1–16.

Ibisate A, Díaz E, Ollero A, Acin V, Granado D. 2013. Channel response to multiple damming in a meandering river, middle and lower Aragon River (Spain). *Hydrobiologia,* 712, 5–23.

Ishiguro, S.; Yamano, H.; Oguma, H. (2016). Geomorphology Evaluation of DSMs generated from multi-temporal aerial photographs using emerging structure from motion – multi-view stereo technology. *Geomorphology*, 268, 64–71.

Lague D, Brodu N, Leroux J. 2013. Accurate 3D comparison of complex topography with terrestrial laser scanner : Application to the Rangitikei canyon (NZ). ISPRS Journal of Photogrammetry and Remote Sensing. 82: 10–26.

Lane SN, Chandler JH, Richards KS. 1994. Developments in Monitoring and Modeling Small-Scale River Bed Topography. *Earth Surface Processes and Landforms* 19: 349-368.

Lane SN, Richards KS, Chandler JH. 1996. Discharge and sediment supply controls on erosion and deposition in a dynamic alluvial channel. *Geomorphology* 15: 1–15.

Latapie A, Camenen B, Rodrigues S, Paquier A, Bouchard JP, Moatar F. 2014. Assessing channel response of a long river influenced by human disturbance. *Catena* 121: 1–12.

Leys K, Werritty A. 1999. River channel planform change: software for historical analysis, *Geomorphology* 29: 107-120.

Llena M, Cavalli M, Vericat D, Crema S. 2018. Assessing landscape changes associated to anthropic disturbances by means of the application of Structure from Motion photogrammetry using historical aerial imagery. *Rendiconti Online Società Geologica Italiana* 46: 74-81.

Llena M, Vericat D, Martínez-Casasnovas JA, Smith M. (En revision). Geomorphic responses to natural and human disturbances in a mountain river: a century of observations. *Geomorphology.*

Mertes JR, Gulley JD, Benn DI, Thompson SS, Nicholson LI. 2017. Using structure-from-motion to create glacier DEMs and orthoimagery from historical terrestrial and oblique aerial imagery. *Earth Surface Processes and Landforms* 42: 2350-2364.

Micheletti N, Chandler JH, Lane SN. 2015a. Structure from Motion (SfM) Photogrammetry. Photogrammetric heritage. *British Society for Geomorphology: Geomorphological Techniques* 2: 1–12.

Micheletti N, Lane SN, Chandler JH. 2015b. Application of Archival Aerial Photogrammetry to Quantify Climate Forcing of Alpine Landscapes. *The Photogrammetric Record* 30: 143-165.

Midgley NG, Tonkin TN. 2017. Geomorphology Reconstruction of former glacier surface topography from archive oblique aerial images. Geomorphology 282: 18–26.

Moretto J, Rigon E, Mao L, Picco L, Delai F, Lenzi MA. 2014. Channel adjustments and island dynamics in the Brenta River (Italy) over the last 30 years. *River Research and Applications* 30: 719–732.

Mosley PM. 1981. Semi-determinate hydraulic geometry of river channels, South Island, New Zealand. *Earth Surface Processes and Landforms* 6: 127–137.

Muñoz-Narciso E, Béjar M, Tena A, Vericat D, Ramos E, Brasington J, Gibbins CN, Batalla RJ. 2014. Generación de modelos topográficos a partir de fotogrametría digital automatizada en un río de gravas altamente dinámico. In: *Avances de la Geomorfología en España 2012-2014*. XIII Reunión Nacional de Geomorfología (Schnabel, S.; Gómez-Gutiérrez, A. Eds.). ISBN: 978-84-617-1123-9, Universidad de Extremadura, Cáceres, 335-338.

Passalacqua P, Belmont P, Staley DM, Simley JD, Arrowsmith JR, Bode CA, Crosby C, DeLong SB, Glenn NF, Kelly SA, Lague D, Sangireddy H, Schaffrath K, Tarboton DG, Wasklewicz T, Wheaton JM. 2015. Analyzing high resolution topography for advancing the understanding of mass and energy transfer through landscapes: a review. *Earth-Science Reviews* 148: 174-193.

Sanchis-Ibor C, Segura-Beltrán F, Almonacid-Caballer J. 2017. Channel forms recovery in an ephemeral river after gravel mining (Palancia River, Eastern Spain). *Catena* 158: 357–370.

Seitz SM, Diebel J, Scharstein D, Szeliski R. 2006. A Comparison and Evaluation of Multi-View Stereo Reconstruction Algorithms. *IEEE Computer Society Conference* 1: 519–528.

Semyonov D. 2011. Algorithms used in Photoscan [Msg 2]. Retrieved 3 May 2011. Message posted to www.agisoft.ru/forum/index.php?topic=89.0.

Smith MW, Vericat D. 2015. From experimental plots to experimental landscapes: topography, erosion and deposition in sub-humid badlands from Structure-from-Motion photogrammetry. *Earth Surface Processes and Landforms* 40: 1656–1671.

Smith MW, Carrivick JL, Quincey DJ. 2016. Structure from motion photogrammetry in physical geography. *Progress in Physical Geography* 40: 247–275.

Surian N, Ziliani L, Comiti F, Lenzi MA, Mao L. 2009. Channel adjustments and alteration of sediment fluxes in gravel-bed rivers of north-eastern Italy: potentials and limitations for channel recovery. *River Research and Applications* 25: 551-567.

Ullman S. 1979. *The interpretation of structure from motion*. The Royal Society, London. 203, 405–442.

Vericat D, Brasington J, Wheaton J, Cowie M. 2009. Accuracy assessment of aerial photographs acquired using lighter-than-air blimps: low-cost tools for mapping river corridors. *River Research and Applications* 25: 985–1000.

Vericat D, Múñoz-Narciso E, Béjar M, Ramos-Madrona E. 2016. Case study: Multitemporal reach-scale topographic models in a wandering river – uncertainties and opportunities. In: *Structure from Motion in the Geosciencies. New Analytical Methods in the Earth Environmental Science* (J. L. Carrivick, M. W. Smith, D. J. Quincey, eds.). Willey, 194 pp.

Vericat D, Wheaton J, Brasington J. 2017. Revisiting the Morphological Approach: Opportunities and Challenges with Repeat High-Resolution Topography. In: *Gravel-Bed Rivers: Processes and Disasters* (D. T. Tsutsumi, J. B. Laronne, eds.). Wiley, 121-158.

Vericat D, Batalla RJ. 2016. Morfodinámica fluvial. In: *Procesos hidrosedimentarios en medios fluviales* (R.J. Batalla, A. Tena, eds.). Editorial Milenio, Lleida, 19-74.

Wackrow R, Chandler JH. 2008. A convergent image configuration for DEM extraction that minimises the systematic effects caused by an inaccurate lens model. *The Photogrammetric Record* 23(121): 6–18.

Warrick JA, Ritchie AC, Adelman G, Adelman K, Limber W, Warrick JA, Limber PW. 2017. New techniques to measure cliff change from historical oblique aerial photographs and Structure-from-Motion Photogrammetry. *Journal of Coastal Research* 33: 39–55.

Westoby MJ, Brasington J, Glasser NF, Hambrey MJ, Reynolds JM. 2012. "Structure-from-Motion" photogrammetry: A low-cost, effective tool for geoscience applications. *Geomorphology* 179, 300–314.

Wheaton JM, Brasington J, Darby SE, Sear DA. 2010. Accounting for uncertainty in DEMs from repeat topographic surveys: improved sediment budgets. *Earth Surface Processes and Landforms* 35: 136-156.

Williams RD. 2012. DEMs of Difference. *Geomorphological Techniques (British Society for Geomorphology)* 2: 1-17.

Williams RD, Brasington J, Vericat D, Hicks DM. 2013. Hyperscale terrain modelling of braided rivers: Fusing mobile terrestrial laser scanning and optical bathymetric mapping. *Earth Surface Processes and Landforms* 39: 167–183.

## 2.5. References not cited in the papers

Borselli L, Cassi P, Torri D. 2008. Prolegomena to sediment and flow connectivity in the landscape: a GIS and field numerical assessment. *Catena* 75: 268–277.

Cavalli M, Trevisani S, Comiti F, Marchi L. 2013. Geomorphometric assessment of spatial sediment connectivity in small Alpine catchments. *Geomorphology* 188: 31–41.

Schick AP. 1967. Gerlach troughs, overland flow traps. Field methods for the study of slope and fluvial processes. *Revue de Géomorphologie Dynamique* 4: 170–172

# CHAPTER 3

## MULTI-TEMPORAL GEOMORPHIC PROCESSES SIGNATURES RESHAPING SUB-HUMID MEDITERRANEAN BADLANDS

# CHAPTER 3: Multi-temporal geomorphic processes signatures reshaping sub-humid Mediterranean badlands

This chapter contains the following submitted paper (14/08/2019) in the journal Earth Surface Processes and Landforms. JCR-SCI Impact Factor (2018): 3.598. Category: Earth-Surface Processes; 1st Quartile.

Llena M, Smith MW, Wheaton JM, Vericat D. 2019. Multi-temporal geomorphic processes signatures reshaping sub-humid Mediterranean badlands. *Earth Surface Processes and Landforms* (Under revision).

**ABSTRACT:** Badland landscapes exhibit high erosion rates and represent the main source of fine sediments in some catchments. Advances in High Resolution Topographic methods allow analysis of topographic changes at high temporal and spatial scales. We apply the Mapping Geomorphic Processes in the Environment (MaGPiE) algorithm to infer the main geomorphic processes signatures operating in two sub-humid badlands with contrasting morphometric attributes located in the Southern Pyrenees. By interrogating a five-year dataset of seasonal and annual topographic changes, we examine the variability of geomorphic processes at multiple temporal scales. The magnitude of geomorphic processes is linked to landform attributes and meteorological variables. Morphometric differences between both adjacent badlands allow analysing the role of landform attributes on main geomorphic process re-shaping landscapes subjected to the same external forcing (i.e. rainfall and temperature). The dominant geomorphic processes signatures observed in both badlands are different, despite their close proximity and same rainfall and temperature regimes. Process signatures determining surface lowering in the gentle-sloping south-facing badland, characterised by lower connectivity and more vegetation cover, are driven by surface runoff-based processes, both diffuse, causing Sheet Washing, and concentrated, determining Cutting and Filling and Rilling and Gullying. The steeper and more connected north-facing slopes of the other badland are re-shaped by means of gravitational processes with Mass Wasting dominating topographic changes. In terms of processes determining surface raising, both Mass Wasting and Cutting and Filling are most frequently observed in both badlands. There is a clear near-balanced feedback between both surface-raising and lowering processes that becomes unbalanced at larger temporal scales due to the thresholds overcoming, as the volume associated with surface lowering becomes higher than that associated with raising-based processes. Rainfall variables control surface flow processes while those variables associated with low temperature have a significant relation with mass movement-based processes and other localised processes as Regolith Cohesion Loss. Finally, our results point out as morphometry (slope and connectivity) together with vegetation cover are key factors determining geomorphic processes and associated topographic changes.

**KEYWORDS**: *Sediment connectivity, Index of Sediment Connectivity, Land use and topographic changes, Mountain catchments, Afforestation, Terracing.*

## 1. INTRODUCTION

Badlands are described as dissected landscapes with little or no vegetation cover developed on unconsolidated or poorly consolidated sedimentary deposits (Yair et al., 1980; Clotet et al., 1987; Gallart et al., 2002). Badlands are usually subjected to high erosion rates, representing the main source of fine sediments in some catchments (e.g. López-Tarazón et al., 2012; Richard and Mathys 1999). High erosion rates implies high sediment transfer downstream, with associated environmental (e.g. channel clogging, Piqué et al., 2014; alluvial plain dynamics alteration, Aucelli et al., 2016) and management implications (e.g. reservoir siltation, Martínez-Casasnovas and Poch, 1998; reduction of water quality, Pimentel et al., 1995). The significance of geomorphic processes in badlands will be determined, mainly, by their morphometric characteristics, including lithology, together with external forcing (i.e. rainfall and temperature). Gallart et al. (2002) proposed three badlands types in terms of the climate: (i) Arid badlands (i.e. annual rainfall below 200 mm); (ii) Semi-arid badlands (rainfall between 200-700 mm) and (iii) Sub-humid and Humid badlands (rainfall exceeds 700 mm). Those climates with marked seasonal contrasts (i.e. temperature, rainfall) favour the development of badlands. In that way, Mediterranean regions represent one of the areas with the greatest presence of these types of landscapes (Clotet et al., 1987; Torri et al., 1994).

Lithology and its interaction with the characteristics of the climate, vegetation cover, connectivity and human activity are considered the main factors responsible for badland development (Smith 1958; Clotet et al., 1987; Gallart et al., 2002; Nadal-Romero and Garcia-Ruiz 2018). In a general way, the main geomorphic processes that shape badland landscapes and control their spatial and temporal evolution are weathering (i.e. regolith formation), surface flow-based processes (i.e. diffuse or concentrated), subsurface erosion (i.e. piping or tunnelling) and mass-wasting (i.e. gravitational processes) (Bryan and Yair 1982; Clotet et al., 1988; Kasanin-Grubin 2013; Moreno-de las Heras and Gallart, 2018).

Erosion rates on badlands are mainly analysed by dynamic or volumetric methods (De Ploey and Grabiels, 1980; Nadal-Romero and García-Ruiz, 2018; Sirvent et al., 1997). On one hand, dynamic methods aim at measuring sediment fluxes from plots (e.g. Nadal-Romero et al., 2007; Regüés et al., 1995), micro-catchments (e.g. Mathys et al., 2003) or experimental catchments (e.g. Rainato et al., 2017). On the other hand, volumetric methods aim at measuring sediment erosion rates through the analysis of topographic changes. Historically, volumetric methods were based on sparse observations across relatively small areas, based on erosion pins (e.g. Barnes et al., 2016; Benito et al., 1992) or microprofile metres (e.g. Descroix and Olivri, 2002; Sirvent et al., 1997).

During recent decades, advances in High Resolution Topographic survey methods (see reviews and examples in e.g. Passalacqua et al., 2015; Tarolli, 2014; Vericat et al., 2017) offer the opportunity of examining topographic changes in a spatially-distributed way at multiple temporal and spatial scales. Several authors have used these data sets to monitor topographic changes in badlands (e.g. Aucelli et al., 2016; Ferrer et al., 2017; Krenz and Kuhn, 2018; Lucia et al., 2011; Nadal-Romero et al., 2015; Nobajas et al., 2017; Smith and Vericat, 2015; Stöcker et al., 2015; Vericat et al., 2014). Although these studies have improved the quantification of erosion and deposition rates, and associated sediment yields, to our knowledge, there has yet to be an attempt to quantify the magnitude of the changes in form associated with the main geomorphic processes, its relation with morphometric characteristics, and their spatial and temporal distribution. Most of the studies are concentrated in relatively small temporal and spatial scales that may limit the applicability of findings beyond the period in which observations are obtained. In this way, for a comprehensive understanding of the drivers and processes

reshaping badlands and their role on sediment production, it is necessary to quantify not just topographic changes across these landscapes, but also to infer in the main geomorphic processes being responsible of the changes at multiple temporal and spatial scales.

In this paper we analyse multi-temporal repeat High Resolution Topography obtained during five consecutive years in two morphometrically-contrasted sub-humid badlands to untangle the relative importance of different processes in reshaping badlands and exporting sediments downstream, and their link to landform attributes and meteorological variables. Specifically, we have applied the Mapping Geomorphic Processes in the Environment (MaGPiE) algorithm recently developed by Llena et al. (under revision) to infer into main geomorphic processes signatures shaping these badlands through the analysis of changes in form. It is worth to mention that this paper together with the mentioned methodological paper (Llena et al., under revision) are considered a paper pair. The methodological paper presents the full details of the MaGPiE algorithm. In this article, however, we have applied the aforementioned algorithm to an extensive long-term dataset (i.e. five years) from two experimental badlands located in the Southern Central Pyrenees that are broadly representative of sub-humid badlands developed in Sub-humid Mediterranean landscapes. The starting hypothesis is that morphometric characteristics will determine in a large degree the typology, extension and magnitude of geomorphic process. For this reason, the two adjacent badlands with contrasted landform attributes but subjected to the same external forcing (i.e. temperature and rainfall) provide an idealised design to to analyse the interaction between meteorological variables, landform attributes and main geomorphic processes signatures at multiple temporal scales. Better understanding of main geomorphic processes re-shaping badlands, together with their relation with meteorological variables and morphometric characteristics, will help providing information about cycles of sediment production and their drivers, which could be very useful data to improve environmental management and landscape evolution modelling.

## 2. STUDY SITE

The study site is composed of two adjacent experimental micro-catchments (i.e. Badland 1 -B1- with a surface area of 0.32 ha, and Badland 2 -B2- with a surface of 0.21 ha) situated in the Soto catchment (Figure 1A); a small (10 $km^2$) intermittent tributary of the Upper River Cinca (8275 $km^2$, Central Pyrenees, Ebro Catchment, Iberian Peninsula; Figure 1A). The distance between both micro-catchments is around 50 m. The main land uses of the Soto catchment are forest (56%), badlands (26%) and field crops (18%). Overall, the average altitude of both Badlands is around 600 m a.s.l.; the local relief can be more than 19 m with steep slopes and high degree of dissection (Figure 1A and 1B). In terms of lithology, both experimental badlands are composed by a sequence of Eocene marls with different degrees of compactness with some alternate layers of sandstones and gypsum. Therefore, geomorphic processes are hypothesised to be highly complex and spatially variable (Smith and Vericat, 2015; Figure 1B). In terms of their specific morphometry (Table 1), differences are mainly controlled by the dip of the geological strata. In this way, B2 presents a higher dip of the strata (i.e. 40º) than B1 (i.e. 25º), that determines, among other characteristics, a higher slope and a major network incision, which in turn controls the degree of structural sediment connectivity. Sediment connectivity was estimated by the topographic-based Sediment Connectivity Index modified by Cavalli et al. (2013) and first developed by Borselli et al. (2008). This pixel-based index is computed by on the ratio between an upslope component (i.e. contributing area, roughness and slope) and downslope component (i.e. flow path length, roughness and slope). After its normalization, the Sediment Connectivity Index represents the probability of sediment arriving at each pixel reaching the catchment outlet or a given targeted point. For instance, a low value of the index indicates a lower probability of

the sediment reaching the targeted point, while a high value indicates that the pixel is well connected and there is a high probability that sediment reaches the outlet or targeted point. The aspect of both badlands is also different, being 211º (i.e. SW) for B1 and 171º (i.e. S) for B2 (Figure 1A and 1B and Table 1). In terms of land cover, the two badlands have a low vegetation cover (i.e. <20%), composed by isolated shrubs (e.g. *Buxus sempervirens, Genista scorpius*) in steep slopes and small groups of relatively young trees (e.g. *Pinus halepensis*) on low slopes or in the top of the micro-catchments (Figure 1A). The experimental badland B1 was also presented in Smith and Vericat (2015). More information about the experimental site can be also obtained in https://sites.google.com/site/badlandscan/.

**Table 1.** Main characteristics of the two experimental badlands.

| | **Badland 1 (B1)** | **Badland 2 (B2)** |
|---|---|---|
| **Surface (ha)** | 0.32 | 0.12 |
| **Mean Altitude (m a.s.l)** | 590.74 | 601.70 |
| **Vegetation cover (%)** | 17.70 | 10.88 |
| **Mean aspect (º)** | 210.67 (SW) | 174.08 (S) |
| **Mean Slope (º)** | 31.44 | 37.27 |
| **Mean slope of dip strata (º)** | 25 | 40 |
| **Mean slope of shady aspect (º)** | 34.25 | 48.84 |
| **Mean Roughness (mm)*** | 7.52 | 6.96 |
| **Mean Topographic Wetness Index**** | 0.41 | 0.16 |
| **Normalized mean value of Index of Sediment Connectivity***** | -2.84 | -1.02 |

* Detrended standard deviation of observation elevations per each 0.05 x 0.05 m grid.
** Calculated by means of the expression ln(A/tanβ) where A is referred to the upslope area in a given cell, and β is the local slope.
*** Calculated by the approach of Cavalli et al. (2013) from the ratio between upslope component (i.e. contributing area, roughness and slope) and downslope component (i.e. flow path length, roughness and slope). Index value is normalized by the micro-catchment surface.

The long-term meteorological background is provided by a meteorological station located 250 m from the study site (i.e. Ainsa Station, Spanish Meteorological Agency, AEMET). Mean annual rainfall for the period 1981-2018 is around 755 mm. Maximum rainfall is observed during spring and autumn (e.g. maximum intensities around 47 mm $h^{-1}$ are registered). Mean annual temperature is 13°C, with minimum values around -6°C and maximum around 37°C. During winter, temperatures below freezing are often registered (on average, 60 days every year are exposed to temperatures <0ºC).

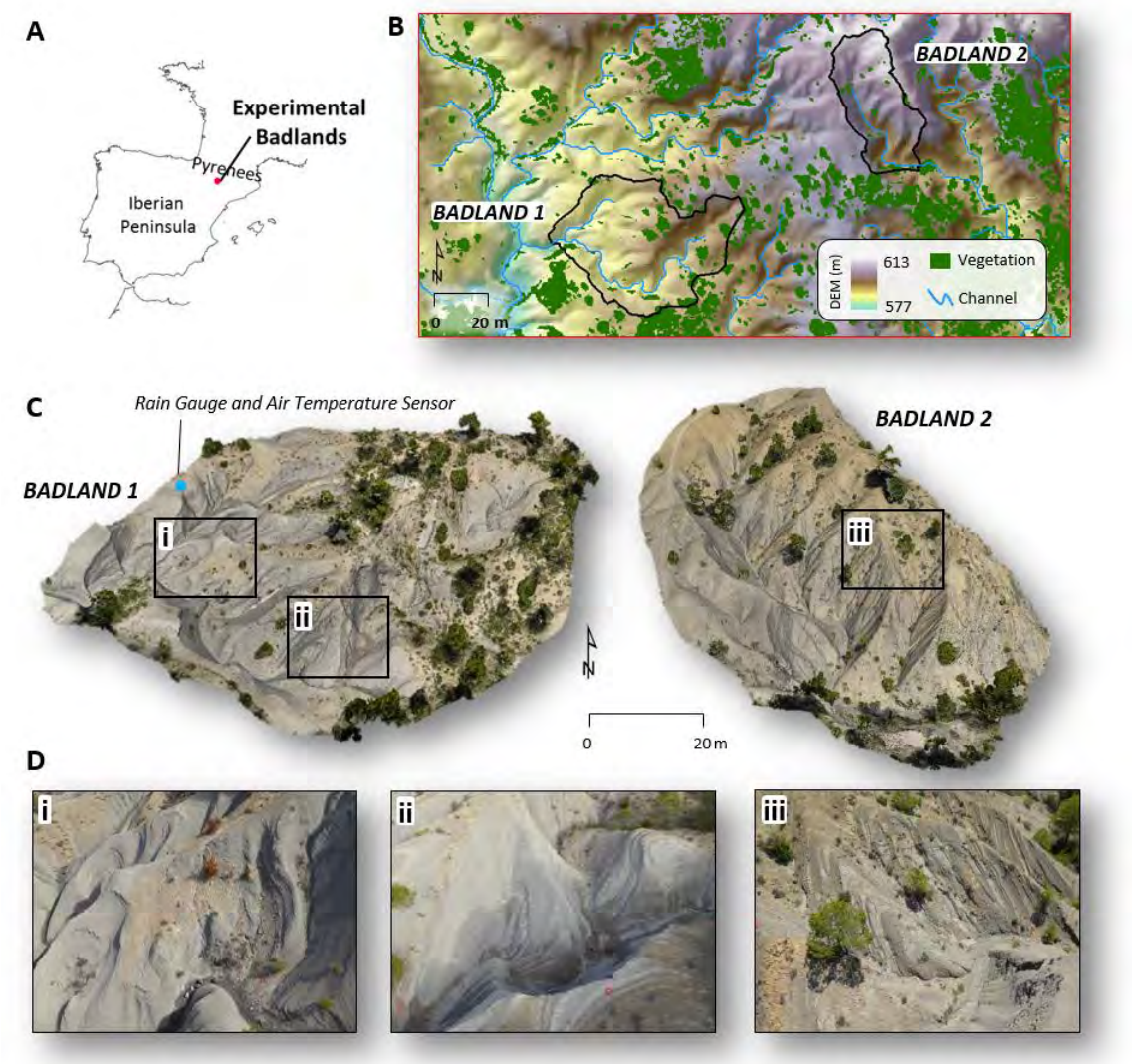


**Figure 1. A.** Location of the experimental badlands in the Iberian Peninsula (red dot) and photo-rendered point clouds of the two badlands (i.e. Badland 1 –B1- and Badland 2 –B2- respectively). The blue dot in B1 indicates the location of both the Rain Gauge and the Temperature Sensors. **B.** Close photo views of the experimental badlands.

## 3. METHODS

### 3.1. Field data collection and preparation

#### 3.1.1. Rainfall & Temperature

Rainfall was measured continuously by a Campbell ARG100 tipping bucket rain gauge, while air temperature was recorded using a Campbell Temperature Probe-109 (see location in Figure 1A). All data were recorded in the same datalogger (Campbell CR200X) at a 5-minute interval. A total of eight meteorological variables were calculated based on the recorded rainfall and temperature (see Table 2 for two for a complete description). Note that the sensors were located in B1; however, the proximity of both badlands (around 50 meters; Figure 1B) together

with the minimum changes in elevation between them (Table 1; Figure 1B) justifies the use of a single station to characterise both badlands.

**Table 2.** Description of the meteorological variables analysed, unites and associated abbreviations.

| Type of variable | Abbreviation | Description | Unit |
|---|---|---|---|
| **Time** | *ND* | Number of days in between surveyed periods | Day |
| **Rainfall** | *TR* | Total rainfall | mm |
| | *RD* | Rainfall duration | Hour |
| | *MRI* | Mean rainfall intensity | mm $hour^{-1}$ |
| | *MaxRI* | Maximum rainfall intensity | mm $hour^{-1}$ |
| **Temperature** | *MT* | Mean temperature | ºC |
| | *Zd* | Days with temperatures <0ºC | Day |
| | *MTZD* | Mean temperature of the minimum temperatures of days <0ºC | ºC |
| | *MinTZD* | Minimum temperature | ºC |

### 3.1.2. Topographic Surveys and Processing Methods

Topographic data sets were obtained through different High Resolution Topographic survey techniques. The number and frequency of the surveys were variable depending on the experimental badland. In B1, 10 topographic surveys were performed between summer 2013 and summer 2018. From 2013 to 2016, surveys were done annually (n=4), while from 2016 to 2018 surveys were done seasonally (n=6; Table 3 and Figure 2). In the case of B2, the surveyed period was between autumn 2016 and summer 2018, with all the surveys at a seasonal interval (n=5; Table 3 and Figure 2). Note that, all the annual surveys were performed in the middle of the summer to ensure that the annual scale is defined by two consecutive summer surveys (e.g. 2017-2018). In the case of the seasonal surveys, these were performed during the middle of summer, at the end of the autumn and at the beginning of the spring (see Figure 1 in supplementary materials section for further information about the survey periods). These surveys yield the following seasonal periods: (i) spring (beginning spring to middle summer; e.g. S2017), (ii) autumn (middle summer to end autumn; e.g. A2017) and (iii) winter (end autumn to beginning spring; e.g. W2017). We selected these periods in order to isolate the potential effects of meteorological drivers (e.g. rainstorms in spring and summer, and temperatures below 0ºC in winter) on weathering and erosion processes. Finally, it is worth noting that the year attributed to every period is always the starting year (e.g. the winter between 2017 and 2018 is named W2017; Table 4).

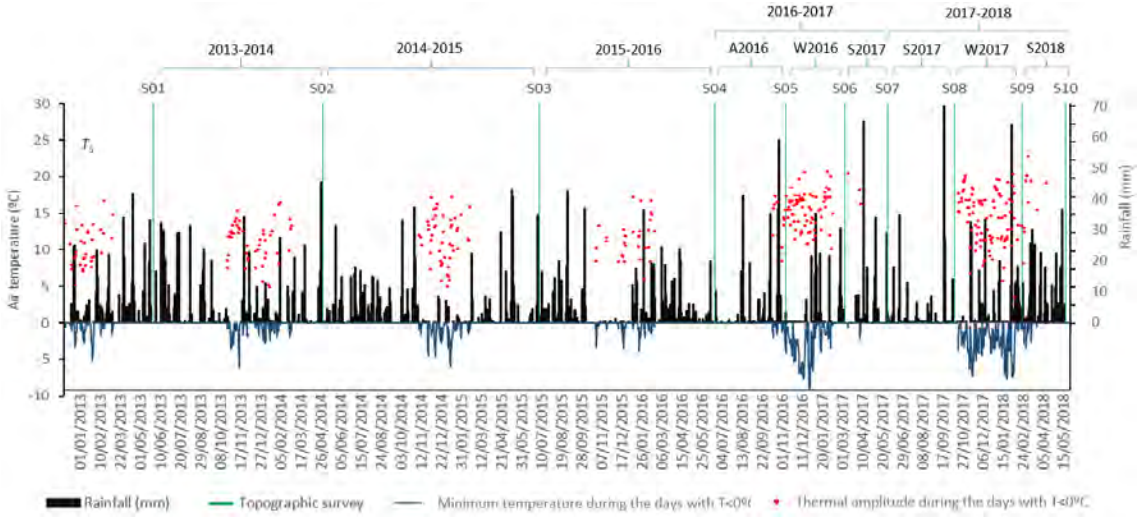


**Figure 2.** Meteorological data registered during all the study period indicating the different topographic surveys (green columns) and analysed periods (blue brackets). Black columns represent total daily rainfall, blue line represents the minimum temperature registered during the days with temperatures below 0ºC, and red dots indicates the thermal amplitude for the days in which temperatures below 0ºC were registered.

Topographic surveys were performed by means of: (i) Terrestrial Laser Scanning (TLS); and (ii) Structure from Motion (SfM) photogrammetry. Note that TLS surveys were only performed in B1 during Survey 1 (S01) and Survey 2 (S02); all other surveys were performed by SfM photogrammetry in both badlands (Table 3).

Specifically, the TLS surveys were performed by a Leica ScanStation C10. The C10 uses a 532-nm pulsed laser with stated precisions of 6 mm for position, 4 mm for distance, and 60 µrad for angles. The maximum data acquisition rate is 50000 points per second while the maximum survey range is 300 m. B1 was surveyed using the same 12 stations in each survey chosen to minimize and eliminate gaps caused by occlusion. Further specific details are provided in Smith and Vericat (2015). In terms of the SfM-based surveys, around 650 pictures per campaign and badland were taken by means of a Panasonic Lumix DMC-TZ60 compact camera (focal length 4 mm which is a 35-mm equivalent of 25 mm; 10 Mpx) mounted on a 10 m telescopic inspection pole. SfM processing was implemented using standard workflows within Agisoft Photoscan Professional 1.3.4. Dense point clouds with an average point density of around $5x10^4$ obs $m^{-2}$ (i.e. 5 obs $cm^{-2}$) were obtained. In terms of georeferencing and scaling, TLS data sets were registered by a floating network of tripod-mounted targets (i.e. 6" circular blue/white targets) used as Ground Control Points (GCPs). SfM data sets were registered by a floating control network of around 30 GCPs per badland, which were spatially distributed. Both GCPs sets were surveyed with a Leica TPS1200 Total Station (TS). The TS was set up based on a primary control network of four (fixed) benchmarks. The coordinates in each benchmark were obtained by means of a Leica Viva GS15 GNSS system and RINEX data from 3 reference stations. 3D data quality after post-processing was 0.006 m on average.

In terms of quality assessment, an independent validation dataset of around 300 Check Points (ChPs) per survey was obtained with the TS. The corresponding differences between ChPs and TLS or SfM-derived point cloud were calculated by the M3C2 plugin implemented in the open source software CloudCompare 2.6.2 (Lague et al., 2013). The validation metrics used to analyse the differences were the Mean Absolute Error (i.e. MAE) as a measure of the accuracy, and the Standard Deviation of the differences (i.e. SDE) as a measure of the precision. Point clouds were

filtered to remove outliers and vegetation. Outliers were filtered by means the Statistical Outlier Filter (SOR) of Cloud Compare 2.6.2 (Girardeau-Montaut, 2016), while the points located in vegetated areas were removed using the combination of the results of the supervised image classification (in case of the SfM-based surveys) and also manually (TLS-based surveys). After that, the open-source Topographic Point Cloud Analysis Toolkit (ToPCAT; Brasington et al., 2012; Rychkov et al., 2012; implemented in the Geomorphic Change Detection extension for ArcMap, available at http://gcd.joewheaton.org/; see Wheaton et al., 2010) was used to regularize the point cloud. A 0.05 x 0.05 m grid was selected taking into account the magnitude of the topographic changes of the study area and the size of the smallest geomorphic features observed in the field (e.g. rills). ToPCAT further allows interrogation and analysis of observations within each grid cell. A series of cell-based statistics were calculated (e.g. maximum, mean and minimum elevations and detrended standard deviation of elevations). The minimum elevation within each grid was used to represent the ground elevation within each cell, while the detrended standard deviation was used as a proxy of surface roughness as previously used by, for instance, Brasington et al. (2012), Smith and Vericat (2015) and Vericat et al. (2014). A Triangular Irregular Network or TIN was calculated based on these observations for each survey. Finally, a 0.05 m resolution DEM and roughness map was computed from each TIN.

## 3.2. Data analyses

### 3.2.1. Geomorphic Change Detection

Figure 3 shows the general workflow applied to analyse topographic changes. Topographic changes were estimated by means of the comparison of DEMs between surveys (DEM of Differencing; i.e. DoD). The old DEM is subtracted from the new one, where negative values indicate surface lowering or erosion, and positive values indicate surface raising or deposition. DoDs were calculated by the Geomorphic Change Detection 7.2 (GCD) extension for ArcMap (Wheaton et al., 2010). GCD also allows adding uncertainty analysis based on simple minimum Level of Detection (minLoD), propagated errors or probabilistic thresholding. Given the relatively low magnitude of the expected topographic changes in the study area compared with other landscapes (e.g. gravel-bed rivers), a robust approach for the estimation of these changes was necessary to discriminate the real changes from noise. In that way, the three steps proposed by Wheaton et al. (2010) were applied to assess DoD uncertainty: (i) quantifying spatially distributed uncertainty for each DEM; (ii) propagating identified uncertainties into each DoD; and (iii) determining the significance of the propagated uncertainty based on a minimum Level of Detection (minLoD). The assessment of the spatially distributed uncertainty was addressed by the application of a Fuzzy Inference System (FIS) to consider errors from different sources (Wheaton et al., 2010). In this study we have used the FIS model proposed by Rossi (2018). This model takes into account the slope and the roughness as main factors determining the vertical uncertainty. Roughness and slope were categorised based on four different levels: low, moderate, high and extreme. These were combined to determine 4 levels of uncertainty (see Figure 2 of Supplementary Materials section for additional information). The values defining or associated to these 4 levels were adapted to the study site by Llena et al. (2018). A critical t-value at a confidence interval of 85% was applied to calculate the spatially distributed minLoD (e.g. Brasington et al., 2000; Lane et al., 2003; Smith and Vericat, 2015). Those DoD cells with absolute values below the minLoD were considered uncertain and not used in the computation of the thresholded DoD.

### 3.2.2. Geomorphic Processes Signatures

The Mapping Geomorphic Processes in the Environment (MaGPiE) algorithm presented by Llena et al. (under revision) was used to infer on the main geomorphic processes signatures controlling topographic changes.

Main geomorphic processes signatures were grouped into: (i) weathering-based processes, (ii) water-based (surface) processes, and (iii) mass movement-realated processes (following Barnes et al., 2016; Bryan and Yair, 1982; Clotet et al., 1987; Gallart et al., 2002; Nadal-Romero and Regües, 2010; Nadal-Romero and García-Ruiz, 2018; Moreno-de las Heras and Gallart, 2018; Vergari et al., 2019). According to these, a total of a total of 6 specific geomorphic processes signatures were identified: (1) *Sheet Washing*; (2) *Rilling and Gullying*; (3) *Cutting and Filling*; (4) *Mass Wasting* (5) *Regolith Cohesion Loss*; and (6) *Overlapping Processes*. Full details of MaGPiE can be obtained in Llena et al. (under revision).

Briefly, the algorithm allows pixel-based identification of the specific geomorphic processes signatures by the combination of (i) landform attributes (i.e. Slope, Roughness and a new Concentrated Runoff Index) and (ii) topographic changes, represented by the results of the thresholded DoD. The landform attributes were extracted from the second (or most recent) DEM (see Figure 3 for the general workflow). The local Slope was calculated by means of the maximum rate of change in elevation from each cell to its neighbours. The Roughness was calculated using ToPCAT-derived detrended standard deviation of the elevations in each grid cell (0.05 m). The Concentrated Runoff Index (i.e. CRI) was calculated based on the Topographic Wetness Index (TWI) and Planform Curvature (PC) by means of the expression TWI+(PC×-1); where the TWI was computed as $\ln(A/\tan\beta)$, A is referred to the upslope area of a given cell ($m^2$), and β is the local gradient (in degrees). PC represents the normalised (from -1 to 1) planform curvature value obtained from the most recent DEM (see more details in Llena et al., under revision). Finally, topographic changes were obtained by the comparison of the DEMs between surveys as described above (i.e. thresholded DoD). To define the signature of each process, each attribute and the DoD was grouped into different classes. An expert-map of the main geomorphic processes signatures was created in order to (a) establish the thresholds of the classes of each attribute and DoD, and (b) to define the signatures (i.e. combination of classes) of each geomorphic process. As a proxy of the accuracy of the classification, 100 random points were distributed per each study period along the study area. The classification results in these points based on the expert-map (observed processes) were compared with the MaGPiE results by a confusion matrix calculated following the method described by Chuvieco (2016). This comparison allows assessing the percentage agreement of the method . Finally, the thresholded DoDs were segmented based on each geomorphic process through the GCD ArcMap-based extension (Figure 3). This last step allows the assessment of areal, vertical and volumetric changes associated to each process and for each study period (see more specific details in Llena et al., under revision).

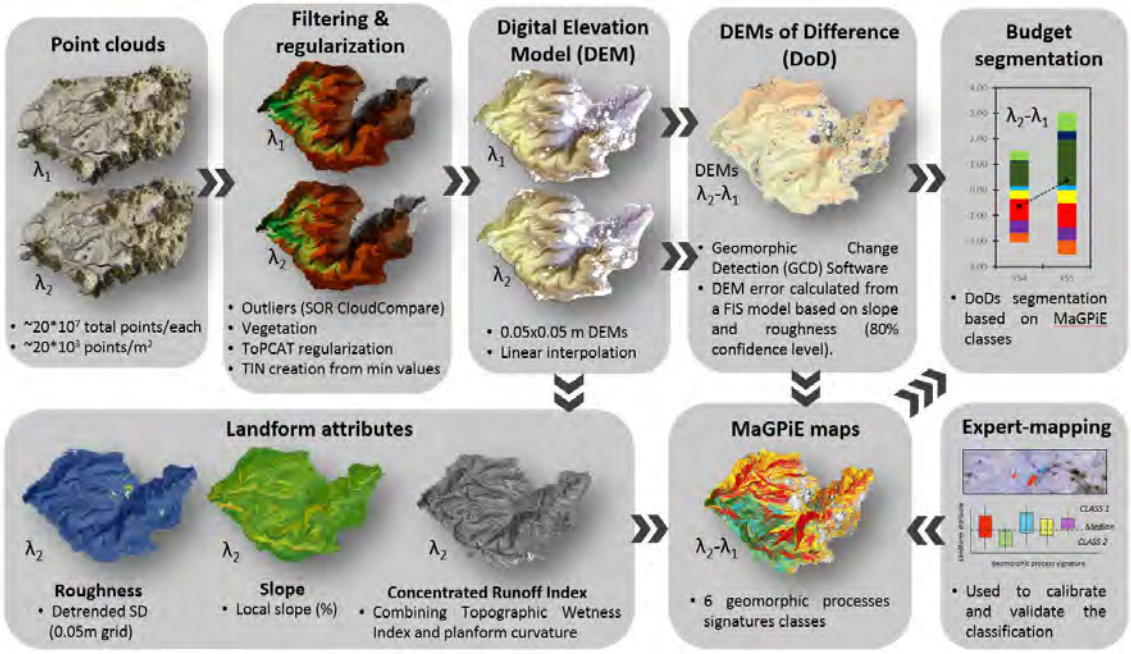


**Figure 3.** General workflow to obtain the geomorphic processes maps from the starting point clouds through several intermediate steps (i.e. filtering, DEMs obtaining, DoDs calculation, MaGPiE parametrization). See more details in Figures 2 of the Supplementary Materials and in Llena et al. (under revision)

### 3.2.3. Statistical analysis

The role of the meteorological variables on the geomorphic processes and associated topographic changes was analysed by means of Pearson correlation coefficients. A p-value of 0.05 was established to consider the correlations statistically significant.

## 4. RESULTS

## 4.1. Quality assessment

### 4.1.1. Topographic data sets

*Registration and georeferencing*

TLS-based surveys (i.e. S01 and S02) presented a registration error of 0.31 cm and 0.27 cm respectively. Both point clouds had an average point density larger than 6.7 points $cm^{-2}$. As mentioned above, the SfM-based surveys (i.e. S03-S11) were georeferenced by means of around 30 floating GCPs per badland. Table 3 shows the different Georeferencing Errors associated with each SfM-derived point cloud. Reported 3d errors range from 1.80 cm to 4.11 cm, with an average error of 2.32 cm. The highest errors were observed in the surveys S05 (i.e. 3.52 cm) and S06 (i.e. 4.11 cm) of the B2, and were mainly due to problems caused by the poor image overlapping in some areas. These problems were corrected in the following surveys, decreasing the errors to values smaller than the average (Table 3). The average point density of SfM-based ranged between 5 and 10 points $cm^{-2}$.

*Point cloud validation*

All the point clouds were independently validated by the ChPs surveyed by the TS, except S01 in which no ChPs were obtained. Results are presented in Table 3. The average MAE (i.e. 1.93 cm) is slightly smaller than the average SDE (2.52 cm) but with the same range, indicating that surveys have similar accuracy and precision. B2 presented, on average, higher MAE and SDE, especially in S05 (i.e. MAE of 2.49 cm and SDE of 3.27 cm) and S06 (i.e. MAE of 3.48 cm and SDE of 3.98 cm). As mentioned above, high errors in these surveys could have been due to the limited overlapping between photographs in some areas.

Both methods (TLS and SfM-based) were used in S03 in B1 to assess the differences between them (see more details in Llena et al., 2018). Briefly, a total of 4 patches (around 5 $m^2$) were selected. These patches were considered representative of flat surfaces, steep slopes, and high and low surface roughness for both micro-catchments. Both TLS and SfM-based point clouds in these patches were compared. Results indicated a MAE of 0.64 cm and a SDE of 0.71 cm, concluding that the differences between methods would not have a direct impact on the analyses of topographic changes.

### 4.1.2. Geomorphic processes signatures maps

Overall, the average percentage of agreement of the MaGPie classification is 77 % for B1 and 73 % for B2 (Table 3). In B1, the highest accuracy was obtained in S06 (i.e. 84 %) and the lowest in S07 (i.e. 62%), while in B2 the highest was obtained in S08 (i.e. 85%) and the lowest in S07 (i.e. 64%). There is no ay correlation between the topographic errors and the accuracy of the MaGPiE classification. In terms of the accuracy per each class, in B1 the most reliable signature is *Regolith Cohesion Loss* (86 % of agreement) with *Sheet Washing* signatures being the most challenging to identify (63 % of agreement). In B2 the most reliable signature is *Rilling and Gullying* (i.e. 85 % of agreement), while *Mass Wasting* (67 % of agreement) and *Cutting and Filling* (66 % of agreement) are identified least readily.

**Table 3**. Summary of the topographic surveys and quality assessment for both badlands. Note that the Georreferencing Errors (GE) of the Structure from Motion (SfM) based surveys were calculated from the Root Mean Square Error (RMSE) of the Ground Control Points (GCPs). In the case of the Terrestrial Laser Scanner (TLS) surveys, the GE includes the error associated to the registration of the different stations and the georereferencing of the point clouds. Mean Absolute Error (MAE) and Standard Deviation Error (SDE) were calculated based on the check points (ChPs). The accurazy of the MaGPiE classification results is also presented by the Classification Agreement (CA).

| Survey | Date | Badlands surveyed | Method | BADLAND 1 | | | | | | BADLAND 2 | | | | | |
|---|---|---|---|---|---|---|---|---|---|---|---|---|---|---|---|
| | | | | Photos (nº) | GE (cm) | ChPs (nº) | MAE (cm) | SDE (cm) | CA (%) | Photos (nº) | GE (cm) | ChPs (nº) | MAE (cm) | SDE (cm) | CA (%) |
| **S01** | 26/06/2013 | 1 | TLS | - | 0.31 | - | - | - | 81 | - | - | - | - | - | - |
| **S02** | 29/05/2014 | 1 | TLS | - | 0.27 | 568 | 1.16 | 1.66 | 67 | - | - | - | - | - | - |
| **S03** | 04/08/2015 | 1 | SfM | 237 | 2.25 | 260 | 1.60 | 2.09 | 77 | - | - | - | - | - | - |
| **S04** | 19/07/2016 | 1 | SfM | 475 | 1.87 | 270 | 1.87 | 2.61 | 81 | - | - | - | - | - | - |
| **S05** | 07/12/2016 | 1 and 2 | SfM | 740 | 2.19 | 256 | 1.57 | 2.14 | 82 | 320 | 3.52 | 95 | 2.49 | 3.27 | 68 |
| **S06** | 04/04/2017 | 1 and 2 | SfM | 525 | 1.91 | 238 | 1.25 | 1.67 | 84 | 332 | 4.11 | 244 | 3.48 | 3.98 | 65 |
| **S07** | 28/06/2017 | 1 and 2 | SfM | 889 | 2.22 | 413 | 1.72 | 2.29 | 62 | 326 | 2.64 | 357 | 1.82 | 2.29 | 64 |
| **S08** | 08/11/2017 | 1 and 2 | SfM | 497 | 2.14 | 518 | 2.25 | 2.81 | 82 | 305 | 1.78 | 572 | 2.21 | 2.29 | 85 |
| **S09** | 23/03/2018 | 1 and 2 | SfM | 579 | 1.80 | 271 | 2.36 | 2.82 | 81 | 372 | 1.79 | 116 | 1.71 | 2.21 | 83 |
| **S10** | 18/06/2018 | 1 and 2 | SfM | 446 | 2.23 | 259 | 1.60 | 2.09 | 72 | 225 | 1.46 | 128 | 1.79 | 2.43 | 73 |

## 4.2. Meteorological characterization of the periods

Main meteorological variables calculated for all the surveyed periods are presented in Table 4 and Figure 2. Annual average rainfall was 818 mm, ranging from 657 mm registered during 2015-2016, to 1001 mm registered in 2017-2018 (Table 4). According to the long-term data (1981-2018) from a nearby station (as stated in the study area section), we consider 2015-2016 as a dry year (i.e. -12 % of the mean long-term rainfall, i.e. 755 mm), while 2017-2018 can be categorised a wet year (i.e. +32% of the long-term mean). The lowest rainfall intensities (i.e. *MRI* and *MaxRI*) were registered during the wettest periods (i.e. 2016-2017 and 2017-2018). Contrary, highest intensities were registered in the driest periods (i.e. 2014-2015 and 2015-2016; Table 4). In terms of temperature, as for the total rainfall, the annual periods in which the highest number of days in which the temperature was below 0ºC were registered were 2016-2017 and 2017-2018 (i.e. 109 and 86 days respectively); while 2014-2015 and 2015-2016 presented fewer days with temperature below 0ºC (i.e. 49 and 31 days respectively). The magnitude of the minimum temperatures was associated with the number of days in which temperatures below 0ºC were registered. Both the minimum temperature and number of days bellow 0ºC were lower and larger respectively in 2016-2017 and 2017-2018.

**Table 4**. Summary of the meteorological variables during the study period grouped on annual and seasonal scales (see table 3 for the meaning of the abbreviations).

| | Code | Period | Survey period | ND (days) | TR (mm) | RD (hours) | MRI (mm/hour) | MaxRI (mm/hour) | MT (ºC) | Zd (days) | MTZD (ºC) | MinTZD (ºC) |
|---|---|---|---|---|---|---|---|---|---|---|---|---|
| Annual Scale | 13-14 | 2013-2014 | S01 – S02 | 338 | 794 | 299.00 | 2.65 | 20.40 | 12.60 | 50 | -1.44 | -6.20 |
| | 14-15 | 2014-2015 | S02 – S03 | 433 | 819 | 321.75 | 2.54 | 25.60 | 14.80 | 49 | -1.79 | -6.00 |
| | 15-16 | 2015-2016 | S03 – S04 | 351 | 657 | 168.08 | 3.91 | 21.60 | 13.10 | 31 | -1.29 | -3.90 |
| | 16-17 | 2016-2017 | S04 – S07 | 345 | 818 | 519.67 | 1.57 | 24.60 | 13.40 | 86 | -1.90 | -9.89 |
| | 17-18 | 2017-2018 | S07 – S10 | 356 | 1001 | 550.08 | 1.82 | 17.40 | 11.80 | 109 | -2.25 | -7.66 |
| Seasonal Scale | A2016 | Autumn 2016 | S04 – S05 | 142 | 355 | 163.42 | 2.17 | 20.40 | 18.20 | 13 | -1.35 | -4.19 |
| | W2016 | Winter 2016 | S05 – S06 | 119 | 254 | 171.25 | 1.49 | 10.20 | 5.10 | 70 | -3.28 | -9.89 |
| | S2017 | Spring 2017 | S06 – S07 | 86 | 209 | 185.00 | 1.13 | 24.60 | 17.10 | 3 | -1.06 | -2.16 |
| | A2017 | Autumn 2017 | S07 – S08 | 134 | 246 | 117.50 | 2.09 | 17.40 | 19.00 | 0 | - | - |
| | W2017 | Winter 2017 | S08 – S09 | 136 | 362 | 158.42 | 2.29 | 7.99 | 3.80 | 102 | -2.94 | -7.66 |
| | S2018 | Spring 2018 | S09 – S10 | 88 | 393 | 232.58 | 1.69 | 16.59 | 13.30 | 7 | -1.56 | -3.54 |

*Note that ND > 365 indicates the second survey was performed slightly ahead of one year after the first.

Results also indicate a high seasonal variability. Maximum rainfall was registered in Spring 2018 (S2018), while the highest intensity was observed in S2017, the driest season in the study period. The number of days with temperature below 0ºC in each season was highly variable, ranging from 102 in W2017 to none in A2017. Although W2017 was the season with more days below freezing, W2016 was the coldest season with an average below 0ºC temperature of -3.28 ºC, and a minimum temperature of -9.89 ºC (see Table 4 and Figure 2 for more details).

## 4.3. Topographic Changes

Table 5 presents the DoD results for both badlands and for the different study periods. Figure 4 and Figure 5 show the DoD maps of representative areas in each badland. The magnified representative areas are presented to facilitate the visualization and interpretation of the results. Maps of the entire badlands are provided in Figures 3 and 4 of the Supplementary Materials. It should be noted that negative and positive DoD values do not imply always erosion and sedimentation processes. For instance, a positive value of the DoD could reflect elevation increases due to both sedimentation or surface swelling; while a negative value may reflect surface lowering due to erosional or shrink processes. Therefore, to avoid confusion, we consider that red colours indicate surface lowering while blue represent surface raising.

**Table 5**. Summary of observed topographic changes extracted from thresholded DoDs for the different temporal scales analysed in the paper.

| | Study period | BADLAND 1 | | | | | | | BADLAND 2 | | | | | | |
|---|---|---|---|---|---|---|---|---|---|---|---|---|---|---|---|
| | | Areal changes ($m^2$) | | Volume Difference ($m^3$) | | | Average Net Thickness Difference (cm) | Area with changes above the minLoD (% total) | Areal changes ($m^2$) | | Volume Difference ($m^3$) | | | Average Net Thickness Difference (cm) | Area with changes above the minLoD (% total) |
| | | Lowering | Raising | Lowering | Raising | Net change | | | Lowering | Raising | Lowering | Raising | Net change | | |
| Annual Scale | 13-14 | 39.11 | 3.57 | 4.17 | 0.3 | -3.86 | -0.15 | 1.66 | - | - | - | - | - | - | - |
| | 14-15 | 14.24 | 17.92 | 1.22 | 1.37 | 0.15 | 0.01 | 1.22 | - | - | - | - | - | - | - |
| | 15-16 | 21.75 | 5.42 | 1.78 | 0.69 | -1.09 | -0.05 | 1.14 | - | - | - | - | - | - | - |
| | 16-17 | 65.65 | 11.22 | 5.3 | 1.96 | -3.34 | -0.13 | 3.10 | 28.22 | 11.62 | 2.1 | 1.47 | -0.63 | -0.06 | 5.07 |
| | 17-18 | 41.78 | 34.69 | 3.83 | 3.08 | -0.75 | -0.03 | 3.11 | 25.6 | 25.76 | 2.58 | 2.94 | 0.36 | 0.04 | |
| Seasonal Scale | A2016 | 44.79 | 9.21 | 3.42 | 1.71 | -1.7 | -0.07 | 2.08 | - | - | - | - | - | - | - |
| | W2016 | 14.69 | 28.07 | 1.52 | 2.28 | 0.77 | 0.03 | 1.59 | 24.42 | 19.18 | 2.51 | 2.09 | -0.42 | -0.04 | 4.17 |
| | S2017 | 43.13 | 34.58 | 3.42 | 3.09 | -0.33 | -0.01 | 3.11 | 26.69 | 14.58 | 2.14 | 1.69 | -0.45 | -0.04 | 3.95 |
| | A2017 | 15.08 | 31.09 | 1.23 | 2.63 | 1.4 | 0.06 | 1.83 | 18.96 | 8.37 | 1.84 | 0.66 | -1.18 | -0.11 | 2.6 |
| | W2017 | 32.52 | 35.9 | 2.92 | 3.14 | 0.23 | 0.01 | 2.47 | 13.58 | 22.67 | 1.54 | 2.48 | 0.94 | 0.09 | 3.43 |
| | S2018 | 45.54 | 21.5 | 4.29 | 1.88 | -2.41 | -0.09 | 2.59 | 15.61 | 19.17 | 1.51 | 2.01 | 0.5 | 0.05 | 3.44 |
| Totals | 16-18 | 84.62 | 20.67 | 7.2 | 2.89 | -4.31 | -0.86 | 4.19 | 69.64 | 27.31 | 5.74 | 3.48 | -2.26 | -0.22 | 9.62 |
| | 13-18 | 247.97 | 9.93 | 21.95 | 1.03 | -20.92 | -4.09 | 10.54 | - | - | - | - | - | - | - |

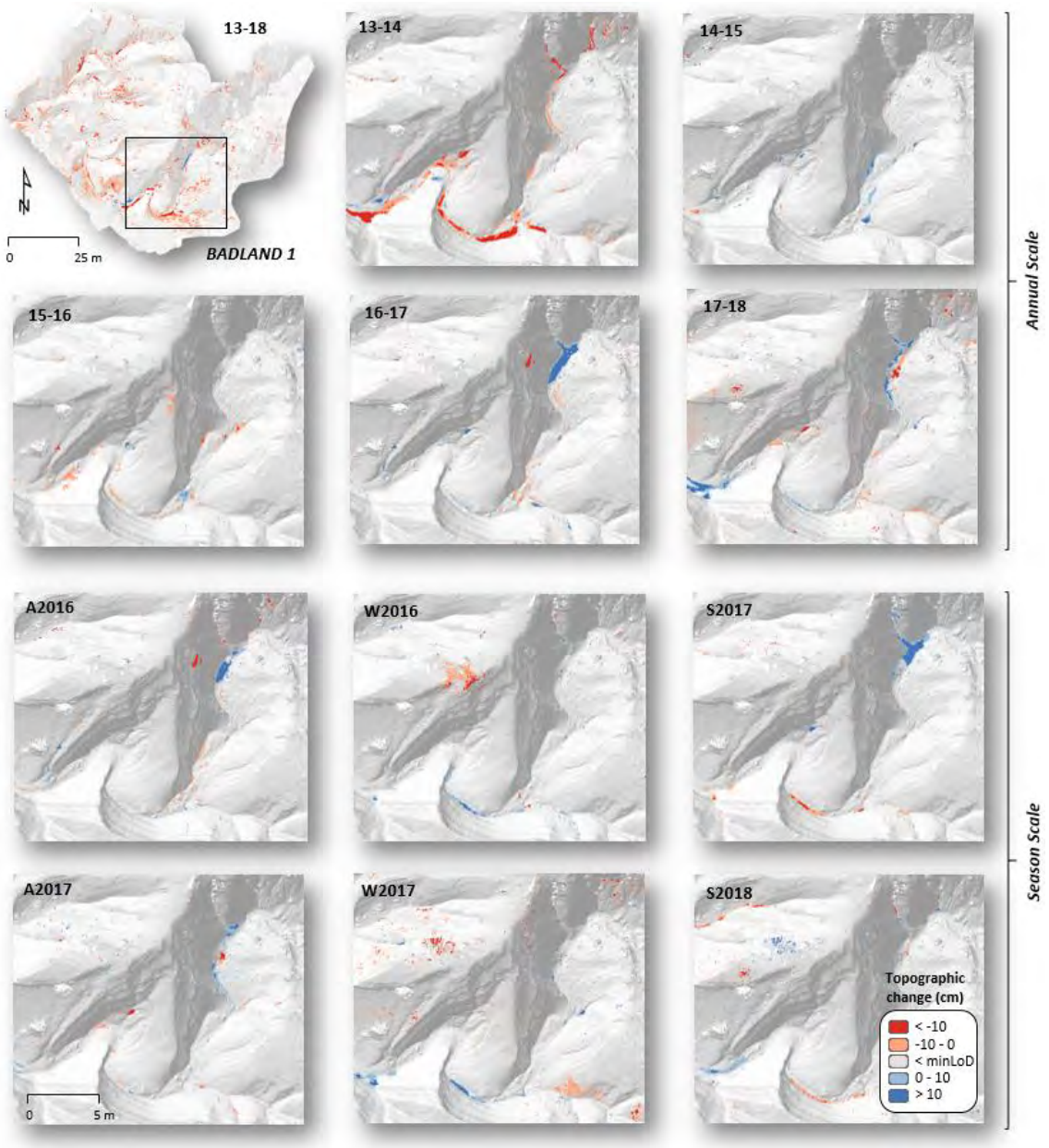


**Figure 4**. DoD maps of a representative area of B1 for the different analysed temporal scales: annual (upper part) and seasonal (lower part) scales. Note that the DoD of the entire badland (top left) corresponds to the map associated with the complete study period (2013-2018) in this badland. The location of the representative area is also shown. Changes below the minimum level of detection (i.e. minLoD) are not presented (considered uncertain) and an underlying shaded DEM is provided to give the context. The entire DoDs maps are presented in Figure 3 of the Supplementary Materials section.

Overall, the areas presenting topographical changes above the minLoD were relatively small, indicating that the magnitude of topographic changes was relatively low and in the range of the uncertainty of the surveys. Topographic changes were spatially and temporally concentrated; intermittent high magnitude changes were observed over the five-year dataset. These observations indicate that although significant changes are only observed in less than a 5% of the total area (on average for all surveys), surface raising and lowering in these areas may be significant, up to 10 cm of change. Surface lowering was mainly located in high slope areas and

in the main channels (see examples in Figures 4 and 5); yet, surface raising was mainly observed in the accumulation zones located at the toe of the slopes near the main channels, and also in the main channels themselves (Figures 4 and 5). These patterns are observed at all temporal scales, annually and seasonally, and in both badlands, B1 and B2. Finally, in terms of the areal changes, our results indicate that both areas associated with surface lowering and those with surface raising are relatively more widespread in the seasonal analyses compared with annual observations.

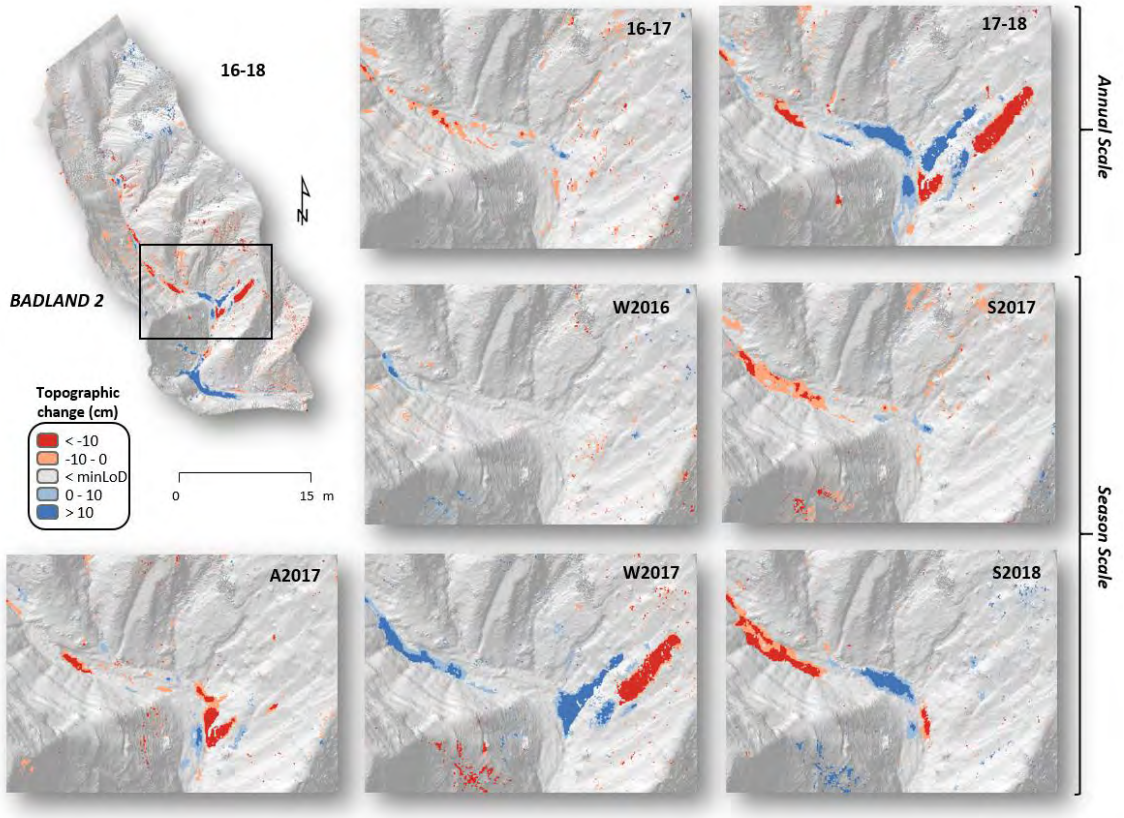


**Figure 5**. DoD maps of a representative area of B2 for the different analysed temporal scales: annual (upper part) and seasonal (lower part) scales. Note that the DoD of the entire badland (top left) corresponds to the map associated with the complete study period (2016-2018) in this badland. The location of the representative area is also shown. Changes below the minLoD are not presented (considered uncertain) and an underlying shaded DEM is provided to give the context. The entire DoDs maps are presented in Figure 4 of the Supplementary Materials section.

Annually, net changes ranged between virtually none (i.e. 0.01 cm $yr^{-1}$) in 2014-2015 to -0.15 cm $yr^{-1}$ in 2013-14 (yielding a maximum net export of -3.86 $m^3$). A similarly high value to the latter was also observed in 2016-17 (i.e. -0.13 $yr^{-1}$, -3.34 $m^3$ $yr^{-1}$). Net changes near or above -1 cm were observed at temporal scales larger than the annual (Table 5). The net change observed in B1 for the period 2016-18 was -0.86 cm (-4.31 $m^3$), a larger value compared to the net change in B2 for the same period (i.e. -0.22 cm or -2.26 $m^3$, values yielding annual values of -0.11 cm $yr^{-1}$ or -1.13 $m^3$ $yr^{-1}$). Long term topographic changes observed in B1 (2013-18) yielded a net change of -4.09 cm (-0.8 cm $yr^{-1}$, -4.18 $m^3$ $yr^{-1}$). Differences in mean annual net changes based on the

length of the period analysed indicate processes that are heavily variable through time and, consequently, values may be highly biased based on the period used to study topographic changes. Additionally, changes can be highly variable spatially too. Seasonally, net topographic changes are very low; the largest value was observed in B2 in A2017 (i.e. -0.11 cm). The largest volumetric change was observed in B1 in S2008 (-2.41 $m^3$). The sign of the net change fluctuates between positive and negative values. All the periods with positive net values of change presented relatively very low values, with the exception of the winter seasons were positive net changes are higher (Table 5). It is worth noting that values obtained for short temporal scales (seasonal and annual) do not add up to longer term values when compared. For example, net change observed in B1 for the period 2016-18 (i.e. 0.86 cm) yielded an average annual net change of -0.43 cm $yr^{-1}$, but the average value of net changes assessed based on the annual scale observations was -0.08 cm $yr^{-1}$. In B2, for the same period, annual changes oscillate between -0.11 cm $yr^{-1}$ and -0.02 cm $yr^{-1}$, depending the temporal scales used to estimate the mean annual change. These differences are attributed to the effect of the minLoD. Areas subjected to changes below the minLoD (i.e. uncertain changes) are generally more extensive when a shorter survey interval is analysed. In terms of differences between badlands, Figure 6 shows that as the total changes observed in B2 are between 2 and 4 times higher than the computed for B1. In general, both volumes attributed to surface lowering and raising are always higher in B2 than in B1. Additionally, the seasonal evolution of the specific net changes show that dominant processes are variable in space.

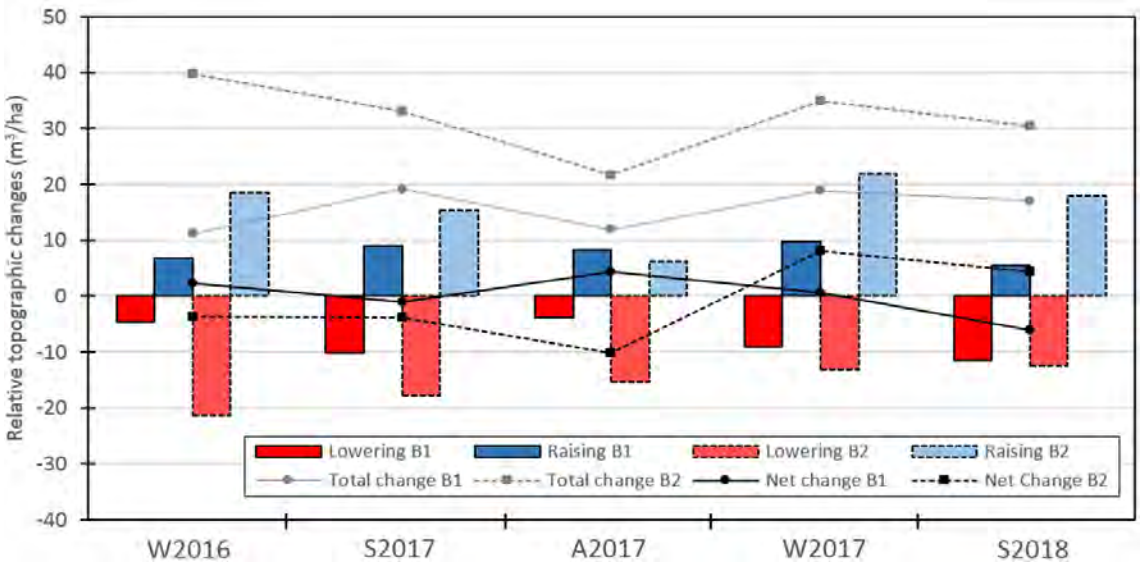


**Figure 6**. Specific topographic changes (expressed as m3 ha-1) in both badlands for the period 2016-2018 (the fully coincident period between B1 and B2). Total lowering (red columns), total raising (blue columns), total topographic change (grey lines) and net topographic change (black lines) are presented. Lines correspond to B1, while dotted lines correspond to B2.

In terms of the relation between the magnitude of change and surveyed time span, Figure 7 shows topographic changes (i.e. Lowering, Raising, Net Topographic Change and Total Topographic Change) observed at different temporal scales in each badland. When temporal scales are smaller than one year (i.e. seasonal), both badlands did not present a clear trend, presenting net changes around zero, while negative net changes are obtained at longer temporal scales.

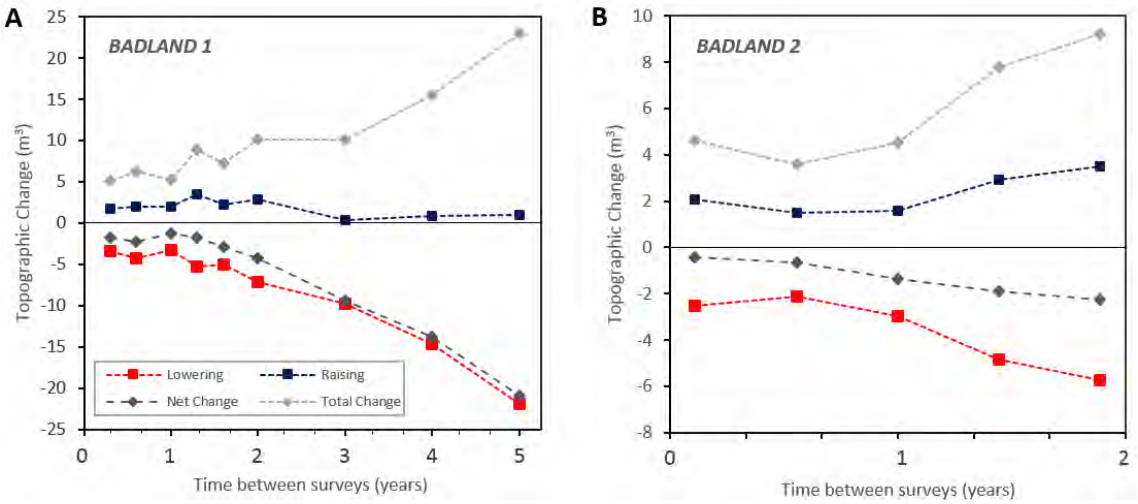


**Figure 7**. Evolution of volumetric topographic changes (i.e. lowering, raising, total change and net change) for different temporal scales in B1 (**A**) and B2 (**B**). Note that the legend only appears in A but remains the same for B.

## 4.4. Geomorphic processes signatures

Figure 8 shows the distribution of each geomorphic process signature identified by the MaGPiE algorithm. Although results indicate that signatures are variable through time, the main signatures observed during the study period are: *Cutting and Filling* in B1 and *Mass Wasting* in B2. Information about area occupied by each geomorphic processes in both experimental badlands and both temporal scales (i.e. annual and seasonal) is presented in Figure 5 of the Supplementary Materials. In particular, the process observed over the largest area was *Cutting and Filling* during the annual scale 2016-17 in B1 (i.e. 31 $m^2$); specifically, 42 % of the area above the minLoD for this period was attributed to this process signature. In both badlands, the geomorphic process signature observed with lower magnitude, both in terms of volume and area, was *Overlapping Processes.* It is worth noting that this process signature is attributed when an observed topographic change cannot be attributed to any other process classification. As such, the overlapping processes class may also include other processes not identified or selected as the main geomorphic processes signatures.

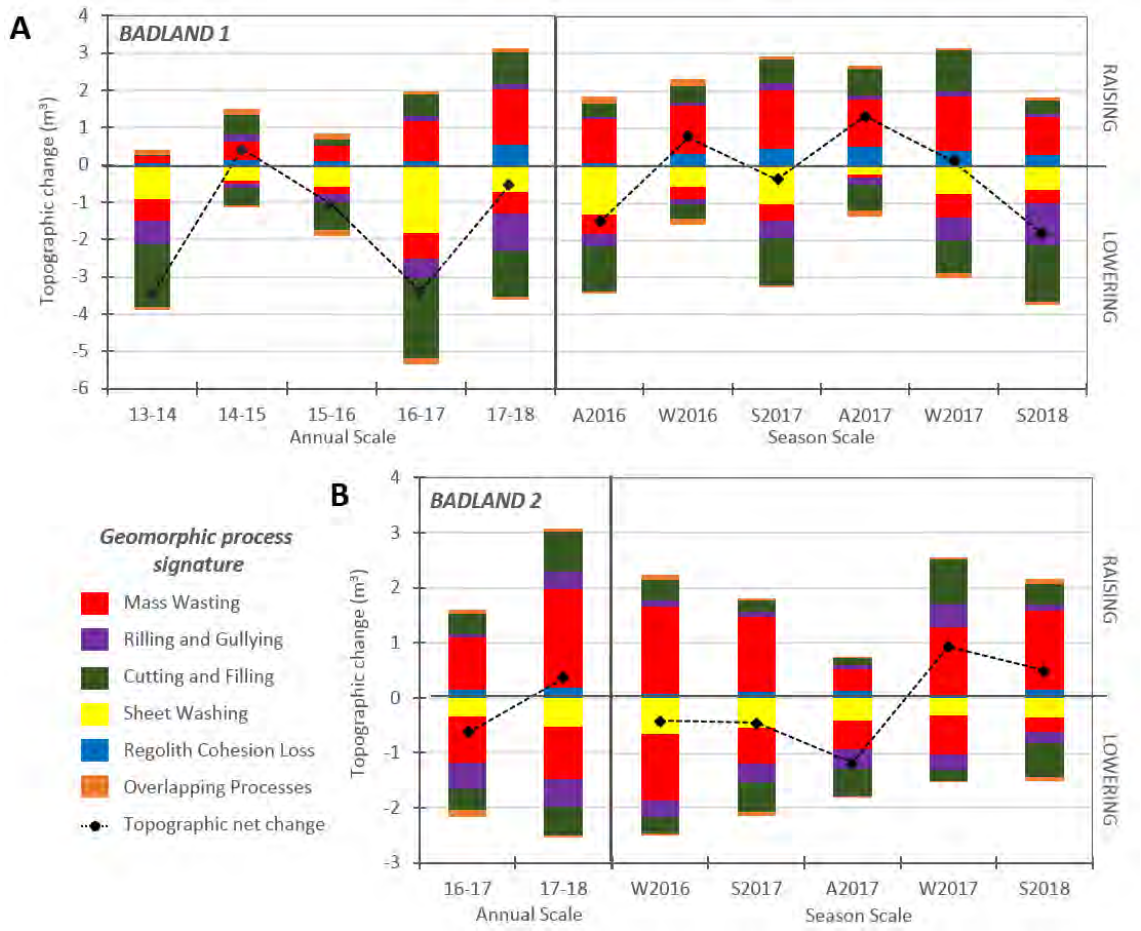


**Figure 8**. Volumetric changes associated to geomorphic processes obtained from the MaGPiE algorithm for B1 (**A**) and B2 (**B**) experimental badlands and at the different temporal scales analysed (i.e. annual and seasonal). The net topographic change is also presented with a dotted black line for all the periods.

Figure 8A and 8B show the volume of change attributed to each process signature together with the evolution of the volumetric net change for all the study periods and for B1 and B2, respectively. Main surface lowering-based processes responsible for the volumetric changes observed in B1 were those driven by surface runoff either diffuse (e.g. *Sheet Washing*) or concentrated (e.g. *Rilling and Gullying*, *Cutting and Filling*). *Sheet Washing* occurred in less steep but highly exposed slopes (e.g. ii in Figure 9). Erosion caused by *Rilling and Gullying* was observed in steep slopes perpendicular to main channels (e.g. i in Figure 10), while *Cutting and Filling* occurred in the main channel bottoms (i and iii in Figure 10). The main lowering-based process observed in B2 was *Mass Wasting,* although, occasionally, processes driven by surface runoff also caused high magnitude changes (e.g. S2018). Erosion caused by *Mass Wasting* were mainly observed in the steepest north-face slopes (e.g. iii in Figure 9 and i and ii in Figure 10) and triggered by gravitational processes together with rainsplash erosion, mobilisingthe regolith that was previously weathered by freeze-thaw and soil moisture changes (e.g. Barnes et al., 2016).

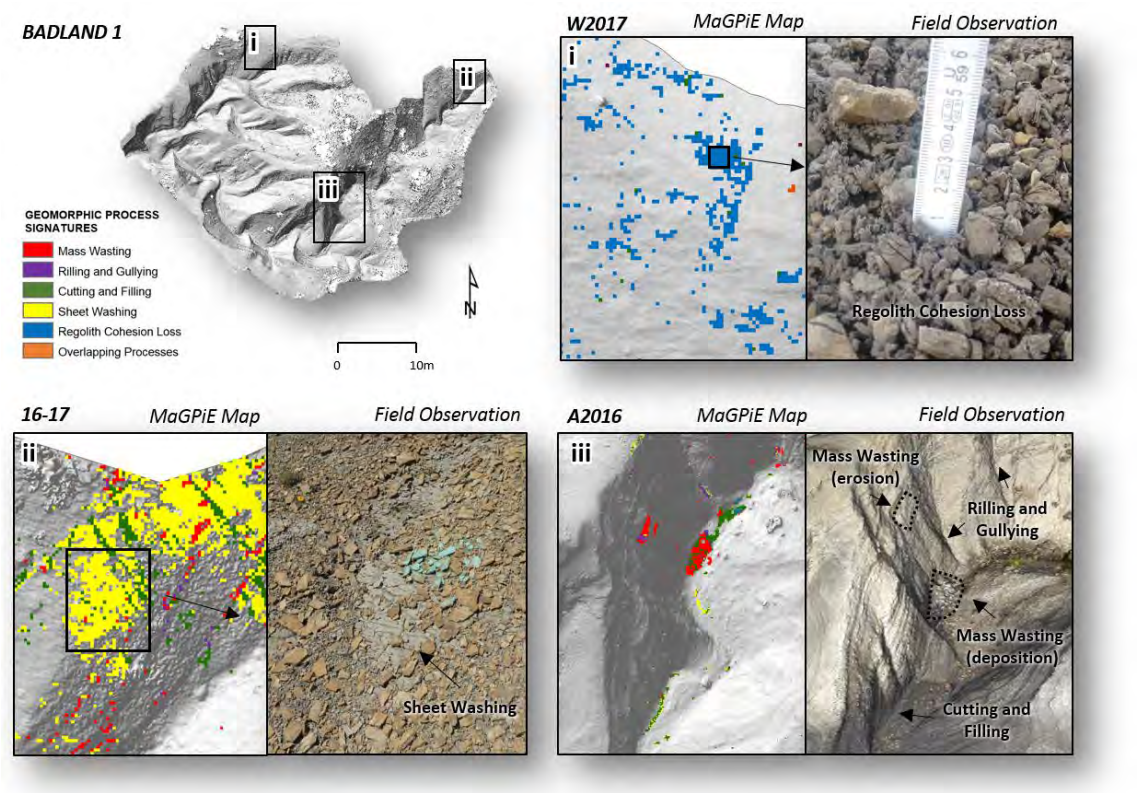


**Figure 9.** Examples of geomorphic maps of processes linked to field observations for different periods in some specific areas of B1. Note that the entire maps are presented in Figure 6 of the Supplementary Materials section.

In relation to surface raising-based processes signatures, deposition caused by *Mass Wasting* is the principal process observed in both badlands for all time scales, followed by *Cutting and Filling* and *Regolith Cohesion Loss* in the case of B1, and *Rilling and Gullying* in B2. Deposition caused by *Mass Wasting* was mainly observed in the bottom of the main channels, associated with the fallen regolith coming from steep slopes (e.g. iii in Figure 9 and ii in Figure 108), or with small accumulation zones located at the base of the slopes near the main channel (e.g. ii in Figure 10). In the latter case, gelivation processes and rainsplash erosion in the slopes are considered to be the main drivers (e.g. Nadal-Romero and Regüés, 2010). The magnitude of these processes signatures was generally low and, consequently, likely below the minLoD and thus not mapped. The magnitude of deposition caused by *Mass Wasting* trends to be larger, mainly due to both the accumulation of materials in small areas and the increase of the volume of the regolith after its fracture (e.g. iii in Figure 9; Nadal-Romero et al., 2007); consequently, these process signatures are less biased and clearly observed in the map. Deposition caused by *Rilling and Gullying* had a relatively low magnitude, especially in B1; mainly due to the low stability of regolith sedimentation deposits in steep slopes (i.e. where mainly rills and gullies are developed). Finally, *Regolith Cohesion Loss* was one of the surface-raising processes that yielded lower volumetric changes, especially in B2. Surface rising associated to this process is mostly due to the fracture of the regolith caused by both the freeze-thaw (e.g. Barnes et al., 2016; Tsutsumi and Fujita, 2016) and moisture-change cycles (e.g. Nadal-Romero and Regüés, 2010). The main location of this process is in flat and north slopes (shaded areas; e.g. i in Figure 9). Figures 9 and 10 only show some examples of geomorphic maps of processes signatures linked to field observations for different periods in some specific areas; the entire geomorphic maps are presented in Figure 6 and 7 of the Supplementary Materials.

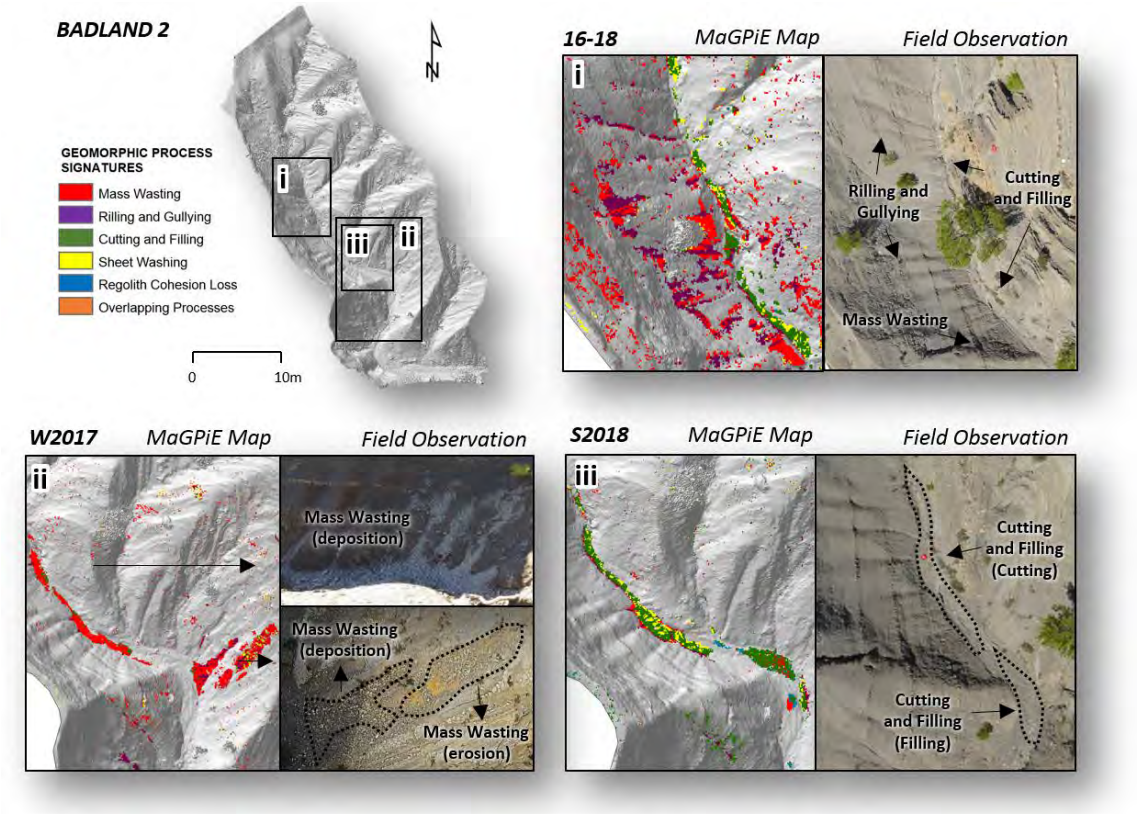


**Figure 10**. Examples of geomorphic processes maps linked to field observations for different periods in some specific areas of B2. Note that the entire maps are presented in Figure 7 of the Supplementary Materials section.

## 4.5. Statistical correlations between meteorological variables and geomorphic processes

Table 6 show the results of the Pearson correlation matrix between topographic changes segmented by the main geomorphic process and the meteorological variables. Rainfall variables are well correlated with lowering processes driven by surface flow. For instance, *In-channel Erosion* is significantly correlated with Rainfall Duration (*RD*) in B1, and *Rill and Gully Erosion* is correlated with Total Rainfall (*TR*) and *RD* in B2. Variables associated with minimum temperatures are significantly correlated with *Regolith Fall Erosion* in the two badlands (i.e. days with temperatures lower than 0º -*Zd*- in B1, and minimum temperature –*MinTZD*- in B2). In B2, surface raising processes such as *Rill and Gully Deposition are* correlated with *Zd*, while *In-channel Deposition* is significantly correlated with mean temperature (*MT*) and *Zd*. Our results also indicated that *Regolith Cohesion Loss* is significantly correlated with the mean temperature of days below 0ºC (*MTZD*) in B2. Finally, *Overlapping Processes* are not correlated with any of the measured meteorological variables.

**Table 6**. Pearson correlation results between meteorological variables and topographic changes segregated by the main geomorphic processes in Badland 1 (B1) and Badland 2 (B2). Highlighted values represent significant correlations at $p < 0.05$. Note that the abbreviations of the variables are presented in table 2.

| | | Change | ND | TR | RD | MRI | MaxRI | MT | Zd | MTZD | MinTZD |
|---|---|---|---|---|---|---|---|---|---|---|---|
| B1 | Mass Wasting | - | 0.02 | 0.23 | 0.46 | 0.33 | 0.15 | 0.33 | **0.55** | 0.42 | 0.55 |
| | | + | **-0.64** | -0.48 | -0.04 | **-0.73** | -0.40 | -0.11 | 0.12 | -0.18 | 0.01 |
| | Rilling and Gullying | - | 0.11 | 0.25 | 0.43 | 0.29 | 0.18 | 0.14 | 0.23 | 0.14 | 0.09 |
| | | + | 0.02 | 0.00 | 0.28 | **-0.53** | 0.17 | 0.03 | 0.24 | -0.12 | -0.10 |
| | Cutting and Filling | - | -0.10 | 0.33 | **0.54** | 0.28 | -0.35 | -0.21 | 0.08 | -0.15 | 0.15 |
| | | + | -0.22 | -0.12 | 0.15 | -0.42 | -0.40 | -0.28 | 0.46 | -0.27 | -0.13 |
| | Sheet Washing | - | -0.08 | 0.19 | 0.44 | 0.31 | -0.34 | -0.10 | 0.21 | 0.11 | 0.39 |
| | Regolith Cohesion Loss | + | -0.44 | -0.32 | -0.05 | -0.48 | -0.44 | -0.13 | 0.10 | -0.02 | 0.21 |
| | Overlapping Proccesses | - / + | 0.35 | -0.15 | -0.48 | 0.36 | 0.31 | 0.32 | 0.41 | 0.10 | -0.06 |
| | TOTAL CHANGE | | 0.25 | 0.05 | 0.48 | **0.65** | 0.08 | 0.07 | 0.35 | 0.18 | 0.25 |
| B2 | Mass Wasting | - | 0.40 | 0.26 | 0.28 | -0.18 | -0.23 | -0.52 | 0.65 | 0.64 | **0.73** |
| | | + | 0.12 | 0.31 | 0.32 | -0.35 | -0.21 | -0.49 | 0.42 | -0.19 | -0.48 |
| | Rilling and Gullying | - | **0.93** | **0.81** | **0.82** | -0.04 | 0.45 | 0.18 | 0.54 | -0.01 | 0.38 |
| | | + | 0.18 | 0.28 | 0.11 | 0.60 | -0.61 | -0.64 | **0.68** | -0.55 | -0.33 |
| | Cutting and Filling | - | -0.05 | 0.10 | 0.16 | -0.37 | 0.58 | **-0.77** | -0.62 | -0.65 | -0.63 |
| | | + | 0.38 | 0.50 | 0.35 | 0.52 | -0.54 | **-0.72** | **0.83** | -0.55 | -0.57 |
| | Sheet Washing | - | -0.10 | -0.14 | -0.06 | -0.59 | -0.05 | -0.11 | -0.01 | 0.25 | 0.15 |
| | Regolith Cohesion Loss | + | 0.61 | 0.65 | 0.42 | -0.20 | 0.66 | 0.62 | -0.07 | **0.73** | 0.13 |
| | Overlapping Proccesses | - / + | -0.43 | -0.07 | -0.16 | 0.44 | 0.14 | -0.2 | 0.22 | 0.39 | 0.24 |
| | TOTAL CHANGE | | 0.43 | 0.53 | 0.51 | 0.16 | 0.24 | 0.54 | **0.70** | **0.71** | 0.63 |

Overall, geomorphic process observed in B1 presented better correlations with rainfall-based variables, while those observed in B2 presented better correlations with the variables related to minimum temperatures. This is verified when the results for the total change are observed (Table 6). For instance, a significant positive correlation between total topographic change and Maximum Rainfall Intensity (*MRI*) is observed in B1, while, in B2, total topographic change is significantly correlated with the number of days below 0ºC (i.e. *Zd*) and the mean temperature of the minimum temperatures of the days below 0ºC (i.e. *MTZD*).

## 5. DISCUSSION

### 5.1. The role of meteorological variables on geomorphic processes

Several authors have observed correlations between erosional processes and rainfall events such as the ones observed in this study. Canton et al. (2000) described how, in arid badlands of SE Spain, main erosive processes were driven by high-intensity rainfall events, while in nearby badlands, Solé-Benet et al. (2012) observed as erosional processes and rainfall intensity were more correlated than with the total rainfall. Desir and Marín (2013) observed, in a badland located in the NE of Spain with similar characteristics to our study area, that erosional processes

were mainly controlled by both the amount of rainfall and its intensity. Although the method used to assess erosion differs to our approach (i.e. sparse observations versus continuous spatial distributed erosion and sedimentation values), their results are in agreement to our observations.

Correlations between variables associated with minimum temperatures and *Regolith Fall Erosion for both badlands* are in agreement with those reported by Barnes et al. (2016), who concluded that mass wasting processes produced in sidewalls (i.e. *Mass Wasting* in our study) are mainly controlled by freeze-thaw events in a scarcely vegetated area of the East of the USA. Although a substantial volume of the materials mobilised by *Mass Wasting Erosion* is deposited in the toe of the slopes, a large proportion of these materials is transported by surface flows and finally deposited in the main channels of the badlands. These interactions may explain the significant correlation between variables associated with minimum temperatures and depositional processes in channels in B2; and were also observed by Descroix and Olivry (2002), who noted that runoff caused by rainfall events mobilize the regolith previously weathered by freeze-thaw cycles in the Black marls of Draix (Southern Alps, France). At the same time, the significant correlation between *Regolith Cohesion Loss* and the mean temperature of the minimum temperatures of the days below 0ºC (*MTZD*) in B2, indicates that *Regolith Cohesion Loss* is probably mainly controlled by freeze-thaw cycles. Nadal-Romero and Regüés (2010) observed that, in sub-humid badlands developed on marls (Central Pyrenees, NE Iberian Peninsula, Spain), maximum regolith alteration was produced during winter periods, mainly due to the freeze-thaw cycles that caused the so-called *popcorn* morphology. As stated, weathered surfaces will be the main source of sediments during subsequent rainfall events. In this way, Regüés et al. (1995) also proved that the main erosional processes in badlands of the eastern Pyrenees (NE Iberian Peninsula, Spain), were controlled by weathering, freeze-thaw cycles, and that these materials were depleted form the slopes after rainfall events.

Generally, geomorphic process observed in B1 presented better correlations with rainfall-based variables, while those observed in B2 presented better correlations with the variables related to minimum temperatures. Due to the fact that the meteorological variables are the same in both badlands, differences between correlations may be explained by the existence of other controlling factors such as, for instance, the morphometry of the badands (see details in Table 1).

## 5.2. The role of morphometry on geomorphic processes

As presented in Section 4.4., the contribution of the main geomorphic processes signatures in each badland to sediment transfer and export was slightly different. In terms of surface lowering-based processes, B1 mainly demonstrated processes driven by surface runoff, both diffuse (i.e. *Sheet Washing*) and concentrated (i.e. *Cutting and Filling, Rilling and Gullying*). In B2 *Mass Wasting* were the main observed processes. The MaGPIE algorithm permitted the mapping of geomorphic processes based on the magnitude and sign of the topographic changes and several variables related to the morphometry of the badlands. The significance of surface-runoff based processes in B1 can be partly explained by the larger catchment area compared to B2 (i.e. around 30% more; Table 1), meaning that B1 potentially has a greater propensity toward runoff concentration than B2 due to its relatively higher upslope catchment areas. B2, however, has higher slopes (i.e. 16% more than B1; Table 1). The local slope is one of the main parameters that determine stability, and consequently, has a direct control on triggering mass movements (i.e. *Mass Wasting*; Bishop and Morgenstern, 1960; Morgenstern and Price, 1965). Additionally, several authors have pointed out that the aspect is, together with the slope, one of the main

factors determining geomorphic processes since they have a direct control on freeze-thaw and dry-wet cycles which are active regolith-weathering agents in shady aspects (e.g. Yair et al., 1980; Calvo-Cases and Harvey, 1996; Nadal-Romero et al., 2007; Vericat et al., 2014; Nadal-Romero et al., 2015). Mean slope on shady aspects in B2 is 31% higher than in B1, proving an explanation as to why *Mass Wasting* processes are higher than in B1.

In terms of surface raising-based processes, *Mass Wasting* is the main geomorphic process observed in both badlands. Even so, the magnitude of change for this process was higher in B2. This difference can be explained by the higher slopes in B2 compared to B1 (Table 1) as stated above. *Mass Wasting* is followed by *Cutting and Filling* processes in both badlands, presenting approximately the same magnitude in terms of surface raising. The third main raising-based process signature differs in each badland: *Regolith Cohesion Loss* in B1 and *Rilling and Gullying* in B2. High slopes in B2 determined the accumulations of sediments in the lower parts of rills and gullies. High slopes also favour the instability of the regolith after its fracture (e.g. gelivation process), causing the dislodgment to the lower parts (i.e. *Mass Wasting*). In areas with low slope (e.g. B1), the fractured regolith remains stable and could present popcorn morphologies (i.e. *Regolith Cohesion Loss*).

As discussed, morphometry determines both the typology of the dominant geomorphic process and the magnitude of these, although the absolute magnitude of these is, of course, influenced by the extension of the badlands too. As observed in Table 2, the surface area of both badlands is different; B2 is 62.5% smaller than B1. Specific seasonal (2016-2018) volumetric changes (i.e. $m^3\ ha^{-1}$) were computed to compare the magnitude of the topographic changes through time in the two badlands. Total changes observed in B2 are between 2 and 4 times higher than the obtained for B1 (Figure 6). Differences between badlands may be attributed to the slope and aspect, as discussed previously, but also to the differences in terms of vegetation cover and sediment connectivity. Broadly, B2 has a lower vegetation cover and higher sediment connectivity than B1 (Table 1). Different studies have focused on the role of vegetation cover preventing erosion in badlands (e.g. Regüés et al., 2000; Gallart et al., 2002; Gallart et al., 2013; Nadal-Romero et al. 2014; Torri et al., 2018). In the Biancana badlands (south of Italy), Torri et al. (2018) observed that the presence of vegetation controls soil properties and the resistance to erosion and degradation. In terms of sediment connectivity, several authors have analysed the feedbacks between badland morphology its evolution, and sediment connectivity (e.g. Faulkner, 2008; Grenfell et al., 2012; Marchamalo et al., 2016). For instance, in semi-arid badlands located in SE Spain, Marchamalo et al. (2016) noted that a high degree of connectivity had a positive and direct relation to the frequency of water and sediment fluxes and, consequently, to slope erosion.

Finally, it is worth mentioning that lithology also plays an important role on the geomorphic processes reshaping badlands. Lithology determines key physical characteristics of badlands landscapes (e.g. hardness, density) and, consequently, has a direct effect on the potential degree of erosion of these materials. For instance, Cerdá (1997) analysed erosion on badlands developed on two different lithologies, marls and clays, and under the same rainfall conditions. He showed that erosion on marls was two orders of magnitude higher than in clays. At the same time, the lithological typology and the structure of geological features (e.g. dip and strike) has also an influence on the morphometry (Table 1) which, in turn, as seen above, determines the typology of the dominant geomorphological process. Our study area is a clear example of how the geological structure controls badland landscape morphometry and associated geomorphic processes. Regarding the effect of lithology on morphometry, Moreno-de las Heras and Gallart (2016) observed how badlands developed on Eocene marls in the eastern Pyrenees (NE Iberain Penninsula, Spain) presented a preferential distribution on north-slope aspects with higher

slope degree than the ones in badlands developed on Garumnian lutites in the same study area, which did not reveal a clear slope-aspect pattern.

The degree of compactness of the marl outcrops in the experimental badlands region is relatively high, which, added to the intercalation of hard layers of sandstones and gypsum, means that the badlands of the study area have a relatively low degree of erosion in comparison with other studies in the same region. For instance, Vericat et al. (2014) reported annual net changes of around 6 cm in a small (90 $m^2$) experimental badland located in a nearby catchment with no vegetation cover. Meanwhile, Francke et al. (2008) reported a minimum mean erosion value of 2.1 cm $y^{-1}$ in the same study area measured by spatially distributed erosion pins. Also in a nearby badlands developed on Eocene marls, Nadal-Romero et al. (2015) observed a mean annual erosion value that range from 0.2 to 7 cm depending on the aspect and survey technique. The differences between these studies and the results reported here may be attributed to the extent over which data were obtained, the method used to acquire the data (punctual observations versus spatially distribute observations), the precision and accuracy of the measurements and the temporal scale in which observations were obtained (as discussed previously). Despite these differences, the experimental badlands can be considered representative, specifically, of all the south face of the Pyrenees' badlands developed on Eocene marls. In a broader sense, they are also representative of badlands developed on these type of materials in sub-humid mountain areas worldwide.

## 5.3. The role of the temporal scale on depicting main geomorphic processes

As observed in Table 5 and previously stated in other studies (e.g. Balasch et al., 1988; Descroix and Olivry, 2002; Nadal-Romero et al., 2007; Vericat et al., 2014; Aucelli et al., 2016; Ballesteros-Cánovas et al., 2017), topographic changes are sensitive to the temporal scale over which they are computed. This, although self-evident, will influence our understanding of the main geomorphic processes reshaping badlands at longer temporal scales. Thus, having a continuity of five years of study, allows to observe see certain patterns in the geomorphic processes, which are not possible with shorter study periods. Geomorphic processes are acting at different temporal scales, driven by meteorological variables and also by other internal factors such as morphometry and lithology, and also conditioned by the effects of the minLoD on the computation of the thresholded DoDs as discussed above. Within this context, processes observed to dominate during winter months may not be the principal agents of change at annual scales, but nevertheless, may have a direct influence on the preparation of the sediments that eventually will be exported from badlands (at larger temporal scales, e.g. annually). In the same way, results observed during short periods of time may be biased, representing neither the general trend of these landscapes nor gross erosion rates. This is evident when net changes are positive or near zero; a larger temporal scale is required to investigate the net export of sediment. Taking the results of short temporal scales to predict long term patterns would bias the interpretations. In summary, short term surveys capture real changes that might be later masked by compensatory changes acting at longer temporal scales; however, they suffer from the minLoD filtering out small changes, a problem less of an issue over longer timescales.

As stated above, when temporal scales are smaller than one year (i.e. seasonal), both badlands do not present a clear trend in terms of topographic change, presenting net changes around zero (Figure 7). Vericat et al. (2014) analysed the importance of the temporal scale on the analysis of the topographic changes, concluding that although event scale changes are heavily variable, from net surface raising to net lowering, a significant negative pattern (surface lowering, i.e. net export) is observed at the annual scale. Therefore, they suggested the need of

appropriately-scaled spatial and temporal data to understand topographic changes and their drivers in badlands.

Increasing the temporal scale to periods of at least one year increases the magnitude of changes, especially in terms of lowering, total and net change (Figure 7). This pattern is observed in both badlands: despite the differences in size and morphometry (Table 1), the average time required to export the sediments weathered and eroded from the slopes is around 1 year, even the geomorphic processes acting in the slopes may differ in time and space. Is worth noting that this time will depend on the magnitude of the assigned minLoD, a fact that reinforces the need to calculate this parameter in the most rigorous possible way. Our observations, in terms of the average time required for that the sediment be depleted from badlands are in agreement with the study of Descroix and Olivry (2002) in the badlands of Draix (South Alps, France), in which they noted that the detached material weathered in the slopes during winter was not completely exported from the catchment until the spring and autumn rainfall. Our observations demonstrate that surveys at seasonal temporal scales allow depiction of specific geomorphological processes preparing and detaching sediments from the slopes, while annual temporal scales are required to estimate average values of erosion (i.e. denudation), masking the geomorphic processes responsible of long-term changes.

## 5.4. Limitations and further work

Repeated High Resolution Topography obtained by means of TLS and SfM photogrammetry was used to study topographic changes across multiple temporal scales in two sub-humid Mediterranean badlands. Errors in topographic surveys propagate into uncertainties in the estimates of topographic change (i.e. changes cannot be considered real, e.g. Brasington et al., 2000; Lane et al., 2003; Wheaton et al., 2010), and may also have an indirect impact on the interpretation of geomorphic processes signatures. These uncertainties may be relevant in landscapes or over temporal scales in which the change is relatively low compared to the potential errors subjected to the surveys, such as our experimental badlands. In order to depicting topographic changes that are being considered noise to these represent real change, we have applied a thresholding to the DoDs (see section 3.2.1. for further information).

Even so, the use of different error and thresholding propagation methods may yield different results in our estimates since the number of cells above or below the minLoD would change, affecting the computation of topographic changes in both signs. Although our method is widely used in the literature (e.g. Brasington et al., 2000; Lane et al., 2003; Milan et al., 2011; Wheaton et al., 2010), Anderson (2018) has recently demonstrated that net changes estimated from repeat high density observations may be affected by correlated or fully systematic errors and uncorrelated or random errors. He concluded that any attempt to remove these errors may cause a misinterpretation of the results. The same author argued that thresholding (i.e. applying a minLoD) may be a biased correction tool for the estimates of total erosion, total sedimentation and total topographic change. Net changes will be less affected by random errors since errors of opposite sign tend to offset each other, but may be largely affected by correlated or systematic errors (e.g. survey method, Anderson, 2018). In our case, we were not able to correct such systematic errors. Although the comparison of both survey methods provided very close results indicating systematic errors in both would be similar, we are not able to quantify the degree in which such errors (if present) may affect the magnitude of the net changes, especially at the shortest temporal scales analysed.

Our results indicate that High Resolution Topography obtained at different temporal scales (i.e. annual and seasonal) during five consecutive years allows analysis of the relations between main

geomorphic processes reshaping badlands and their role on sediment production and transfer. As far as we aware, there are no previous studies analysing topographic changes in badlands at the spatial and temporal resolutions analysed here. Data provided from natural laboratories such as the one presented here (https://sites.google.com/site/badlandscan/) are also fundamental to study long-term changes in relation to the frequency and magnitude of rainfall events and future trends in a context of global change.

## 6. CONCLUSIONS

This paper analyses multi-temporal repeat High Resolution Topography obtained during five consecutive years in two morphometrically-contrasted but adjacent badlands subjected to the same external forcing to untangle the relative importance of different geomorphic processes in reshaping badlands and exporting sediments downstream. The main conclusions are:

1. Both experimental badlands are subjected to low erosion rates (between 0.07 and 0.01 cm/yr on average in B1 and B2 respectively) in comparison with badlands developed on the same lithology in the southern Pyrenees where annual erosion rates can be up to 3 cm/yr. We hypothesise that these differences may be attributed to the morphometry of the experimental badlands, the method used to monitor topographic changes and the higher degree of compactness, which entails highly complex and spatially variable processes.

2. The dominant geomorphic processes signatures observed in both badlands are different. Processes signatures determining surface lowering in the gentle-sloping south-facing badland (B1), characterised by lower connectivity and more vegetation cover, are driven by surface runoff-based processes, both diffuse, causing *Sheet Washing*, and concentrated, determining *Cutting and Filling* and *Rilling and Gullying*. The steepest and more connected north-facing slopes of B2 are re-shaped by means of gravitational processes, with *Mass Wasting* being dominant. In terms of processes determining surface raising, both *Mass Wasting* and *Cutting and Filling* are considered the main in both badlands.

3. There is a clear near-balanced feedback between both surface-raising and lowering processes, that gets unbalanced at larger temporal scales, as the volume associated with surface lowering becomes higher than that associated to raising-based processes, indicating that the time required to export the sediments that are weathered and detached form the slopes is around 1 year. This time will depend on the magnitude of the assigned minLoD, a fact that reinforces the need to calculate this parameter in the most rigorous and consistent possible way.

4. Rainfall variables control surface flow processes while those variables associated with low temperature have a significant relation with mass movement-based processes and other localised processes as *Regolith Cohesion Loss*.

5. Morphometry is a key factor that determine geomorphic processes and associated topographic changes. Our results suggest that slope, connectivity and vegetation cover have a direct impact in triggering determinate geomorphic processes.

6. Geomorphic processes are acting at different temporal and spatial scales, driven by meteorological variables and also by other internal factors such as morphometry and lithology. We demonstrated that seasonal temporal scales are optimum for analysing specific geomorphic processes preparing and detaching sediments from the slopes and these are spatially different; conversely, annual temporal scales are required to estimate average values of erosion (i.e.

denudation), diverging to similar gross estimates but masking the short-term geomorphic processes responsible of long-term changes.

Better understanding of main geomorphic processes together with their relation with meteorological variables and morphometric characteristics as the results presented here can be very useful data to improve environmental management and landscape evolution modelling.

## 7. ACKNOWLEDGEMENTS

This research was carried out within the framework of two research projects funded by the Spanish Ministry of Economy and Competitiveness and the European FEDER funds: MORPHSED (CGL2012-36394) and MORPHPEAK (CGL2016-78874-R). The first author has a grant funded by the Ministry of Education, Culture and Sports, Spain (FPU016/01687). The last author is a Serra Húnter Fellow at the University of Lleida. The first and last authors are part of the Fluvial Dynamics Research Group-RIUS, a Consolidated Group recognized by the Generalitat de Catalunya (2017 SGR 459645). We also acknowledge the support of the CERCA Program of the Generalitat de Catalunya. Finally, we also thank the British Society for Geomorphology to support the long-term geomorphological monitoring program in the experimental badland that started in 2013; and the members of the Fluvial Dynamics Research Group for their assistance during the fieldwork campaigns. We thank Prof. Stuart Lane, acting as editor in chief of the journal Earth Surface Processes and Landforms, his suggestion of considering the methodological paper submitted by Llena et al. (under revision) where the MaGPiE algorithm is presented and this one as a paper pair or two connected papers.

## 8. REFERENCES

Aucelli PPC, Conforti M, Della Seta M, Del Monte M, D'uva L, Rosskopf CM, Vergari F. 2016. Multi-temporal Digital Photogrammetric Analysis for Quantitative Assessment of Soil Erosion Rates in the Landola Catchment of the Upper Orcia Valley (Tuscany, Italy). *Land Degradation and Development* 27: 1075– 1092

Anderson SW. 2019. Uncertainty in quantitative analyses of topographic change: error propagation and the role of thresholding. Earth Surface Processes and Landforms 44: 1015-1033.

Balasch JC, Clotet N, Gallart F. 1988. Validación a escala temporal de tasas de erosión en áreas de badlands (Prepirineo Catalán). *Comunicaciones Congreso Geológico de España* 1: 359-362.

Ballesteros-Cánovas JA, Stoffel M, Martín-Duque JF, Corona C, Lucía A, Bodoque JM, Montgomery DR. 2017. Gully evolution and geomorphic adjustments of badlands to reforestation. *Scientific Reports.* 8 pp.

Barnes N, Luffman I, Nandi A. 2016. Gully erosion and freeze-thaw processes in clay-rich soils, northeast Tennessee, USA. *GeoResJ* 1-12: 67-76

Benito G, Gutiérrez M, Sancho C. 1992. Erosion Rates in Badland Areas of the Central Ebro Basin (NE-Spain). *Catena* 19: 269-286.

Bishop A and Morgenstern N. 1960. Stability coefficients for earth slopes. *Geotechnique* 10: 129–150.

Borselli L, Cassi P, Torri D. 2008. Prolegomena to sediment and flow connectivity in the landscape: A GIS and field numerical assessment. *Catena* 75: 268–277.

Brasington J, Rumsby B, McVey R, 2000. Monitoring and Modelling Morphological Change in a Braided Gravel-Bed River Using High Resolution GPS-Based Survey. *Earth Surface Processes and Landforms* 25: 973-990.

Brasington J, Vericat D, Rychkov I. 2012. Modelling river bed morphology, roughness, and surface sedimentology using high resolution terrestrial laser scanning. *Water Resources Research*. 48: 1-18.

Bryan R, Yair A. 1982. Perspectives on studies of badland geomorphology. In: *Badland Geomorphology and Piping*, Bryan RB, Yair A (Eds.). Geobooks: Norwich; 1–12.

Calvo-Cases A, Harvey AM. 1996. Morphology and development of selected badlands in Southeast Spain: Implications of climatic change. *Earth Surface Processes and Landforms* 21: 725-735.

Canton Y, Domingo F, Solé-Benet, Puigdefábregas J. 2000. Hydrological and erosion response of a badlands system in semiarid SE Spain. *Journal of Hydrology* 252: 65-84.

Cavalli M, Trevisani S, Comiti F, Marchi L, 2013. Geomorphometric assessment of spatial sediment connectivity in small Alpine catchments. *Geomorphology* 188: 31–41.

Cerdà A. 1997. Influencia de la Litología en los procesos de erosión en badlands. Los casos de Anna (Valencia) y Petrer (Alicante. *Pirineos* 149: 3-20.

Clotet N, Gallart F, Sala M. 1987. Los badlands: características, interés teórico, dinámica y tasas de erosión. *Notes de Geografía Física* 15-16: 28-37.

Clotet-Perarnau N, Gallart F, Balasch JC.. 1988. Medium-term erosion rates in small scarcely vegetated catchment in the Pyrenees. *Catena Supplement* 13: 37-47.

De Ploey J, Gabriels D. 1980. Measuring soil loss and experimental studies. In: M.J. Kirkby and R.P.C. Morgan (Editors). *Soil Erosion*. Willey, 63-108 pp.

Descroix L, Olivry JC. 2002. Spatial and temporal factors of erosion by water of black marls in the badlands of the French southern Alps. *Hydrological Sciences Journal* 47(2): 227-242.

Desir G, Marín C. 2013. Role of erosion processes on the morphogenesis of a semiarid badland area. Bardenas Reales (NE Spain). *Catena* 106: 83-92.

Gallart F, Solé A, Puigdefàbregas J, Lázaro R. 2002. Badland Systems in the Mediterranean. In: Dryland Rivers: Hydrology and Geomorphology of Semi-arid Channels. Bull LJ, Kirkby MJ (Eds.). John Wiley & Sons, Ltd. 299-326.

Gallart F, Marignani M, Pérez-Gallego N, Santi E, Maccherini S. 2013. Thirty years of studies on badlands, from physical to vegetational approaches. A succinct review. *Catena* 106: 4-11.

Girardeau-Montaut D. 2019. CloudCompare - Open Source Project. http://www.danielgm.net/cc/ (accessed 01 February 2019).

Grenfell SE, Rowntree KM, Grenfell MC. 2012. Morphodynamics of a gully and floodout system in the Sneeuberg Mountains of the semi-arid Karoo, South Africa: Implications for local landscape connectivity. *Catena* 89: 8-21.

Faulkner H. 2008. Connectivity as a crucial determinant of badland morphology and evolution. *Geomorphology*. 100: 91-103.

Ferrer V, Errea P, Alonso E, Gómez-Guitierrez A, Nadal-Romero E. 2017. A Multiscale Approach to asses Geomorphological Processes in a semiarid badland area (Ebro Depression, Spain). *Cuadernos de Investigación geográfica* 43: 41-62.

Francke T, López-Tarazón JA, Vericat D, Bronstert A, Batalla RJ. 2008. Flood-based analysis of high-magnitude sediment transport using a non-parametric method. *Earth Surface Processes and Landforms* 33: 2064-2077.

Kasanin-Grubin M. 2013. Clay mineralogy as a crucial factor in badlands hillslope processes. *Catena* 106: 54–67.

Krenz J, Kuhn NJ. 2018. Assesing Badland Sediment Sources Using Unmanned Aerial Vehicles. In: *Badland Dynamics in the Context of Global Change*. Nadal-Romero E, Martínez-Murillo JF, Kuhn NJ. (Eds.). Elsevier, Amsterdam. 320 pp.

Lague D, Brodu N, Leroux J. 2013. Accurate 3D comparison of complex topography with terrestrial laser scanner: Application to the Rangitikei canyon (N-Z). *ISPRS Journal of Photogrammetry and Remote Sensing* 82: 10-26.

Lane SN, Westaway RM, Hicks DM. 2003. Estimation of Erosion and Deposition Volumes in a Large, Gravel-Bed, Braided River Using Synoptic Remote Sensing. *Earth Surface Processes and Landforms* 28: 249-271.

Llena M, Smith MW, Vericat D. 2018. The role of the altitude and surface morphometric proprieties in the quality of SfM-based High Resolution Topography. In *Geomorfología del Antropoceno. Efectos del Cambio Global sobre los procesos geomorfológicos*. Garcia C, Gómez--Pujol L, Morán-Tejeda E, Batalla RJ (eds). Universitat de les Illes Balears - Sociedad Española de Geomorfología: Palma. 402 pp.

Llena M, Vericat D, Smith MW, Wheaton JM. Under revision. Inferring geomorphic processes signatures in badlands from the measurement of changes in form. *Earth Surface Processes and Landforms*.

Lucia A, Martín-Duque JF, Laronne JB, Sanz-Santos MA. 2011. Geomorphic dynamics of gullies developed in sandy slopes of Central Spain. *Landform Analysis* 17: 91-97.

Marchamalo M, Hooke JM, Sandercocket PJ. 2016. Flow and sediment connectivity in semi-arid landscapes in SE Spain: patterns and controls. *Land Degradation and Development* 27: 1034-1044.

Martínez-Casasnovas JA, Poch RM. 1998. Estado de la Conservación de los suelos de la cuenca del embalse Joaquín Costa. *Limnimética* 14: 83-91.

Mathys N, Brochot S, Meunier M, Richard D. 2003. Erosion quantification in the small marly experimental catchments of Draix (Alpes de Haute Provence, France). Calibration of the ETC rainfall–runoff–erosion model. *Catena* 50: 527-548.

Milan DJ, Heritage GL, Large ARG, Fuller IC. 2011. Filtering spatial error from DEMs: implications for morphological change estimation. *Geomorphology* 125: 160–171.

Moreno-de las Heras M, Gallart F. 2016. Lithology controls the regional distribution and morphological diversity of montane Mediterranean badlands in the upper Llobregat basin (eastern Pyrenees). *Geomorphology* 273: 107-115.

Moreno-de las Heras M, Gallart F. 2018. The Origin of Badlands. In: *Badland Dynamics in the Context of Global Change*. Nadal-Romero E, Martínez-Murillo JF, Kuhn NJ. (Eds.). Elsevier, Amsterdam. 320 pp.

Morgenstern N, Price VE. 1965. The analysis of the stability of general slip surfaces. *Geotechnique* 15(1): 79–93.

Nadal-Romero E, Regüés D, Martí-Bono C, Serrano-Muela P. 2007. Badland dynamics in the Central Pyrenees: temporal and spatial patterns of weathering processes. *Earth Surface Processes and Landforms* 32: 888-904.

Nadal-Romero E, Regüés D. 2010. Geomorphological dynamics of sub-humid mountain badland areas: weathering, hydrological and suspended sediment transport processes. A case of study in the Araguás catchment (Central Pyrenees), and implications for altered hydro-climatic regimes. *Progress in Physical Geography* 34 (3): 123–150.

Nadal-Romero E, Petrlic K, Verachtert, Bochet E, Poesen J. 2014. Effects of slope angle and aspect on plant cover and species richness in a humid Mediterranean badland. *Earth Surface Processes and Landforms* 39: 1705-1716.

Nadal-Romero E, Revuelto J, Errea P, López-Moreno JI. 2015. The application of terrestrial laser scanner and SfM photogrammetry in measuring erosion and deposition processes in two opposite slopes in a humid badlands area (central Spanish Pyrenees). SOIL 1, 561–573.

Nadal-Romero E, García-Ruiz JM. 2018. Rethinking Spatial and Temporal Variability of Erosion in Badlands. In: *Badland Dynamics in the Context of Global Change*. Nadal-Romero E, Martínez-Murillo JF, Kuhn NJ. (Eds.). Elsevier, Amsterdam. 320 pp.

Nobajas A, Waller RI, Robinson ZP, Sangonzalo R. 2017. Too much of a good thing? the role of detailed UAV imagery in characterizing large-scale badland drainage characteristics in South-Eastern Spain. International Journal of Remote Sensing 38: 2845-2860.

Pimentel D, Harvey C, Resosudamo P, Sinclair K, Kurz D, McNair M, Crist S, Shpritz L, Fitton L, Saffouri R, Blair R. 1995. Environmental and Economic Costs of Soil Erosion and Conservation Benefits. *Science* 267: 1117-1122.

Passalacqua P, Belmont P, Staley DM, Simley JD, Arrowsmith JR, Bode CA, Crosby C, DeLong SB, Glenn NF, Kelly SA, Lague D, Sangireddy H, Schaffrath K, Tarboton DG, Wasklewicz T, Wheaton JM. 2015. Analyzing high resolution topography for advancing the understanding of mass and energy transfer through landscapes: a review. *Earth-Science Reviews* 148: 174-193.

Piqué G, López-Tarazón JA, Batalla RJ. 2014. Variability of in-channel sediment storage in a river draining highly erodible areas (the Isábena, Ebro basin). J Soils Sediments 12: 2031-2044.

Rainato R, Mao L, García-Rama A, Picco L, Cesca M, Vianello A, Preciso E, Scussel GR, Lenzi MA. 2017. Three decades of monitoring in the Rio Cordon instrumented basin: Sediment budget and temporal trend of sediment yield. *Geomorphology* 291: 45-56.

Regüés D, Pardini G, Gallart F. 1995. Regolith behavior and physical weathering of claey mudrock as dependent on seasonal weather conditions in a badland area at Vallcebre, Eastern Pyrenees. *Catena* 25: 199-212.

Regüés D, Guàrdia R, Gallart F. 2000. Geomorphic agents versus vegetation spreading as causes of badland occurrence in a Mediterranean subhumid mountainous area. *Catena* 40(2): 173–187.

Richard D, Mathys N. 1999. Historique, contexte technique et scientifique des BVRE de Draix. In: N. Mathys (Ed.), *Caractéristiques, données disponibles et principaux résultats acquis au cours des dix ans de suivi*. Actes du séminaire Les bassins versants expérimentaux de Draix. Cemagref-Editions, Coll. Actes de colloques, Grenoble, 11-28 pp.

Rossi RK. 2018. *Evaluation of `Structure-from-Motion' from a Pole-Mounted Camera for Monitoring Geomorphic Change*. Master Dissertation. Utah State University. 211 pp.

Rychkov, I., Brasington, J., Vericat D. 2012. Computational and methodological aspects of terrestrial surface analysis based on point clouds. *Computers & Geosciences*. 42: 64-70.
Sirvent J, Desir G, Gutierrez M, Sancho C, Benito G. 1997. Erosion rates in badland areas recorded by collectors, erosion pins and profi lometer techniques (Ebro Basin, NE-Spain). *Geomorphology* 18: 61–75.

Smith KG. 1958. Erosional processes and landforms in Badlands National Monument, South Dakota. *Bulletin of the Geological Society of America* 69: 975-1008.

Smith MW, Vericat D. 2015. From experimental plots to experimental landscapes: topography, erosion and deposition in sub-humid badlands from Structure-from-motion photogrammetry. *Earth Surface Processes and Landforms* 40: 1656-1671.

Smith MW, Carrivick JL, Quincey DJ. 2016. Structure from motion photogrammetry in physical geography. *Progress in Physical Geography* 40(2): 247-275.

Solé-Benet A, Afana A, Cantón Y. 2012. Erosion pins, profile and laser scanners for soil erosion monitoring in active hillsopes in badlands of SE Spain. *Actas XII Reunión Nacional de Geomorfología, Santander* 575-578.

Stöcker C, Eltner A, Karrasch P. 2015. Measuring gullies by synergetic application of UAV and close range photogrammetry — a case study from Andalusia, Spain. *Catena* 132: 1–11.

Tarolli, P. 2014. High-resolution topography for understanding Earth surface processes: opportunities and challenges. *Geomorphology* 216: 295–312.

Torri D, Colica A, Rockwell D. 1994. Preliminary study of the erosion mechanisms in a biancana badland (Tuscany, Italy). *Catena* 23: 281-294.

Torri D, Rossi M, Brogi F, Marignani M, Bacaro G, Santi E, Tordoni E, Amici V, Maccherini S. 2018. Badlands and the Dynamics of Human History, Land Use, and Vegetation Through Centuries. In: *Badland Dynamics in the Context of Global Change*. Nadal-Romero E, Martínez-Murillo JF, Kuhn NJ. (Eds.). Elsevier, Amsterdam. 320 pp.

Tsutsumi D, Fujita M. 2016. Field observations, experiments, and modeling of sediment production from freeze and thaw action on a bare, weathered granite slope in a temperate region of Japan. *Geomorphology* 267: 37-47.

Vericat D, Smith MW, Brasington J. 2014. Patterns of topographic change in sub-humid badlands determined by high resolution multi-temporal topographic surveys. *Catena* 120: 164–176.

Vericat D, Wheaton J, Brasington J. 2017. Revisiting the Morphological Approach: Opportunities and Challenges with Repeat High-Resolution Topography. In: Gravel-Bed Rivers: Processes and Disasters. Tsutsumi DT, Laronne JB. (Eds.). Wiley, 121-158.

Wheaton JM, Brasington J, Darby SE, Sear DA. 2010. Accounting for uncertainty in DEMs from repeat topographic surveys: improved sediment budgets. Earth Surface Processes and Landforms 35(2): 136–156.

Yair A, Lavee H, Bryan RB, Adar E. 1980. Runoff and erosion processes and rates in the Zin Valley badlands, Northern Negev, Israel. *Earth Surface Processes* 5: 205-225.

## SUPPLEMENTARY MATERIALS:

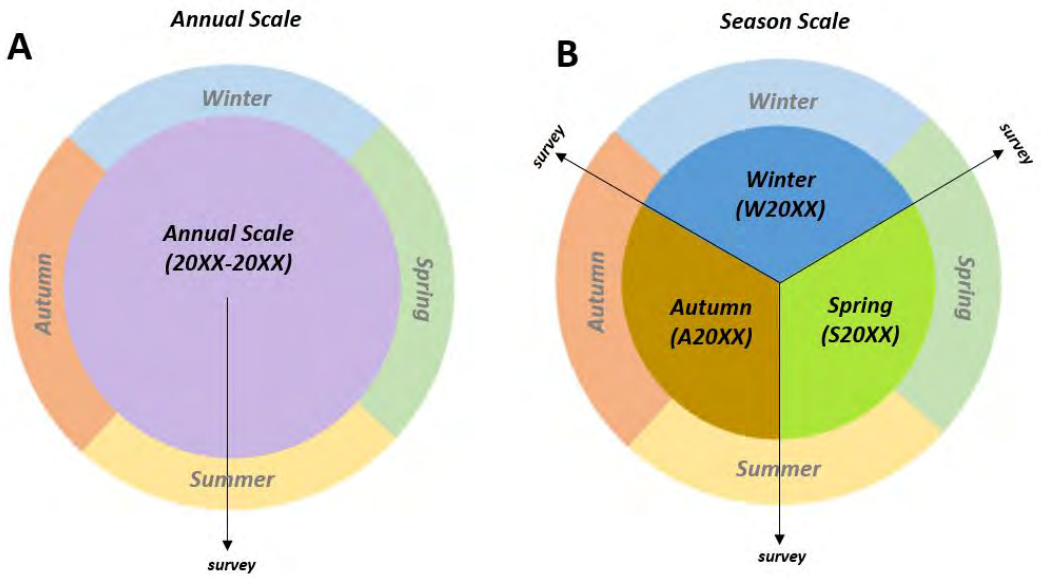


**Figure SM 1.** Temporal distribution of annual (**A**) and seasonal (**B**) topographic surveys and corresponding study periods during an entire natural year.

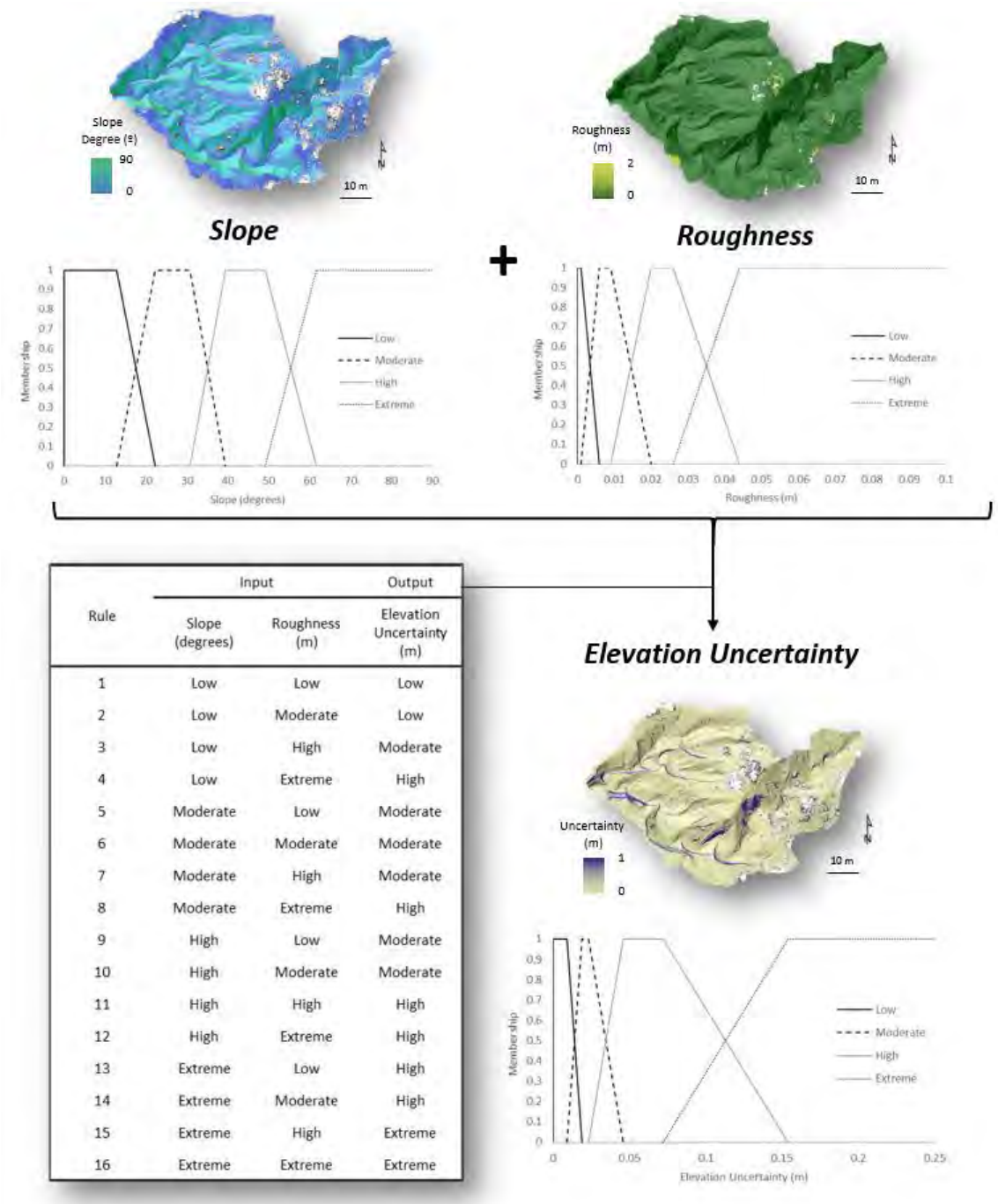


| Rule | Input | | Output |
|---|---|---|---|
| | Slope (degrees) | Roughness (m) | Elevation Uncertainty (m) |
| 1 | Low | Low | Low |
| 2 | Low | Moderate | Low |
| 3 | Low | High | Moderate |
| 4 | Low | Extreme | High |
| 5 | Moderate | Low | Moderate |
| 6 | Moderate | Moderate | Moderate |
| 7 | Moderate | High | Moderate |
| 8 | Moderate | Extreme | High |
| 9 | High | Low | Moderate |
| 10 | High | Moderate | Moderate |
| 11 | High | High | High |
| 12 | High | Extreme | High |
| 13 | Extreme | Low | High |
| 14 | Extreme | Moderate | High |
| 15 | Extreme | High | Extreme |
| 16 | Extreme | Extreme | Extreme |

**Figure SM 2.** Inputs (slope and roughness) and output (elevation uncertainty) FIS membership functions used in the present study to propagate DEM errors. The table on the left shows the ruleset used for the 2 FIS components (inputs) of the error model.

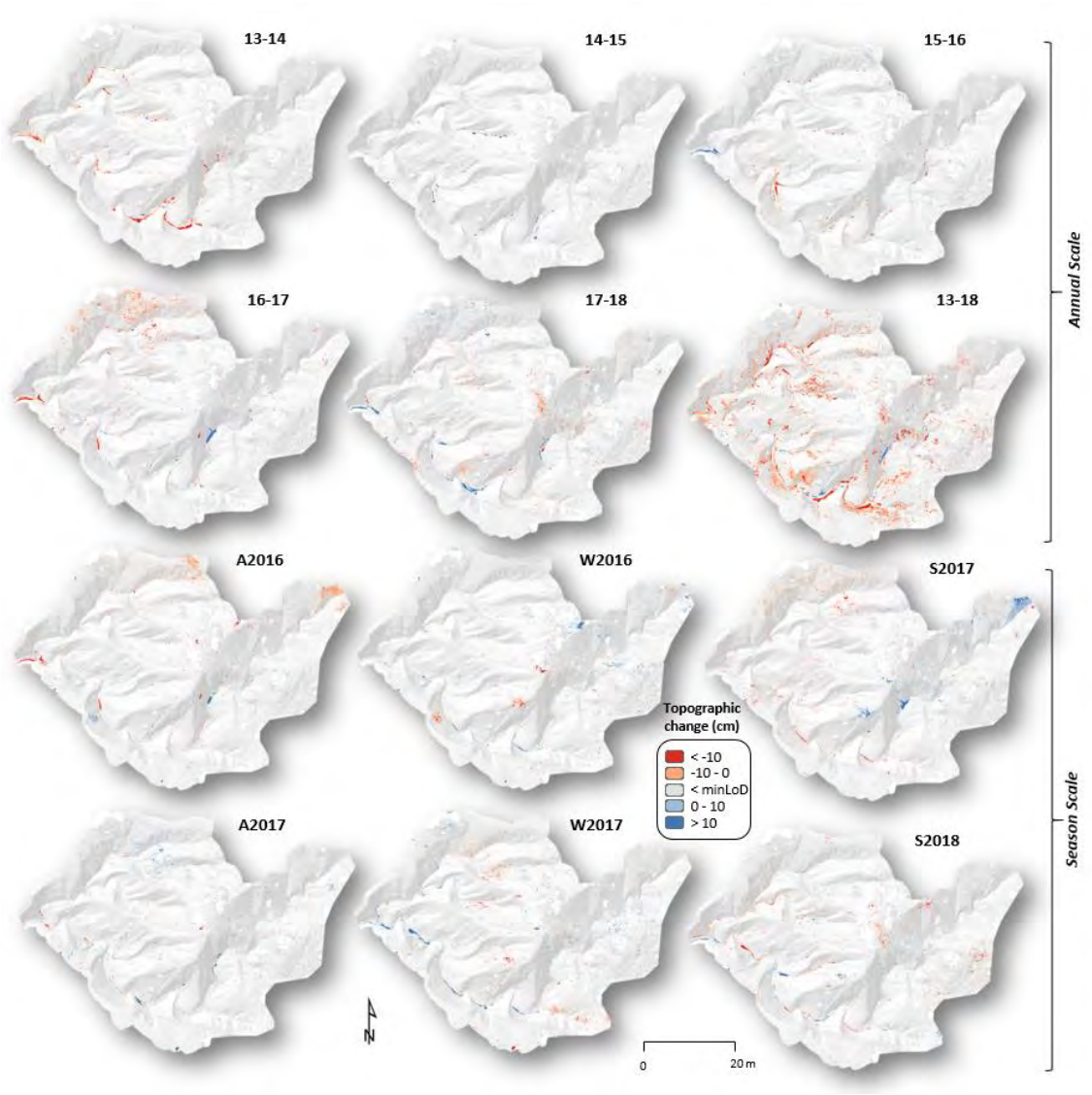


**Figure SM 3.** DoDs maps for the entire Badland 1 (B1) during all the temporal scales analysed (i.e. seasonal and annual).

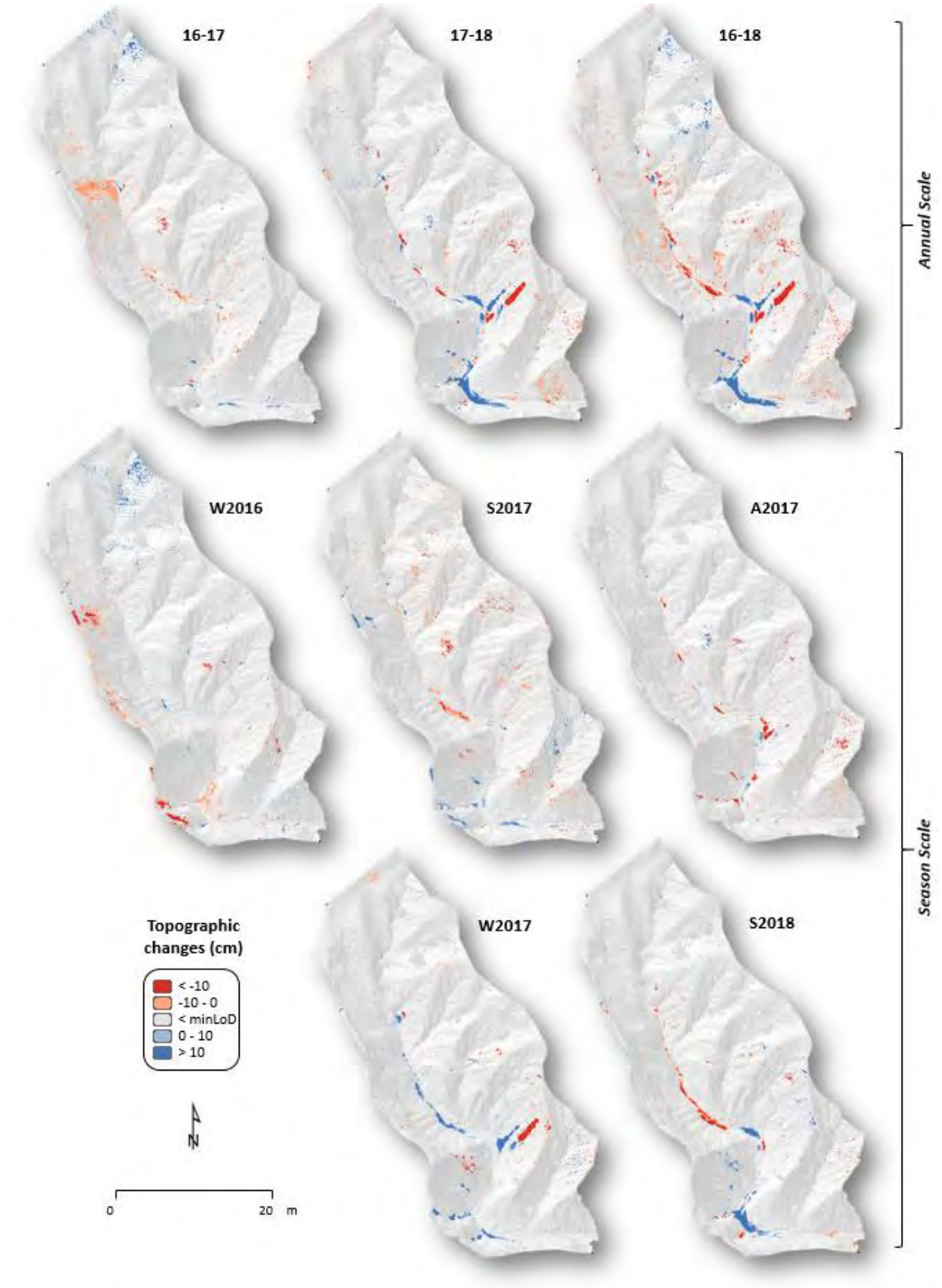


**Figure SM 4.** DoDs maps for the entire Badland 2 (B2) during all the temporal scales analysed (i.e. seasonal and annual).

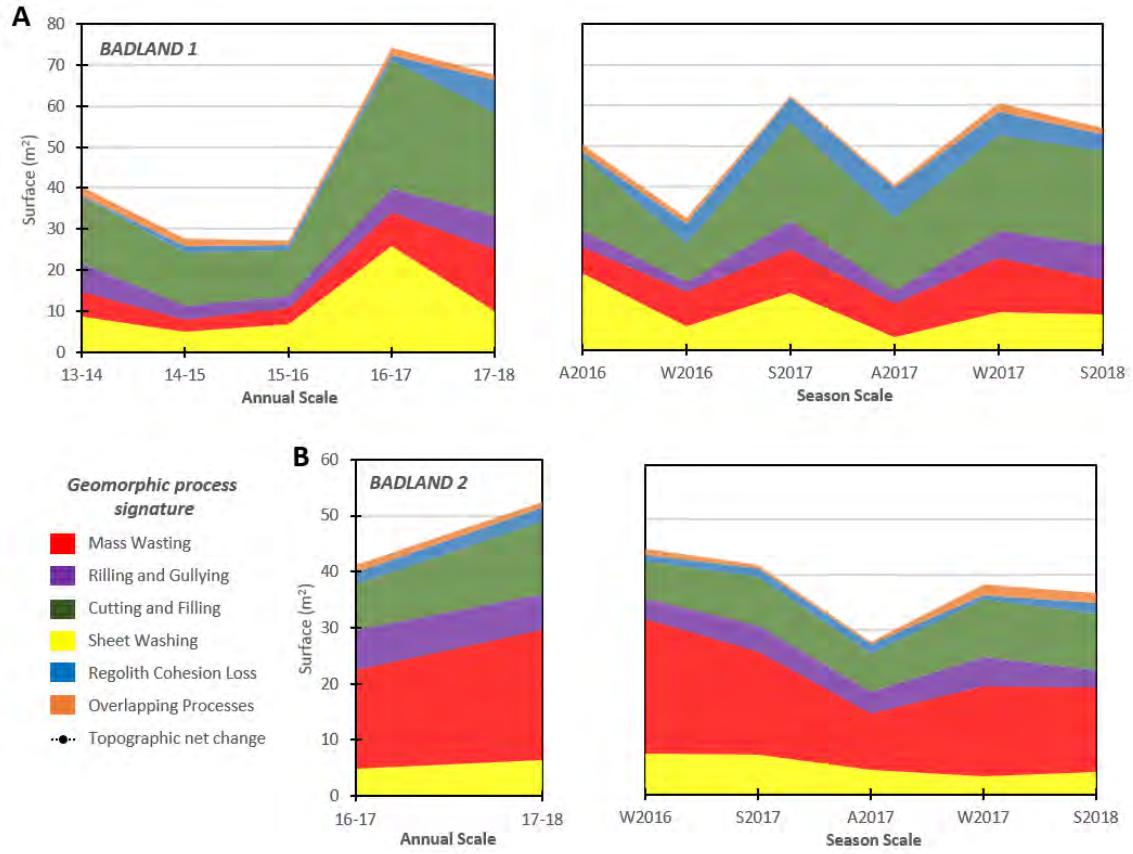


**Figure SM 5.** Area occupied by each geomorphic process in B1 (**A**) and B2 (**B**) experimental badlands and both analysed temporal scales (i.e. annual and seasonal).

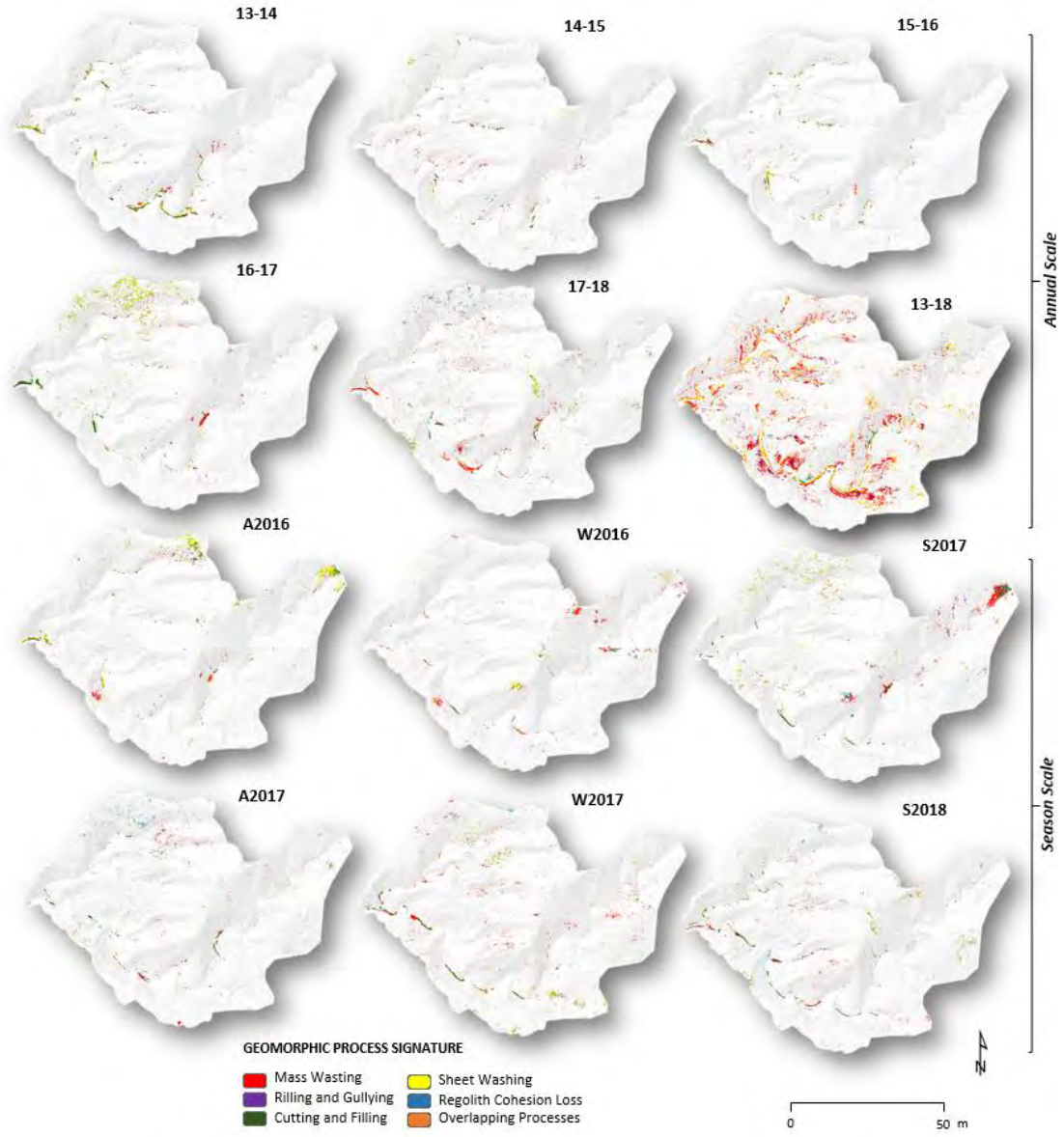


**Figure SM 6.** Geomorphic processes maps for the entire Badland 1 (B1) during all the analysed temporal scales (i.e. seasonal and annual).

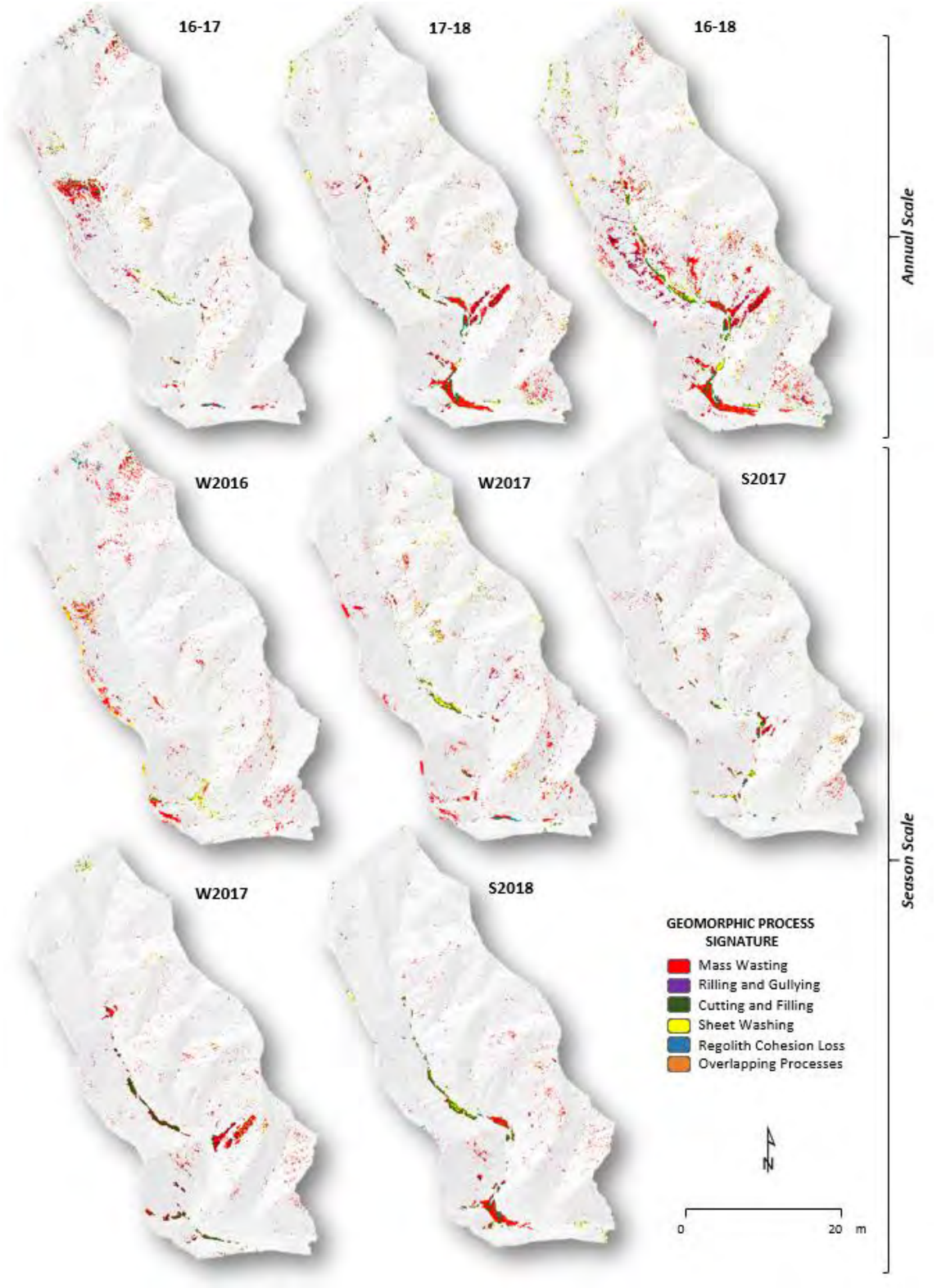


**Figure SM 7.** Geomorphic processes maps for the entire Badland 2 (B2) during all the analysed temporal scales (i.e. seasonal and annual).

# CHAPTER 4

## DO BADLANDS (ALWAYS) CONTROL SEDIMENT YIELD? EVIDENCE FROM SMALL INTERMITTENT CATCHMENT

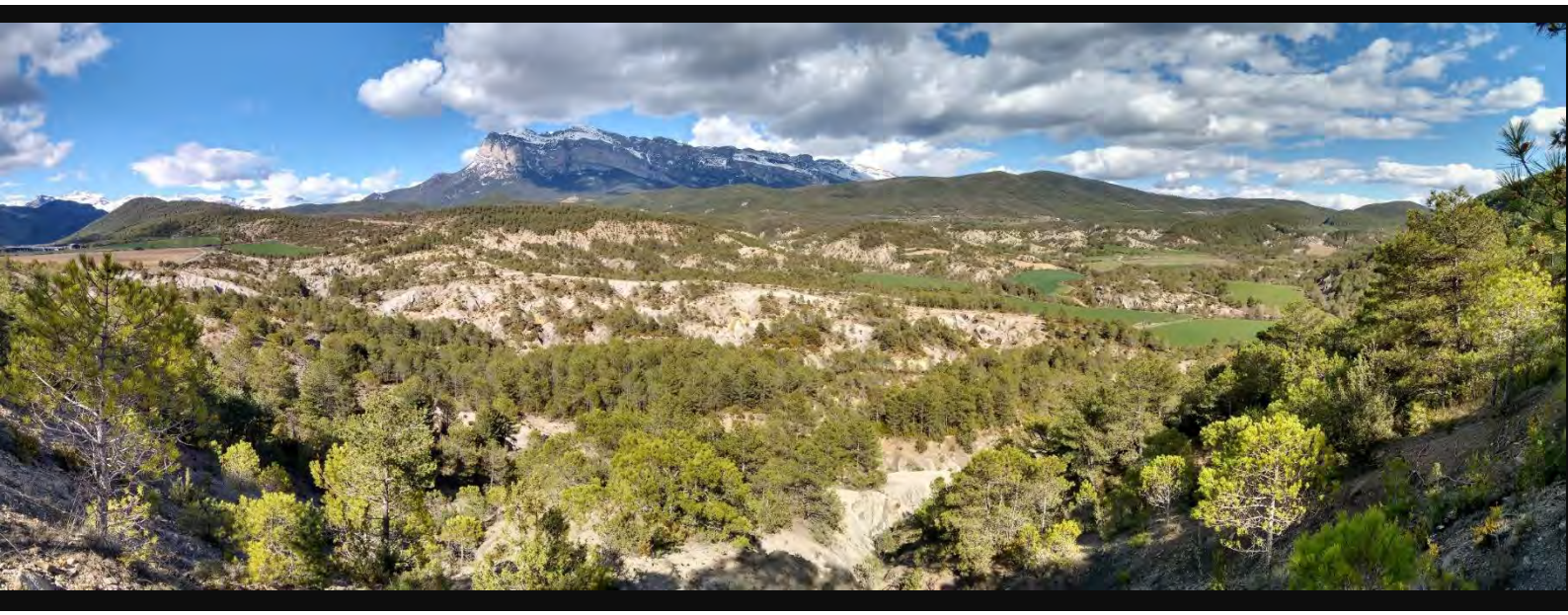

# CHAPTER 4: Do badlands (always) control sediment yield? Evidence from small intermittent catchment

This chapter contains the following pending to be submitted paper to the journal Land Degradation and Development. JCR-SCI Impact Factor (2018): 4.275. Category: Soil Science; 1st Quartile.

2019. Do badlands (always) control sediment yield? Evidence from small intermittent catchment. *Land Degradation and Development* (To be submitted).

**ABSTRACT:** Badlands frequently represent the main sediment source in catchments. In many small mountain intermittent catchments stream flow is often flashy, which determines much of the transfer of water and sediments through the drainage network. This transfer typically takes place in the form of pulses, out-of-phase with hillslope sediment production or erosion processes. The objective of this paper is to analyse the sediment production and the sediment yield in a small mountain catchment (10 $km^2$) characterised by patches of badlands and drained by intermittent streams located in the Southern Pyrenees. The study is performed at multiple temporal scales to further highlight: (i) the effect of specific pulses in the transfer of water and sediment; (ii) the contribution of the sediment production from badlands to the sediment yield at the outlet of the catchment; and (iii) the role of the drainage network as a sediment source and sink.

Significant correlations between meteorological and runoff variables were observed; specifically, the strongest positive correlations were found between stream flashiness and the duration of the period in which the stream is dry, sediment production and suspended sediment concentration. Sediment yield is well correlated with rainfall and flood duration. Results indicated that badlands do not always control the export of sediments. Although sediment produced in badlands can be higher than the amount exported in the catchment outlet during specific seasons in the year. At an annual scale badlands, occupying the 25% of the catchment area) supply around 54% of the total catchment sediment export. Sediments transferred from agricultural fields and forest also contribute substantially to the sediment yield. Additionally, our results also emphasised the key role of the channel network, caused by the intermittent character of the stream in the development of water and sediment pulses during flash floods. The frequency and magnitude of the water and sediment pulses determines changes in Sediment Delivery Ratio (SDR) at the catchment outlet, depending on whether the drainage network acts as a sediment sink (i.e. SDR < 1) or source (i.e. SDR > 1).

**KEYWORDS**: *Badlands, sediment production, sediment yield, pulses, Sediment Delivery Ratio, flow intermittency.*

## 1. INTRODUCTION

Plant cover, together with rainfall intensity and slope, are considered the most important factors controlling soil erosion (e.g. Borrelli et al., 2013; Cerovski-Darriau and Roering, 2016). *Badlands* are described as highly-dissected landscapes with little or no vegetation cover and high erosion rates (Yair et al., 1980; Clotet et al. 1987; Gallart et al 2002; Francke, 2009). They are frequently reported as being the main sediment source in catchments worldwide, notably in Mediterranean climate regions (e.g. Richard and Mathys 1999; Llorens et al., 2018). Besides badlands, agricultural areas are also important sediment sources, with moderate to high rates of soil erosion (e.g. Casalí et al., 2008), whereas forested areas present lower rates (e.g. Zabaleta et al., 2007). However, and despite the fact that these two types of surfaces typically display lower sediment production rates than those observed in badlands (e.g. Mathys et al., 2003; García-Ruíz et al., 2015; Llorens et al., 2018), they should not be dismissed in the estimation of sediments yields, especially in mountain regions where they usually cover large swathes of territory. Moreover, streamflow in catchments exhibiting patches of badlands is often intermittent and flashy (MacDonough et al., 2011), mostly due to the rapid concentration of surface runoff caused by the large presence of bare surfaces (e.g. Gallart and Llorens, 2004; García-Ruiz et al., 2008). These characteristics determine much of the transfer of water and sediments through the drainage network, which occur typically in the form of pulses (Junk et al., 1989) out-of-phase with hillslope sediment production or erosion (e.g. Puigdefabregas et al., 1999; Cui et al., 2003; Gran and Czuba, 2017).

Erosion rates in badlands have been mainly analysed by means of dynamic (i.e. sediment fluxes; e.g. Nadal-Romero et al., 2007; Mathys et al., 2003) and volumetric methods (i.e. topographic changes; Benito et al., 1992; Vericat et al., 2014). High Resolution Topography developed from advanced surveying platforms, sensors and algorithms (e.g. Structure from Motion photogrammetry, SfM), has permitted the quantification of topographic changes in different types of surfaces at high spatial and temporal resolutions (Tarolli, 2014; Passalacqua et al., 2015; Vericat et al., 2017), including badlands. Therefore, erosion rates and the subsequent sediment production of badland landscapes can be now inferred from topographic change detection at multiple temporal scales (e.g. Vericat et al., 2014; Stöcker et al., 2015; Smith and Vericat, 2015; Neugirg et al., 2016; Llena et al., Under revision).

Most studies of sediment delivery from catchments patched with badlands focus on the sediment production from a specific area (e.g. Barnes et al., 2016; Benito et al., 1992), while others quantify the total sediment yield at the catchment outlet (e.g. Nadal-Romero et al., 2007; Regüés et al., 1995). However, fewer studies encompass both type of analysis (e.g. Mathys et al., 2003; López-Tarazón et al., 2012). The integration of measurements at multiple temporal scales allows analysis of the role of specific sediment sources, such as the badlands, and their contribution to the total sediment yield for different time spans and in relation to meteorological and hydrological variables.

Moreover, it is worth noting the role of the drainage network (river channels) as a sediment sink and source, an element of riverscapes that is often neglected from sediment budgets, especially in small mountain areas, where channel related processes are seemingly less evident. For instance, López-Tarazón et al. (2011) examined the contribution of badlands to the sediment yield of th meso-scale Isábena catchment in the Southern Pyrenees Although virtually all of the sediments at the outlet of the catchment were produced and eroded from the sub-catchments draining badlands, the channel network acted as source and sink of these sediments, controlling the dynamics observed at the outlet. López-Tarazón et al. (2011) concluded that, annually, all sediments were exported (i.e. Sediment Delivery Ratio  around 1) but with marked seasonal

changes, implying sedimentation and erosion of fine sediment in the channel bed. This type of integrated analysis is key to catchment-to-stream management, especially in rivers that present acute flashiness behaviour (e.g. flash floods; e.g. Marchi et al., 2010; Tarolli et al., 2012; Surian et al., 2016; Amponsah et al., 2016), high sediment yields (e.g. reservoir siltation, Martínez-Casasnovas and Poch, 1998), and reduced water quality (e.g. high sediment concentrations and load, Pimentel et al., 1995).

Within this context, this paper aims to analyse the sediment production and sediment yield in a small mountain catchment characterised by patches of badlands and drained by intermittent streams. The study is performed at multiple temporal scales in order to further highlight: (i) the effect of specific pulses in the transfer of water and sediment; ii) the contribution of the sediment production from badlands to the sediment yield at the catchment outlet; and (iii) the role of the drainage network as a sediment source and sink. Additionally, statistical correlations between meteorological, sediment and flow variables are investigated. Our working hypothesis, based on preliminary field observations of badlands' responses in the study area, is that despite their high sediment production, badlands do not fully control the catchment's sediment yield, nor completely explain the seasonal variability of it. We further hypothesize that the role of the drainage network is key to understanding the sediment transfer in these type of catchments, which are typically dominated by intermittent flashy streams.

## 2. STUDY AREA

The River Soto is a tributary of the Upper River Cinca (Central Pyrenees, Ebro Catchment, Iberian Peninsula; Figure 1A). This is a small mountain catchment (i.e. 10 $km^2$) whose altitude ranges from 540 m a.s.l. at the outlet to 1047 m a.s.l. in the headwaters. Eocene grey marls with different degree of compactness and harder layers of sandstones underlay most part of the catchment. Due to the high erodibility of these materials, the study area is characterized by a dense network of badlands that occupy the 25% of the catchment's area. The remainder of the catchment is covered by Mediterranean forest (56%; mainly *Pinus halepensis*) and winter cereal (18%). The catchment has a continental Mediterranean climate with a mean annual rainfall of 755 mm (period 1981-2018). Maximum rainfall intensities are observed in spring and autumn, occasionally attaining 50 mm $h^{-1}$. Mean annual temperature is 13°C, ranging from -6°C and to 37°C (daily values). During winter, temperatures below freezing are often registered (on average, 60 days every year are exposed to temperatures <0ºC). The flow regime is intermittent (according to the classification by McDonough et al., 2011) with the stream normally drying out during August and September. Average daily discharge was 0.05 $m^3$ $s^{-1}$ during the study period (2016-2018; no further data is available since the river was ungauged before the study period). The streamflow is characterized by the succession of flash floods with an average of 30 events per year (according to data between 2016 and 2018). Flash-floods typically last for 1 day and occur following intense thunderstorms (e.g. >25 mm accumulated rainfall). The low degree of forest cover and the high erosion rates of bare surface areas (badlands) means that during floods, the river transports large amounts of sediment (in suspension) to the River Cinca that immediately drains into the Mediano Reservoir (435 $hm^3$, finalised in 1974).

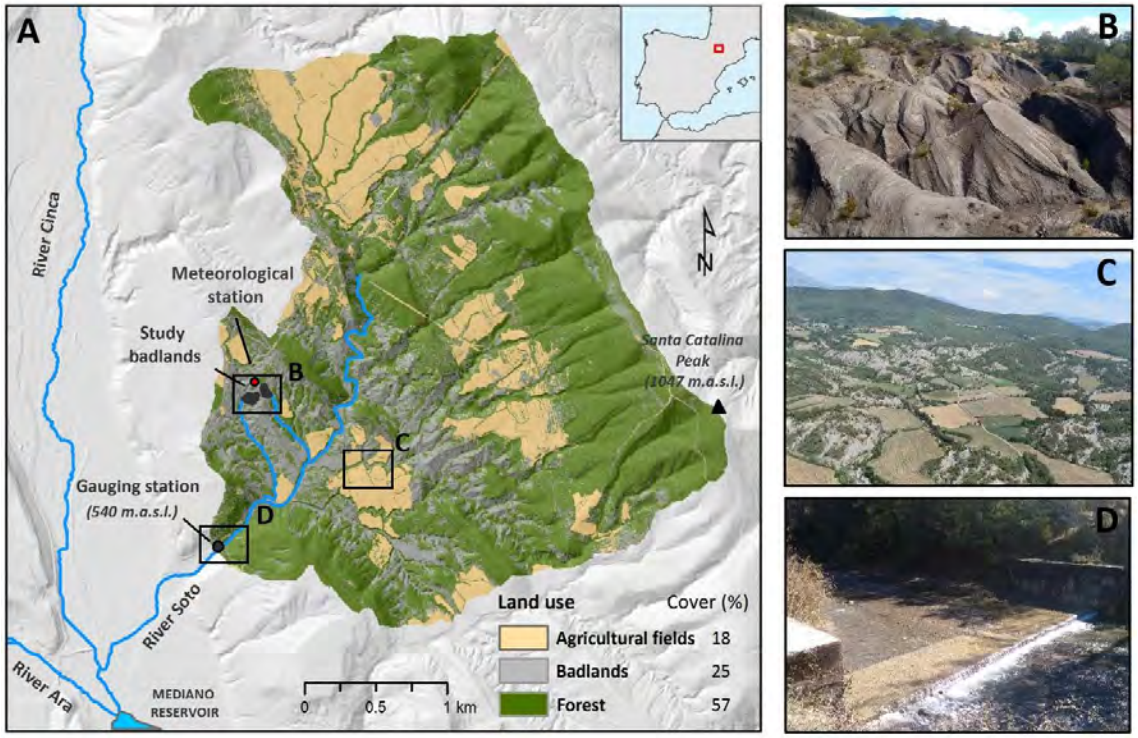


**Figure 1. (A)** Land cover map of the Soto study catchment in the context of the Upper Cinca basin (southern Pyrenees) and the Iberian Peninsula. **(B)** Image of one of the study badlands used in this paper to estimate the overall sediment production of the rest of badland surfaces in the catchment. **(C)** General view of the middle part of the study catchment with a land cover mosaic composed by agricultural fields, badlands and forest. **(D)** Gauging station at the outlet of the catchment (channel width = 14 m).

## 3. METHODS

### 3.1. Data acquisition and treatment

The study period covers two years from July 2016 to June 2018. Three types of data were obtained: (i) meteorological-based data (rainfall and air temperature); (ii) sediment production from two experimental badlands through repeat High Resolution Topography; and (iii) water and sediment fluxes at the outlet of the catchment. Rainfall, air temperature, discharge and suspended sediment concentrations were acquired continuously, while topographic surveys were acquired seasonally. Specifically, surveys were performed in the middle of summer, at the end of autumn and at the beginning of spring, yielding a total of six *seasonal* study periods (Table 1). This allowed the study of the effect of distinct seasonal climatic characteristics (e.g. rainstorms in spring and summer, temperatures below 0ºC in winter) on weathering and erosion processes. Note that the summer seasons are included in the spring and autumn periods defined here (Table 1).

**Table 1.** Distribution of the study periods: starting and ending dates, called period and name.

| Scale | Name[1] | Period | Study period | |
|---|---|---|---|---|
| | | | Start | End |
| SEASONAL | A2016 | Autumn 2016 | 19/07/2016 | 07/12/2016 |
| | W2017 | Winter 2016 | 07/12/2016 | 01/04/2017 |
| | S2017 | Spring 2017 | 01/04/2017 | 28/06/2017 |
| | A2017 | Autumn 2017 | 28/06/2017 | 08/11/2017 |
| | W2018 | Winter 2017 | 08/11/2017 | 23/03/2018 |
| | S2018 | Spring 2018 | 23/03/2018 | 18/06/2018 |
| ANNUAL | 2016-17 | 2016-2017 | 19/07/2016 | 28/06/2017 |
| | 2017-18 | 2017-2018 | 28/06/2017 | 18/06/2018 |

[1] The year attributed to each period is the starting year (e.g. the winter between 2017 and 2018 is named W2017).

### 3.1.1. Rainfall and temperature

Rainfall and temperature were obtained from an *in-situ* meteorological station (see Figure 1A for location details). Rainfall was measured continuously by means of a Campbell ARG100® tipping bucket rain gauge, while air temperature was recorded by a Campbell Temperature Probe-109®. All data were recorded in the same data logger (Campbell CR200X®) at a 5-min interval. There is a significant relationship between these recorded values and the nearest meteorological stations (5 and 10 km away, respectively) operated by the Ebro Water Authorities (i.e. $r^2$=0.91, $p<0.01$), hence justifying the use of a single station to characterise the whole study catchment.

### 3.1.2. Sediment production from badlands

The sediment production from badlands was detailed by Llena et al. (Under revision) from the comparison of repeat High Resolution Topography in two representative badlands of the study area. Despite the two monitored badlands having the same lithology, each one presented a specific morphometry (i.e. slope, aspect, network pattern) and vegetation cover, thereby encompassing the influence of morphometric and land cover characteristics on geomorphic processes re-shaping the badlands and, consequently, sediment production (e.g. Yair et al. 1980; Nadal-Romero et al 2007; Vericat et al. 2014; Marchamalo et al. 2016; Vergari et al., 2019). In this way, these surveyed badlands are representative of all the badlands in the study catchment. More information about the experimental baldand can be also obtained in https://sites.google.com/site/badlandscan/. Specific details of both badlands are described in Llena et al. (Under review), but here we present a summary of the methods.

Topographic surveys were performed by means of Structure from Motion (SfM) photogrammetry. Around 650 pictures per campaign and site were taken using a Panasonic Lumix DMC-TZ60® compact camera (focal length 4 mm which is a 35-mm equivalent of 25 mm; 10 Mpx) mounted on a 10-m telescopic inspection pole. SfM processing was implemented using standard workflows within Agisoft Photoscan Professional® 1.3.4. Dense point clouds with an average point density of around $5\times10^4$ observations $m^{-2}$ (i.e. 5 obs $cm^{-2}$) were obtained. In terms of georreferencing and scaling, SfM data sets were registered by a floating control network of around 30 Ground Control Points (GCPs) per badland, set up based on a permanent network control. GCPs were spatially distributed, with an average mean absolute error of 0.023 m. In terms of quality assessment, an independent validation dataset of around 300 Check Points (ChPs) per survey were obtained with an average mean absolute error of 0.021 m. Point clouds were filtered to remove outliers and vegetation. The open-source Topographic Point Cloud Analysis Toolkit (ToPCAT; Brasington et al., 2012; Rychkov et al., 2012) was then used to regularize the point cloud (implemented in the Topographic Analysis Tools Software (TAT) extension for ArcMap®, available at http://tat.riverscapes.xyz/). A 0.05 × 0.05 m grid was selected, taking into account the magnitude of the topographic changes on the study area and the size of the smallest geomorphic features observed in the field (e.g. rills). ToPCAT allows the analysis of topographic data within each grid cell ad calculation of a series of sub-grid statistics (e.g. maximum, mean and minimum elevations and detrended standard deviation of elevations). The minimum elevation within each cell was used to represent the ground elevation. A Triangular Irregular Network (TIN) was calculated based on these observations for each survey. Finally, a 0.05 m resolution DEM from each TIN was obtained.

Topographic changes were estimated by the comparison of DEMs between surveys (DEM of Differencing; i.e. DoD). DoDs were calculated by the Geomorphic Change Detection 7.4 (GCD) extension for ArcMap® (available at http://gcd.joewheaton.org/; see Wheaton et al. 2010). GCD also allows adding uncertainty analysis based on simple minimum Level of Detection (minLoD), propagating errors and performing probabilistic thresholding. The assessment of the spatially distributed uncertainty was addressed by the application of a Fuzzy Inference System (FIS) to consider errors from different sources (Wheaton et al., 2010). In this study we have used the FIS model proposed by Rossi (2018), which takes into account the slope and the roughness as the main factors determining the vertical uncertainty in SfM topographic datasets. A critical *t*-value at a confidence interval of 85% (i.e. the default value in GCD) was applied to calculate the spatially distributed minLoD (e.g. Brasington et al., 2000; Lane et al., 2003; Smith and Vericat, 2015). Those DoD cells with absolute values below the minLoD were considered uncertain and hence were not used in the computation of the thresholded DoDs.

The measured net topographic changes in the two study badlands were extrapolated to all the surface occupied by badlands in the study area; this was performed by multiplying the average net change (i.e. reference sediment production rate) for each period by the total surface occupied by badlands in the entire basin. As stated, the reference sediment production rate is the average between the two study badlands; however, in order to characterize the full spectrum of sediment production rates, the maximum and the minimum values were also used. Note that these extreme values (i.e. minimum and maximum) correspond to the values measured in the two badlands; for instance, if the sediment production in Badland 1 is less than in Badland 2 then value of Badland 1 is taken as the minimum while the value of the Badland 2 is taken as the maximum. Average surface net changes (m $year^{-1}$) were multiplied by the area of the badlands ($m^2$), and transformed to sediment production (t $year^{-1}$) using a bedrock density of 2.61 t $m^{-3}$ reported by López-Tarazón et al. (2012) for badlands in the neighbouring Isábena catchment.

### 3.1.3. Discharge and suspended sediment transport at the basin outlet

Water depth and suspended sediment transport were monitored continuously in the gauging section located at the catchment outlet (see location in Figure 1). Water depth (h) was measured with capacitive water stage sensors/loggers (TruTrack WT-HR®) at 5-minute intervals and subsequently converted to a discharge (*Q*) using the formula for open rectangular-notch weirs to derive the *h*/*Q* relation (see Figure 1D). Suspended sediment transport was also recorded at a 5-minute interval as turbidity using an ANALITE® NEP9350® turbidity probe attached to a Campbell CR200® data logger. The range of the probe was 0-3000 NTU, equating to approximately 0-3 g $l^{-1}$. Turbidity values were subsequently converted to suspended sediment concentrations using specifically collected water samples (*n* = 110). Samples were obtained using a 1.7 m water stage sampler with a bottle spacing of 5 cm (i.e. one sample every 5 cm water stage increment; designed and built following the initial model developed by Schick, 1967). Samples were filtered by means of 45 μm pore cellulose filters. When concentrations were >2 g $l^{-1}$ samples were decanted (i.e. samples were left immobile until sediments settled and the water was extracted from the samples) then oven-dried, and weighed to determine the suspended sediment concentration (SSC). The turbidity sensor was not able to measure the whole sediment concentration range, which eventually attained 10 g $l^{-1}$ during floods. The out-of-range periods were thus derived from the SSC extracted from the samples obtained by the water stage sampler (i.e. one sample every 5 cm stage increment). Linear interpolation between sampled-based SSCs was performed to extract a SSC value per each value of flow (i.e. 5-minute data).

## 3.2. Data analysis

A total of 23 variables were derived from meteorological (*n* = 8), discharge (*n* = 9) and sediment records (*n* = 6) in order to search for statistical relationships that help explain the sediment yield of the catchment and the contribution of badlands to it (see Table 2 for a complete description of the variables and their units). Meteorological variables include rainfall and temperature. The selection of variables was informed by the observation that low temperatures and rainfall are the main drivers of weathering and erosion processes in badlands areas, respectively (e.g. Yair et al., 1980; Clotet et al., 1987; Gallart et al., 2002). We define a flood as a hydrological event in which discharge exceeded 1.5 times the base flow at the beginning of the rainfall (e.g. García-Ruiz et al., 2005; López-Tarazón et al., 2010; Tuset et al., 2016). Sediment production variables are estimated for all the baldland surfaces in the study catchment, obtained using the reference

sediment production rates measured in the experimental badlands (section 3.1.2) and the total area of the study catchment occupied by badlands.

**Table 2.** Meteorological, discharge and sediment-based variables, showing the corresponding abbreviations and measuring units.

| Type of variable | Abbreviation | Description | Unit |
|---|---|---|---|
| Time | *ND* | Number of days | Day |
| Meteorological | *TR* | Total rainfall | mm |
| | *RD* | Rainfall duration | hour |
| | *MRI* | Mean rainfall intensity | mm $hour^{-1}$ |
| | *MaxRI* | Maximum rainfall intensity | mm $hour^{-1}$ |
| | *MT* | Mean temperature | ºC |
| | *Zd* | Days with temperature <0ºC | Nº of days |
| | *MTZD* | Mean of minimum temperatures of days <0ºC | ºC |
| | *MinTZD* | Absolute minimum temperature | ºC |
| Discharge | *R* | Runoff | $hm^{-3}$ |
| | $Q_m$ | Mean discharge | $m^3\ s^{-1}$ |
| | *RC* | Runoff coefficient | |
| | *DR* | % time channel dry | % |
| | *NF* | Number of floods | nº |
| | $Q_{ci}$ | Maximum instantaneous flood | $m^3\ s^{-1}$ |
| | *FD* | Flood duration | hours |
| | $Q_{mf}$ | Mean flood discharge | $m^3\ s^{-1}$ |
| | *FI* | Flashiness Index[1] | $m^3\ s^{-1}\ h^{-1}$ |
| Sediment transport | *SY* | Sediment yield | t |
| | *SSY* | Specific sediment yield | t $ha^{-1}$ $year^{-1}$ |
| | $SSC_{max}$ | Maximum suspended sediment concentration | g $l^{-1}$ |
| | $SSC_m$ | Mean suspended sediment concentration | g $l^{-1}$ |
| | *SDR* | Sediment Delivery Ratio | $SY/\ SP_{mean}$ |
| | $SP_{min}$ | Minimum sediment production | t |
| | $SP_{max}$ | Maximum sediment production | t |
| | $SP_{mean}$ | Mean sediment production | t |

[1] Note that FI was estimated as the rate of increment of discharge per unit of time (as per Batalla and Vericat, 2009).

Normality of the study variables was evaluated using the Shapiro-Wilk test (Royston, 1982). Results indicated that 6 variables (i.e. 26% of the total variables used) were not normally distributed (i.e. *p*-value > 0.01). In this way, the non-parametric Spearman's Rank correlation coefficient was used instead a Pearson correlation matrix. The analysis was perform for each of the study periods ($n$ = 6) to investigate statistical correlations between variables. A *p*-value of 0.05 was set to consider the relations statistically significant, while correlations at a *p*-value smaller than 0.01 were highlighted to indicate the strongest correlations.

## 4. RESULTS

Figure 2 shows temperature, rainfall, runoff and suspended sediment transport for the whole study period. Visual relations between variables can be observed. For instance winter registered the lowest temperatures and precipitation, with consequently fewer floods and low suspended sediment concentrations; in turn, the spring and autumn periods (the latter including most of the summer season) registered the highest temperatures and rainfall which resulted in a higher occurrence of floods and largest suspended sediment concentrations. Mean annual temperature (*MT*) ranged between 12 and 13 ºC. Maximum temperature was registered during August of 2016 (i.e. 42ºC) while the minimum was recorded in January 2017 (i.e. -10ºC). A total of 61 floods were registered (22 in 2016-17 and 39 in 2017-18), with peak flows ($Q_{ci}$) raging from 4.32 to 15.97 $m^3$ $s^{-1}$. Mean peak flow ($Q_{mf}$) for the entire period was 1.30 $m^3$ $s^{-1}$. Maximum registered SSC was 118.06 g $l^{-1}$ ($SSC_{max}$), with a mean flood-based SSC of 7.80 g $l^{-1}$ ($SSC_{mean}$). Annual rainfall (*TR*) varied between 818 and 1001 mm. Maximum intensity (*MaxRI*) was registered during June of 2017 (i.e. 24 mm $h^{-1}$).

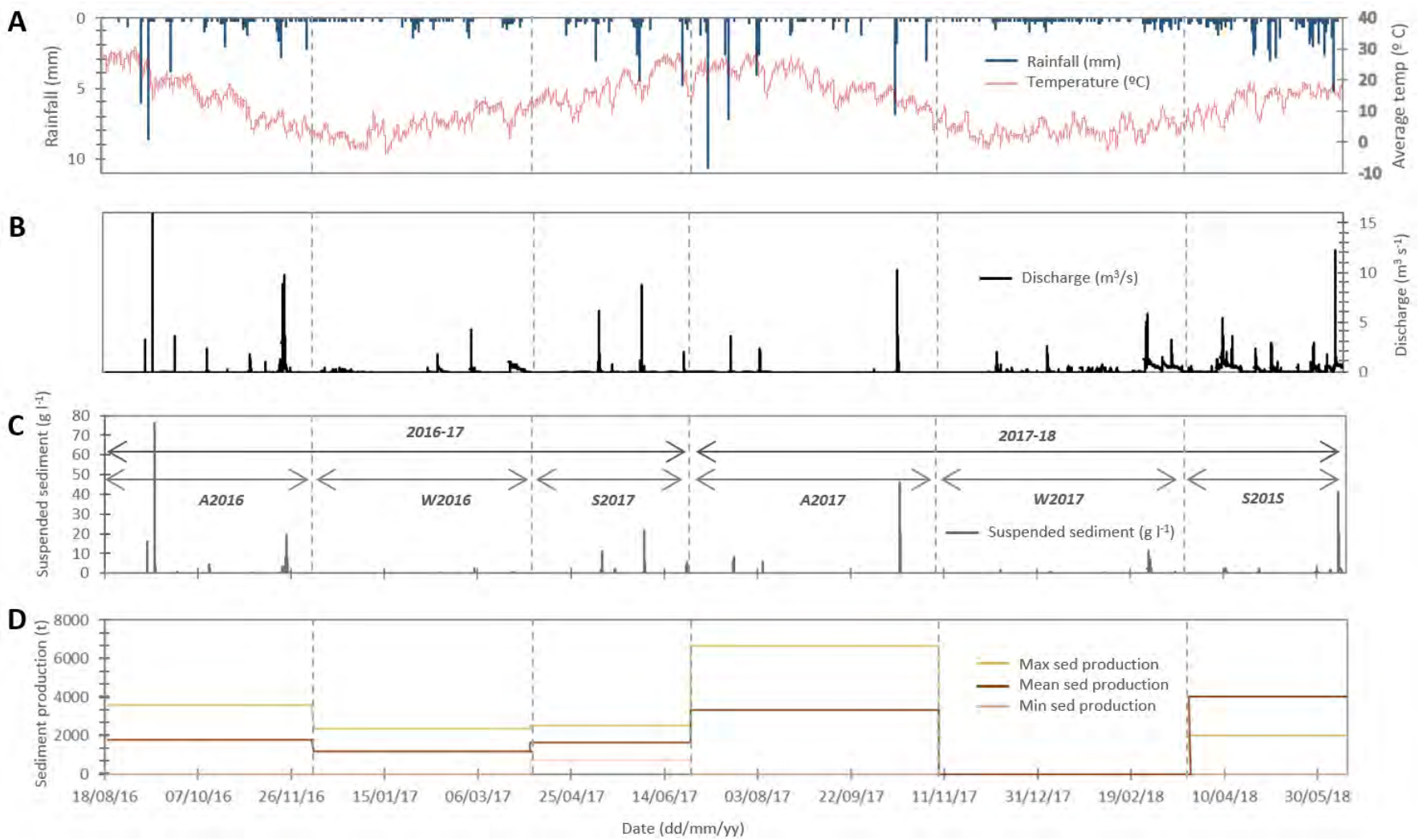


**Figure 2.** Variables recorded in the Soto catchment during 2016-2018. (A) Rainfall and temperature; (B) Flow discharge (*Q*); (C) Suspended sediment concentrations (*SSC*); (D) Sediment production in badlands. All variables are recorded at 5-min intervals.

## 4.1. Temperature, rainfall and runoff

Table 3 presents temperature, rainfall and runoff variables measured in the Soto catchment in each of the study periods. In summary, the highest mean temperature (*MT)* was registered during A2017 and A2016, whereas W2018 registered the highest *Zd* and W2017 recorded the lowest mean of minimum temperatures of days <0ºC (*MTZD)* and the absolute minimum temperature (*MinTZD)*. Regarding rainfall, maximum total rainfall (*TR)* and rainfall duration (*RD)* were registered during S2018, while maximum values of mean rainfall intensity (*MRI*) and maximum rainfall intensity (*MaxRI*) were registered in W2018 and S2017, respectively; maximum rainfall typically occurs in autumn. At the annual scale, 2017-18 was wetter and cooler than 2016-17, while 2016-17 registered more extreme rainfall events (*MaxRI*) in all seasons, and lower minimum temperatures (*MinTZD*). Conversely, runoff variables do not show clear seasonal patterns. Instead, W2018 and S2018 presented the highest values of runoff (*R*), mean discharge ($Q_m$), runoff coefficient (*RC*), number of floods (*NF*) and flood duration (*FD*). In contrast, A2017 showed the highest percentage of time with the channel dry (*DR*; almost 60%). This period also presented the highest flashiness index (*FI*). Finally, A2016 registered the highest peak discharges, both maximum instantaneous flood ($Q_{ci}$) and mean flood discharge ($Q_{mf}$). At the annual scale runoff variables during 2017-18 were double the 2016-17 values, including maximum discharges, thereby highlighting the higher hydrological variability of this second study year.

**Table 3.** Meteorological and runoff variables registered in the Soto catchment during 2016-2018 (see Table 2 for a description of variables). For reference, largest values of each variable are highlighted in bold.

| | Period | TR | RD | MRI | MaxRI | MT | Zd | MTZD | MinTZD | R | $Q_m$ | RC | DR | NF | $Q_{ci}$ | FD | $Q_{mf}$ | FI |
|---|---|---|---|---|---|---|---|---|---|---|---|---|---|---|---|---|---|---|
| | | *mm* | *hour* | mm hour$^{-1}$ | mm hour$^{-1}$ | *ºC* | *Nº of days* | *ºC* | *ºC* | hm$^3$ | m$^3$ s$^{-1}$ | | % | *Nº* | m$^3$ s$^{-1}$ | *hour* | m$^3$ s$^{-1}$ | m$^3$ s$^{-1}$ h$^{-1}$ |
| SEASONAL | **A2016** | 355 | 163.4 | 2.17 | 20.4 | 18.2 | 13 | -1.35 | -4.19 | 0.94 | 0.09 | 0.26 | 21 | 9 | **16.0** | 172.0 | **2.22** | 3.43 |
| | **W2017** | 254 | 171.3 | 1.49 | 10.2 | 5.1 | 70 | **-3.28** | **-9.89** | 0.92 | 0.09 | 0.36 | 0 | 6 | 4.3 | 641.8 | 0.82 | 0.96 |
| | **S2017** | 209 | 185.0 | 1.13 | **24.6** | 17.1 | 3 | -1.06 | -2.16 | 0.47 | 0.06 | 0.22 | 4 | 7 | 8.8 | 122.3 | 1.25 | 4.62 |
| | **A2017** | 246 | 117.5 | 2.09 | 17.4 | **19.0** | 0 | - | - | 0.34 | 0.03 | 0.14 | **58** | 4 | 10.3 | 174.8 | 1.88 | **8.70** |
| | **W2018** | 362 | 158.4 | **2.29** | 8.0 | 3.8 | **102** | -2.94 | -7.66 | **1.84** | 0.18 | **0.50** | 0 | **18** | 5.8 | **975.0** | 0.91 | 0.74 |
| | **S2018** | **393** | **232.6** | 1.69 | 16.6 | 13.3 | 7 | -1.56 | -3.54 | 1.83 | **0.26** | 0.46 | 0 | 17 | 12.2 | 696.7 | 0.63 | 2.51 |
| ANNUAL | **2016-17** | 818 | 519.7 | 1.57 | **24.6** | **13.4** | 86 | -1.90 | **-9.89** | 2.32 | 0.08 | 0.28 | 8 | 22 | **16.0** | 936.1 | **1.43** | 3.01 |
| | **2017-18** | **1001** | **550.1** | **1.82** | 17.4 | 11.8 | **109** | **-2.25** | -7.66 | **4.01** | **0.16** | **0.40** | **19** | **39** | 12.2 | **1846.5** | 1.14 | **3.98** |

Figure 3 shows the results of the Spearman's Rank correlation matrix between runoff, rainfall and temperature variables highlighting in bold the statistically significant correlations. The number of days (*ND*) is positively related with mean rainfall intensity (*MRI*), while maximum rainfall intensity of rainfall (*MaxRI*) is positively related with mean temperature (*MT*) and inversely related with days with temperature <0ºC (*Zd*). Temperature variables, as expected, show significant correlations between each other. Runoff (*R*) presented a high positive relation (*p*-value < 0.01) with mean discharge ($Q_m$), runoff coefficient (*RC*), number of floods (*NF*), and it is inversely correlated with flashiness (*FI*). Mean discharge ($Q_m$) presented a positive relationship with runoff coefficient (*RC*) and number of floods (*NF*). Runoff coefficient (*RC*) is positively related with total rainfall (*TR*), days with temperature <0ºC (*Zd*), number of floods (*NF*) and flood

duration (*FD*), and it is inversely related with mean temperature (*MT*), mean of minimum temperatures of days <0ºC (*MTZD*), percentage of time with the channel dry (*DR)* and flashiness (*FI*). *FI* also presented a positive and strong relationship with the percentage of time with the channel dry (*DR)* and it is inversely correlated with runoff (*R*), indicating that drier periods have a lower runoff but have a higher rate of flow increase when a flood occurs. Furthermore, total rainfall (*TR*) is positively related with total runoff (*R*), mean discharge ($Q_m$) and runoff coefficient (*RC*), while maximum rainfall intensity (*MaxRI*) is inversely related with flood duration (*FD*). In turn, *FD* presented negative and positive relations with maximum rainfall intensity (*MaxRI*) and runoff coefficient (*RC*), respectively. Overall, *FI* shows the strongest relation with other variables, notably *MT*, *MTZD*, *MinTZD, RC* and *DR*.

**Figure 3.** Spearman's Rank correlation coefficient matrix between temperature, rainfall, runoff, sediment production from badlands and catchment sediment yield for the 6 different seasonal periods analysed (see Table 2 for a description of each variable). Values in bold indicate that statistical relations are significant at $p < 0.05$, while bold and italic values indicate that relations are significant at $p < 0.01$.

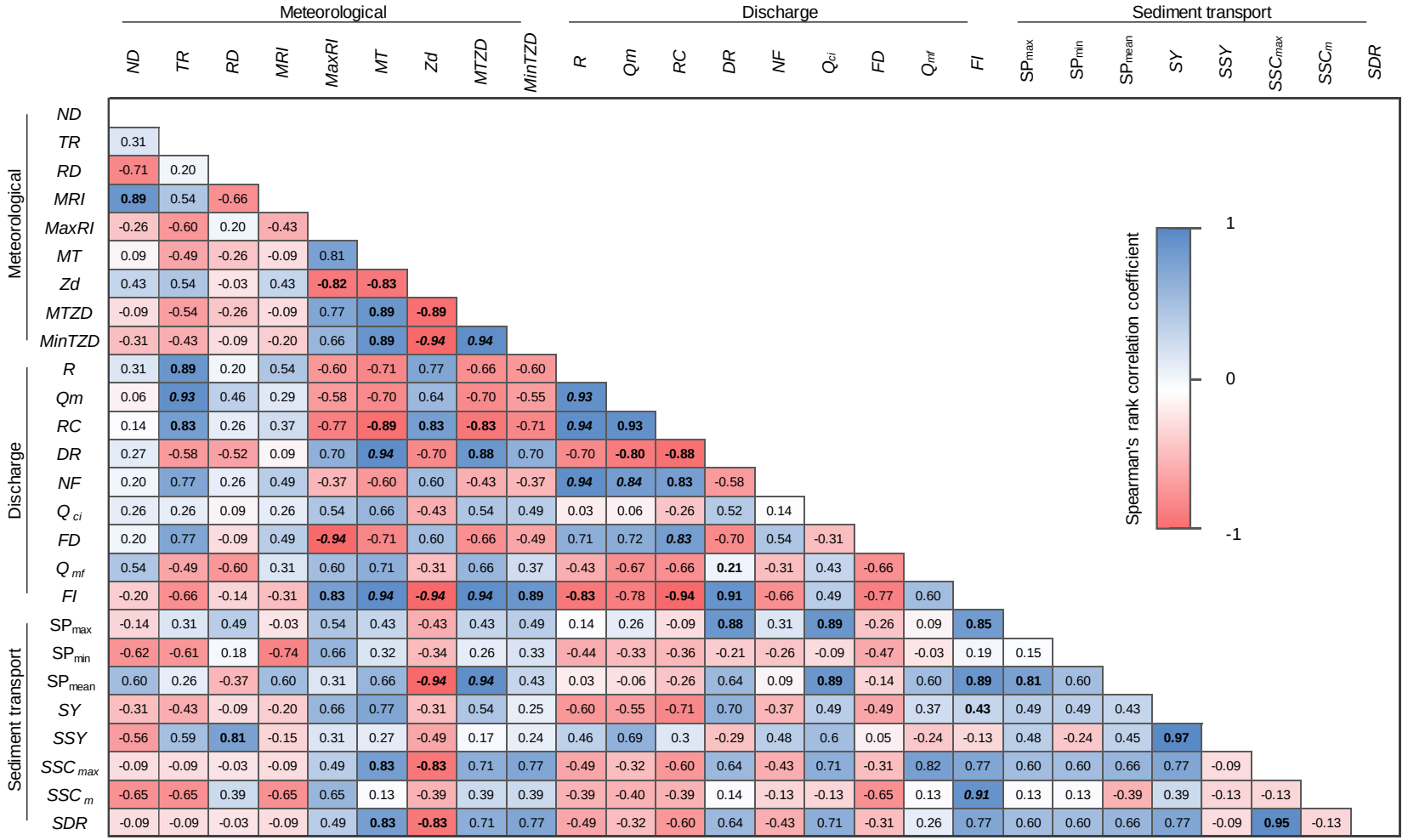


| | ND | TR | RD | MRI | MaxRI | MT | Zd | MTZD | MinTZD | R | Qm | RC | DR | NF | $Q_{ci}$ | FD | $Q_{mf}$ | FI | $SP_{max}$ | $SP_{min}$ | $SP_{mean}$ | SY | SSY | $SSC_{max}$ | $SSC_m$ | SDR |
|---|---|---|---|---|---|---|---|---|---|---|---|---|---|---|---|---|---|---|---|---|---|---|---|---|---|---|
| ND | | | | | | | | | | | | | | | | | | | | | | | | | | |
| TR | 0.31 | | | | | | | | | | | | | | | | | | | | | | | | | |
| RD | -0.71 | 0.20 | | | | | | | | | | | | | | | | | | | | | | | | |
| MRI | **0.89** | 0.54 | -0.66 | | | | | | | | | | | | | | | | | | | | | | | |
| MaxRI | -0.26 | -0.60 | 0.20 | -0.43 | | | | | | | | | | | | | | | | | | | | | | |
| MT | 0.09 | -0.49 | -0.26 | -0.09 | 0.81 | | | | | | | | | | | | | | | | | | | | | |
| Zd | 0.43 | 0.54 | -0.03 | 0.43 | **-0.82** | **-0.83** | | | | | | | | | | | | | | | | | | | | |
| MTZD | -0.09 | -0.54 | -0.26 | -0.09 | 0.77 | **0.89** | **-0.89** | | | | | | | | | | | | | | | | | | | |
| MinTZD | -0.31 | -0.43 | -0.09 | -0.20 | 0.66 | **0.89** | ***-0.94*** | ***0.94*** | | | | | | | | | | | | | | | | | | |
| R | 0.31 | **0.89** | 0.20 | 0.54 | -0.60 | -0.71 | 0.77 | -0.66 | -0.60 | | | | | | | | | | | | | | | | | |
| Qm | 0.06 | ***0.93*** | 0.46 | 0.29 | -0.58 | -0.70 | 0.64 | -0.70 | -0.55 | ***0.93*** | | | | | | | | | | | | | | | | |
| RC | 0.14 | **0.83** | 0.26 | 0.37 | -0.77 | **-0.89** | **0.83** | **-0.83** | -0.71 | ***0.94*** | **0.93** | | | | | | | | | | | | | | | |
| DR | 0.27 | -0.58 | -0.52 | 0.09 | 0.70 | ***0.94*** | -0.70 | **0.88** | 0.70 | -0.70 | **-0.80** | **-0.88** | | | | | | | | | | | | | | |
| NF | 0.20 | 0.77 | 0.26 | 0.49 | -0.37 | -0.60 | 0.60 | -0.43 | -0.37 | ***0.94*** | ***0.84*** | **0.83** | -0.58 | | | | | | | | | | | | | |
| $Q_{ci}$ | 0.26 | 0.26 | 0.09 | 0.26 | 0.54 | 0.66 | -0.43 | 0.54 | 0.49 | 0.03 | 0.06 | -0.26 | 0.52 | 0.14 | | | | | | | | | | | | |
| FD | 0.20 | 0.77 | -0.09 | 0.49 | ***-0.94*** | -0.71 | 0.60 | -0.66 | -0.49 | 0.71 | 0.72 | ***0.83*** | -0.70 | 0.54 | -0.31 | | | | | | | | | | | |
| $Q_{mf}$ | 0.54 | -0.49 | -0.60 | 0.31 | 0.60 | 0.71 | -0.31 | 0.66 | 0.37 | -0.43 | -0.67 | -0.66 | **0.21** | -0.31 | 0.43 | -0.66 | | | | | | | | | | |
| FI | -0.20 | -0.66 | -0.14 | -0.31 | **0.83** | ***0.94*** | ***-0.94*** | ***0.94*** | **0.89** | **-0.83** | -0.78 | **-0.94** | **0.91** | -0.66 | 0.49 | -0.77 | 0.60 | | | | | | | | | |
| $SP_{max}$ | -0.14 | 0.31 | 0.49 | -0.03 | 0.54 | 0.43 | -0.43 | 0.43 | 0.49 | 0.14 | 0.26 | -0.09 | **0.88** | 0.31 | **0.89** | -0.26 | 0.09 | **0.85** | | | | | | | | |
| $SP_{min}$ | -0.62 | -0.61 | 0.18 | -0.74 | 0.66 | 0.32 | -0.34 | 0.26 | 0.33 | -0.44 | -0.33 | -0.36 | -0.21 | -0.26 | -0.09 | -0.47 | -0.03 | 0.19 | 0.15 | | | | | | | |
| $SP_{mean}$ | 0.60 | 0.26 | -0.37 | 0.60 | 0.31 | 0.66 | ***-0.94*** | ***0.94*** | 0.43 | 0.03 | -0.06 | -0.26 | 0.64 | 0.09 | **0.89** | -0.14 | 0.60 | **0.89** | **0.81** | 0.60 | | | | | | |
| SY | -0.31 | -0.43 | -0.09 | -0.20 | 0.66 | 0.77 | -0.31 | 0.54 | 0.25 | -0.60 | -0.55 | -0.71 | 0.70 | -0.37 | 0.49 | -0.49 | 0.37 | **0.43** | 0.49 | 0.49 | 0.43 | | | | | |
| SSY | -0.56 | 0.59 | **0.81** | -0.15 | 0.31 | 0.27 | -0.49 | 0.17 | 0.24 | 0.46 | 0.69 | 0.3 | -0.29 | 0.48 | 0.6 | 0.05 | -0.24 | -0.13 | 0.48 | -0.24 | 0.45 | **0.97** | | | | |
| $SSC_{max}$ | -0.09 | -0.09 | -0.03 | -0.09 | 0.49 | **0.83** | **-0.83** | 0.71 | 0.77 | -0.49 | -0.32 | -0.60 | 0.64 | -0.43 | 0.71 | -0.31 | 0.82 | 0.77 | 0.60 | 0.60 | 0.66 | 0.77 | -0.09 | | | |
| $SSC_m$ | -0.65 | -0.65 | 0.39 | -0.65 | 0.65 | 0.13 | -0.39 | 0.39 | 0.39 | -0.39 | -0.40 | -0.39 | 0.14 | -0.13 | -0.13 | -0.65 | 0.13 | ***0.91*** | 0.13 | 0.13 | -0.39 | 0.39 | -0.13 | -0.13 | | |
| SDR | -0.09 | -0.09 | -0.03 | -0.09 | 0.49 | **0.83** | **-0.83** | 0.71 | 0.77 | -0.49 | -0.32 | -0.60 | 0.64 | -0.43 | 0.71 | -0.31 | 0.26 | 0.77 | 0.60 | 0.60 | 0.66 | 0.77 | -0.09 | **0.95** | -0.13 | |

## 4.2. Sediment production from badlands

Net changes from the two badlands ranged between 0.07 and 0.13 cm $ha^{-1}$. Mean annual sediment production was 0.07 cm $ha^{-1}$ in 2016-17 and 0.10 cm $ha^{-1}$ in 2017-18. Note that a complete analysis of the spatio-temporal changes on sediment erosion and export from these two experimental badlands, together with the study of the main geomorphic process signatures responsible for these, is presented in Llena et al. (Under revision). Table 4 summarises the sediment production from badlands in the Soto catchment for the whole study period. The highest values of sediment production from badlands were measured during spring and autumn periods (which includes most of the summer months), while the minimum values were registered during winter. These patterns are similar to those observed for sediment yield variables (see section 4.3 below). More specifically, the highest maximum sediment production ($SP_{max}$) and mean sediment production ($SP_{mean}$) were registered in A2017 while the highest minimum sediment production ($SP_{min}$) was measured in S2017. The minimum values were measured during W2018. At the annual scale, both years presented similar values, being $SP_{mean}$ and $SP_{max}$ slightly higher during 2017-18. In turn, $SP_{min}$ was higher during 2016-17.

**Table 4.** Sediment production from badlands registered in the Soto catchment during 2016-2018 (see Table 2 for a description of each variable). The largest values of each variable are highlighted in bold. Note that these data are extracted from Llena et al. (Under revision).

| | Period | $SP_{min}$[1] | $SP_{max}$ | $SP_{mean}$ |
|---|---|---|---|---|
| | | *t* | *t* | *t* |
| SEASONAL | **A2016** | 0 | 3588.3 | 1794.2 |
| | **W2017** | 0 | 2372.2 | 1186.1 |
| | **S2017** | **755.4** | 2541.7 | 1648.6 |
| | **A2017** | 0 | **6664.8** | **3332.4** |
| | **W2018** | 0 | 0 | 0 |
| | **S2018** | 0 | 4029.0 | 2014.5 |
| ANNUAL | **2016-17** | **755.4** | 8502.2 | 4628.8 |
| | **2017-18** | 0 | **10693.8** | **5346.9** |

The results of the Spearman's Rank correlation coefficient show several statistically significant relations (Figure 3); $SP_{mean}$ is the sediment production variable that exhibits the strongest relationships with the meteorological and hydrological variables, followed by $SP_{max}$. $SP_{mean}$ is positively related with *MTZD,* $Q_{ci}$*, Fi and* $SP_{max}$ , and is negatively related with *Zd*. In turn, $SP_{max}$ presented positive relations with *DR,* $Q_{ci}$ and *FI*. $SP_{min}$ in turn did not present any significant statistical relation.

## 4.3. Catchment sediment yield

Table 5 summarises the catchment sediment yield for each study period. The highest values of sediment yield (*SY*), specific sediment yield (*SSY*), maximum suspended sediment concentration ($SSC_{max}$) and mean suspended sediment concentration ($SSC_m$) are registered during spring and autumn, while the lowest values are recorded in winter. At the annual scale, 2017-18 presents the highest values of sediment transport (the wettest year), except for the maximum suspended

sediment concentration, which was registered in 2016-17, when the maximum rainfall intensity was also observed as indicated above.

**Table 5.** Summary of flow and sediment transport variables registered in the Soto catchment during 2016-2018 (see Table 2 for a description of each variable). The largest values of each variable are highlighted in bold. Note that flow-related variables are also included for reference.

| | | *Flow* | | | *Sediment transport* | | | |
|---|---|---|---|---|---|---|---|---|
| | ***Period*** | ***$Q_m$*** | ***NF*** | ***$Q_{ci}$*** | ***SY*** | ***SSY*** | ***$SSC_{max}$*** | ***$SSC_m$*** |
| | | $m^3 s^{-1}$ | *Nº* | $m^3 s^{-1}$ | *t* | t $ha^{-1}$ $year^{-1}$ | g $l^{-1}$ | g $l^{-1}$ |
| SEASONAL | **A2016** | 0.09 | 9 | **16.0** | 7344.4 | 7.8 | **118.1** | 7.8 |
| | **W2017** | 0.09 | 6 | 4.3 | 314.6 | 1.2 | 7.3 | 1.2 |
| | **S2017** | 0.06 | 7 | 8.8 | 2584.1 | 14.1 | 37.0 | 14.1 |
| | **A2017** | 0.03 | 4 | 10.3 | 620.1 | **19.6** | 78.5 | **19.6** |
| | **W2018** | 0.18 | **18** | 5.8 | 420.0 | 5.8 | 38.3 | 5.8 |
| | **S2018** | **0.26** | 17 | 12.2 | **11165.6** | 11.1 | 49.3 | 11.1 |
| ANNUAL | **2016-17** | 0.08 | 22 | **16.0** | 10243.09 | 7.7 | **118.1** | 7.7 |
| | **2017-18** | **0.16** | **39** | 12.2 | **12205.73** | **11.60** | 78.5 | **12.2** |

According to the Spearman's Rank correlation coefficient results (Figure 3), overall,; specific sediment yield (*SSY*) is positively related with rainfall duration (*RD*) and sediment yield (*SY*), while maximum suspended sediment correlation ($SSC_{max}$) is positively related with mean temperature (*MT*) and mean *Q* of floods ($Q_{mf}$), and inversely correlated with days with temperatures below 0ºC (*Zd*). Mean suspended sediment correlation ($SSC_m$) is positively correlated with flashiness (*FI*); and Sediment Delivery Ratio (*SDR*) is correlated with mean temperatures (*MT*) and maximum suspended sediment correlation ($SSC_m$), and inversely correlated with days with temperatures below 0ºC (*Zd*).

## 5. DISCUSSION

### 5.1. Pulses of water and sediment fluxes

Meteorological and runoff variables present the most significant correlations, specifically: (i) total rainfall largely explains total runoff and mean discharge, more so than rainfall intensity. These findings are in agreement with results obtained by Tuset et al. (2016) in the Ribera Salada, a catchment with a long-term record in the eastern Pyrenees with no badlands, where main land use is composed by forest. (ii) Sediment yield is well correlated with rainfall duration; the longer the duration of the rainfall event, the higher the sediment yield observed at the outlet of the catchment. This fact was also reported by López-Tarazón et al. (2010) in the River Isábena, a neighbouring basin with similar characteristics to our study catchment, despite its larger size and perennial regime. The authors emphasised that river responses are controlled by the distance between the main sediment sources (i.e. badlands) and the catchment outlet. They stated that not all sediment eroded during a given rainfall event is exported out of the catchment immediately. Thus, the longer the event, the greater the opportunity for the system to export the sediment, and hence the higher the sediment yield. Finally, our results also indicated that:

(iii) temperature-based variables influence sediment production, suspended sediment concentrations, and flow variables such as flood duration and flashiness. As already reported in previous studies (e.g. Nadal-Romero and Regüés, 2010; Llena et al. Under review), low temperatures (typically recorded in winter) lead to a reduction of the erosion processes in badlands areas in favour of weathering processes. Under such circumstances, rates of suspended sediment transport and yield decrease. At the same time, the negative relationship between temperature and flood variables can be explained by changes in surface runoff generation by the low temperatures (e.g. Ollesch et al., 2005; Gallart et al., 2008).

Flashiness is the *runoff variable* that best correlates with the duration of the period in which the stream is dry, sediment production and suspended sediment concentration. Flashiness is rather pronounced in the study catchment. As an example, Figure 4 shows a representative (flash) flood registered in the Soto catchment: (i) surface runoff quickly concentrates in badlands after the rainfall, which is subsequently followed by a rapid response at the catchment outlet (*Q* reached 3.75 $m^3 s^{-1}$ in 15 minutes, *FI* = 15 $m^3 s^{-1} h^{-1}$); and (ii) the rapid increase of the suspended sediment concentration following runoff increase (reaching a value of almost 75 g $l^{-1}$), indicating that sediment was readily available in the drainage network (i.e. the channel acting as a source of sediment). In terms of the relationship between flashiness and the period when the channel remains dry (*DR*), Estrany et al. (2010) observed that during dry periods, runoff generation is limited due to the low saturation of the drainage network, and only rainfall episodes exceeding infiltration rates, thus producing Hortonian overland flow, are the responsible for the sudden *Q* increases at the catchment outlet (i.e. high flashiness caused by flash floods). Moreover, Batalla and Vericat (2009) explain that the increase of flashiness implies a higher rate of energy expenditure in the channel per unit time, increasing the magnitude of potential channel erosion and sediment transport, which may be directly reflected in an increase of suspended sediment concentrations if in-channel fine sediment is available, hence sediment load.

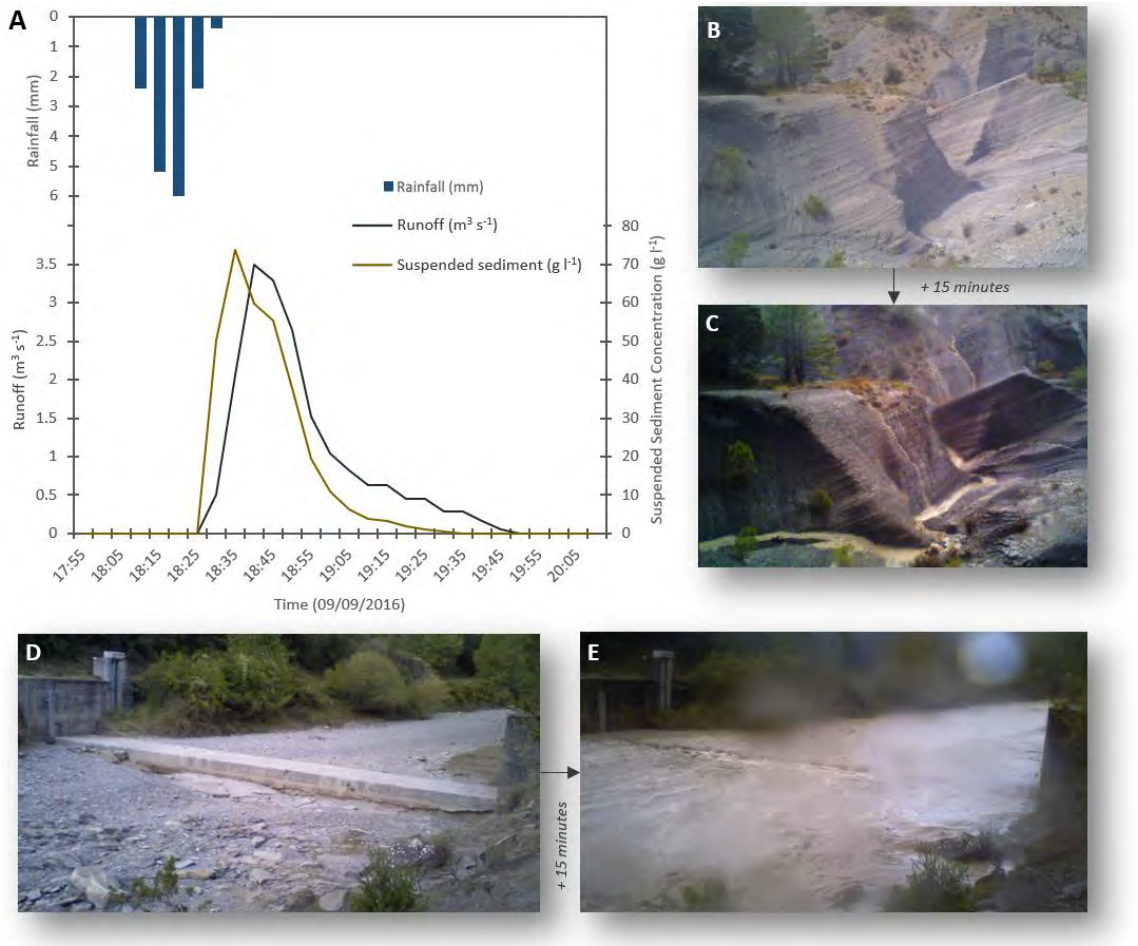


**Figure 4.** (A) Rainfall, discharge and suspended sediment concentration measured at 5-min interval for the flash flood of 9th September 2016. (B) An area of badlands just before the onset of rainfall and (C) at the highest rainfall intensity (i.e. 6 mm in 5 minutes). (D) Gauging station located at the catchment outlet (see location in Figure 1) just before the flood started and (E) during peak *Q*. Note that (i) the rainfall gauge is located in B and C, and (ii) the time between B and C, and D and E indicates the time-lapse between both photographs were taken.

Water and sediment transfer through fluvial systems is comprised of pulses (floods); a fact that is especially evident in systems characterised by intermittent regimes under highly variable hydroclimatic conditions such as that studied here. The degree of connectivity between sources and sinks will depend on the availability of sediments and on the capacity of running waters to transfer them through the drainage network that ultimately will be controlled by the flow peak but also the duration of competent flows. Sediment yield in catchments without constant base flow is more dependent on high magnitude pulses than catchments with perennial streams, especially if the sediment production rates in source areas are elevated (for instance in areas of badlands). The Soto basin represents a system with high structural connectivity, but with intermittent functional connectivity (i.e. fluxes), which is mainly controlled by pulses. Evidence of this low level of functional connectivity is provided by the absence of any correlation between sediment production and export at the seasonal scale (Figure 3). In order to understand the flashy response of these types of catchments it is important to analyse the dynamics of sediment source areas as well as to role of the drainage network in buffering the sediment load to downstream (i.e. acing as source or sink of fine sediments).

## 5.2. The role of badlands and land cover on catchment sediment yield

Our results indicate that both sediment production in badlands and sediment yield at the catchment outlet is very variable, with autumn and spring periods showing the highest values (Figure 5A). This fact was also observed by several authors in catchments exhibiting badlands (e.g. Regüés et al., 1995; Römkens et al., 2001; Nadal-Romero et al., 2007; Lana-Renault and Regüés 2009; Nadal-Romero and Regüés, 2010; López-Tarazón et al., 2011; Desir and Marin 2013; Piqué et al., 2014; Barnes et al., 2016; Vercruyse et al., 2017) and is mainly controlled by the seasonality of weathering and erosion processes, in turn controlling sediment production and yield. For instance, in the Vallcebre catchment (Southern Pyrenees), Regüés et al. (1995) described how during winter, regolith is weathered mainly by freeze-thawing processes, while during summer convective storms (included in both spring and autumn periods in this study) most of the regolith is eroded and transferred, and consequently sediment production increases. In terms of sediment yield, Lobera et al. (2016) also observed in the neighbouring River Ésera, that the highest suspended sediment loads occurred in summer and autumn, when high magnitude rainfall episodes lead to important flood events carrying large sediment loads. Similarly, Béjar et al. (2018) identified summer and autumn as the seasons with higher sediment loads for the Upper Cinca catchment (which includes the Soto study basin).

The variability of sediment production mostly depends on badland morphometric characteristics, including vegetation cover, a fact that has been widely analysed (e.g. Yair et al. 1980; Nadal-Romero et al., 2007; Vericat et al. 2014; Nadal-Romero et al 2015; Marchamalo et al. 2016; Bonetti et al., 2019; Vergari et al., 2019). For instance, Vericat et al. (2014) stated that, at the annual scale, aspect, surface roughness and slope were significant predictors of topographic change. In SE Spain, Marchamalo et al. (2016) analysed the influence of micro-topographic factors on pathways and frequency of water and sediment fluxes, which control runoff and erosion rates. In our case we use the mean rate of sediment production obtained in both badlands as a representative value for these types of surfaces throughout the basin, since it correctly represents their morphometric and vegetation variability. The use of single values to generalise to the catchment is in fact a limitation may have an influence to the results. However, it should be noted that maximum and minimum rates of sediment production were also used to search for correlations, in order to encompass the influence of a range of morphometric characteristics on the on sediment production.

Figure 5A shows the sediment production in badlands areas based on the mean value, but also the envelope defined by the minimum and maximum specific values observed during each study period, both seasonally and annually. The Figure also represents the sediment yield at the Soto catchment outlet for each of the study period. Despite the fact that, as explained above, temporal trends for badland sediment production and catchment sediment yield are similar (i.e. higher rates in spring and autumn, and lower rates in winter) a mismatch between the frequency and the magnitude of sediment production and sediment yield is evident. Several periods show larger sediment yield than production (A2016, S2017, W2018, A2018; brown areas in Figure 5A), whereas others show the opposite behaviour (W2017, S2017; grey areas in Figure 5A), production higher than the yield at the outlet. Moreover, at the annual scale, sediment production in the badlands accounts for half of the sediment yield in both study periods (i.e. 55% and 46% for 2016-17 and 2017-18 respectively). It is necessary to then analyse the role of other factors that can potentially effect the production, transfer and export of sediment in the basin: (i) the role of other land uses as sediment source occupying the 75% of the catchment area; and (ii) the role of drainage network acting as sediment source/sink.

As stated, land uses of the Soto catchment are mainly forest (56%), badlands (25%) and agricultural fields (19%). Only data from to experimental badlands was available in this study.

Thus, in order to analyse the potential role of non-badlands areas on sediment production in the Soto catchment, erosion values of forested ($n$ = 43) and agricultural ($n$ = 69) areas with similar characteristics (e.g. precipitation) were extracted from the literature, mostly from the review provided by García-Ruiz et al. (2015). These values are summarized in Table 1 in the Supplementary Materials. Values were combined following all possible combinations in order to extract a distribution of potential sediment production from forest and agricultural fields. An accumulated frequency distribution for each study period was calculated and presented in Figure 5B. The percentile 50 of these distributions (i.e. values associated to an accumulated frequency of 50 % of time) was used to compute the potential sediment production from these land uses.

Figure 5C shows the total sediment production in the Soto catchment for each study period after measured values in badlands and estimated values in forests and agriculture surfaces were integrated. As stated in the results, despite representing ¼ of the catchment area badlands still produce more than half (54%) of the sediment, being the main source of sediments; however, these results are far from those reported for instance in the neighbouring Isábena basin by Lopez-Tarazón et al. (2012), where 1% of badlands surface almost accounted for all of the basin's sediment yield at the annual scale. It is worth highlighting the different catchment area of the Isábena (445 $km^2$) compared to the Soto, which may have a direct impact on these differences. In the same way, Nadal-Romero and Regüés (2010) stated that, for the Araguás catchment (located around 80 km west of the study area, 0.45 $km^2$), sediment production in badlands are of three orders of magnitude higher than the values observed in other land uses in the same catchment.

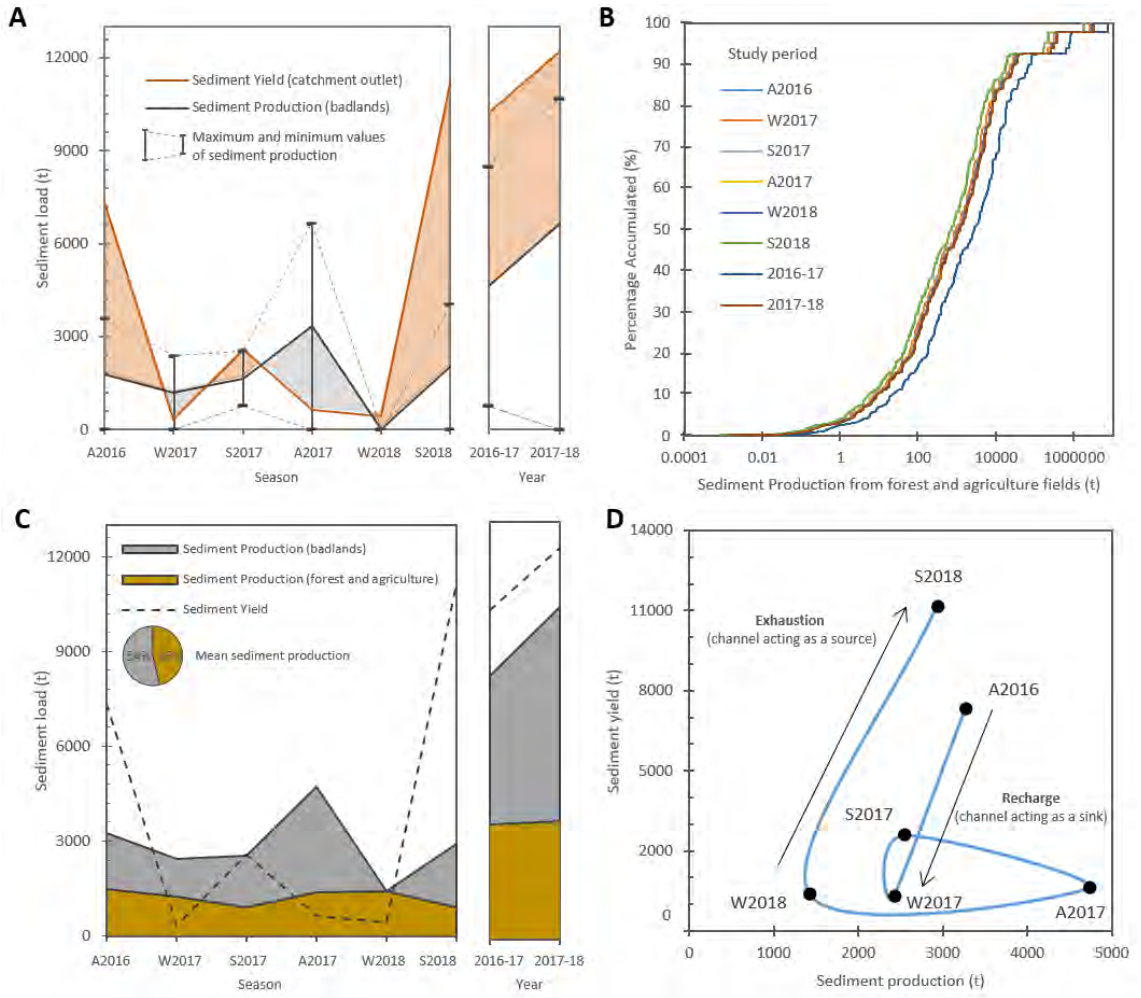


**Figure 5.** (A) Badlands' sediment production (grey line) and catchment sediment yield (brown line) for each study period (see section 3.1. for details). Brown areas represent the periods in which catchment sediment yield is higher than sediment production from badlands, while grey areas represent the opposite, i.e. periods in which sediment production is higher than sediment yield. Dotted lines represent the minimum and the maximum sediment production values registered in the two study badlands. Vertical lines represent the amplitude of the sediment production based on these extreme values. (B) Accumulated frequency distribution curves of sediment production values associated to forest and agricultural fields for each study period. These curves were estimated based on values obtained from the literature (Table 7; see section 5.2. for further details). (C) Comparison between measured sediment production in badlands (i.e. based on the mean or reference value) and estimated sediment production in agricultural and forested surfaces based on the median value (percentile 50$^{th}$) of the curves in B. (D) Hysteresis between sediment production and sediment yield for each study period in the Soto catchment.

## 5.3. Temporal dynamics of sediment transport

The analysis of the relationship between sediment production and sediment yield at the seasonal scale permits us to infer the sediment transfer dynamics within the catchment. Moreover, the seasonal scale helps to identify temporal trends related to the main characteristics of the meteorological variables within each season. Figure 5D illustrates the relation between total sediment production and sediment yield in the Soto catchment, which shows a double clockwise-loop with different consecutive phases: (i) exhaustion; (ii) inactivity; (iii) recharge; (iv) inactivity; and (v) exhaustion. During the first exhaustion phase (i), sediment export at the outlet changed from a high value in A2016 to a low value in W2017, while sediment

production remained more or less constant. From W2017 to S2017, although the sediment yield at the outlet increased, this was not substantial and can be considered as a phase of inactivity since sediment production remained constant. Phase (ii) was related to the low occurrence of erosive meteorological events during the winter months, as well as the low availability of sediment after previous exhaustion. In Phase (iii), from S2017 to A2017, the system was *recharged* following intense sediment production and low sediment yield at the outlet, i.e. produced sediments were not exported. Again, Phase (iv), from A2017 to W2018, represented a period of inactivity mainly due to the low occurrence of erosive meteorological events and the low and constant sediment yield at the outlet. Finally, Phase (v), from S2018 to S2018, was characterized by a high sediment export (sediment yield increased more than order of magnitude) as a response to the high availability of sediment in the catchment due to the previous recharge period (iii), as well as to the high production during that period.

In the case of the neighbouring Isábena catchment, López-Tarazón et al. (2011) and Piqué et al. (2014) observed that fine sediment in the drainage network has a mean residence time of around 1 year, which corroborates the high network connectivity and the role of baseflows allowing continuous sediment transfer. Continuous sediment transfer was not observed in the Soto due to its intermittent character. More recently, Keesstra et al. (2019) observed that clockwise-loops could be explained by the temporal storage of sediment along the drainage system due to its morphological complexity as well as to in-stream vegetation structures, which could act as disconnecting landscapes features. The latter process seems not to be in operation in the Soto catchment although no data is available to investigate this fully; however, we next discuss the potential role of the stream network in buffering the sediment yield and modulating the sediment export at the catchment outlet based on our observations.

## 5.4. Sediment delivery and the role of the channel as sediment buffer

Throughout the study period, rates of sediment production and yield are not synchronised except for S2017. This variability is presented graphically in Figure 6A. Sediment production and export values for each period are indicated in each compartment (i.e. each study period). When the compartment is coloured in red, it indicates that the export is higher than the production, that is a sediment delivery ratio (SDR) >1. When the compartments are blue the export is smaller than the production and the SDR is <1 (Figure 6B). Finally, when the SDR is 1 the compartment is coloured grey. SDR is subjected to two main sources of uncertainty: (i) the uncertainty in the methods used for the quantification of sediment yield (e.g. Regüés and Nadal-Romero, 2013; Vercruysse et al., 2017); and/or (ii) the uncertainty associated to the estimation of sediment production from topographic changes (e.g. Smith and Vericat, 2015; James et al., 2017), or, in the particular case of this study the estimates obtained from the literature. Despite these, the observed cycles and the hysteretic behaviour (that correlate with meteorological variables), point to role of the channel network as an important role in the regulation of sediment transfer. The channel network is acting as sediment sink (transient storage) for periods with SDR <1 in which sediment production is higher than the yield (W2017, A2017 and W2018 in Figure 6B), while it is acting as sediment source when SDR>1 (A2016, S2017 and S2018 in Figure 6B).

Sediment storage can be characterized, for instance, from the study of functional sediment connectivity through the use of tracers (i.e. fingerprinting). For instance, by using lead-210 ($^{210}$Pbex) in catchments draining badlands in NE of Spain, Moreno-de las Heras et al. (2018) observed how bare surfaces were weathered in winter and eroded during spring-autumn. Moreover, they reported a high connectivity between badlands, streams and the catchment outlet for fine sediments, and much lower connectivity for coarser sediments, which remained

in the stream bed for longer periods. Jantzi et al. (2017), using volumetric changes in the channel network (i.e. repeated topographic surveys), reported residence times of around 3 years in badland catchments in the South of France, mainly controlled by the degree of confinement of the stream network. In the Central Pyrenees, several authors (e.g. López-Tarazón et al., 2011; Gallart et al., 2013; Piqué et al., 2014; Buendia et al., 2015) observed that the residence time of the produced sediments is around 1 year (i.e. annually, the SDR equals 1). They also concluded that the sedimentary cycles along the catchment are not hydraulically driven, but directly driven by the amount of sediments available in the riverbed mainly controlled by sediment supply from badlands. In the case of the Soto, and given its particular physiographic characteristics (e.g. a highly coupled drainage network), sedimentary dynamics (i.e. intermittent sediment production), and the intermittent character of the river, we argue that the drainage network acts alternatively as sediment source or sink according to the supply of sediments from the catchment, and the magnitude and frequency of the hydrological pulses.

Besides sediment conveyance, the channel network can also act as an important sediment source through river bed erosion and transport. Gaspar et al. (2019) and Lizaga et al. (2019) stated using fingerprinting methods in Mediterranean catchments of NE Spain that the river channel can contribute up to 90% of the sediment exported during exceptional rainstorm events. Similarly, Kronvang et al. (2013) observed that bank erosion was the dominant sediment source (>90%) in the River Odense (Denmark). Despite the fact that events recorded in the Soto cannot be considered as extreme events, we hypothesise that SDR fluctuations may be in some cases explained by the succession of aggradation and degradation cycles in the channel network. The area of the fluvial channel network in the Soto is estimated at 6.25 ha by the digitalization of an orthophotomosaic of 0.5 m resolution of the study area obtained in 2015 (Spanish National Centre of Geographic Information, CNIG). Taking this into account and considering a sediment density of 2.61 t $m^{-3}$, the maximum negative net difference of -8237 t measured for S2018 (Figure 6B) could be balanced by a mean degradation rate of 0.13 m in the channel network (without considering contributions form bank erosion), which seems a plausible value of *fluvial* activity. Similarly, a mean net difference of -1949 t for the whole study period (i.e. 2016-18) would require a mean channel degradation of 0.03 m, which again seems to be a feasible value. These values are in agreement with erosion rates measured by Llena et al (Under revision) in the channel bottom of the experimental badlands for the same study period, which lends further support to our hypothesis of the active role of stream bed as sediment sink and source.

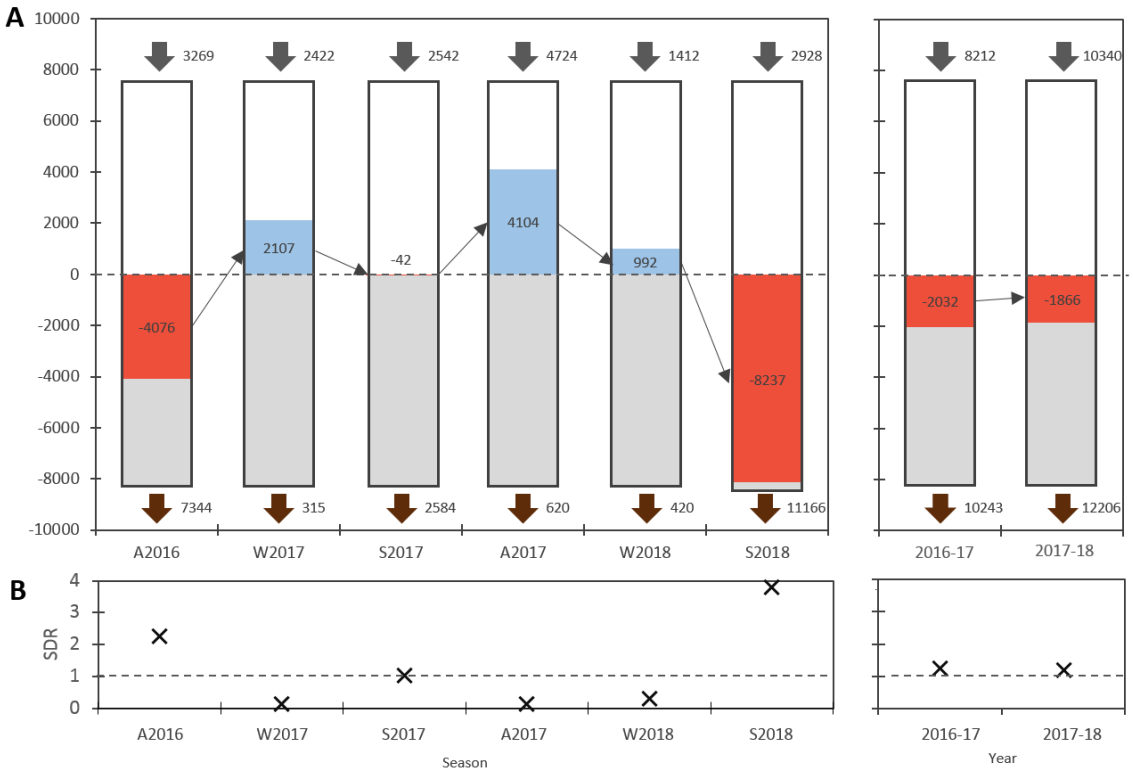


**Figure 6.** (A) Model of in-channel sediment storage fluctuations in relation to sediment production (inputs, grey arrows) and sediment export at the catchment outlet (outputs, brown arrows). (B) Changes in the sediment delivery ratio SDR for each study period.

## 5.5. The sediment budget of the Soto catchment

The sediment budget of the Soto catchment for the period 2016-18 is constructed from the following elements: (i) estimation of erosion in badlands from high temporal and spatial resolution topographic surveys; (ii) estimation of erosion from other land uses from a broad systematic literature review in similar hydro climatic areas, and (iii) *seasonal* and annual suspended yield (export) for the whole catchment (i.e. sediment output) based on continuous SSC and *Q* data. The estimates of (i) and (ii) constitute the sediment input (sediment source) to the system. The compiled sediment budget allows the construction of a quantitative framework to infer the role of the channel network as a sediment buffer (sink and source dynamics). Sediment input for the whole period 2016-18, reaches 9250 t $y^{-1}$, whereas sediment output amounted to 11225 t $y^{-1}$ (which equates to a SDR = 1.2), altogether yielding a sediment deficit of 1979 t $y^{-1}$ for the entire basin, which we attribute to the role of the channel network supplying fine sediment.

SDR observed in the Soto is higher in comparison with catchments with similar characteristics (e.g. Walling et al., 1983; de Vente et al., 2007) a fact that, additionally to the source of uncertainty already discussed above, it could be due to: (i) the relatively low erosional rates from badlands (i.e. around 1 mm $y^{-1}$ on average) in comparison to catchments in the same mountain region (i.e. from 5 to 30 mm $y^{-1}$; e.g. Clotet et al., 1988; Gallart et al., 2002; Nadal-Romero et al., 2007; Vericat et al., 2014); and (ii) the role of the intermittent stream and its flashiness behaviour, a fact that may exert an effect on the magnitude and frequency on the catchment sediment export. Intermittency poses a challenge in terms of the minimum time need to completely characterize a full sedimentary cycle in such type of small basins (for instance, in our case the study period is two years that were characterized by hydroclimatic values below the

mean, i.e. drier and cooler). Flashiness implies a high erosive potential in the main channel during floods, which suggest a relatively higher rate of sediment contribution (e.g. Kronvang et al., 2013; Gaspar et al., 2019) in comparison to streams where there is constant flow, that in turn controls in-channel sediment storage and depletion. It is worth noting that, as stated in section 5.2, badland morphometry has a direct effect on the sediment production, which could also modify the proposed sediment budget for the catchment. For instance, the use of the maximum sediment production rates in the two experimental badlands would drop SDR to 0.9, similar to the value reported by López-Tarazón et al. (2012) for the neighbouring Isábena catchment. Altogether, although the change on the SDR is not extremely high, reinforces the need to take into account the effects of morphometry on erosion processes in dryland and semiarid areas, and on the other, to account for the errors associated with techniques used to estimate rates of sediment production.

## 6. CONCLUSIONS

This paper has analysed the sediment production and the sediment yield in a small mountain catchment characterised by patchy badlands and drained by intermittent streams at multiple temporal scales. The main conclusions can be drawn as follows:

1. Meteorological and runoff variables exhibit the most significant correlations. Flashiness is the runoff variable that best correlates with the duration of the period in which the stream is dry, sediment production and suspended sediment concentration. Sediment yield is well correlated with rainfall and flood duration.
2. Although being the main source of sediments, badlands do not always control the export of sediments, confirming our initial hypothesis.
3. Sediment production of the two badlands is relatively low when compared to catchments with similar characteristics, a fact that can be attributed to the size of the experimental badlands, the method used to monitor topographic changes and the higher degree of compactness of the materials, which exhibits highly complex and spatially variable geomorphic processes, of lower magnitude when compared with other sub-humid Mediterranean badlands.
4. There exists a fluctuation of the functional connectivity of the channel network caused by water and sediment pulses during flashy floods and the intermittent character of the stream.
5. The drainage network acts as a temporally variable sediment source and sink. This situation, driven by the frequency and magnitude of the water and sediment pulses, will dictate changes in sediment delivery at the catchment outlet, depending on whether the drainage network acts as a sediment sink (i.e. SDR < 1) or sediment source (i.e. SDR > 1).

## 7. ACKNOWLEDGMENTS

This research was carried out within the framework of two research projects funded by the Spanish Ministry of Economy and Competitiveness and the European FEDER funds: MORPHSED (CGL2012-36394) and MORPHPEAK (CGL2016-78874-R). The author has a grant funded by the Spanish Ministry of Education Culture and Sports (FPU016/01687), and he is part of the Fluvial Dynamics Research Group-RIUS, which is a Consolidated Group recognized by the Generalitat de Catalunya (2017 SGR 459645). There is also acknowledge the support of the CERCA Program of the Generalitat de Catalunya.

## 8. REFERENCES

Alatorre LC, Beguería S, Lana-Renault N, Navas A, García-Ruiz JM. 2012. Soil erosion and sediment delivery in a mountain catchment under scenarios of land use change using a spatially distributed numerical model. *Hydrology and Earth System Sciences* 16: 1321-1334.

Barnes N, Luffman I, Nandi A. 2016. Gully erosion and freeze-thaw processes in clay-rich soils, northeast Tennessee, USA. *GeoResJ* 9-12: 67-76.

Batalla RJ, Vericat D. 2009. Hydrological and sediment transport dynamics of flushing flows: implications for management in large Mediterranean rivers. *River Research and Applications.* 25: 297-134.

Béjar M, Vericat D, Batalla RJ, Gibbins CN. 2018. Variation in flow and suspended sediment transport in a montane river affected by hydropeaking and instream mining. *Geomorphology*. 310: 69-83.

Benito G, Gutiérrez M, Sancho C. 1992. Erosion rates in badland areas of the Central Ebro basin (NE-Spain). *Catena* 19: 269-286.

Bonetti S, Richter DD, Porporato A. 2019. The effect of accelerated soil erosion on hillslope morphology. *Earth Surface Processes and Landforms*.

Borrelli P, Robinson DA, Fleischer LR, Lugato E, Ballabio C, Alewell C, Meusburger K, Madugno S, Schütt; Ferro V, Bargarello V, Van Oost K, Montanarella L, Panagos P. 2013. An assessment of the global impact of 21st century land use change on soil erosion. *Nature Communications.* DOI: 10.1038/s41467-017-02142-7

Borrelli P, Marker M, Panagos P, Schutt B. 2014. Modeling soil erosion and river sediment yield for an intermountain drainage basin of the Central Apennines, Italy. *Catena* 114: 45-58.

Brasington J, Rumsby B, McVey R, 2000. Monitoring and Modelling Morphological Change in a Braided Gravel-Bed River Using High Resolution GPS-Based Survey. *Earth Surface Processes and Landforms* 25: 973-990.

Brasington J, Vericat D, Rychkov I. 2012. Modelling river bed morphology, roughness, and surface sedimentology using high resolution terrestrial laser scanning. *Water Resources Research*. 48: 1-18.

Buendia C, Vericat D, Batalla RJ, Gibbins CN. 2016. Temporal dynamics of sediment transport and transient in-channel storage in a highly erodible catchment. *Land Degradation and Development.* 27: 1045-1063.

Casalí J, Gastesi R, Álvarez-Mozos J, De Santisteban LM, Lersundi JDV, Giménez R, Larrañaga A, Goñi M, Agirre U, Campo MA, López JJ, Donézar M. 2008. Runoff, erosion, and water quality of agricultural watersheds in central Navarre (Spain). *Agricultural Water Management* 95 (10): 1111-1128.

Casalí J, Giménez R, De Santisteban L, Álvarez-Mozos J, Mena J, Del Valle de Lersundi J. 2009. Determination of long-term erosion rates in vineyards of Navarre (Spain) using botanical benchmarks. *Catena* 78: 12-19.

Cerovski-Darriau C, Roering JJ. 2016. Influence of anthropogenic land-use change on hillslope erosion in the Waipaoa River Basin, New Zealand. *Earth Surface Processes and Landforms.* 41: 2167-2176.

Chambers BJ, Garwood TWD. 2000. Monitoring of water erosion on arable farms in England and Wales. 1990-1994. *Soil Use and Management* 16: 93-99.

Clotet N, Gallart F, Sala M. 1987. Los badlands: características, interés teórico, dinámica y tasas de erosión. *Notes de Geografía Física* 15-16: 28-37.

Clotet-Perarnau N, Gallart F, Balasch JC. 1988. Medium-term erosion rates in small scarcely vegetated catchment in the Pyrenees. *Catena Supplement* 13: 37-47.

Cui Y, Parker G, Lisle TE, Gott J, Hansler-Ball ME, Pizzuto JE, Allmendinger NE, Reed JM. 2003. Sediment pulses in mountain rivers: 1. *Experiments. Water Resources Research*. 39(9): 1239-1251.

Desir G, Marín C. 2013. Role of erosion processes on the morphogenesis of a semiarid badland area. Bardenas Reales (NE Spain). *Catena* 106: 83-92.

Djorovic, M. 1992. Soil erosion problem in Yugoslavia (Republics: Serbia, Bosnia-Herzegovina, Macedonia and Montenegro). In: Safley, M., Várallyay, G., (Eds.), *Soil Erosion Prevention and Remediation Workshop*, US–Central and Eastern European Agro-Environmental Program, Budapest, Hungary. 158-174 pp.

Erskine WD, Saynor MJ. 1996. Success of soil conservation works in reducing soil erosion rates and sediment yields in central eastern Australia. In: *Erosion and Sediment Yield: Global and Regional Perspectives* (Proceedings of the Exter Symposium, July 1996). IAHS Publ. 236. 523-530 pp.

Erskine WD, Mahmoudzadeh A, Myers C. 2002. Land use effects on sediment yields and soil loss rates in small basins of Triassic sandstone near Sydney, NSW, Australia. *Catena* 49: 271-287.

Estrany J, Garcia C, Batalla RJ. 2010. Hydrological response of a small Mediterranean agricultural catchment. *Journal of Hydrology*. 380: 180-190.

Francke, T. 2009. Measurement and Modelling of Water and Sediment Fluxes in Meso-Scale Dryland Catchments. PhD thesis, Universität Potsdam, Germany. http://opus.kobv.de/ubp/volltexte/2009/3152/.

Gallart F, Solé A, Puigdefàbregas J, Lázaro R. 2002. Badland Systems in the Mediterranean. In: *Dryland Rivers: Hydrology and Geomorphology of Semi-arid Channels*. Bull LJ, Kirkby MJ (Eds.). John Wiley & Sons, Ltd. 299-326.

Gallart F, Llorens P. 2004. Observations on land cover changes and water resources in the headwaters of the Ebro catchment, Iberian Peninsula. *Physics and Chemistry of the Earth*. 29: 769–773.

Gallart F, Amaxidis Y, Botti P, Canè G, Castillo V, Chapman P, Froebrich J, García-Pintado J, Latron J, Llorens P, Lo Porto A, Morais M, Neves R, Ninov P, Perrin JL, Ribarova I, Skoulikidis N, Tournoud MG. 2008. Investigating hydrological regimes and processes in a set of catchments with temporary waters in Mediterranean Europe. *Hydrological Sciences Journal*. 53(3): 618-628.

Gallart F, Marignani M, Pérez-Gallego N, Santi E, Maccherini S. 2013. Thirty years of studies on badlands, from physical to vegetational approaches. A succinct review. *Catena* 106: 4-11.

Gallart F, Pérez-Gallego N, Latron J, Catari G, Martínez-Carreras N, Nord G. 2013b. Short- and long-term studies of sediment dynamics in a small humid mountain Mediterranean basin with badlands. *Geomorphology* 196: 242-251.

García-Ruiz JM. Arnáez J, Beguería S, Seeger M, Martí-Bono C, Regüés D, Lana-Renault N, White S. 2005. Runoff generation in an intensively disturbed, abandoned farmland catchment, Central Spanish Pyrenees. *Catena*. 59: 79-92.

García-Ruiz JM, Regüés D, Alvera B, Lana-Renault N, Serrano-Muela P, Nadal-Romero E, Navas A, Latron J, Martí-Bono, Arnáez J. 2008. Flood generation and sediment transport in experimental catchments affected by land use changes in the central Pyrenees. *Journal of Hydrology*. 356: 245-260.

García-Ruiz JM, Beguería S, Nadal-Romero E, González-Hidalgo JC, Lana-Renault N, Sanjuán Y. 2015. A meta-analysis of soil erosion rates across the world. *Geomorphology*. 239: 160-173.

Gaspar L, Lizaga I, Blake WH, Latorre B, Quijano L, Navas A. 2019. Fingerprinting changes in source contribution for evaluating soil response during an exceptional rainfall in Spanish pre-Pyrenees. *Journal of Environmental Management*. 240: 136-148.

Geilhausem M, Otto JC, Morche D, Schrott L. 2012. Decadal sediment yield from an Alpine proglacial zone inferred from reservoir sedimentation (Pasterze, Hohe Tauern, Austria). In: *Erosion and Sediment Yield in the Changing Environment*. IAHS Publ. 356. 161-172 pp.

Giménez R, Casalí J, Díez J. 2012. Evaluación de la producción de sedimentos y calidad de las aguas en cuencas agrarias de Navarra. *Cuadernos de Investigación Geográfica* 38 (1): 7-25.

Giménez R, Casalí J, Grande I, Díez I, Díez J, Campo MA, Álvarez-Mozos J, Goñi M. 2012. Factors controlling sediment export in a small agricultural watershed in Navarre (Spain). *Agricultural Water Management* 110, 1-8.

Giménez-Morera A, Ruiz-Sinoga JD, Cerdà A. 2010. The impact of cotton geotextiles on soil and water losses in Mediterranean rainfed agricultural land. *Land Degradation and Development* 21: 210-217.

Gran KB, Czuba JA. 2017. Sediment pulse evolution and the role of network structure. *Geomorphology*. 277: 17-30.

Helming K. Prasad SN. 2002. Soil erosion under different rainfall intensities, surface roughness, and soil water regimes. *Catena* 46(2-3): 103-123.

James MR, Robson S, Smith, MW. 2017. 3-D uncertainty-based topographic change detection with structure-from-motion photogrammetry: precision maps for ground control and directly georeferenced surveys. *Earth Surface Processes and Landforms* 42: 1769–1788.

Jantzi H, Liébault F, Klotz S. 2017. Sediment residence time in alluvial storage of black marl badlands. *Catena*. 156: 82-91.

Junk JW, Bayley PB, Sparks RE. 1989. The flood pulse concept in river flood plain systems. *Can. Spec. Publ. Fish. Aquat. Sci*. 106: 110–121.

Keesstra SD, Davis J, Masselink RH, Casalí J, Peeters ETHM, Dijksma R. 2019. Coupling hysteresis analysis with sediment and hydrological connectivity in three agricultural catchments in Navarre, Spain. *Journal of Soils and Sediments*. 19:1598-1612.

Khanchoul K, Boukhrissa ZE, Acidi A, Altschul R. 2012. Estimation of suspended sediment transport in the Kebir drainage basin, Algeria. *Quaternary International* 262: 25-31.

Kronvang B, Andersen HE, Larsen SE, Audet J. 2013. Importance of bank erosion for sediment input, storage and export at the catchment scale. *Journal Soils Sediments*. 13: 230-241.

Kuo CW, Brierley GJ. 2013. Importance of bank erosion for sediment input, storage and export at the catchment scale. *Geomorphology*. 180: 255-266.

Lana-Renault N, Regüés D. 2009. Seasonal patterns of suspended sediment transport in an abandoned farmland catchment in the Central Spanish Pyrenees. *Earth Surface Processes and Landforms*. 34: 1291-1301.

Lane SN, Westaway RM, Hicks DM. 2003. Estimation of Erosion and Deposition Volumes in a Large, Gravel-Bed, Braided River Using Synoptic Remote Sensing. *Earth Surface Processes and Landforms* 28: 249-271.

Lizaga I, Gaspar L, Blake W, Latorre B, Navas A. 2019. Fingerprinting changes of source apportionments from mixed land uses in stream sediments before and after an exceptional rainstorm event. *Geomorphology*. https://doi.org/10.1016/j.geomorph.2019.05.015

Llena M, Smith MW, Wheaton JM, Vericat D. Under review Multi-temporal geomorphic processes reshaping sub-humid Mediterranean badlands. *Earth Surface Processes and Landforms.*

Llorens P, Gallart F, Cayuela C, Roig-Planasdemunt M, Casellas E, Molina AJ, Moreno-de Las Heras M, Bertran G, Sánchez-Costa E, Latron J. 2018. What have we learnt about Mediterranean catchment hydrology? 30 years observing hydrological processes in the Vallcebre research catchments. *Geographical Research Letters*. 44(2): 475-502.

Lobera G, Batalla RJ, Vericat D, López-Tarazón JA, Tena A. Sediment transport in two mediterranean regulated rivers. *Science of the Total Environment*. 540: 101:113.

López-Tarazón JA, Batalla, RJ, Vericat D, Balasch JC. 2010. Rainfall, runoff and sediment transport relations in a mesoscale mountainous catchment: The River Isábena (Ebro basin). *Catena*. 82: 23-34.

López-Tarazón JA, Batalla RJ, Vericat D. 2011. In-channel sediment storage in a highly erodible catchment: the River Isábena (Ebro Basin, Southern Pyrenees). *Zeitschrift für Geomorphologie*. 55(3): 365-382.

López-Tarazón JA, Batalla RJ, Vericat D, Francke T. 2012. The sediment budget of a highly dynamic mesoscale catchment: the river Isábena. *Geomorphology* 138: 15–28.

MacDonough OT, Hosen JD, Palmer M. 2011. Temporary streams: The hydrology, Geography and ecology of non-perennially flowing water. In: *River ecosystems: Dynamics, management and conservation*. Elliott, H. and Martin, L. (eds). Nova Scotia Publishers. 259-289 pp.

Marchamalo M, Hooke JM, Sandercocket PJ. 2016. Flow and sediment connectivity in semi-arid landscapes in SE Spain: patterns and controls. *Land Degradation and Development* 27: 1034-1044.

Marchi L, Borga M, Preciso E, Gaume E. 2010. Characterisation of selected extreme flash floods in Europe and implications for floods risk management. *Journal of Hydrology* 394(1-2): 118-133.

Martínez-Casasnovas JA, Poch RM. 1998. Estado de conservación de los suelos de la cuenca del embalse Joaquín Costa. *Limnética* 14: 83-91.

Mathys N, Brochot S, Meunier M, Richard D. 2003. Erosion quantification in the small marly experimental catchments of Draix (Alpes de Haute Provence, France). Calibration of the ETC rainfall–runoff–erosion model. *Catena* 50: 527-548.

Mingyi F, Walling DE, Zinbao Z, Anbang W. 2003. A study on responses of soil erosion and sediment yield to closing cultivation on sloping land in a small catchment using 137Cs technique in the Rolling Loess Plateau, China. *Chinese Science Bulletin* 48 (19: 2093-2100.

Moreno-de las Heras M, Gallart F, Latron J, Martínez-Carreras N, Ferrer L, Estrany J. 2018. Testing the use of $^{210}Pb_{ex}$ to study sediment connectivity in a Mediterranean mountain basin with badlands. *Land Degradation and Development*. 29: 676-689.

Nadal-Romero E, Regüés D, Martí-Bono C, Serrano-Muela P. 2007. Badland dynamics in the Central Pyrenees: temporal and spatial patterns of weathering processes. *Earth Surface Processes and Landforms* 32: 888-904.

Nadal-Romero E, Regüés D. 2010. Geomorphological dynamics of sub-humid mountain badland areas: weathering, hydrological and suspended sediment transport processes. A case of study in the Araguás catchment (Central Pyrenees), and implications for altered hydro-climatic regimes. *Progress in Physical Geography* 34 (3): 123–150.

Nadal-Romero E, Revuelto J, Errea P, López-Moreno JI. 2015. The application of terrestrial laser scanner and SfM photogrammetry in measuring erosion and deposition processes in two opposite slopes in a humid badlands area (central Spanish Pyrenees). *SOIL* 1, 561–573.

Nadal-Romero E, Lasanta T, García-Ruiz JM. 2013. Runoff and sediment yield from land under various uses in a Mediterranean mountain area: long-term results from an experimental station. *Earth Surface Processes and Landforms* 38: 346-355.

Navas A, López-Vicente M, Gaspar L, Machín J. 2013. Assessing soil redistribution in a complex karst catchment using fallout 137Cs and GIS. *Geomorphology* 196: 231-241.

Navratil O, Esteves M, Legout C, Gratiot N, Nemery J, Willmore S, Grangeon T. 2011. Global uncertainty analysis of suspended sediment monitoring using turbidimeter in a small mountainous river catchment. *Journal of Hydrology* 398 (3-4): 246-259.

Navratil O, Evrard O, Esteves M, Legout C, Ayrault S, Némery J, Mate-Marin A, Ahmadi M, Lefèvre I, Poirel A, Bonté P. 2012. Temporal variability of suspended sediment sources in an alpine catchment combining river/rainfall monitoring and sediment fingerprinting. *Earth Surface Processes and Landforms* 37: 828-846.

Neugirg F, Stark M, Kaiser A, Vlacilova M, Della Seta M, Vergari F, Schmidt J, Becht M, Haas F. 2016. Erosion processes in calanchi in the Upper Orcia Valley, Southern Tuscany, Italy based on multitemporal high-resolution terrestrial LiDAR and UAV surveys. *Geomorphology* 269: 8–22.

Oeurng C, Sauvage S, Sánchez-Pérez JM. 2010. Dynamics of suspended sediment transport and yield in a large agricultural catchment, southwest France. *Earth Surface Processes and Landforms* 35: 1289-1301.

Passalacqua P, Belmont P, Staley DM, Simley JD, Arrowsmith JR, Bode CA, Crosby C, DeLong SB, Glenn NF, Kelly SA, Lague D, Sangireddy H, Schaffrath K, Tarboton DG, Wasklewicz T, Wheaton JM. 2015. Analyzing high resolution topography for advancing the understanding of mass and energy transfer through landscapes: a review. *Earth-Science Reviews* 148: 174-193.

Pimentel D, Harvey C, Resosudarmo P, Sinclair K, Kurz D, McNair M, Crist S, Shpritz L, Fitton L, Saffouri R, Blair R. 1995. Environmental and Economic Costs of Soil Erosion and Conservation Benefeits. *Science*. 179: 1117-1123.

Piqué G, López-Tarazón JA, Batalla RJ. 2014. Variability of in-channel sediment storage in a river draining highly erodible areas (the Isábena, Ebro basin). *Journal Soils Sediments* 12: 2031-2044.

Porto P, Walling DE. 2012. Validation the use of 137Cs and 210Pbex measurements to estimate rates of soil loss from cultivated land in southern Italy. *Journal of Environmental Radioactivity* 106: 47-57.

Puigdefabregas J, Sole A, Gutierrez L, del Barrio G, Boer M. 1999. Scales and processes of water and sediment redistribution in drylands: results from the Rambla Honda field site in Southeast Spain. *Earth-Sci. Rev*. 48: 39–70.

Regüés D, Pardini G, Gallart F. 1995. Regolith behavior and physical weathering of claey mudrock as dependent on seasonal weather conditions in a badland area at Vallcebre, Eastern Pyrenees. *Catena* 25: 199-212.

Regüés D, Nadal-Romero E. 2013. Uncertainty in the evaluation of sediment yield from badland areas: Suspended sediment transport estimated in the Araguás catchment (central Spanish Pyrenees). *Catena* 106: 93-100.

Richard D, Mathys N. 1999. Historique, contexte technique et scientifique des BVRE de Draix. In: N. Mathys (Ed.), *Caractéristiques, données disponibles et principaux résultats acquis au cours des dix ans de suivi*. Actes du séminaire Les bassins versants expérimentaux de Draix. Cemagref-Editions, Coll. Actes de colloques, Grenoble, 11-28 pp.

Rodríguez-Blanco ML, Taboada-Castro MM, Taboada-Castro MT. 2013. Linking the field to the stream: Soil erosion and sediment yield in a rural catchment, NW Spain. *Catena* 102: 74-81.

Rodríguez-Blanco ML, Taboada-Castro MM, Palleiro L, Taboada-Castro MT. 2010. Temporal changes in suspended sediment transport in an Atlantic catchment, NW Spain. *Geomorphology* 123: 181-188.

Rossi RK. 2018. *Evaluation of `Structure-from-Motion' from a Pole-Mounted Camera for Monitoring Geomorphic Change*. Master Dissertation. Utah State University. 211 pp.

Rovira A, Batalla RJ. 2006. Temporal distribution of suspended sediment transport in a Mediterranean basin: The Lower Tordera (NE Spain). *Geomorphology* 79: 58-71.

Royston P. 1982. An extension of Shapiro and Wilk's W test for normality to large samples. *Applied Statistics* 31: 115–124.

Römkens MJM, Helming K. Prasad SN. 2002. Soil erosion under different rainfall intensities, surface roughness, and soil water regimes. *Catena* 46(2-3): 103-123.Rychov I, Brasington J, Vericat D. 2012. Computational and methodological aspects of terrestrial surface analysis based on point clouds. *Computers and Geosciences* 42:64–70.

Schick AP. 1967. Gerlach troughs, overland flow traps. Field methods for the study of slope and fluvial processes. *Revue de Géomorphologie Dynamique* 4: 170–172.

Shao Q, Xiao T, Liu JY, Qi Y. 2011. Soil erosion rates and characteristics of typical alpine meadow using 137Cs technique in Qinghai-Tibet Plateau. *Chinese Science Bulletin* 56 (16): 1708-1713.

Shao Y, Lunetta RS, Macpherson J, Luo J, Chen G. 2013. Assessing Sediment Yield for selected watersheds in the Laurentian Great Lakes Basin Under Future Agricultural Scenarios. *Environmental Management* 51: 59-69.

Smith MW, Vericat D. 2015. From experimental plots to experimental landscapes: topography, erosion and deposition in sub-humid badlands from Structure-from-motion photogrammetry. *Earth Surface Processes and Landforms* 40: 1656-1671.

Stöcker C, Eltner A, Karrasch P. 2015. Measuring gullies by synergetic application of UAV and close range photogrammetry — a case study from Andalusia, Spain. *Catena* 132: 1–11.

Surian N, Righini M, Lucía A, Nardi L, Amponsah W, Benvenuti M, Borga M, Cavalli M, Comiti F, Marchi L, Rinaldi M, Viero A. 2016. Channel response to extreme floods: Insights on controlling factors from six mountain rivers in northern Apennines, Italy. *Geomorphology* 272, 78-91.

Sutherland RA, Bryan RB. 1991. Sediment budgeting: A case study in the Katiorin drainage basin, Kenya. *Earth Surface Processes and Landforms* 16: 383-398.

Tarolli P, Borga M, Morin E, Delrieu G. 2012. Analysis of flash flood regimes in the North-Western and South-Eastern Mediterranean regions. *Natural Hazards and Earth System Sciences*. 12: 1255- 1265.

Tarolli, P. 2014. High-resolution topography for understanding Earth surface processes: opportunities and challenges. *Geomorphology* 216: 295–312.

Turnage KM, Lee SY, Foss JE, Kim KH, Larsen IL. 1997. Comparison of soil erosion and deposition rates using radiocesium, RUSLE, and buried soils in dolines in East Tennessee. *Environmental Geology* 29 (1/2): 1-10.

Tuset J, Vericat D, Batalla RJ. 2016. Rainfall, runoff and sediment transport in a Mediterranean mountainous catchment. *Science of Total Environment*. 540: 114-132.

Ollesch G, Sukhanovski Y, Kistner I, Rode M, Meissner R. 2005. Characterization and modelling of the spatial heterogeneity of snowmelt erosion. *Earth Surface Processes and Landforms*. 30: 197–211.

Porto P, Walling DE, Callegari G. 2011. Using 137Cs measurements to establish catchment sediment budgets and explore scale effects. *Hydrological Processes* 25: 886-900.

Vercruyse K, Grabowski RC, Rickson RJ. 2017. Suspended sediment transport dynamics in rivers: Multi-scale drivers of temporal variation. *Earth-Science Reviews.* 166: 38-52.

Vergari F, Troiani F, Faulkner H, Del Monte M, Della Seta M, Ciccacci S, Fredi P. 2019. The use of the slope-area function to analyse process domains in complex badland landscapes. *Earth Surface Processes and Landforms* 44: 273-286.

Vericat D, Smith MW, Brasington J. 2014. Patterns of topographic change in sub-humid badlands determined by high resolution multi-temporal topographic surveys. *Catena* 120: 164–176.

Vericat D, Wheaton J, Brasington J. 2017. Revisiting the Morphological Approach: Opportunities and Challenges with Repeat High-Resolution Topography. In: *Gravel-Bed Rivers: Processes and Disasters*. Tsutsumi DT, Laronne JB. (Eds.). Wiley, 121-158.

Walling DE. 1983. The sediment delivery problem. *Journal of Hydrology*. 65(1–3): 209–237.

Walling DE, Russell MA, Hodgkinson RA, Zhan Y. 2002. Establishing sediment budgets for two small lowland agricultural catchments in the UK. *Catena* 47: 323-353.Williams GP. 1989. Sediment concentration versus water discharge during single hydrologic events in rivers. *Journal of Hydrology* 111: 89-106.

Wheaton JM, Brasington J, Darby SE, Sear DA. 2010. Accounting for uncertainty in DEMs from repeat topographic surveys: improved sediment budgets. *Earth Surface Processes and Landforms* 35(2): 136–156.

Yair A, Lavee H, Bryan RB, Adar E. 1980. Runoff and erosion processes and rates in the Zin Valley badlands, Northern Negev, Israel. *Earth Surface Processes* 5: 205-225.

Zabaleta A, Martínez M, Uriarte JA, Antigüedad I. 2007. Factors controlling suspended sediment yield during runoff events in small headwater catchments of the Basque Country. *Catena* 71: 179-190.

## 9. SUPPLEMENTARY MATERIAL

**Table 1**. References consulted to estimate specific sediment production rates (SSP) in agricultural and forest areas.

| Reference | Study Area | Land use | Mean annual rainfall (mm) | SSP (Mg/ha/yr) |
|---|---|---|---|---|
| Alatorre et al., 2010 | West southern Pyrenees (Spain) | Agricultural | - | 75.5000 |
| Arthonditsis et al., 2000 | Greece | Agricultural | - | 0.0013 |
| Bruggeman et al., 2005 | Syrian Arab Republic | Agricultural | - | 26.5500 |
| Casalí et al., 2008 | Latxaga (Spain) | Agricultural | 835 | 0.0010 |
| Casalí et al., 2008 | Latxaga (Spain) | Agricultural | 835 | 0.0043 |
| Casalí et al., 2008 | Latxaga (Spain) | Agricultural | 835 | 0.0156 |
| Casalí et al., 2008 | Latxaga (Spain) | Agricultural | 835 | 0.0203 |
| Casalí et al., 2008 | Latxaga (Spain) | Agricultural | 835 | 0.0232 |
| Casalí et al., 2008 | La Tejería (Spain) | Agricultural | 725 | 0.0249 |
| Casalí et al., 2008 | La Tejería (Spain) | Agricultural | 725 | 0.1301 |
| Casalí et al., 2008 | Latxaga (Spain) | Agricultural | 835 | 0.1362 |
| Casalí et al., 2008 | La Tejería (Spain) | Agricultural | 725 | 0.1396 |
| Casalí et al., 2008 | La Tejería (Spain) | Agricultural | 725 | 0.2325 |
| Casalí et al., 2008 | La Tejería (Spain) | Agricultural | 725 | 0.2550 |
| Casalí et al., 2008 | Latxaga (Spain) | Agricultural | 835 | 0.2628 |
| Casalí et al., 2008 | Latxaga (Spain) | Agricultural | 835 | 0.3386 |
| Casalí et al., 2008 | La Tejería (Spain) | Agricultural | 725 | 0.7905 |
| Casalí et al., 2008 | La Tejería (Spain) | Agricultural | 725 | 0.8148 |
| Casalí et al., 2008 | La Tejería (Spain) | Agricultural | 725 | 3.3189 |
| Chahor et al., 2014 | Laxaga (Spain) | Agricultural | 800 | 0.0330 |
| Chahor et al., 2014 | Laxaga (Spain) | Agricultural | 800 | 0.0509 |
| Chambers and Garwood, 2000 | Bollitree (England) | Agricultural | - | 0.1626 |
| Chambers and Garwood, 2000 | Morfe Valley (England) | Agricultural | - | 0.3673 |
| Chambers and Garwood, 2000 | Kenton (England) | Agricultural | - | 0.9910 |

| | | | | |
|---|---|---|---|---|
| Chambers and Garwood, 2000 | Llanishen (England) | Agricultural | - | 1.0598 |
| Chambers and Garwood, 2000 | Ashcombe (England) | Agricultural | - | 1.2097 |
| Chambers and Garwood, 2000 | Bicton (England) | Agricultural | - | 1.8966 |
| Chambers and Garwood, 2000 | Starcross (England) | Agricultural | - | 4.2500 |
| Chambers and Garwood, 2000 | Penalt (England) | Agricultural | - | 6.8750 |
| Dunjó et al., 2004 | West southern Pyrenees (Spain) | Agricultural | - | 0.5596 |
| Erskine et al., 2002 | 20 (Australia) | Agricultural | 1363 | 1.3019 |
| Erskine et al., 2002 | 22 (Australia) | Agricultural | 1217 | 3.0357 |
| Erskine et al., 2002 | 10 (Australia) | Agricultural | 966 | 16.0000 |
| Erskine et al., 2002 | 11 (Australia) | Agricultural | 940 | 22.9323 |
| Geilhausen et al., 2012 | Pasterze catchment (Austria) | Agricultural | - | 0.0073 |
| Giménez et al., 2012 | La Tejería (Spain) | Agricultural | 724 | 0.0180 |
| Giménez et al., 2012 | Latxaga (Spain) | Agricultural | 830 | 0.0590 |
| JRC, 2012 | All Europe | Agricultural | - | 9.2600 |
| Mingyi et al., 2003 | Zhaojia catchment (China) | Agricultural | 528.4 | 25.6045 |
| Nadal-Romero et al. 2012 | West southern Pyrenees (Spain) | Agricultural | - | 3.7850 |
| Nadal-Romero et al., 2013 | EEVA (Spain) | Agricultural | 1216.7 | 841.1111 |
| Nadal-Romero et al., 2013 | EEVA (Spain) | Agricultural | 1216.7 | 971.7778 |
| Nobre, 2011 | Northwest Portugal | Agricultural | - | 0.2188 |
| Nunes et al., 2011 | Northwest Portugal | Agricultural | - | 3.2395 |
| Oeurng et al., 2010 | Save catchment (France) | Agricultural | 603 | 0.0001 |
| Oeurng et al., 2010 | Save catchment (France) | Agricultural | 787 | 0.0006 |
| Ordoñez-Fernández et al., 2007 | South Spain | Agricultural | - | 1.4000 |
| Porto et al. 2011 | Trionto (Italy) | Agricultural | - | 0.0002 |
| Porto et al. 2012 | Trionto (Italy) | Agricultural | - | 0.0004 |
| Shao et al., 2013 | Peshtigo River (EEUU) | Agricultural | - | 0.0000 |
| Shao et al., 2013 | St. Joseph River (EEUU) | Agricultural | - | 0.0000 |
| Shao et al., 2013 | St. Mary River (EEUU) | Agricultural | - | 0.0000 |
| Shao et al., 2013 | Cattaraugus Creek (EEUU) | Agricultural | - | 0.0003 |
| Turnage et al. 1997 | East Tennesse (EEUU) | Agricultural | 1300 | 0.3876 |
| Turnage et al. 1997 | East Tennesse (EEUU) | Agricultural | 1300 | 1.6524 |
| Ursic and Dendy, 1963 | Northern Mississippi (U.S.A.) | Agricultural | - | 8.8021 |
| Walling et al., 2002 | New Cliftonthorp (UK) | Agricultural | 644 | 0.0063 |
| Walling et al., 2002 | Lower Smisby (UK) | Agricultural | 644 | 0.2715 |
| Walling et al., 2002 | Lower Smisby (UK) | Agricultural | 758 | 0.3465 |
| Alatorre et al., 2010 | West southern Pyrenees (Spain) | Forestal | - | 22.8571 |
| Arthonditsis et al., 2000 | Greece | Forestal | - | 0.0002 |
| Borrelli et al., 2014 | Upper Turano River watershed (Italy) | Forestal | 1205 | 0.0087 |
| Bruggeman et al., 2005 | Syrian Arab Republic | Forestal | - | 5.1000 |
| Djorovic, 1992 | Jasenica River Basin (Serbia) | Forestal | 760 | 0.0003 |
| Djorovic, 1992 | Jasenica River Basin (Serbia) | Forestal | 760 | 0.0074 |
| Djorovic, 1992 | Jasenica River Basin (Serbia) | Forestal | 760 | 0.0561 |
| Dunjó et al., 2004 | West southern Pyrenees (Spain) | Forestal | - | 0.0784 |
| Duvert et al., 2012 | Cal Rodo (Spain) | Forestal | 862 | 0.1190 |
| Duvert et al., 2012 | Ca ´'Isard (Spain) | Forestal | 862 | 0.6769 |
| Erskine et al., 2002 | 18 (Australia) | Forestal | 962 | 4.7727 |
| Erskine et al., 2002 | 15 (Australia) | Forestal | 907 | 8.3333 |

| | | | | |
|---|---|---|---|---|
| Erskine et al., 2002 | 16 (Australia) | Forestal | 1008 | 10.3333 |
| Gallart et al., 2013b | Ca L'Isard (Spain) | Forestal | 862 | 0.4444 |
| Giménez et al., 2012 | Oskotz (Spain) | Forestal | 1137 | 0.0003 |
| JRC, 2012 | Europe | Forestal | - | 0.0700 |
| Khanchoul et al., 2012a | Wadi Cherf (Algeria) | Forestal | 290 | 0.0001 |
| Khanchoul et al., 2012a | Kebir (Algeria) | Forestal | 700 | 0.0005 |
| Khanchoul et al., 2012a | Kebir (Algeria) | Forestal | 700 | 0.0005 |
| Nadal-Romero et al. 2012 | West southern Pyrenees (Spain) | Forestal | - | 0.4150 |
| Navas et al., 2013 | Estanque de Arriba Lake (Spain) | Forestal | 595 | 0.0000 |
| Navratil et al., 2012 | Bleéone at Chaffaut (France) | Forestal | 820 | 0.0023 |
| Navratil et al., 2012 | Bes at Pérouré (France) | Forestal | 820 | 0.0209 |
| Nobre, 2011 | Northwest Portugal | Forestal | - | 0.0102 |
| Nunes et al., 2011 | Northwest Portugal | Forestal | - | 0.0120 |
| Ordoñez-Fernández et al., 2007 | South Spain | Forestal | - | 0.3000 |
| Porto et al. 2011 | Bonis (Italy) | Forestal | 1250 | 0.0600 |
| Porto et al. 2012 | W2 (Italy) | Forestal | 670 | 107.6605 |
| Porto et al. 2012 | W2 (Italy) | Forestal | 670 | 47.7108 |
| Porto et al. 2012 | W2 (Italy) | Forestal | 670 | 87.3950 |
| Porto et al. 2012 | W2 (Italy) | Forestal | 670 | 31.8937 |
| Porto et al. 2012 | W3 (Italy) | Forestal | 670 | 16.9118 |
| Porto et al. 2012 | W3 (Italy) | Forestal | 670 | 11.3372 |
| Rodríguez-Blanco et al., 2010 | Corbeira (Spain) | Forestal | 895 | 0.0034 |
| Rodríguez-Blanco et al., 2010 | Corbeira (Spain) | Forestal | 1397.2 | 0.0069 |
| Rodríguez-Blanco et al., 2010 | Corbeira (Spain) | Forestal | 1191.6 | 0.0054 |
| Rovira and Batalla, 2006 | Tordera (Spain) | Forestal | - | 0.0004 |
| Turnage et al. 1997 | East Tennesse (EEUU) | Forestal | 1300 | 6.5178 |
| Turnage et al. 1997 | East Tennesse (EEUU) | Forestal | 1300 | 1.6000 |
| Ursic and Dendy, 1963 | Northern Mississippi (U.S.A.) | Forestal | - | 0.2428 |
| Walling et al., 2002 | Belmont (UK) | Forestal | 691 | 0.5347 |
| Walling et al., 2002 | Belmont (UK) | Forestal | 694 | 0.5580 |
| Walling et al., 2002 | New Cliftonthorp (UK) | Forestal | 758 | 1.2777 |
| Walling et al., 2002 | Jubilee (UK) | Forestal | 694 | 2.6503 |
| Walling et al., 2002 | Jubilee (UK) | Forestal | 691 | 5.9183 |
| Walling et al., 2002 | Moorfield (UK) | Forestal | - | 10.4500 |
| Walling et al., 2002 | New Cliftonthorp (UK) | Forestal | - | 14.0000 |
| Walling et al., 2002 | Foxbridge (UK) | Forestal | - | 16.3390 |
| Walling et al., 2002 | Foxbridge (UK) | Forestal | - | 16.5763 |
| Walling et al., 2002 | Longlands (UK) | Forestal | - | 17.7931 |
| Zabaleta et al., 2007 | Aixola (Spain) | Forestal | 1200 | 0.0365 |

# CHAPTER 5

# THE EFFECTS OF LAND USE AND TOPOGRAPHIC CHANGES ON SEDIMENT CONNECTIVITY IN MOUNTAIN CATCHMENTS

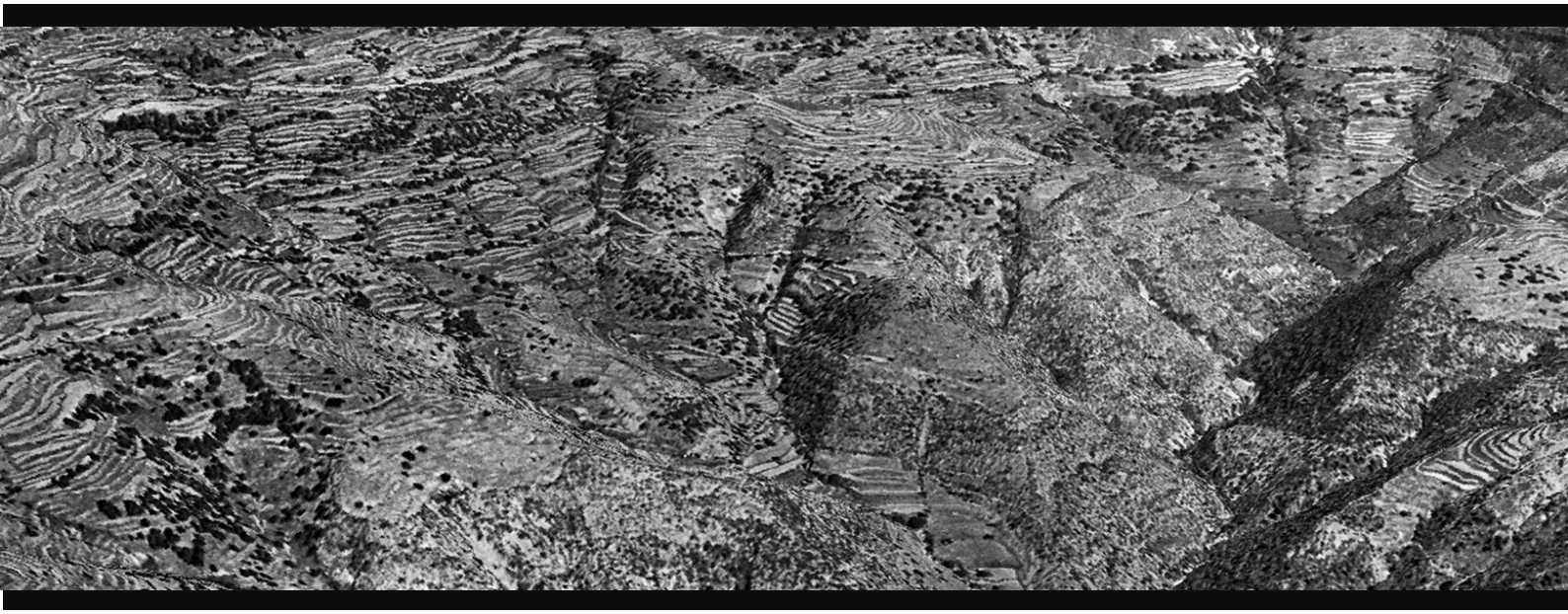

# CHAPTER 5: The effects of land use and topographic changes on sediment connectivity in mountain catchments

This chapter contains the following accepted paper in the journal *Science of Total Environment.* JCR-SCI Impact Factor (2018): 5.589. Category: Environmental Engineering; 1st Quartile.

Llena M, Vericat D, Cavalli M, Crema S, Smith M. 2019. The effects of land use and topographic changes on sediment connectivity in mountain catchments. *Science of the Total Environment* 660: 899-912.

**ABSTRACT:** Understanding the evolution of sediment connectivity associated with different land use and topographic changes is a prerequisite for a better understanding of sediment budgets and sediment transport processes. We used the Index of Sediment Connectivity (IC) developed by Cavalli et al. (2013) based on the original approach by Borselli et al. (2008) to study the effects of decadal-scale land use and topographic changes on sediment connectivity in mountain catchments. The input variables of the IC (i.e. land cover and topography) were derived from historical aerial photos using Structure from Motion-Multi View Stereo algorithms (SfM-MVS). The method was applied in different sub-catchments of the Upper River Cinca Catchment (Central Pyrenees), representative of three scenarios: (a) Land cover changes; (b) Topographic changes in agricultural fields (terracing); and (c) Topographic changes associated with infrastructure (road construction). In terms of land cover changes, results show that although connectivity is increased in some areas due to the establishment of new field crops, for most of the study area connectivity decreased due to afforestation caused by rural abandonment. Topographic changes due to the establishment of agricultural terraces affected connectivity to a larger degree than land cover changes. Terracing generally reduced connectivity due to the formation of flat areas in step slopes, but in certain points, an increase in connectivity caused by the topographic convergence produced by terraces was observed. Finally, topographic changes associated with road construction greatly modified surface flow directions and the drainage network, resulting in changes in connectivity that may affect erosional processes nearby. The methodology used in this paper allows to study the effects of real decadal-scale land use and topographic changes on sediment connectivity and also evaluating and disentangling those changes. Furthermore, this approach can be a useful tool to identify potential risks associated with morphological and land use changes, involving road infrastructures.

**KEYWORDS**: *Sediment connectivity, Index of Sediment Connectivity, Land use and topographic changes, Mountain catchments, Afforestation, Terracing.*

## 1. INTRODUCTION

Connectivity is an emergent property of a geomorphic system (Wohl et al., 2018) and can be defined as the degree to which a system facilitates the transfer of water and sediment through coupling relationships among its components (Heckmann et al., 2018). Sediment connectivity represents the potential for a specific particle to move through the compartments of a system at different temporal scales (Hooke, 2003; Bracken and Croke, 2007; Fryirs, 2013). In the particular case of the fluvial system, this term refers to the transfer of sediments from the hillslopes to the channels (lateral connectivity *sensu* Fryirs et al., 2007), and along the channels (longitudinal connectivity *sensu* Fryirs et al., 2007). Sediment connectivity depends on the structural characteristics of the surfaces (e.g. topography, roughness) and the processes driven by the fluxes of water and sediments (e.g. erosion and sedimentation). The interaction of these two components will determine the sediment balance at multiple temporal scales and, consequently, the evolution of landforms and the changes in landscape properties (Bracken et al., 2015). Therefore, connectivity is not static and varies over time and space due to the interaction between the external forcing (mainly precipitation and temperature), landscape properties (i.e. structural connectivity), and the magnitude of the water and sediment fluxes (i.e. functional connectivity), that will ultimately determine the frequency, distribution and magnitude of erosional and sedimentation processes. Additionally, connectivity can be modified by anthropogenic changes that affect these processes and interactions. The significance of these impacts on connectivity will be determined by the geomorphic sensitivity of the landscape: the response of the system to an environmental change or disturbance and its recovery (Brunsden and Thornes, 1979; Harvey 2001; Wohl, 2017).

The assessment of sediment connectivity is particularly relevant in mountain environments because they are characterized by a complex and rugged morphology (Cavalli et al., 2013) and are very sensitive to disturbances by human activities. Population increased in Mountain areas of the Mediterranean region since the end of the 15$^{th}$ century, reaching a peak in the middle of the 19$^{th}$ century. In the case of the Pyrenees, in both the mountain areas and the valley bottoms, population growth was responsible for the progressive expansion of the cultivated area at the expense of forest cover (García-Ruiz and Lopez-Bermudez, 2009). In addition, steep slope areas in this region were gradually transformed into terraced arable lands (Larsen et al., 2016). Agricultural terraces have significant impacts on hydrological and geomorphological processes as they alter the distribution of local slopes and soil properties, and frequently modify the natural drainage patterns of the landscape (Arnáez et al., 2015; Lizaga et al., 2016; Calsamiglia et al., 2017). Terrace construction significantly reduces water and sediment connectivity between the hillslopes and the channels; ultimately, terraces interrupt or delay overland flow and consequently soil erosion and sediment transport (Van Dijk et al., 2005; Bellin et al., 2009).

During the second half of the 20th century, however, the majority of the mountain areas in the Mediterranean region suffered significant land use changes driven by agricultural abandonment as a consequence of the strong depopulation (García-Ruiz and Lana-Renault, 2011; Lopez-Moreno et al., 2011). This abandonment induced an increase in the vegetation cover, both by planting by public administrations (Gracía-Ruiz and Lopez-Bermudez, 2009) and by natural recolonization (Keesstra et al., 2009). The impacts of these land use changes on catchment-scale sediment and water supply, have been intensified by the effects of climate change (Macklin et al., 2012; Buendia et al., 2016; Coulthard and Van de Wiel, 2017). Several studies have pointed to a decrease of the hydrological and geomorphic activity due to climate change (Gallart and Llorens, 2003; Liébault et al., 2005; Beguería et al., 2006; López-Moreno et al., 2009; Garcia-Ruiz, 2010). For instance, Beguería et al. (2006) reported a runoff reduction of around 30% for the past 50 years in the Pre-Pyrenean region, while Buendía et al. (2015) concluded that climate

change and afforestation reduced sediment yield by around 8% in a 65 $km^2$ basin. More recently, Lizaga et al. (2019) analysed the impact of land use changes in soil properties in a catchment of the Pyrenees during the second half of the 20$^{th}$ century, reporting an increase of the soil properties, in terms of soil organic carbon and total nitrogen, related to the afforestation process. In addition to these environmental changes, it is worth considering all direct impacts on hydro-sedimentary processes caused by urbanization and associated constructions (Ferreira et al., 2017). Although the impacts of disturbances due to road construction are very localized (i.e. space and time), they heavily modify the topography and, consequently, connectivity, affecting the fluxes of water and sediment, and, potentially triggering a series of hydrological and geomorphological adjustments well beyond the disturbed zone (Jones et al., 2000, Tague and Band 2001; Bordoni et al., 2018).

The potential of a landscape to be connected has been widely analysed through the application of Sediment Connectivity Indices (e.g. Borselli et al., 2008; Cavalli et al., 2013; Quiñonero et al., 2013; Gay et al., 2015; Heckmann et al., 2018). Raster-based indices provide an opportunity to quantitatively assess the spatial distribution of sediment connectivity. The Index of Sediment Connectivity (hereafter IC) developed first by Borselli et al. (2008), and further modified by Cavalli et al. (2013), has been used in many applications (e.g. Goldin et al., 2016; Lopez-Vicente et al., 2013; Lopez-Vicente et al., 2016; Ortíz-Rodríguez et al., 2017; Persichillo et al., 2018). In mountain environments, Goldin et al. (2016) applied the IC to infer the changes in sediment dynamics as a result of glacier retreat. In terms of land use changes, Lopez-Vicente et al. (2013) and Lopez-Vicente et al. (2016) applied the first version of the IC to analyse changes in connectivity under different scenarios of land uses and land abandonment in two Mediterranean mountain catchments. Results show that erosion rates decrease inversely with the increase of vegetation cover and with the preservation of the agricultural terraces. Quiñonero et al. (2013) developed and applied the Catchment Connectivity Index (hereafter CCI) in a Mediterranean catchment with different land uses and check dam scenarios. Results indicate that the CCI allows identification of landscape properties that have a larger impact on sediment (dis)connectivity at the catchment scale. Persichillo et al. (2018) applied IC in two small catchments in the Apennines (Italy) to investigate three different scenarios of changes induced by human activities related to drainage system, road network, and land use. Results highlighted the changes in the distribution of connectivity as a function of human-induced variations. Finally, in active volcanic areas, Ortíz-Rodríguez et al. (2017) used a modified version of the IC to assess the lateral flow contribution of pyroclastic sediments on the main channels.

This paper analyses the effects of land use changes on sediment connectivity using the IC developed by Cavalli et al. (2013). It is worth noting that IC is primarily a structural sediment connectivity index: it aims to express the control of topography on the potential of the different compartments of a system to be connected. The novelty of the approach used here lies in the dual consideration of both land cover and topographic variations on the assessment of sediment connectivity through time. The previous studies that applied the IC to investigate the effects of land use changes on connectivity (e.g. Lopez-Vicente et al., 2016; Lizaga et al., 2016; Persichillo et al., 2018), simply modified a land-cover based weighting factor that represents the impedance to sediment flux (e.g. *C*-factor or Manning's *n*) implemented in the IC, and topography, another input variable for the computation of the IC, often is assumed to remain unchanged (i.e. a single digital terrain model is used). Therefore, there is a knowledge gap related to studies which analyse changes in the IC through taking into account not just the land cover properties but also the topography (i.e. using the 'real' terrain model in each IC assessment). We argue herein that the use of static topography may not adequately capture the changes in connectivity and, consequently, we have attempted to consider the topography associated to each period under investigation. From the methodological point of view, the

novelty of our study lies in the application of Structure from Motion (SfM) photogrammetry using historical aerial photos to obtain historical orthomosaics and topography for quantitative landscape analyses as the bases of the assessment of multi-temporal changes on sediment connectivity.

Specifically, IC maps were produced before and after the *landscape disturbances*. Three different scenarios of land use change were analysed in a representative Pyrenean Mountain catchment (the Upper Cinca). Changes associated with (i) land cover; (ii) terracing; and (iii) road construction were quantified. These three scenarios provide an ideal data set to analyse the sensitivity of the different changes on the potential of the sediment to be transferred through the different compartments of the catchment (i.e. structural connectivity) and, ultimately, to be supplied to the mainstream.

## 2. STUDY AREA

The Upper Cinca catchment is located in the headwaters of the river Cinca catchment (8300 $km^2$), in the centre of the south face of the Pyrenees (NE Iberian Peninsula; Figure 1). The upper catchment, above the Mediano Reservoir (435 $hm^3$), covers a total area of 1565 $km^2$ and is composed by two sub-catchments: the Ara (715 $km^2$) and the Cinca (850 $km^2$). The Upper Cinca catchment is characterized by a complex morphology. The elevation ranges from 522 m.a.s.l. at the outlet to 3375 m.a.s.l. on the Posets Peak at the headwaters (Figure 1A). The climate is typical of Mediterranean mountainous areas with a mean annual precipitation of around 1100 mm, ranging from 800 mm in the lowlands to 1600 mm at high elevations (López-Martín et al., 2007). Strong inter-annual and seasonal variability of precipitation and temperature, and local conditions (e.g. due to relief, lithology and land use) create a highly heterogeneous landscape. Higher parts of the catchment are dominated by bare soil/rock, meadow and scrublands, valley bottoms are mainly used for agriculture, and intermediate elevations covered by woodlands and scrublands comprise the majority of the catchment.

Four small sub-catchments (around 10 $km^2$) of the Upper Cinca catchment were selected to represent three different scenarios of land use changes: Aran and Soto (Scenario 1: Changes associated with land cover); Pocinos (Scenario2: Changes by terracing); and Fiscal sub-catchments (Scenario 3: Changes by road construction; see the location in Figure 1 and sub-catchments characteristics in Table 1). In the following sections the main characteristics of the sub-catchments are presented along with the reasons for including each study area in a specific scenario.

### 2.1. Aran sub-catchment

The Aran sub-catchment (9.2 $km^2$) is located in the upper part of the Ara River. Between 1957 and 2010, forest cover in this basin almost doubled from 43% to 81% of the total surface of the catchment (Figure 3). This increase resulted in a decrease in meadow and pasture areas, mainly located above the timberline, and also a decrease in bare soil areas, such as land crops in the lower parts of the valley, and sediment active areas located in the upper parts of the catchment (i.e. erosional features) and in the valley bottom (i.e. active channels; Figure 3). The increase in forest cover during the second half of $20^{th}$ century is representative of many Pyrenean mountain catchments and mainly driven by both land crop abandonment and decreasing grazing due to depopulation (e.g. García-Ruiz et al., 1996; Gallart and Llorens, 2003; García-Ruiz and Lana-Renault, 2011; Lopez-Moreno et al., 2011) and climate change (e.g. Lopez-Moreno et al., 2011; Macklin et al., 2012; Buendia et al., 2016; Coulthard and Van de Wiel, 2017).

### 2.2. Soto sub-catchment

The Soto sub-catchment (10.1 $km^2$) is located in the lower part of the Upper Cinca near the outlet and is characterized by a large bare surface area composed mainly of field crops and badlands. This basin is virtually the only sub-catchment in the Upper Cinca that has not suffered agricultural abandonment during the study period (1957-2010); contrarily, an increase of the area of crop fields has been observed. There was a small decrease in forested areas (from 57 to 51%) and a corresponding increase in bare soil area (from 14 to 20%; Figures 4A and 4B). In 1957 there was a heterogeneous or patchy spatial distribution of the different land uses, sparse forest in the highest parts of the sub-catchment and a few patches of forest cover in the lower parts of the sub-catchment (Figure 4A and 4B). Bare areas composed of small land crops, agricultural terraces, and badlands. However, in 2010 the tree density in the forested areas increased, especially the upper parts. This is mainly due to the decrease of the extensive activities caused by rural abandonment and changes of the main economic activities in mountain areas (García-Ruiz and Valero-Garcés, 1998; Lasanta-Martinez et al., 2005). Badland surface area remained stable throughout the study period. Additionally, the maps indicate that the small crop fields located in the upper parts of the sub-catchment were abandoned and the crop fields in the flatter areas remained, even increasing their surface due to the unification of existing plots or the creation of new ones by means of ploughing and forest harvesting (Tague and Band, 2000; Figure 4A). The abandonment of upland small plots was also driven by the mechanization of the agriculture; except for rare occasions, only the farmlands where (i) machinery can enter, (ii) an access road is available, (iii) a certain slope threshold is not exceeded, and (iv) a size threshold is exceeded, are cultivated (García-Ruiz and Lopez-Bermudez, 2009).

### 2.3. Pocinos sub-catchment

The Pocinos sub-catchment (7.4 $km^2$), located in the middle part of the Upper Cinca. Most of the surface is covered by agricultural terraces, which due to rural abandonment, have been fully covered by vegetation. The forest surface doubled (from 31% in 1957, to 64% in 2010), while the meadow (from 44% to 18%, respectively) and bare soil (from 25% to 18%) tend to decrease. The main part of the sub-catchment (i.e. 58%) did not undergo significant changes. The rest of the sub-catchment experienced afforestation (i.e. 37%), especially the areas with abandoned terraced fields. Finally, only 5% of the surface suffered deforestation during the study period. These changes are driven by the construction of new roads or the creation of firewalls in the middle part of the sub-catchment and also a little area near to the outlet which was affected by a forest fire in 1991 (Figure 5A).

### 2.4. Fiscal sub-catchment

The Fiscal sub-catchment (15.6 $km^2$) is located in the middle part of the River Ara catchment. This sub-catchment has also experienced a significant increase in forest cover (i.e. from 50% of the total surface in 1977 to 72% in 2010) and a reduction in meadow and bare surfaces during the study period (Figure 7A and 7B). Furthermore, during the beginning of the 21$^{st}$ century, a road with a length of 5 km and an average width of 20 m was constructed in this sub-catchment. Regarding the impacts of the road construction, Llena et al. (2018) recently analysed the magnitude of the topographic changes along the road, which resulted in a net sediment mobilization of about 900,000 $m^3$ of material, mainly due to the excavation of material in the slopes (i.e. extraction) and to the infilling in depressions or deep channels (i.e. deposition). Roads influence the overall sediment transfer in two ways, by inducing erosion downslope of the road, and by capturing sediment coming from above the road and delivering them downstream

(Wemple et al., 2001). Due to the induced effects on flow paths and consequently on runoff, topographic changes due to roads may have a localised effect on connectivity.

**Table 1**. Main characteristics of the four study sub-catchments

| Catchment | Catchment Area ($km^2$) | Minimum and maximum elevation (masl) | Mean slope (º) | Percentage of forested cover (%) |
|---|---|---|---|---|
| **Fiscal** | 15.6 | 750 - 1925 | 29 | 72 |
| **Arán** | 9.2 | 1045 - 2025 | 17 | 81 |
| **Pocinos** | 7.4 | 758 - 2013 | 28 | 52 |
| **Soto** | 10.1 | 540 - 1046 | 30 | 51 |

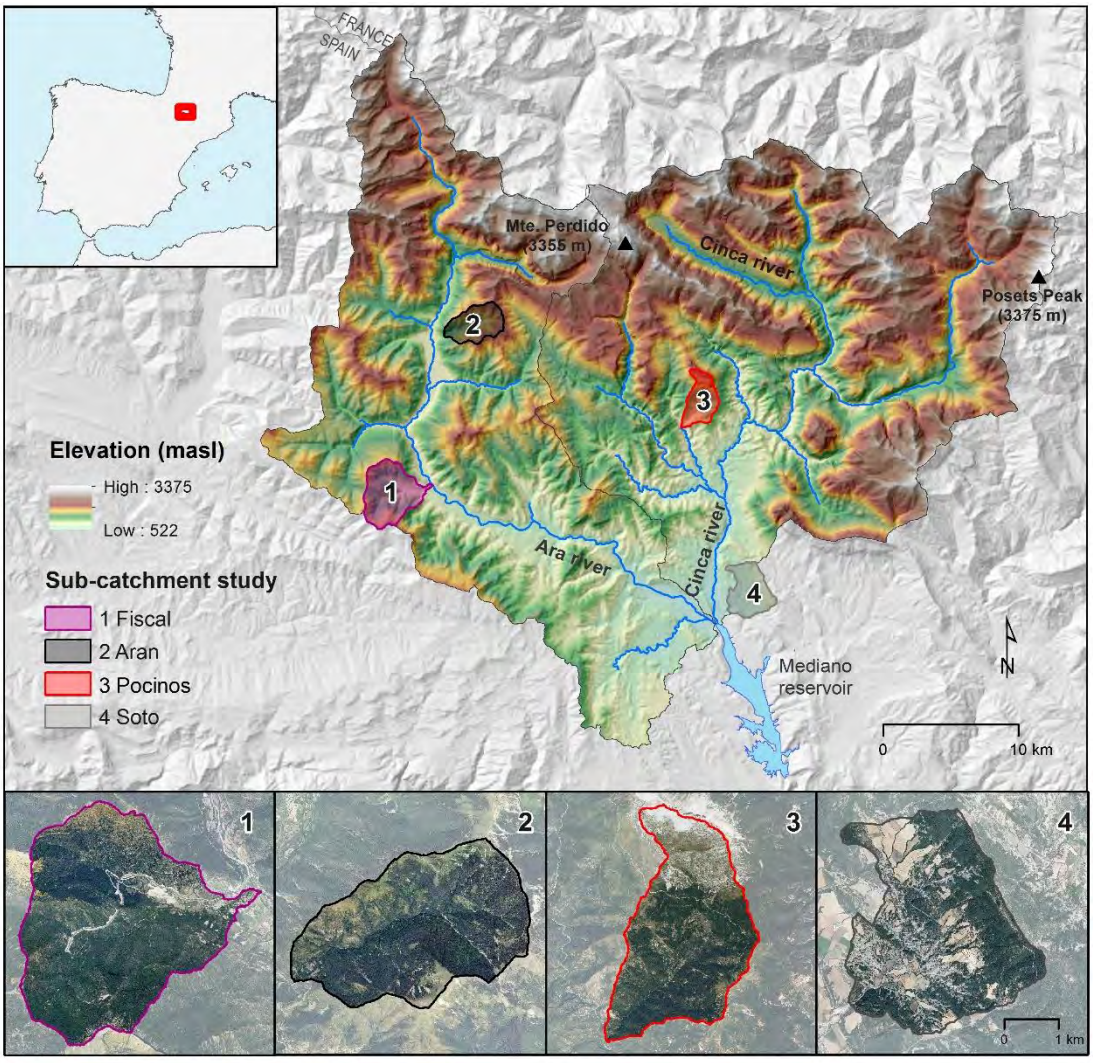


**Figure 1**.Upper Cinca river catchment and study sub-catchments

# 3. METHODS

## 3.1 Data preparation

Sediment connectivity for the different scenarios was mapped using the Index of Connectivity (IC) developed by Cavalli et al. (2013), which is based upon the original approach by Borselli et al. (2008). This index aims at evaluating, at the pixel scale, potential connectivity between hillslopes and features which act as targets or storage areas (e.g. catchment outlet, channel network). Specific information on the computation of the IC is provided in section 3.3.1. In summary, the inputs needed by the IC are: (i) a Digital Elevation Model (DEM), and (ii) land use maps used to calculate the Weighting factor (obtained from orthophotos, see section 3.3.2 for more information). Input variables to compute the IC are obtained differently for historical and contemporary study periods. In the case of the historical study period, black and white aerial photographs from 1957 and 1977 were used. Structure from Motion and Multi-View Stereo Photogrammetry (SfM-MVS) were applied to produce both orthomosaics and point clouds. The complete SfM-MVS workflow is presented in Llena et al. (2018). The 1957 photographs were obtained from Cartographic and Photographic Centre of the Spanish Army (CECAF), and the 1977 photographs from the National Geographic Spanish Institute (IGN). The use of historical aerial photographs to obtain spatial data through SfM-MVS is influenced by the quality and overlap of photograms and the ground control network (see Micheletti et al., 2015; Bakker and Lane 2017 for additional details). In the particular case of this study, we obtained point clouds with an average spatial resolution of 1 pts/$m^2$ and an average Standard Deviation Error (SDE) of the elevation of 2 m. Additionally, orthomosaics with a resolution of 1 m and an average Root Mean Square Error (RMSE) less than 1 m were also obtained.

In terms of the contemporary period, information from 2010 was used. For this year, a LiDAR dataset (i.e. point clouds) with a resolution of 0.5 pts/$m^2$ and an elevation accuracy of less than 0.2 m, and an orthomosaic of 0.5 m resolution were both available from the National Geographic Spanish Institute (IGN).

### 3.1.1 Image classification: land use maps

A supervised image classification of the multi-temporal orthomosaics for each of the study areas was carried out in order to obtain land use maps to derive the different weighting factors required to compute the IC (see more details in 3.3.2.). Three different classes were identified in terms of land cover: bare, meadow and forest. The identification of these classes was limited by the scale, properties (e.g. black and white) and the quality of the aerial photographs. Forest polygons were also used to filter the point clouds in order to create the DEMs as explained below.

### 3.1.2 Post-processing point clouds: Digital Elevation Models

Each point cloud (SfM-MVS or LiDAR-based) was regularized to the desired resolution using the ToPCAT algorithm (Brasington et al., 2012), as implemented in ArcGIS through the open source Geomorphic Change Detection extension (GCD, available at http://gcd.joewheaton.org/; Wheaton et al., 2010). This algorithm allowed first defining a regular grid of analysis, second sorting all points in each cell, and finally, calculating a series of elevation statistics for each cell. The mean elevation value in each cell was used as an estimate of the mean ground elevation. The grid resolutions were based on the typology and magnitude of the topographic change in

each scenario and in relation to the errors reported below (See section 3.3.2 for more details). Finally, the regularised data representing the mean elevation value per grid cell were interpolated to create the DEMs. For this purpose, we used the Natural Neighbours interpolation method implemented in ArcGIS 10.3. It is worth to mention that, for the 1977 series, we used the polygons associated with forest cover to filter the point cloud before to run ToPCAT. We considered the ground elevation in forested areas not well represented when the point cloud is extracted using SfM-MVS applied to aerial photos. This is a common limitation of this method, not present in the LiDAR data sets where the vegetation is already filtered. Therefore, the SfM-MVS-based topographic observations within those areas were erased before running ToPCAT and creating the DEMs.

## 3.2 Scenarios of change

The three different scenarios were considered representative of changes in Mediterranean mountain catchments. Figure 2 illustrates each of the scenarios including the data set used.

### 3.2.1. Scenario 1: Changes in land cover

Land cover changes were analysed in two different sub-catchments (Soto and Aran, Figure 1) during two study periods (1957 and 2010). The Aran sub-catchment, as detailed introduced above, is representative of those where forest cover increased (afforestation) by reducing the area of bare soil, meadows and former cultivate areas. On the other hand, the Soto sub-catchment is considered representative of areas that have not experienced changes in land use during the last 50 years. Only a small increase in crop field areas is observed in this sub-catchment (tillage).

### 3.2.2. Scenario 2: Terracing: topographic changes in agricultural fields

The effect of terraces on sediment connectivity was analysed in a terraced sub-catchment with an important increase of vegetated area due to the land abandonment during the period 1957-2010. In this scenario, the objective was to compare both the effects of afforestation and of the construction of terraces on sediment connectivity, and evaluate which of them have a more significant role on sediment connectivity (i.e. sensitivity of the IC changes). The effect of terracing (alone) was studied for the Pocinos sub-catchment by analysing the surface with the presence and absence of terraces. The situation of 'terrace presence' was analysed using the contemporary (2010) LiDAR-based DEM. In the case of the situation with the 'absence of terraces', these were filtered out (removed) from the 2010 DEM. The terraces observed in 1957 are actually the same as those observed currently, although almost all the field crops have been abandoned and afforestation took place. Terraces were removed by smoothing the 2010 DEM (see section 3.3.2 for more details). In this case, the same land use map (the one obtained for the year 1957) was used to compute the IC for both conditions: terraces and no-terraces. Therefore, considering that the land uses in 1957 were representative of those before terraces were built, we are able to analyse the effects of these structures on sediment connectivity. Additionally, the effect of just land use changes was assessed with a unique topography (i.e. 2010 DEM containing terraces) but using different land use maps (i.e. 1957 and 2010 respectively) to compute the IC. All these combinations permit analysis of which impacts (terracing vs land use changes in a terraced landscape) have a greater effect on sediment connectivity.

### 3.2.3. Scenario 3: Road construction: topographic changes associated with infrastructure

This scenario is focused in the Fiscal sub-catchment, where a road was built during the period 2006-2010. We compared the IC maps extracted from the contemporary DEM (i.e. 2010 LIDAR dataset) with the 1977 DEM (i.e. SfM-MVS based dataset). The results for both years could not be statistically compared due to the different accuracy associated to each DEM. However, results permit analysis of the impact of the road on connectivity patterns and identification of areas where changes in connectivity may prompt additional impacts (i.e. potential erosion hot spots).

**A**

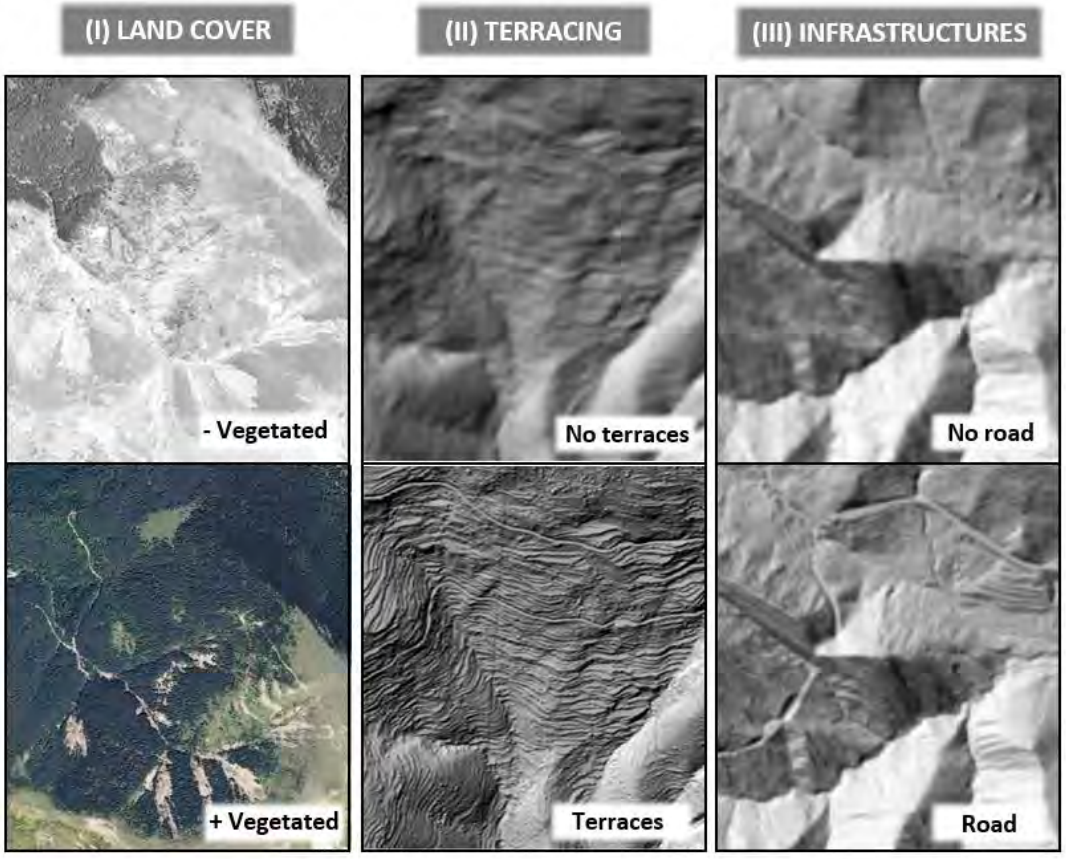


**B**

| Scenario | (I) | (II) | (III) |
|---|---|---|---|
| **DEMs (resolution and time)** | 5x5 m 2010 | 1x1 m 2010 and 2010 modified | 10x10 m 1977 and 2010 |
| **LAND USE MAPS (time)** | 1957 and 2010 | 1957 and 2010 | 1977 and 2010 |

**Figure 2**. **A**. Representation of the three scenarios of change analysed in the Upper Cinca catchment: (a) Changes in land cover; (b) Topographic changes on agricultural fields (i.e. terracing) and (c) Topographic changes associated with infrastructures (i.e. road construction). **B**. Maps and DEM's used for each of the scenarios.

## 3.3. Assessment of changes in Sediment Connectivity associated with selected scenarios

### 3.3.1. Index of Sediment Connectivity (IC)

The Index of Sediment Connectivity (IC) was computed using the software SedInConnect 2.3 (Crema and Cavalli, 2018). The IC is defined as:

$$IC = log_{10}\left(\frac{D_{up}}{D_{dn}}\right)$$

where $D_{up}$ is the upslope component and $D_{up}$ is the downslope component. The upslope component ($D_{up}$) describes the potential for downward routing of the sediment produced upslope, and is estimated as follows:

$$D_{up} = W\ S\ \sqrt{A}$$

where *W* is the weighting factor (i.e. a proxy of impedance to the sediment flux; dimensionless), *S* is the slope (%) and *A* is the upslope contributing area ($m^2$). The downslope component ($D_{dn}$) takes into account the flow path length that a particle has to travel to reach the nearest target or sink. It is expressed as:

$$D_{dn} = \sum_i \frac{d_i}{W_i S_i}$$

Where $d_i$ is the length of the flow path along the $i^{th}$ cell, $W_i$ and $S_i$ are the weighting factor and the slope gradient of the $i^{th}$ cell, respectively.

The computation of the IC is mainly based on topography but information on land use cover can be integrated into the analysis by using the weighting factor (e.g. based on *C*-factor as in Borselli et al., 2008 or Manning's *n* as in Brardinoni et al. (2015) and Pesrsichillo et al. (2018). More details on IC can be found in Cavalli et al. (2013) and complemented by the original work by Borselli et al. (2008).

### 3.3.2. Computing the IC for the different scenarios

In this section we describe the specific methods adopted in each scenario and catchment for the computation of the two main data sets needed for IC computation: (a) Terrain Data (i.e. topography expressed by the DEMs), and (b) Weighting Factor (i.e. land use expressed by the Manning's *n* roughness coefficient).

*Terrain Data*

Topography determinates the slope and the drainage network characteristics, and both parameters are taken into account in the calculation of the upslope and downslope components of the IC. In the present paper, as explained above (see Figure 2), different DEMs were used based on the objective of each scenario:

Scenario 1: Changes in land cover. A DEM of 5 m resolution was extracted from the 2010 LIDAR dataset with a density of 0.5 pts/$m^2$. This resolution was considered sufficient to represent the macro-topography at the catchment scale. From the interpretation of the aerial photos we assume that the topographic changes during the study period (1957-2010) would have a

minimum effect on the computation of the IC at the targeted scale, therefore the IC was assessed just changing the W factor and using the same terrain data.

Scenario 2: Terracing. First, a DEM of 1 m resolution obtained from the 2010 LIDAR dataset was used. Taking into account that the typical length and width of the terraces in the study area is >2 m, the use of 1 m DEM resolution is considered appropriate to represent the alteration that the terraces caused on the topography. Then, in order to eliminate possible point cloud noise (i.e. interpolation artifacts) a smoothing filter (low pass) was applied to the original 1 m DEM. Finally, to recreate the landscape without terraces the DEM was smoothed in order to eliminate the micro-topography maintaining the macro-topography. To this end, a DEM resampling from 1 m to 5 m (using the Resample ArcGIS 10.3 tool), and a subsequent resampling again to the original resolution of 1 m was performed. The later resampling was performed because maintaining the resolution of the DEM has been considered very important since coarsening implies an increase in the estimated IC value (Goldin, 2015; Brardinoni et al., 2015; Cantreul et al., 2018; López-Vicente and Álvarez, 2018). Therefore, this scenario is evaluated using two DEMs, one representing the landscape without terraces and a second one representing the actual situation, i.e. the landscape with terraces (both at 1 m resolution).

Scenario 3: Road Construction. In the case of the contemporary topography (i.e. after road construction), a DEM of a 10 m resolution derived from the LIDAR 2010 dataset was used. To represent the historical topography (i.e. before the construction of the road) a DEM with 10 m resolution extracted from a 1977 point cloud obtained by means of SfM-MVS applied to aerial historical photos was used. A 10 m resolution was selected to minimize the irregularities observed in the historical point cloud (e.g. bumping surface; Bakker and Lane 2017; Llena et al., 2018). Additionally, this resolution is considered enough to represent the topographic changes associated to the construction of the road, which in some parts were greater than 30 m. Again, this scenario is analysed by means of two DEMs: one representing the landscape before the road was constructed and a contemporary model that contains the road (both at 10 m resolution).

*Weighting factor*

In the original IC of Borselli et al. (2008), the C-factor based on USLE-RUSLE models was used to parameterize the weighting factor (*W*). In studies like this, where the evaluation of the role of different vegetation cover and land use changes on sediment connectivity is one of the main objectives, an alternative approach to the C-factor using a parameter related to hydraulic roughness. In particular, roughness is needed for a better representation of the impedance to the water and sediment fluxes since the C-factor only refers to cover and management related to erosion. An option is to use the Manning's *n* roughness coefficient (*n*), which represents the resistance to flow, with values varying according to different surface characteristics affecting roughness (Goldin, 2015; Brardinoni et al., 2015; Pesrsichillo et al., 2018). For this study, an image classification of all orthomosaics orthophoto mosaics was performed in order to obtain land use maps. A different Manning's *n* value was assigned to each of land use classes taking into account the *n*-values described in Goldin (2015). Although the study area in Goldin (2015) is located in a different geographical context than the areas studied in this work (i.e. the Italian Alps), the use of *n*-values extracted from this study is justified due to the similarity of the characteristics of the land uses. In spite of this, it is necessary to take into account the simplification that implies the use of the same *n*-value value for each land use class. Evidently, the variability of the *n*-value within each use can be notable although we have considered that this intra-variability has a minor effect on the computation of the IC at the catchments scale. It is important to highlight that the number of land use classes was determined based on the

quality (e.g. blurred), characteristics (e.g. number of bands) and resolution (i.e. pixel size) of the aerial images; the images with most limiting conditions (i.e. usually historical images) determined the number of final classes. In this case, we defined three different classes: forest, meadow, and bare (with respective Manning's *n* values of 0.4, 0.1 and 0.05). Finally, the weighting factor W is computed as W = 1 – n (following Goldin et al., 2015; Persichillo et al., 2018). The three land uses classes are representative of the land cover of the study sub-catchments and also of many mountain catchments in the Mediterranean.

*IC computation and comparison*

Once the IC maps were calculated for each scenario, IC values, as also suggested by Crema and Cavalli (2018), were reclassified into four classes for a better interpretation of the results: Low, Medium-Low, Medium-High and High Connectivity. The mean IC value was used as a limit between the Medium-Low and Medium-High classes, while the mean value plus two times the standard deviation of the IC values was used to define the threshold between the Medium-High and High classes. Finally, the mean value minus two times the standard deviation was the criterion used to establish the limit between the Medium-Low and Low classes. The same criteria were used for the representation of the difference of the IC between the analysed periods.

## 4. RESULTS AND DISCUSSION

### 4.1 Changes in sediment connectivity driven by land cover changes (Scenario 1)

In this section, we present two conditions in which land uses can affect sediment connectivity: afforestation and tillage, the latter of which is highly representative of most of the surface of Pyrenean catchments (e.g. García-Ruiz et al., 1996; Lasanta-Martínez et al., 2005), and many mountain catchments in Europe in general (e.g. MacDonald et al., 2000; Liébault et al., 2005) which have undergone afforestation in the last century. In the particular case of the Upper Cinca catchment, afforestation is the main observed change; the areas in which the agricultural activity has been maintained are limited to flat areas located in old terraces or valley bottoms in the vicinity of villages and towns (i.e. <5% of the total surface).

#### 4.1.1. Afforestation: the case of the Aran sub-catchment

Figure 3 presents the land cover (Figure 3A) and IC maps for each year (Figure 3B) and also the comparison of the IC (Figure 3D) and land cover maps (Figure 3C). The old IC map (1957) was subtracted from the more recent (2010) map (hereafter IC Differences map), so that a positive value indicates an increase of connectivity and a negative value a decrease of sediment connectivity. Additionally, by comparing the land cover maps three main processes were determined: afforestation, deforestation and no change. The comparison between the 1957 and 2010 IC maps highlights the general decrease of connectivity in almost all the study sub-catchments (i.e. -0.18 median) that is mainly due to the increase of vegetation occurred during this period (Figure 3A and 3C). These results are in line with the findings of several studies in mountain Mediterranean regions that also show a reduction in sediment connectivity caused by an increase of vegetation cover during the second half of 20$^{th}$ century (e.g. Foerster et al., 2014; Lopez-Vicente et al., 2016; Lizaga et al., 2016; Persichillo et al., 2018). As pointed out by Foertser et al (2014) in the case of the nearby Isábena catchment (Southern Pyrenees), the resulting connectivity map depends not only on the land cover fractions but also on the spatial distribution of vegetation abundances and its proximity to the catchment outlet (i.e. target). In

the case of Aran sub-catchment, the majority of the land surface was subject to afforestation (i.e. from bare soil or meadow surface to forest), but the highest decrease in sediment connectivity occurs in the areas where the increase of vegetation is more spatially concentrated and in areas located closer to the outlet (Figures 3C and 3D).

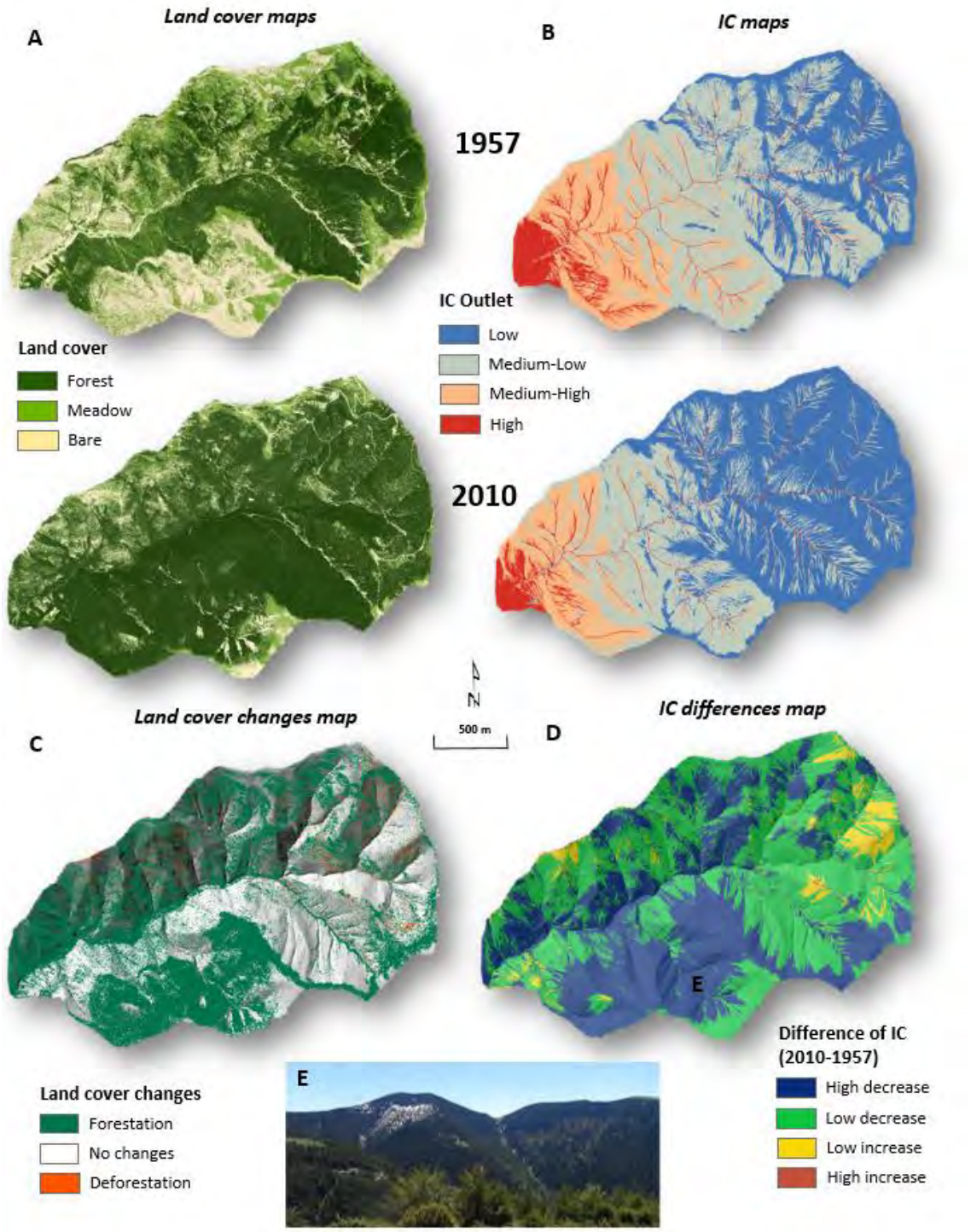


**Figure 3**. Changes on sediment connectivity associated land cover changes (afforestation): **A**. Land use maps for the two study periods (1957-2010). **B**. Map of the Connectivity Index (IC) for the two study periods. **C**. Maps of land cover changes between the two study periods where 3 main processes can be observed (afforestation, deforestation and no change). **D**. Maps of the difference of the ICs between the two study periods. **E**. Example of an area in which there has been a decrease in connectivity due to the increase in forest.

### 4.1.2. Tillage: the case of the Soto sub-catchment

For almost all the sub-catchment (i.e. 74%) there was a small increase in sediment connectivity (around 1% on average). Only for isolated patches located in the upper part of the catchment did connectivity decrease (i.e. 21% of total surface). These were areas that became forested during the analysed period. Results also indicate that connectivity increased in areas (i.e. 5% of the total surface) characterised by the establishment of farmlands in previously forested areas (Figures 4B and 4D). Although the surface occupied by badlands did not change significantly, it is very important to pay particular attention to these areas because they have because they have the highest values of connectivity. The high dynamism in these landscapes is also clear in the topographic changes observed by Smith and Vericat (2015) for some Badlands of the Soto, and in nearby badlands located in the River Isábena by Vericat et al. (2014). Overall, the median increment of the IC changes during the period 1957-2010 can be considered marginal (i.e. 0.05).

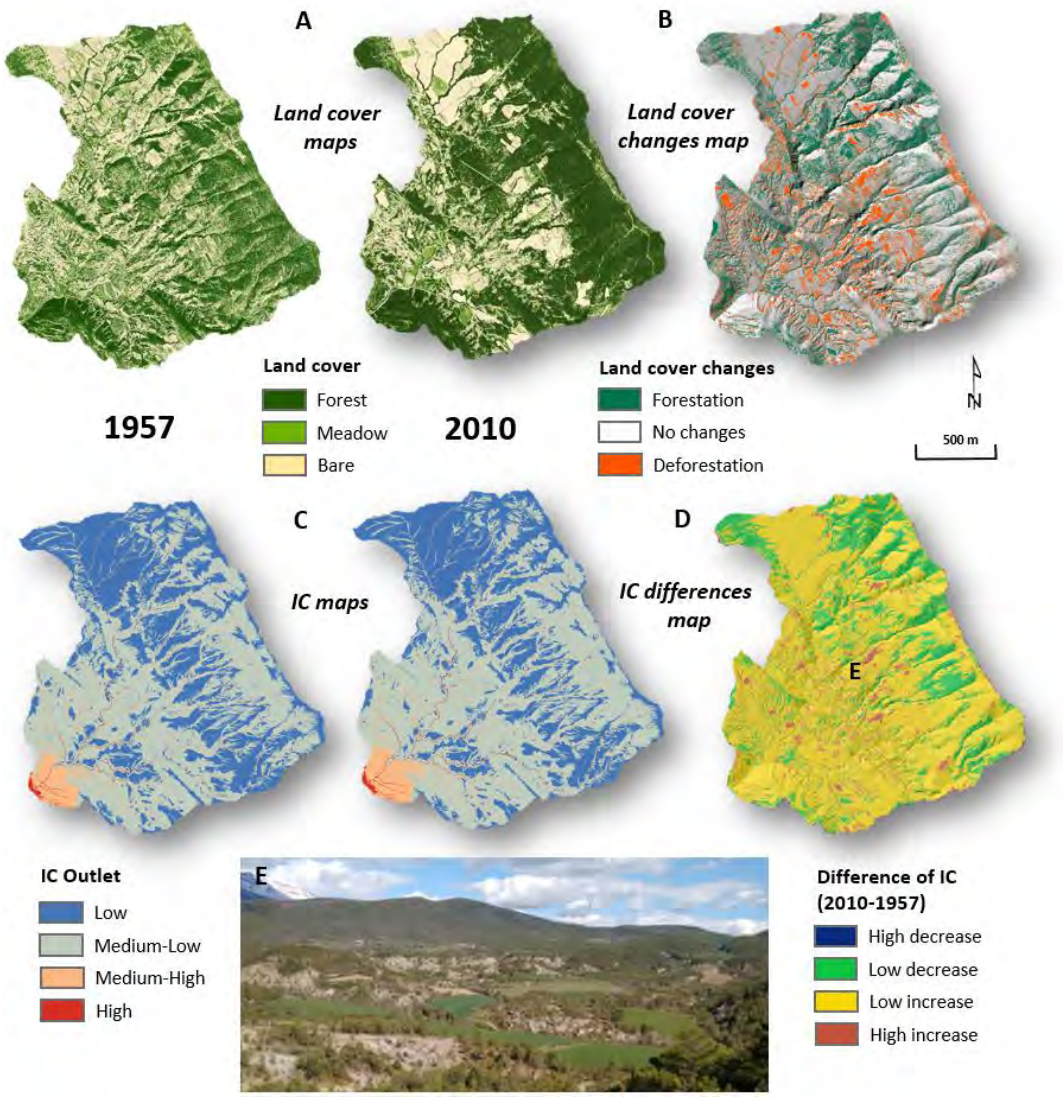


**Figure 4**. Changes on sediment connectivity associated with land cover changes (tillage): **A**. Land use maps of the Soto sub-catchment for the two study periods (1957-2010). **B**. Map of land cover changes between the two study periods (afforestation, deforestation and no change). **C**. Connectivity Index (IC) maps for the two study periods. **D**. Maps of the difference of the ICs between the two study periods. **E**. Photograph showing an example of an area in which there has been a large increase of sediment connectivity due to the creation of new cropland.

## 4.2 Changes in sediment connectivity by terracing (Scenario 2)

Two landscape conditions are analysed in this scenario to study the effects of: (a) land cover changes in a terraced landscape on connectivity; and (b) terracing on connectivity. In the former, the landscape is kept the same (i.e. terraced) and land uses are changed while in the later the land uses are kept the same and the landscape is changed (i.e. no terraces versus terraced). These results differ from the results obtained for scenario 1 in the way that they allow inferring the change (land cover or terracing) that affects sediment connectivity most. Areas characterised by a high increase in forest cover have experienced a high decrease in sediment connectivity (e.g. northeast of the sub-catchment, Figure 6). In contrast, in areas where roads and firewalls were built, connectivity increased, while the area affected by a wild fire near to the outlet is the only section that exhibits a high increase of sediment connectivity due to the deforestation associated to the fire (Figures 5A and 6B). The fast increase of forest cover in abandoned terraced landscapes can be explained by the stability of these areas and the favourable soil properties. Terrace abandonment followed by strong scrub or meadow regeneration in humid areas improves soil quality and creates effective protection against soil erosion, ultimately favouring afforestation (Llorens, 1991; Lana-Renault et al., 2014; Lizaga et al., 2016).

In terms of the effect of terracing on connectivity, the comparison of both DEMs shows that the topographic variations caused by the terraces have an amplitude of around 5 m (see longitudinal profiles in Figures 5B and 5C), while terraces increase the local slope (from 5º to 45º). These changes have a direct effect on the estimates of the IC.

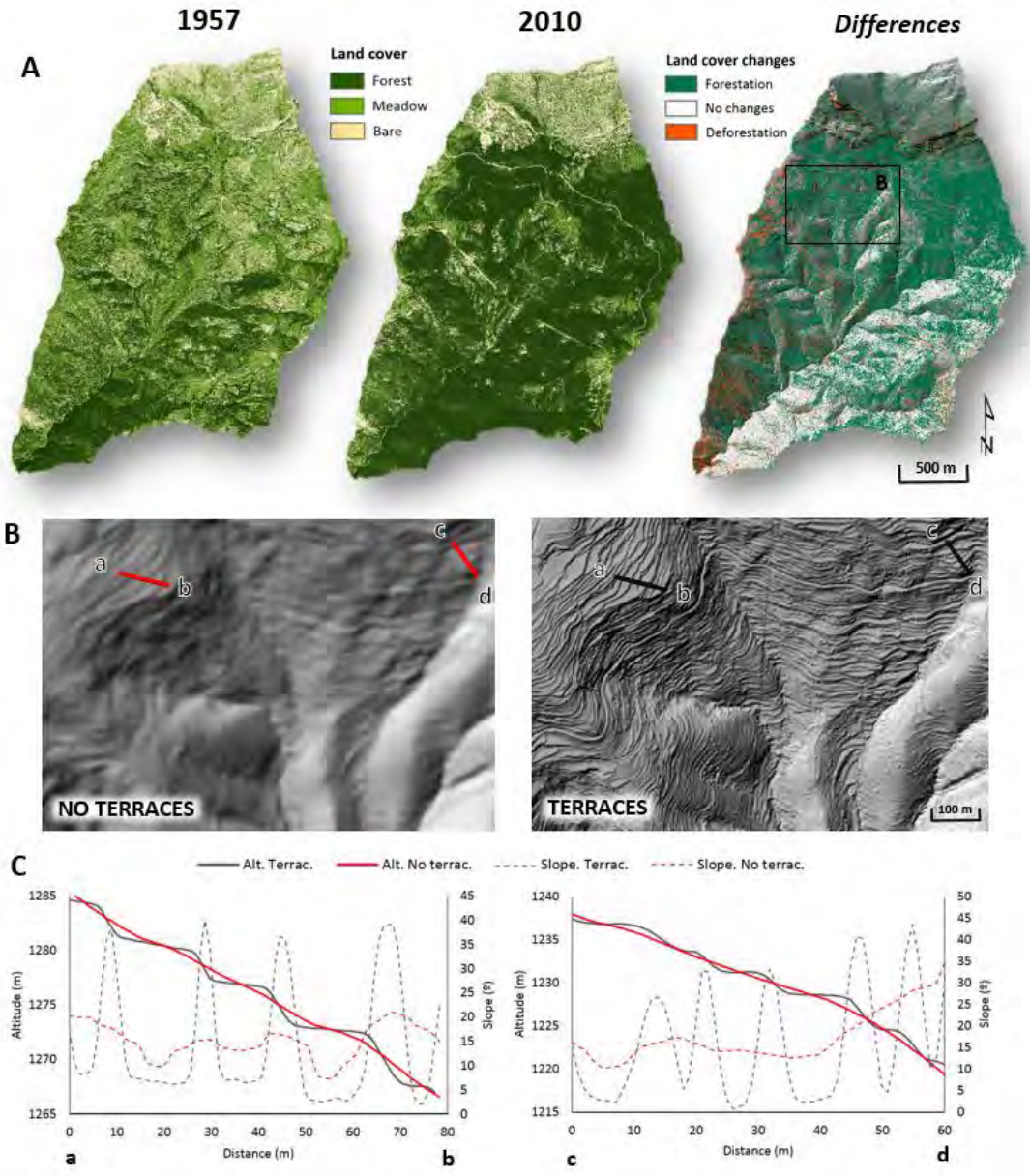


**Figure 5**. Changes in sediment connectivity associated with terracing: **A**. Land cover maps for both study periods (i.e. 1957 and 2010) and map of land cover changes between the two study periods (afforestation, deforestation and no change) in a terraced landscape. **B**. Hillshade model of the DEMs with no terraces (left) and with the presence of terraces (right). **C**. Two profiles (i.e. a-b, c-d) showing the variation of elevation and slope for no terraced (red lines) and terraced (black lines) DEMs.

The maps of IC show a general large decrease of sediment connectivity in all the areas with the presence of terraces (Figure 6B). Topographic conditions in terraced landscapes have a direct influence on infiltration and surface runoff; infiltration tends to increase while surface runoff is typically delayed, resulting in reduced peak flows and a subsequent decrease of connectivity (Garcia-Ruiz, 2010; Preti et al., 2018). Lesschen et al. (2009) also found that the presence of (maintained) terraces largely determines hydrological connectivity at the catchment scale. Inside the terraced landscape areas, connectivity increased locally, mainly due to the convergence caused by artificial structures (e.g. walls, forest roads; Figure 6B). This increase is typically explained by the abandonment of terraced areas triggering localized landslides and wall

failures, resulting in a localized increase in connectivity even in areas with dense vegetation (e.g. Garcia-Ruiz and Lana-Renault, 2010; Lopez-Vicente, 2013; Tarolli et al., 2014; Tarolli and Sofia, 2016). In particular, Calsamiglia et al. (2017) observed a high correlation between the failure of terrace walls and the increase in erosion and sediment connectivity (structural and functional) in a small Mediterranean catchment. Note that in our case the non-terraced landscape was reconstructed by smoothing the 2010 DEM (see methods). This was mainly due to the limitations provided by the quality of the 1957 topography data (i.e. errors around 2 m). Therefore, no further details on the effects of wall failures on connectivity were able to be performed. Our results, however, allow studying the combined effect of terracing and land use changes and the effect of the different topography related just to the presence\absence of terraces. In summary, after isolating the effect of land cover changes on a terraced landscape, and those driven by topographical changes due to terracing, the presence of terraces has a greater effect on sediment connectivity in the whole sub-catchment. Specifically, the IC median reduction due to terracing is more than twice the reduction computed when different land cover conditions are analysed (i.e. IC median reduction of 5 and 2% of respectively).

Although the (re)creation of a DEM without terraces can be considered a landscape simulation, this can be a useful approach to estimate the effect on sediment connectivity before the construction and after the failure of terraces in Mediterranean mountain catchments. In addition, if IC maps are computed based on these terrain models, they can help to better estimate and understand historical sedimentary dynamic providing important indication for its future evolution.

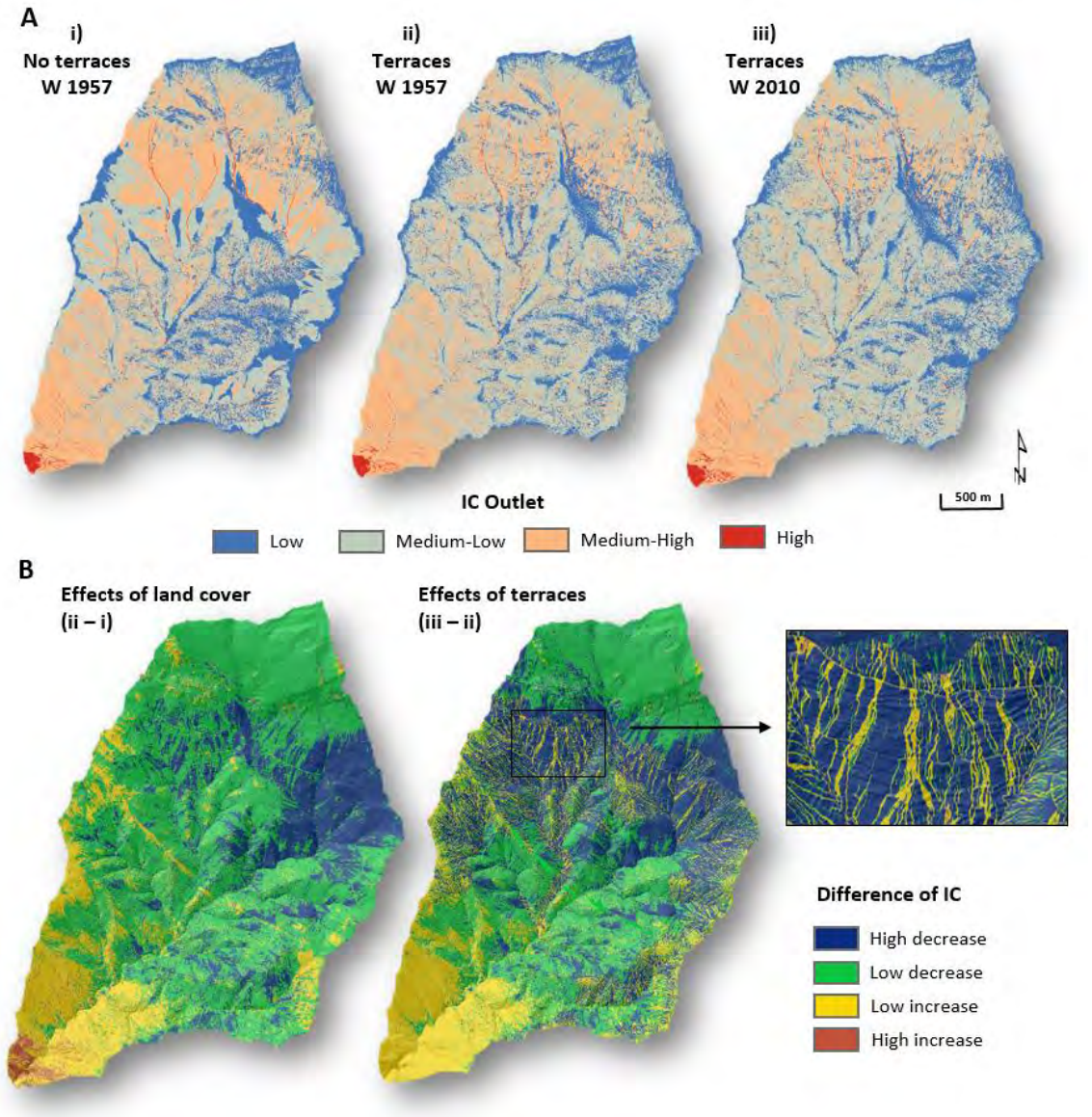


**Figure 6**. Changes in sediment connectivity associated with terracing: **A**. IC maps for different catchment conditions: (i) IC map assessed from the DEM without terraces and a weighting factor (W) extracted from the 1957 land use map; (ii) IC map obtained from the DEM with terraces (2010) and a W extracted from the 1957 land use map; and (iii) IC map assessed from the DEM with terraces (2010) and a W extracted from 2010 land cover map. **B**. Difference of the IC maps comparing the effect of terracing on connectivity (i.e. terraces; left); and the effect of land cover changes on connectivity in a terraced landscape (right).

## 4.3 Changes in sediment connectivity driven by road construction (Scenario 3)

The IC maps of the Fiscal sub-catchment show low values of connectivity in the areas with a high increase of the forest cover. A large part of these areas corresponds to the zones covered by steep slope field crops in 1977. These crops were abandoned and, consequently, covered by scrubs and forest (north part of the sub-catchment; Figure 7A and 7B). The south part of the sub-catchment also shows a decrease of sediment connectivity related to the increase of forest cover. In this case, the increment is due to an increase of tree density due to the decrease of

extensive forest exploitation activities caused mainly by depopulation and also climate change (see IC maps in Figure 7A and 7B).

In terms of stream-road intersections (e.g. Figure 7B and 7D), the road artificially cut the drainage network producing a localized increase in connectivity in the upslope area and a decrease in the potential connectivity downslope. As a consequence, the morphological variation due to road construction led to an increase of erosional activities uphill, triggering in some cases localised landslides (Figure 7D). The IC map also suggests that the sediment involved in the landslide now has a lower probability of reaching the target (i.e. outlet of the catchment) because of the effect of the road in trapping the material produced upslope.

Tarolli and Sofia (2016) analysed how roads could trigger landslides in two different case studies in a mountain watershed in the United States of America. Their results described whether or not the sediment produced by the slides can contribute to the total sediment of the watershed at the outlet. In one of their study cases, when the slide was produced above the road, the road disconnected the source area from the channel network, but move the flows downstream, thus increasing the probability of delivering the sediment to the watershed outlet by changing the path. Other studies analysed the interactions between roads and sediment (dis)connectivity. For instance, Kalantari et al. (2017) recently used the IC, among other indicators, to try to quantify the flood probability in road-stream intersections, demonstrating that the use of the IC as input variable improved the accuracy of a data-driven spatial-statistical model for road flood probability. In a different geographical context, Persichillo et al. (2018) observed a high correlation between the occurrences of shallow landslides with areas with high connectivity caused by the presence of roads in a Mediterranean catchment of the north of Italy. All these studies, both the study case, are good examples of the use of IC as a useful tool to assess potential risks associated with such infrastructure (e.g. identifying hot spots) and to inform also, at a broad spatial scale, those responsible for watershed and road infrastructure management.

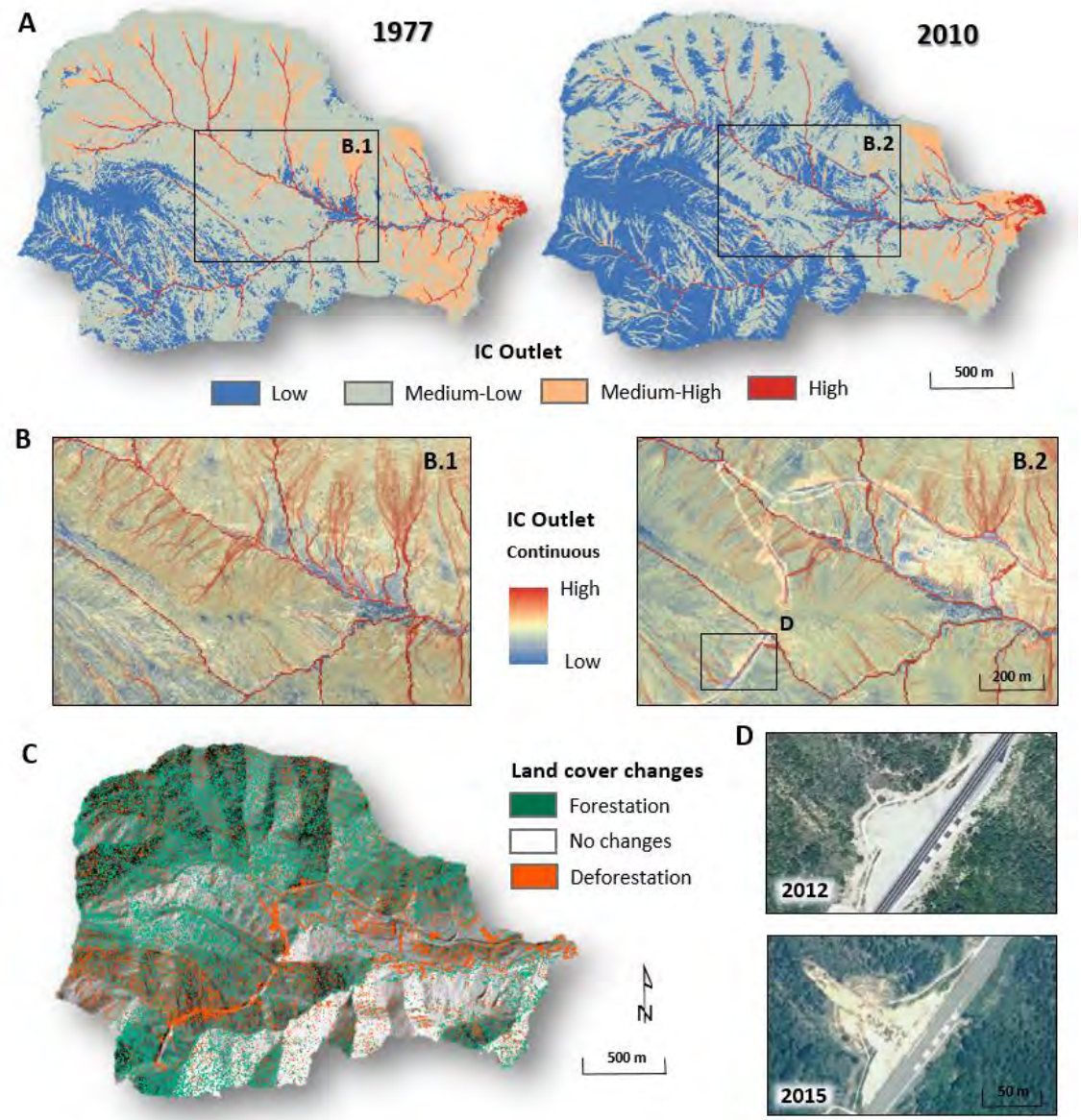


**Figure 7**. Changes on sediment connectivity associated to road construction: **A**. IC maps obtained using the 1977 DEM and land cover map (before road construction) and by the 2010 DEM and land cover map (after road construction). **B**. IC maps for both study periods showing the spatial distribution of the IC values and the changes caused by the construction of the road. **C**. Map of land cover changes between the two study periods (afforestation, deforestation and no change). **D**. Zoom on a hot spot where the morphological variation due to road construction led to an increase of erosional activities on the upslope side of the road (i.e. a landslide); this is also observed by looking at the changes on the IC (indicated with a black rectangle).

## 4.4. General Trends and Limitations

The analyses of land use changes and topographical changes in different scenarios allow us to quantify the effect of these changes on Sediment Connectivity and to estimate what types of change have the greatest effect. Figure 8 summarises the changes associated with each of the scenarios analysed in this study. The increase or decrease of the vegetation cover had a clear effect on the IC (Figure 8) by increasing or decreasing connectivity respectively. If topographic changes, such as the associated with terrace construction, are also taken into account, the

impact of these on connectivity can be even higher than the driven by land use changes. This is clearly observed in the results obtained for the Pocinos catchment. In this case, the percentage of the area in which connectivity highly decreased is 22% when the land use changes are analysed, and 35% when the topographic changes are considered. Moreover, in this latter case, the degree of IC increase is magnified (2.2% of the landscape suffered a high increase in connectivity while only the 0.1% in the case of the analysis just isolating the land use changes).

It is also interesting to note the patterns obtained in catchments where, although no significant general changes are observed (a mean change of the IC around 1% is obtained in the Soto sub-catchment), locally, (i) the unification of existing field crops or the creation of new ones by means of ploughing and forest harvesting, and (ii) patchy afforestation may increase or decrease connectivity. In this case, two main processes can be observed. First, connectivity may change on bare surfaces attributed to topographic changes. These changes, although may be relevant to study changes on connectivity at smaller (detailed) scales, cannot be depicted at the scale analysed in this paper (they are out of the scope of this study). Secondly, land use changes may decrease connectivity locally in those areas where field crops are abandoned or bare surfaces are vegetated (7% of the catchment area of the Soto experimented this change), or may increase in those areas where new field crops are developed or by the unification of existing ones (6% of the Soto). Finally, topographic changes associated with road construction can modify, not only the general IC values but also the patterns and distribution of these (Figure 8), in much more detail than the ones associated with land use changes.

As stated in the methods section, the limits between the different IC classes (including the IC changes) were calculated based on the mean values and the standard deviation of these. In this way, the significance of changes is a relative expression that depends on the distribution of the data of each of the scenarios. In the same way, the values of IC were directly conditioned by the main inputs to calculate the IC: the weighting factor and the topography. On one hand, the selection of the roughness or *n*-values as a weighting factor parameter was based on values presented in the literature (Goldin, 2016). It is very important to take into account the criteria when assigning the different values of *n*, since the variation of these values could lead to completely different IC maps. On the other hand, the resolution of the topography has an inverse effect on the total values of IC (e.g. Cantreul et al., 2018; López-Vicente and Álvarez, 2018), mainly driven by the smoothing of the landscape as the resolution decreases. In this study, the different resolutions were based on the typology and magnitude of the topographic change analysed in each scenario in relation to the errors.

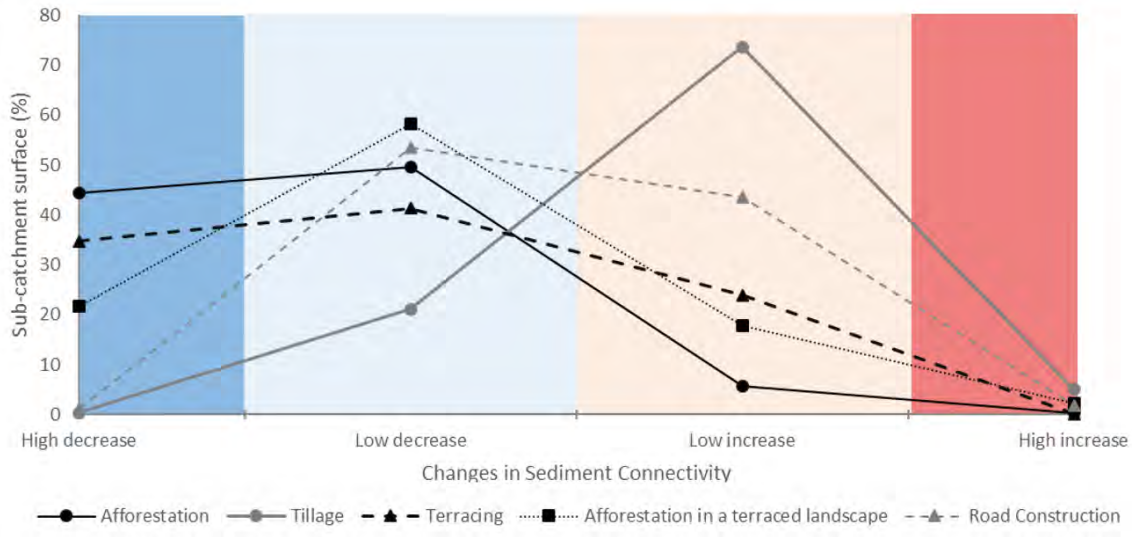


**Figure 8**. Changes in Sediment Connectivity (IC) for each one of the scenarios analysed in this study: Afforestation; Tillage; Terracing; Afforestation in a terraced landscape and Road Construction.

## 5. CONCLUSIONS

Sediment Connectivity Indices are very valuable to analyse the potential of a landscape to transfer sediments through its main compartments; that is to assess structural sediment connectivity through time. The role of land use and topographic changes on sediment connectivity in representative mountain catchments has been analysed for three different scenarios, representative of the main changes observed in many mountain areas. The main findings of the study can be summarized as follows:

- Land cover changes have a direct effect on the impedance to water and sediment fluxes. We identified areas with a slight increase in sediment connectivity due to the establishment of new field crops; however, most of the study area has undergone afforestation which resulted in a decrease of sediment connectivity and potential reduction of sediment supply to the main channel network.

- Terraces affect connectivity to a much greater extent than changes in land cover. The establishment of terraces has a double effect: (a) generally reducing connectivity due to the establishment of flat areas between slopes, and (b) increasing connectivity locally due to the convergence produced by the different human-made structures such as walls or the collapse of terraces due to abandonment. Results indicate that the use of the IC may detect areas of terraced landscapes where further monitoring is required for a better management of such structures, as for instance in vineyards areas where terraces are key for their stability and productivity.

- Topographic changes associated with road construction modify slope, surface flow directions and, consequently, the drainage network. Altogether, this leads to changes in connectivity that could affect erosional processes in the neighbouring areas with a direct impact on the stability of the road and on the transfer of sediments downstream. In this context, the IC is a useful tool to map hot spots, i.e. critical areas where further attention or monitoring would be required for a better maintenance of such infrastructures.

Finally, we argue that the study of historical changes in sediment connectivity due to land use variations, especially if addressed considering also topographic changes, may provide valuable information to understand sediment supply dynamics. This information coupled with hydrological and sediment transport numerical modelling can help understanding of how this has or is affecting the channel adjustments that are observed in many mountain rivers that have experienced land use changes in their headwaters during the 20$^{th}$ century. The novelty of our work lies in the development of an approach to assess multi-temporal changes in sediment connectivity by considering both changes in topography and land use. The methodology we used in this paper allows not just studying the effects of real decadal-scale land use and topographic changes on sediment connectivity, but also evaluating and disentangling those changes. Furthermore, the assessment of connectivity at multiple temporal scales can be also a useful tool to identify potential risks associated with morphological and land use changes, involving road infrastructure.

## 6. ACKNOWLEDGEMENTS

This research was carried out within the framework of two research projects funded by the Spanish Ministry of Economy and Competitiveness and the European FEDER funds: MORPHSED (CGL2012-36394) and MORPHPEAK (CGL2016-78874-R). The first author has a grant funded by the Spanish Ministry of Education Culture and Sports (FPU016/01687). The second author is a Serra Húnter Fellow at the University of Lleida. This manuscript has benefited from the work carried out during a Short Term Scientific Mission funded by the EU Cost Action Connecteur (ES1306: Connecting European Connectivity Research), and all discussions during the different meetings the Working Group 2 and 4 of this Action organised. The first and second authors are part of the Fluvial Dynamics Research Group-RIUS, which is a Consolidated Group recognized by the Generalitat de Catalunya (2017 SGR 459645). We also acknowledge the support of the CERCA Program of the Generalitat de Catalunya.

## 7. REFRENCES

Arnáez J, Lana-Renault N, Lasanta T, Ruiz-Flaño P, Castroviejo J. 2015. Effects of farming terraces on hydrological and geomorphological processes. A review. *Catena* 128: 122-134.

Bakker M, Lane SN. 2017. Archival photogrammetric analysis of river-floodplain systems using Structure from Motion (SfM) methods. *Earth Surface Processes and Landforms* 42: 1274–1286.

Beguería S. 2006. Changes in land cover and shallow landslide activity: A case study in the Spanish Pyrenees. *Geomorphology* 74: 196-206.

Bellin N, van Wesemael B, Meerkerk A, Vanacker V, Barbera GG. 2009. Abandonment of soil and water conservation structures in Mediterranean ecosystems. A case study from south east Spain. *Catena* 76: 114-121.

Bordoni M, Persichillo MG, Meisina C, Crema S, Cavalli M, Bartelletti C, Galanti Y, Barsanti M, Giannecchini R, D'Amato Avanzi G. 2018. Estimation of the susceptibility of a road network to shallow landslides with the integration of the sediment connectivity. *Natural Hazards and Earth System Sciences* 18: 1735-1758.

Borselli L, Cassi P, Torri D. 2008. Prolegomena to sediment and flow connectivity in the landscape: A GIS and field numerical assessment. *Catena* 75: 268–277.

Braken LJ, Tumbull L, Wainwright J, Bogaart P. 2015. Sediment connectivity: a framework for understanding sediment transfer at multiple scales. *Earth Surface Processes and Landforms* 40: 177-188.

Braken LJ, Croke J. 2007. The concept of hydrological connectivity and its contribution to understanding runoff-dominated geomorphic systems. *Hydrological Processes* 21: 1749-1763.

Brardinoni F, Cavalli M, Heckmann T, Liebault F, Rimbock A. 2015. Guidelines for assessing sediment dynamics in Alpine basins and channel reaches. Final project report (WP4), Alpine Space Programme – SedAlp Project. 177 pp.

Brasington J, Vericat D, Rychkov I. 2012. Modelling river bed morphology, roughness, and surface sedimentology using high resolution terrestrial laser scanning. *Water Resources Research* 48: 1-18.

Brunsden D, Thornes JB, 1979. Landscape sensitivity and change. *Transactions of the Institute of British Geographers* 4: 463–484.

Buendia C, Batalla RJ, Sabater S, Palau A, Marcé R. 2015. Runoff trends driven by climate and afforestation in a Pyrenean basin. *Land Degradation and Development* 27: 823-838.

Calsamiglia A, Fortesa J, García-Comendador J, Lucas-Borja ME, Calvo-Cases A, Estrany J. 2018. Spatial patterns of sediment connectivity in terraced lands: Anthropogenic controls of catchment sensitivity. *Land Degradation and Development* 29: 1198-1210.

Cantreul V, Bielders C, Calsamiglia A, Degré A. 2017. How pixel size affects a sediment connectivity index in central Belgium. *Earth Surface Processes and Landforms* 43: 884-893.

Cavalli M, Trevisani S, Comiti F, Marchi L. 2013. Geomorphometric assessment of spatial sediment connectivity in small Alpine catchments. *Geomorphology* 188: 31–41.

Crema S, Cavalli M. 2018. SedInConnect: a stand-alone, free and open source tool for the assessment of sediment connectivity. *Computational Geosciences* 111: 39–45.

Coulthard TJ, Van De Wiel MJ. 2017. Modelling long term basin scale sediment connectivity, driven by spatial land use changes. *Geomorphology* 277: 265-281.

Ferreira CSS, Walsh RPD, Blake WH, Kikuchi R, Ferreira AJD. 2017. Temporal Dynamics of Sediment Sources in an Urbanizing Mediterranean Catchment. *Land Degradation and Development* 28(8): 2357-2369.

Foerster S, Wilezok C, Brosinsky A, Segl K. 2014. Assessment of sediment connectivity from vegetation cover and topography using remotely sensed data in a dryland catchment in the Spanish Pyrenees. *Journal of Soils and Sediments* 14: 1982-2000.

Fryirs KA, Brierley GJ, Preston NJ, Kasai M. 2007. Buffers, barriers and blankets: The (dis)connectivity of catchment-scale sediment cascades. *Catena* 70: 49-67.

Fryirs K. 2013. (Dis)Connectivity in catchment sediment cascades: a fresh look at the sediment delivery problem. *Earth Surface Processes and Landforms* 38: 30–46.

Fryirs KA. 2017. River sensitivity: a lost foundation concept in fluvial geomorphology. *Earth Surface Processes and Landforms* 42: 55-70.

Gallart F, Llorens P. 2003. Catchment Management under Environmental Change: Impact of Land Cover Change On Water Resources. *Water International* 28: 334-340.

García-Ruiz JM. 2010. The effects of land uses on soil erosion in Spain: A review. *Catena* 81: 1-11.

García-Ruiz JM, Lasanta T, Ruiz-Flaño P, Ortigosa L, White S, González C, Martí C. 1996. Land-use changes and sustainable development in mountain areas: a case study in the Spanish Pyrenees. *Landscape Ecology* 11(5): 267-277.

García-Ruiz JM, Valero-Garcés B. 1998. Historical geomorphic processes and human activities in the Central Spanish Pyrenees. *Mountain Research and Development* 18(4): 309-320.

García-Ruiz JM, López-Bermúdez F. 2009. La erosión del suelo en España. *Cuaternario y Geomorfología* 23 (3-4).

García-Ruiz JM, Lana-Renault, N. 2011. Hydrological and Erosive Consequences of Farmland Abandonment in Europe, with Special Reference to the Mediterranean Region—A Review. *Agriculture Ecosystems & Environment* 140(3): 317-338.

Gay A, Cerdan O, Mardhel V, Desmet M. 2015. Application of an index of sediment connectivity in a lowland area. *Journal of Soils and Sediments*. 16(1): 280-293.

Goldin B. 2015. *Geomorphometric Analysis and Sediment Dynamics In Mountainous Basins: Spatial And Temporal Scales*. Doctoral Thesis. Università degli Studi di Padova.

Goldin B, Rudaz B, Bardou E. 2016. Application of a sediment connectivity GIS-based index in a basin undergoing glacier retreat: the case study of the Navizence catchment. *Rendiconti Online Società Geologica Italiana* 6: 35-38.

Grohmann CE, Smith MJ, Riccomini C. 2011. Multiscale Analysis of Topographic Surface Roughness in the Midland Valley, Scotland. *IEEE TRANSACTIONS ON GEOSCIENCE AND REMOTE SENSING* 49(4): 1200-1213.

Harvey AM. 2001. Coupling between hillslopes and channels in upland fluvial systems: implications for landscape sensitivity, illustrated from the Howgill Fells, northwest England. *Catena* 42: 225-250.

Heckmann T, Cavalli M, Cerdan O, Foerster S, Javaux M, Lode E, Smetanová A, Vericat D, Brardinoni F. 2018. Indices of sediment connectivity: opportunities, challenges and limitations. *Earth-Science Reviews* 187: 77-108.

Hooke J. 2003. Coarse sediment connectivity in river channel systems: a conceptual framework and methodology. *Geomorphology* 56: 79-94.

Jones JA, Swanson FJ, Wemple BC, Snyder KU. 2000. Effects of Roads on Hydrology, Geomorphology, and Disturbance Patches in Stream Networks. *Conservation Biology* 14(1): 76-85.

Kalantari Z, Cavalli M, Cantone C, Crema S, Destouni G. 2017. Flood probability quantification for road infrastructure: Data-driven spatial-statistical approach and case study Applications. *Science of the Total Environment*. 581-582: 386-398.

Keestra SD, van Dam O, Verstraeten G, van Huissteden J. 2009. Changing sediment dynamics due to natural reforestation in the Dragonja catchment, SW Slovenia. *Catena* 78: 60-71.

Lana-Renault N, Ruiz-Flaño P, Llorente JA, Arnáez J. 2014. Respuesta hidrológica de una cuenca de bancales abandonados (Camero Viejo, La Rioja). In: Arnáez, J., González-Sampériz, P.,

Lasanta, T., Valero-Garcés, B. (Eds.) *Geoecología, cambio ambiental y paisaje*. CSIC-Universidad de La Rioja.

Larsen A, Robin V, Heckmann T, Fülling A, Larsen JR, Hans-Rudolf B. 2016. The influence of historic land-use changes on hillslope erosion and sediment redistribution. *The Holocene* 26(8): 1248-1261.

Lasanta-Martínez T, Vicente-Serrano SM, Cuadrat-Prats JM. 2005. Mountain Mediterranean landscape evolution caused by the abandonment of traditional primary activities: a study of the Spanish Central Pyrenees. *Applied Geography* 25: 47-65.

Lesschen JP, Cammeraat LH, Nieman T. 2009. Erosion and terrace failure due to agricultural land abandonment in a semi-arid environment. *Earth Surface Processes and Landforms* 33: 1574-1584.

Liébault, F., Gomez, B., Page, M., Marden, M., Peacock, D., Richard, D., Trotter, M. 2005. Land-use change, sediment production and channel response in upland regions. *River Research and Applications* 21: 739-756.

Lizaga I, Quijano L, Palazón L, Gaspar L, Navas A. 2016. Enhancing Connectivity Index to Assess the Effects of Land Use Changes in a Mediterranean Catchment. *Land Degradation and Development* 29(3): 663-675.

Lizaga I, Quijano L, Gaspar L, Ramos MC, Navas A. 2019. Linking land use changes to variation in soil properties in a Mediterranean mountain agroecosystem. *Catena* 172: 516-527.

López-Martín F, Cabrera-Millet M, Cuadrat JM, Saz-Sánchez MA, Martín S, Serrano V. 2007. *Atlas climático de Aragón*. Gobierno de Aragón. Spain

López-Moreno JI, Vicente-Serrano SM, Morán-Tejeda E, Zabalza J, Lorenzo-Lacruz J, García-Ruiz JM. 2011. Impact of climate evolution and land use changes on water yield in the Ebro basin. *Hydrology and Earth System Sciences* 15: 311-322.

López-Moreno JI, Zabalza J, Vicente-Serrano SM, Revuelto J, Gilaberte M, Azorin-Molina C, Morán-Tejeda, García-Ruiz JM, Tague C. 2014. Impact of climate and land use change on water availability and reservoir management: Scenarios in the Upper Aragón River, Spanish Pyrenees. *Science of the Total Environment* 493: 1222-1231.

López-Vicente M, Poesen J, Navas A, Gaspar L. 2013. Predicting runoff and sediment connectivity and soil erosion by water for different land use scenarios in the Spanish PrePyrenees. *Catena* 102: 62–73.

López-Vicente M, Nadal-Romero E, Cammeraat EJH. 2016. Hydrological Connectivity Does Change Over 70 Years of Abandonment and Afforestation in the Spanish Pyrenees. *Land Degradation and Development* 28(4): 1298-1310.

López-Vicente M, Álvarez S. 2018. Influence of DEM resolution on modelling hydrological connectivity in a complex agricultural catchment with woody crops. *Earth Surface Processes and Landforms* 43(7): 1403-1415

Llena M, Cavalli M, Vericat D, Crema S. 2018. Assessing landscape changes associated to anthropic disturbances by means of the application of Structure from Motion photogrammetry using historical aerial imagery. *Rendiconti Online Società Geologica Italiana* 46: 74-81.

Llorens P. 1991. *Resposta hidrològica i dinàmica de sediments en una petita conca perturbada de muntanya mediterrània*. Tesis doctoral. Universitat de Barcelona, Barcelona.

MacDonald D, Crabtree JR, Wiesinger G, Dax T, Stamou N, Fleury P, Gutierrez-Lazpita J, Gibon A. 2000. Agricultural abandonment in mountain areas of Europe: Environmental consequences and policy response. *Journal of Environmental Management* 59: 47-69.

Macklin MG, Lewin J, Woodward JC. 2012. The fluvial record of climate change. *Philosophical Transactions of The Royal Society* 370: 2143-2172.

Micheletti N, Lane SN, Chandler JH. 2015. Application of Archival Aerial Photogrammetry to Quantify Climate Forcing of Alpine Landscapes. *The Photogrammetric Record* 30: 143-165.

Ortíz-Rodríguez AJ, Borselli L, Sarocchi D. 2017. Flow connectivity in active volcanic areas: Use of index of connectivity in the assessment of lateral flow contribution to main streams. *Catena* 157: 90-111.

Persichillo MG, Bordoni M, Cavalli M, Crema S, Meisina C. 2018. The role of human activities on sediment connectivity of shallow landslides. *Cartena* 160: 261–274.

Preti F, Guastini E, Penna D, Dani A, Cassiani G, Boaga J, Deiana R, Romano N, Nasta P, Palladino M, Errico A, Giambastiani Y, Trucchi P, Tarolli P. 2018. Conceptualization of Water Flow Pathways in Agricultural Terraced Landscapes. *Land Degradation and Development* 29(3): 651-662.

Quiñonero-Rubio JM, Boix-Fayos C, de Vente J. 2013. Desarrollo y aplicación de un Índice Multifactorial de Conectividad de Sedimentos a escala de cuenca. *Cuadernos de Investigación Geográfica* 39(2): 203-223.

Smith MW, Vericat D. 2015. From experimental plots to experimental landscapes: topography, erosion and deposition in sub-humid badlands from Structure-from-Motion photogrammetry. *Earth Surface Processes and Landforms* 40: 1656-1671.

Tague C, Band L. 2001. Simulating the impact of road construction and forest harvesting on hydrologic response. *Earth Surface Processes and Landforms* 26(2): 135-151.

Tarolli P, Preti F, Romano N. 2014. Terraced landscapes: From an old best practice to a potential hazard for soil degradation due to land abandonment. *Anthropocene* 6: 10-25.

Tarolli P, Sofia G. 2016. Human topographic signatures and derived geomorphic processes across landscapes. *Geomorphology* 255: 140-161.

Van Dijk, AIJM, Bruijnzeel LA, Vertessy RA, Ruijter J. 2005. Runoff and sediment generation on bench-terraced hillsides: measurements and up-scaling of a field-based model. *Hydrological Processes* 19: 1667-1685.

Van Nieuwenhuyse BHJ, Antoine M, Wyseure G, Govers G. 2011. Pattern-process relationships in surface hydrology: hydrological connectivity expressed in landscape metrics. *Hydrological Processes* 24: 3760–3773.

Vericat D, Smith MW, Brasington J. 2014. Patterns of topographic change in sub-humid badlands determined by high resolution multi-temporal topographic surveys. *Catena* 120: 164-176.

Wemple BC, Swanson FJ, Jones JA. 2001. Forest roads and geomorphic process interactions, Cascade Range, Oregon. *Earth Surface Processes and Landforms* 26(2): 191-204.

Wheaton JM, Brasington J, Darby SE, Sear D. 2010. Accounting for Uncertainty in DEMs from Repeat Topographic Surveys: Improved Sediment Budgets. *Earth Surface Processes and Landforms* 35: 136-156.

Wohl E. 2017. Connectivity in rivers. *Progress in Physical Geography* 41(3): 345–362.

Wohl E, Brierley G, Cadol D, Coulthard TJ, Covino T, Fryirs KA, Grant G, Hilton RG, Lane SN, Magilligan FJ, Meitzen KM, Passalacqua P, Poeppl RE, Rathburn SL, Sklar LS. 2018. Connectivity as an Emergent Property of Geomorphic Systems. *Earth Surface Processes and Landforms* 44: 4-26.

# CHAPTER 6

## GEOMORPHIC RESPONSES TO MULTI-SCALE DISTURBANCES IN A MOUNTAIN RIVER: A CENTURY OF OBSERVATIONS

# CHAPTER 6: Geomorphic responses to multi-scale disturbances in a mountain river: a century of observations

This chapter contains the following submitted paper in the journal Catena. JCR-SCI Impact Factor (2018): 3.851. Category: Water Resources; 1st Quartile.

Llena M, Vericat D, Martínez-Casasnovas JA, Smith M. 2019. Geomorphic responses to multi-scale disturbances in a mountain river: a century of observations. *Catena.* (Submitted).

**ABSTRACT:** River channel forms are considered to be in equilibrium when the imposed water and sediment fluxes do not cause a net change in form. Any alteration caused to these conditions will generate a geomorphic response, a disequilibrium imposed by the water and sediment fluxes, which can have different duration and magnitude depending on these. In this paper we analyse the geomorphic response of a mountain river (Upper Cinca River, Central Southern Pyrenees) in relation to multi-scale disturbances during almost a century (i.e. 1927-2015). The integration of multiple geomorphic descriptors (i.e. morphology and topography) and disturbances (i.e. floods, land use changes, dams, embankments and gravel mining activities) allows to better understanding the cause-effect relations and the time needed to the river to reach a new equilibrium after catchment and reach-scale disturbances. Results show that afforestation was the main land use change exhibited between 1957 and 2015, although mainly concentrated during 1977-2015. Annual runoff presented a general negative trend with a wet (1959-1983) and dry period (1983-2015). Extensive gravel mining occurs after flood events, together with channel engineering works as the construction of embankments. These disturbances, together with the construction of three small dams, had a direct impact on lateral connectivity by confining and constraining channels and concentrating flows, resulting in-channel incision and stability. The evolution of the disturbances, process changes and geomorphic descriptors indicated the existence of three phases in the changes of the river channel during the last century. First, a Regime State 1 (before 1927), where the river was potentially in equilibrium. Second, a Transient State (1927-2012) in which the river adjusted to the disequilibrium imposed by multi-scale disturbances acting at different temporal and spatial scales by means of two contrasted channel states. The period 1927-1984 was characterised by having high geomorphic activity and channel incision. The period 1984-2012 was characterised, however, by having a low geomorphic activity, when channel constraining was the dominant process. Finally, a Regime State 2 (after 2012), a period in which we hypothesise that the river may be reaching again a new equilibrium, adjusting to the imposed water and sediment fluxes and channel configuration. According to our observations, the relaxation time, the period needed to reach a new regime state, was around 85 years. The results of the Upper Cinca may be relevant to infer in future fluvial metamorphosis associated to the effects of global change on water and sediment fluxes in mountain catchments, and to assist objective-based rehabilitation measures of rivers subjected to multi-scale disturbances.

**KEYWORDS**: *Fluvial morphology, geomorphic response, gravel mining, floods, land use changes, fluvial metamorphosis.*

## 1. INTRODUCTION

Rivers are dynamic systems in which their channel morphology is determined by the interaction between water and sediment transfers at different temporal scales. Channel form is considered to be in equilibrium when the imposed water and sediment fluxes do not cause a net change in form (Lane, 1955; Richards, 1982; Church, 2006). Ultimately, the quantity and size of the sediments supplied to the channels will determine channel morphology. Any alteration caused to these conditions (e.g. increase/decrease of sediment supply) will generate a morphological adjustment to the new situation; ultimately, a new equilibrium will be reached. In general, the alteration of the equilibrium state of a fluvial system can be naturally or humanly-driven.

River's morphology is sculpted by competent floods, natural short-term (i.e. days) processes (e.g. Schumm, 1965; Newson, 1980; Baker et al., 1988; Stover and Montgomery, 2001) driven by upstream sediment supply and availability, and flow hydraulics. Climate fluctuations may also have an impact on morphology (e.g. Werritty and Leys, 2001; Lane et al., 2007), although they act at a longer temporal scale (i.e. years, decades). These fluctuations control flood and drought-dominated regimes, altering the frequency and magnitude of floods, thus disturbance. For instance, Batalla et al. (2018) recently observed a simplification of the morphology of a Chilean river channel due to the reduction of geomorphic activity caused by a negative trend of rainfall during a period of around 15 years. In the case of the Pyrenees, several authors have stated a significant decrease of mean annual flow during the second part of the last century (e.g. Beguería et al., 2003; Gallart and Llorens, 2004; López-Moreno et al., 2011; García-Ruiz and Lana-Renault, 2011; Buendia et al., 2015; Ollero et al., 2015). Beguería et al. (2003) reported a volumetric runoff reduction of around 30% for the past 50 years in the Pre-Pyrenean region.

Mountain river systems have been historically modified by humans, either by social or economic purposes (e.g. Hooke, 2006; Wohl, 2006); in Mediterranean areas these modifications have been exaggerated since the middle of the last century. Impacts include dam construction (e.g. Williams and Wolman, 1985; Batalla et al., 2004; Vericat and Batalla, 2006), instream gravel mining (e.g. Kondolf, 1994; Surian and Rinaldi, 2003), construction of channel embankments (e.g. Bravard, 1986; Gilvear, 1999;), and land use changes (e.g. Liébault et al., 2005; Nadal-Romero et al., 2013; López-Vicente et al., 2016). The temporal and spatial scales in which human impacts affect to fluvial systems are also variable (e.g. Downs et al., 2013). For instance, instream gravel mining (example of reach-scale impacts) has a rapid and localised impact on channel morphology that may cause subsequently channel adjustments upstream and downstream (e.g. Kondolf, 1994; Rinaldi et al., 2005); while land use changes (example of catchment-scale impacts) are more extend disturbances or influences (e.g. Murgatroyd and Ternan, 1983; Livers et al., 2018), and require longer temporal scales to the river to react or adjust. Specifically, dams cut the continuity of sediment transport and may alter flow and flood regimes (e.g. Williams and Wolman, 1985, and the example of the large Ebro river in Vericat et al., 2006b), what ultimately will affect river channel morphology by, for instance, vegetation encroachment, channel incision and narrowing (e.g. Kondolf, 1997; Liébault and Hervé, 2002; Aguiar et al., 2016). Instream gravel mining involves the removal of riverbed sediments, directly altering channel geometry and bed-level lowering, locally, upstream and downstream. For instance, Surian (2006) reported an incision up to 5 m along the Brenta river on the north of Italy. Additionally, in several occasions, channel embankments are built up after the extraction of sediments, reducing lateral connectivity and concentrating flows. Consequently, the balance between sediment availability and transport capacity is interrupted, with subsequent changes on to the form of the channel.

During the second half of the 20th century almost all mountain areas in the Mediterranean region suffered significant land use changes driven by agricultural abandonment as a consequence of pronounced depopulation (e.g. García-Ruiz et al., 1996; MacDonald et al., 2000; Taillefumier and Hervé, 2003; Mottet et al., 2006). This abandonment induced an increase of the vegetation cover, both by afforestation by public administrations (e.g. García-Ruiz and López-Bermúdez, 2009) and by natural recolonization (e.g. Keesstra et al., 2009). Reforestation implies an increase in rainfall interception (e.g. Gallart et al., 1997; Llorens et al., 1997) and a reduction in the generation of direct runoff, at least for rainfall events of high frequency. This, combined with the replacement of cereal crops by dense scrub on steep slopes, has led to more moderate hydrological responses, accompanied by a clear decrease in erosion and sediment supply (e.g. García-Ruiz and Ortigosa, 1988; García-Ruiz et al., 1996; López-Moreno et al., 2009). Buendia et al. (2015), for instance, concluded that climate change and afforestation reduced sediment yield by around 8% in a 65 $km^2$ basin also in the Pre-Pyrenees. This sediment deficit may contribute to the adjustment of river channels, causing a series of changes in their channel form and morphology(e.g. Liébault et al., 2002; Gallart and Llorens, 2004; Beguería et al., 2006; López-Moreno et al., 2009; García-Ruiz et al., 2010).

Therefore, channel responses are often the consequence of multiple stimuli (e.g. Downs et al., 2013), which their segregation being a challenging task (e.g. González del Tánago et al., 2016). Within this context, the objective of this paper is to analyse the geomorphic responses of a mountain river reach (Upper River Cinca, Southern Pyrenees) in relation to natural and human disturbances or influences during almost a century: the period 1927-2015. The morphological units of a 12 km braided reach were mapped on 8 occasions, encompassing a period of 88 years. Additionally, topographic changes in the reach were also obtained. Finally, the evolution of channel morphology and topography is analysed in relation to floods, land use changes, hydroelectric infrastructures, river embankment and gravel mining activities. There are several studies trying to link geomorphic adjustments to multiple human disturbances using a data set encompassing almost a century such as the one presented in this paper (e.g. Hoyle et al., 2008; Zilian and Surian, 2012; Bollati et al., 2014; Scorpio and Rosskopf, 2016; Downs and Piégay, 2019). The present work not just represents a very good example of linking geomorphic adjustments and human disturbances, but also an original contribution from a methodological point of view. On one hand, the quite novelty application of Structure from Motion (SfM) to historical imagery (e.g. Bakker and Lane, 2017; Llena et al., 2018) allows to extract channel topography per each of the study periods. On the other hand, the use of statistical tools to find trends and breakpoints in the data sets allow to infer on the existence of significant trends and breakpoints in the temporal evolution of the geomorphic descriptors and disturbances. These analyses allows a better understanding of how the river adjust during the relaxation time needed to the river to reach a new equilibrium after the disequilibrium caused by multiple disturbances. Results may be relevant to infer in future fluvial metamorphosis associated to the effects of global change on water and sediment fluxes in mountain catchments.

## 2. STUDY AREA

The Upper River Cinca catchment has an area of 848 $km^2$ and is located in the southern Pyrenees (Figure 1A) with a maximum altitude of 3375 m a.s.l. (Posets peak). The river flows into Mediano reservoir (built in 1974 with a capacity of 435 $hm^3$, Figure 1), where the study area reach the minimum elevation (522 m a.s.l.). The study reach is 12 km in length and is located in the lower part of the catchment, between the villages of Escalona (upstream part of the reach) and Ainsa (downstream part; Figure 1B). The average channel slope in the reach is 0.7%; it is located downstream of a breakpoint in the longitudinal profile in which the valley opens out and the

slope reduces. Morphologically, the reach is highly dynamic with multiple active channels, different typologies of bars and vegetation cover (Figure 1B and Figure 2B). Average active channel width is around 200 m, while water depth at mean flow averages 0.3 m. Sediments are very poorly sorted, ranging from sands to large boulders (i.e. 0.5 to 2000 mm). The median size of the surface sediments is 67 mm, so the upper Cinca can be considered to be a gravel-bed river, with a notable presence of cobbles and even coarser materials (see more details in Béjar et al., 2017 and Béjar et al., 2018). Mean long-term discharge in the reach is 29 $m^3/s$ (period 1959-2015). Frequent floods (recurrence interval of 2 years, i.e. $T_2$) have a water discharge magnitude of 250 $m^3/s$, while less frequent floods ($T_{10}$) are around 530 $m^3/s$ (based on the analyses presented in Llena, 2016).

During the study period (1927-2015), the study reach has suffered several natural and human disturbances or influences that have affected directly or indirectly the morphology of the channel. These disturbances include high magnitude floods, land use changes, hydroelectric infrastructures (e.g. dams), instream gravel mining and construction of channel embankments (see examples on Figure 1C-E).

## 3. MATERIALS AND METHODS

### 3.1. Runoff and flood frequency and magnitude

Flow and flood regimes were characterized from the available water discharge series (1959-2015) of the Ebro Water Authorities (CHE) at the Escalona (EA051) gauging station, located within the study reach (see Figure 1A). Three variables were analysed at an annual scale: (a) runoff in $hm^3$; (b) annual maximum daily discharge ($Q_c$) in $m^3/s$; and (c) instantaneous maximum discharge ($Q_{ci}$) in $m^3/s$. In general, runoff was used to study total water discharge variability and trend during the study period, while $Q_c$ and $Q_{ci}$ were used to analyse flood frequency and magnitude. $Q_{ci}$ data were not available for the period 1959-1996. In order to populate missing data, a relationship between $Q_c$ and $Q_{ci}$ was established (i.e. $Q_{ci} = 1.73 \cdot Q_c - 1.57$, $r^2 = 0.83$, $p < 0.01$, n= 17) for those periods in which both data were available (i.e. 1994-2015). Around the 30% of the data (n = 7) were used to validate the aforementioned statistical relationship. The residual of these data provide a mean absolute error of 42 $m^3/s$, a relatively small value when compared with the magnitude of the floods analysed (e.g. representing the 10% of the $T_5$). Note that no hydrological data was recorded during the period 1993-1995, consequently no data was used for these years.

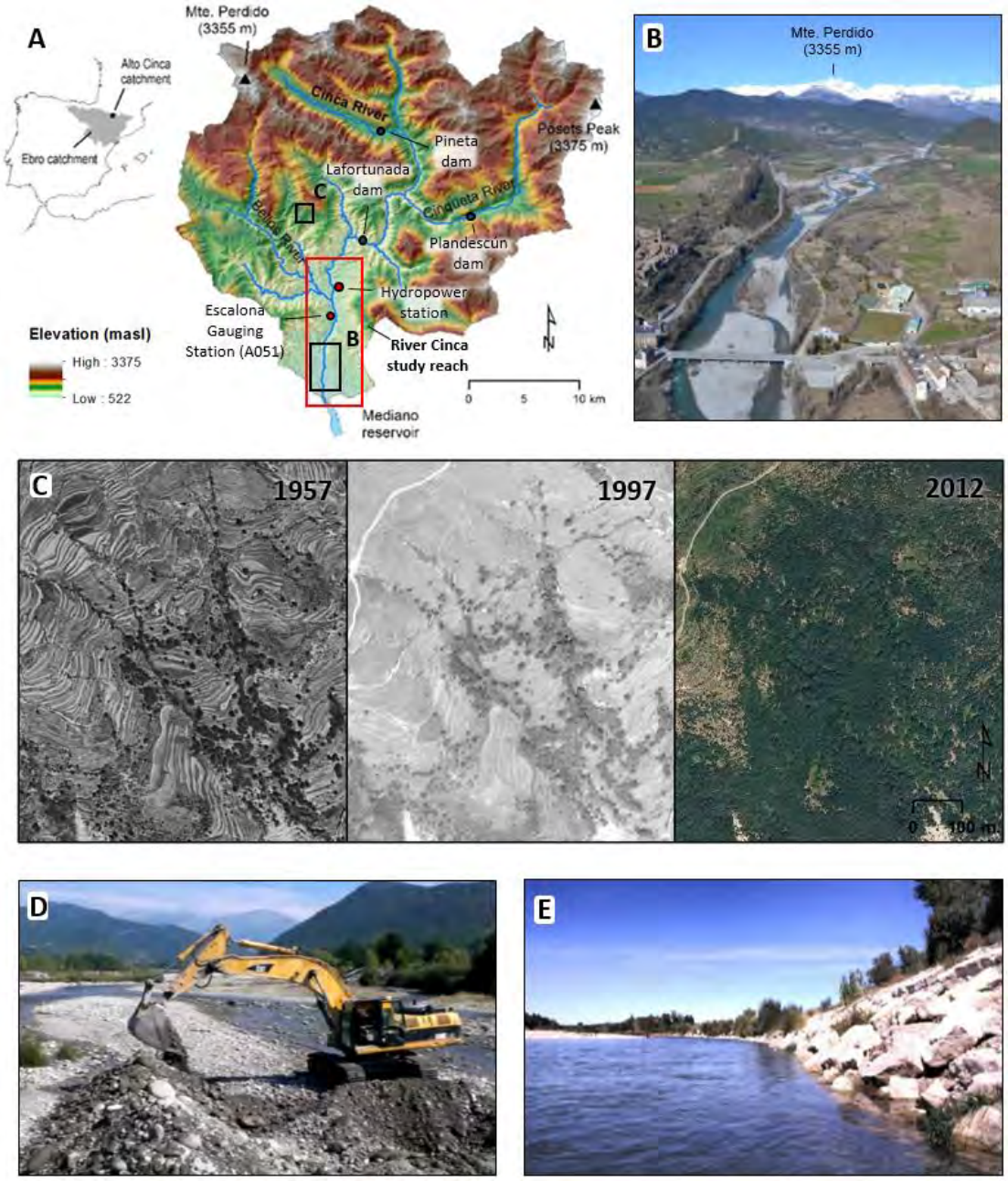


**Figure 1**. **A**. Location of the study reach within the context of the Upper Cinca and Ebro catchments, and the Iberian Peninsula. **B**. Oblique aerial picture of the lower part of the Upper Cinca (study reach). **C**. Aerial photos showing an example of changes on land cover between 1957, 1977 and 2012. Afforestation was the dominant process. **D**. Example of a localised instream gravel mining performed in the middle part of the study reach during the year 2014. **E**. View of the lateral embankment on the left bank of the lower part of the study reach.

## 3.2. Gravel mining and channel embankments

Gravel mining data were obtained from the CHE inventory. Only data from 1974 to 2015 were available, and the type and quality of the information were variable. Mainly, between 1974 and 1990 only information regarding to the number and location of the requested extractions were available. Data on the requested extracted volume were also available from 1990 to 2015; however, these volumes should be treated with caution as no further validation of volumes

actually extracted was possible. Even so, the number of extractions requested as well as their volumes can be used qualitatively to identify the periods when the river channel was subjected to more human disturbances or influences. In the same way, no data on channel embankment construction were available and only qualitative information extracted from local sources, personal communications and from the interpretation of the aerial photos were used.

### 3.3. Aerial photos: orthomosaics, point clouds and land use maps

A total of 8 series of aerial photos were used: 1927, 1957, 1977, 1984, 1997, 2006, 2012 and 2015 (see Table 1 in the supplementary materials for further specific technical information on these). The selection of these series was based on their availability, quality (mainly based on the resolution) and overlap between individual photos (which allows stereo pairs). Additionally, aerial photos from 2015 were taken as part of the MorphSed research project (see Vericat et al., 2016), and were considered to represent the contemporary fluvial morphology. In the case of 1927, the representation of the study area was reduced to 6 km (around the 50% of the total study reach) due to the unavailability of information for the entire area. Even so, the results were expressed in percentage values and the 6-km length was considered representative to show the general trend for the entire reach due to the same distribution of morphological units

Three types of information were obtained: (i) orthomosaics and (ii) point clouds of the study reach; and (iii) land use maps of the whole Upper Cinca catchment. Each survey was used for the orthomosaics, while topography was only extracted for the series in which overlapping between photos was sufficient for 3D reconstruction: 1957, 1977, 1984 and 2015 (Table 1 in the supplementary materials). Finally, the series of 1957, 1977 and 2012 were used to extract a land use map for each period and for the entire catchments. Specific details of each type of information are provided in the supplementary materials section.

### 3.4. Digital Elevation Models (DEM), longitudinal profiles and topographic changes

Point clouds were filtered and regularized with the main purpose to reduce ground elevation uncertainty associated to other covers (e.g. vegetation) or punctual errors (e.g. noise or outliers). The first step consisted in the elimination of outliers by means the Statistical Outlier Filter (SOR) tool available in Cloud Compare 2.6.2. All points located in vegetated areas were then removed using the results of the supervised image classification (see section 3.5). Additionally, the data within the wet channel were also removed. Next, point clouds were regularized by means of the ToPCAT algorithm (Brasington et al., 2012; Rychkov et al., 2012). A grid size of 5mx5m was selected, and the minimum elevation value in each cell was used to estimate the ground elevation. This resolution was set based on the potential extension and magnitude of the impacts in relation to the errors reported above. A Triangular Irregular Network (TIN) for each time series was created based on these elevations, and subsequently transformed to a raster data set of 5 m resolution meanwhile linear interpolation, obtaining the final Digital Elevation Model (i.e. DEM).

Topographic changes were analysed in two different ways. First, the comparison of all time-series for which topographic data was available (Table 1 in thesupplementary materials) was carried out by looking at the differences between longitudinal profiles. The mean elevation of the dry channel at 1-m cross-sections was calculated for each survey, selected because dry areas were subject to minimal errors and are only minimally affected by differences in vegetation cover and wet areas between series (these data removed before the TIN was generated). Longitudinal profiles were extracted using ArcMap 10.5©. Additionally to this, the first (i.e. 1957) and the last (i.e. 2015) DEMs were directly compared through a DEM of Difference (DoD),

providing a gross estimate of the net changes in the study reach during the total study period. Although the errors associated with the 1957 DEM were significant, the low error of the 2015 DEM provided an optimal condition to estimate long-term (58 years) topographic changes within the reach. A minimum Level of Detection (i.e. minLoD) of 2 m was established to reflect DoD uncertainty. This value was calculated with a simple propagation of the errors of the DEMs through the square root of the sum of the square of each error (e.g. Brasington et al., 2000). When the topographic changes are lower than the minLoD, these are considered uncertain and not taken into account in the analyses, therefore, only the changes higher than the minLoD were mapped.

### 3.5. Geomorphic units and complexity of the channel pattern

The literature provides multiple criteria to identify and define geomorphic units, as well as to describe these (e.g. Church, 1972; Smith, 1978; Church and Jones, 1982; Pedraza, 1996; Fryirs and Brierley, 2013). In this paper we apply the framework of Wheaton et al. (2015) to map and classify fluvial landforms based on tiered hierarchical taxonomy from position, shape, specific morphology and vegetative characteristics of geomorphic units. This method allows progression from a first tier into lower tiers, filtering the range of possible choices to a much smaller list of possible units. In this paper this approach was used with some adjustments due to the limitation of the resolution and accuracy of the historical data. The classification provided by the first tier, position, is out of the scope of our work since our analyses were all based on the in-channel morphology. In the same way, it was not possible to define units based on the shape (i.e. concave or convex).

Our analyses concentrated on defining and identifying key attributes to differentiate the geomorphic units present in the study area. The geomorphic units defined were: fluvial channels or wet channels, longitudinal bars, lateral bars, diagonal bars, confluence bars, islands and levees. The extent of these units and all additional calculations derived from these were influenced by the water discharge conditions at the time of the aerial photos. Therefore, the comparison of the geomorphic maps between periods can lead to biased results when the water discharge is significantly different between periods. The average daily flows recorded on the day when the images were taken were compared in order to analyse the existence of significant differences, indicating that in all cases photographs were obtained with relatively low flow conditions (around the average water discharge), in exception of the 2012 series in which flow was slightly higher but with a minimum influence on the extension of the units as revealed by field observations (Table 1 in the supplementary materials).

Geomorphic units were mapped using ArcMap 10.5© by the combination of manual digitalization and supervised image classification of the respective orthomosaics. The percentage of vegetation cover of the different units was estimated by image classification. The unit was considered stabilised when the percentage of vegetation cover was larger than the 60%. Based on these, stable lateral bars were classified as levees, while stable longitudinal or diagonal bars were classified as islands.

The complexity of the channel pattern was analysed by means of three main sets of variables: (i) active channel width; (ii) braiding indices; and (iii) process-based channel change maps obtained by the intersection of units between periods. Active channel width was defined as the river area encompassed within riparian vegetation limits (e.g. Belletti et al., 2013; Picco et al., 2014). Active channel width and braided indices were calculated based on a series of cross sections (Figure 2) which remained constant for the whole series. Cross sections must be perpendicular to the channel centre line, which its direction may change with time. In our case

we used the same sections for all the study periods in order to compare the evolutions of the targeted variables. Although the results (mainly those for the active channel width) may be affected by some errors due to this fact, the magnitude of these would not interfere on the observed general trends. The spacing (i.e. 300 m) between cross sections was established based on: (i) the average length of the main morphological sequence (riffle-pool) in the study reach (i.e. 200-400 m); and (ii) the average active width of the study reach for the entire analysed period (i.e. 300 m; following Arnaud et al., 2015). A total of 40 cross sections segmented the 12 km length study reach. In this way, the active channel width in each cross section was calculated.

Three different braiding indices were also calculated: (i) the Channel Count Index (CCI) presented by Hong and Davies (1979); (ii) the Channel Length Index (CLI) developed by Mosley (1981); and (iii) the Bar Index (BI) presented by Germanoski and Schumm (1993). These indices were selected based on the braided index review provided by Egozi and Ashmore (2008). The CCI was based on the number of channels in a given section and, consequently, was calculated for each cross section (Figure 2). The CLI (based on the length of the channels) and BI (based on the size and frequency of bars) were calculated based on the channel reach (polygon) between two consecutive cross sections and attributed to the downstream section (Figure 2). These three indices were integrated into a single new index: the Braided Complexity Index (BCI), where each index was normalised based on their maximum value and the average value of the normalised indices was computed (i.e. channel complexity increases as the BCI approaches to 1). The combination of these indices in the BCI was carried out with the main objective of having an integrated view of the three indexes, being able to characterise channel complexity with a single value (of which all the indices are indicative).

Maps of processes were elaborated (e.g. Ham and Church, 2012) by analysing the evolution of each unit between periods. Although these maps integrate all process acting between long periods, they provide the distributions and evolution of the main process (net) reshaping channel morphology between the study years. Five main categories of processes were established: sedimentation, constraining, lateral erosion, in-channel erosion and areas which do not experimented any change. These categories were obtained by intersecting the geomorphic maps of two study periods. For instance, if a given pixel in the first period represented the wet channel and this changed to any class of bar in the second period, the main process in this pixel was sedimentation. Constraining was the process attributed to the geomorphic units that became vegetated. Lateral erosion describes areas that in the first period were not classified as geomorphic unit (i.e. out of the active channel boundary), but they were during the second period; meanwhile in-channel erosion describes areas that pass from geomorphic units to channel.

Finally, channel staticity was also analysed by the variation of the position of the wet channel in probability terms. The layers occupied by the wet channel in each survey were intersected; areas classified as wet in all surveys were assigned a high probability of staticity (100%), i.e. a potential indication of incision and lateral disconnectivity. The probability is reduced proportionally when the pixel is not consistently classified as being wet; a low probability (e.g. 25%) means the position of the wet channel in a given area was variable (i.e. dynamism that will ultimately control the size and the evolution of the geomorphic units).

Note that maps of the entire reach cannot be presented due to its length and the space-limitation, for this reason the maps of the results are limited to 2.5 km long representative

subsection located in the lower part of the study reach (Figure 2B), while all general data or analyses are always presented for the entire reach (i.e. 12 km).

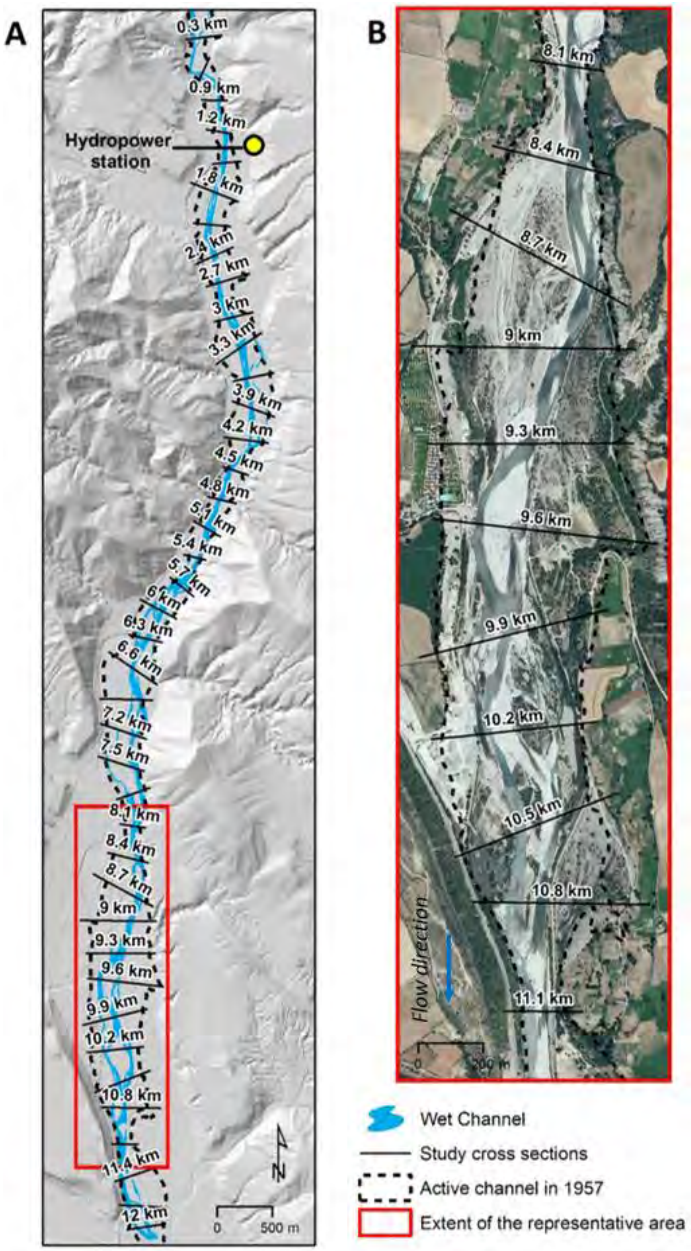


**Figure 2. A**. Schematic view of the study reach segmented by the study cross sections (300 m spacing). Note that the wet channel polygon (blue), active channel width in 1957 (dotted polygon) and location of the Laspuña hydropower station were also presented. **B**. Zoom showing a representative reach that will be used in the rest of the paper when maps are presented. Note that (i) the entire reach cannot be presented due to its length and the space-limitation, and (ii) the rest of the figures and analyses are presented for the entire reach, only maps are limited to this extension.

## 3.6. Statistical analyses

The temporal trends of the data were statistically analysed with two main objectives: (i) to identify significant breakpoints on the series, and (ii) to analyse the significance for the general trends and for the periods defined by the breakpoints (before and after breakpoints) in the case of their existence (significance).

To detect potential breakpoints in the data sets, the Change Point Model procedure (Hawkins et al., 2003; Hawkins and Zamba, 2005) was performed. It considers all possible divisions of data in two consecutive sequences and compares them through a t-test of the mean value of the two periods. The non-parametric Mann–Kendall test (Mann, 1945; Kendall, 1975) was applied to check for the significance of the trends, both general and the periods defined by the breakpoints. The Mann-Kendall's statistic (τ) detects monotonic increases or decreasing trends in a dataset by comparing differences between successive values. These analyses were performed to the following time series data sets: total runoff and maximum discharge, number and quantity of gravel mining, and channel width and Braided Complexity Index. Statistical analysis were performed in the R environment by the software RStudio (v 1.2. 1335).

# 4. RESULTS AND DISCUSSION

## 4.1. Reach and catchment scale disturbances

### 4.1.1. Global changes

Land use maps of the Upper Cinca catchment show a clear trend towards afforestation. Figure 3A shows that the forest cover increased from 34% of the total surface in 1957 to 47% of the total surface in 2012. Meadow decreased from 36% in 1957 to 21% in 2012, while the proportion of bare surfaces remained very similar, from 30% in 1957 to 32% in 2012. Afforestation was mainly concentrated in the period 1977 to 2012. The changes observed between 1957 and 1977 were minimum, from 34% to 37%. During this period, however, the area occupied by meadows increased from 36% to 41%, while bare soil areas decreased from 30% to 22%. These changes are probably attributed to the first phase of land abandonment, in which the abandoned field crops started to be colonized by meadows and small bushes before being covered by forest (e.g. v in Figure 3B). Several studies have observed a reduction of sediment production and connectivity in mountain Mediterranean catchments during the 20th century due to afforestation (e.g. Piégay et al., 2004; Keesstra et al., 2009; García-Ruiz and Lana-Renault, 2011; Nadal-Romero et al., 2013; Buendia et al., 2016; Quiñonero-Rubio et al., 2016; Llena et al., 2019). Our results are within the range reported in other Mediterranean mountain catchments located in the headwaters of the Ebro basin (NE of the Iberian Peninsula). For instance, Gallart and Llorens (2004) reported an average increase of 21% for the Ebro headwaters (1970-1991) while Buendia et al. (2016) obtained an increase of 19% (1957-2009) in the Ribera Salada, an upland meso-scale (102 $km^2$) mountainous Mediterranean catchment in the Pre-Pyrenes. In terms of the spatial distribution of the land use changes (Figure 3A), the increase of the forest cover is mainly located in the lower parts of the valley and terraced slopes that were abandoned (iv, v and vi in Figure 3B), and in sedimentary active areas that were stabilized by vegetation either in the upper parts of the catchment (i.e. erosional features) or in the valley bottom (i.e. active floodplains; see i, ii, and iii in Figure 3B). These patterns have a direct effect in reducing sediment supply and thus sediment fluxes downstream.

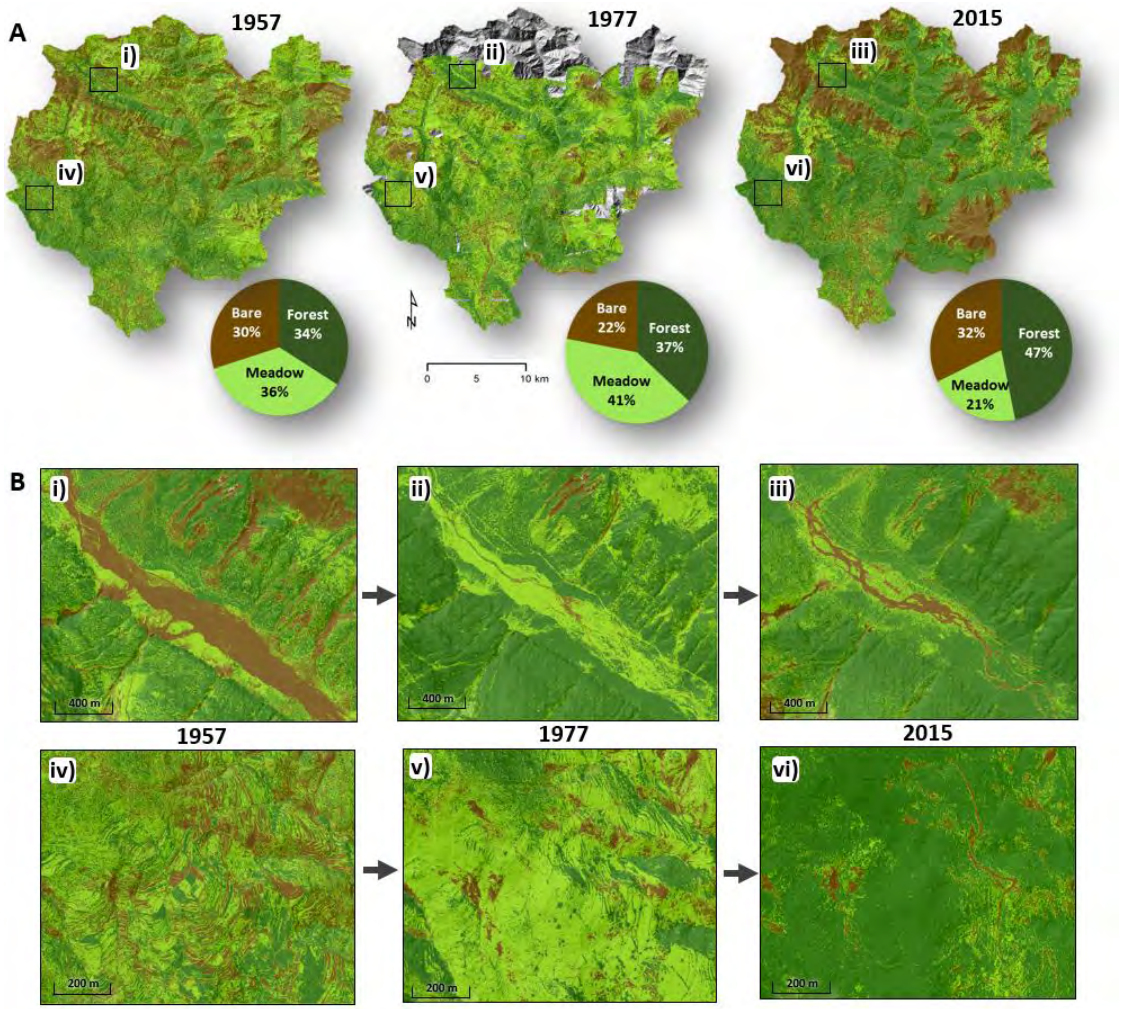


**Figure 3. A**. Land use maps of the Upper Cinca catchment for the 1957, 1977 and 2015 years. Pie charts representing the % of land cover classes (i.e. forest; meadow and bare) in relation to the whole Upper Cinca catchment for the 1957, 1977 and 2015 years. **B**. Zoom in some catchment areas in which afforestation has been intensive during the study period. i) and ii) correspond to the orthomosaics and land cover maps of the years 1957 and 2015 of the upper reach of the River Cinca in the Pineta Valley. Note that the constraining of active geomorphic units, lateral alluvial fans and tributaries can be osberved. iii) and iv) correspond to orthomosaics and land cover maps of the years 1957 and 2015 near the abandoned village of Ceresuela (west part of the catchment). Note that afforestation suffered after farm abandoning during the 1960's decade can be observed.

### 4.1.2 Hydroelectric power generation

The catchment has been heavily regulated since 1923 with the main objective of hydroelectric power generation, as with many such of mountain rivers. Specifically, 3 small dams impounding 1.55 $hm^3$ and 58 km of canals and diversions were constructed during the period compressed between 1918 and 1965 (Galán, 2012). The Pineta reservoir has a storage capacity of 0.3 $hm^3$ (built in 1923); it is located in the headwaters of the River Cinca and the catchment area upstream from the dam is 74 $km^2$ (Figure 1). The Plandescún reservoir (1934) has a storage capacity of 0.9 $hm^3$ (located in the Cinqueta tributary; 156 $km^2$), while the Laspuña Dam is located in the mainstem, 7 km upstream the upstream end of the study reach (521 $km^2$), built in 1965 with a capacity of 0.35 $hm^3$. Although dams cut the transfer of water and sediments, the Laspuña Dam, the one impounding more catchment area, has a wigged gates that, although impound low flows be transferred through the canal network of canals, they are open during

floods facilitating the continuity of the water discharge and sediment transport. The study reach is subjected to daily rapid water discharge fluctuations (hydropeaks) caused by hydropower generation (see location of the hydropower station in Figure 1). Therefore, the study reach is subjected to two contrasted daily water discharge regimes: (i) a low water discharge regime given by environmental flows released from Laspuña Dam that affects the first 2 km of the study reach, and (ii) the hydropeaking-based regime affecting the lowest 10 km of the study reach, due to the location of the hydropower station (Figure 1A and Figure 2A). The relatively low magnitude of the hydropeaks (peak flow around 25 $m^3/s$) only caused localised channel incision processes observed just downstream from the station with no major implication in terms of reach-scale channel adjustments as the ones analysed in this study. Although the impounded ratio of the dams in the catchment is very low and their particularities, specifically in the case of Laspuña Dam (e.g. wigged gates), water and sediment transfer through these is being affected by such infrastructures and the way they are managed to generate hydropower generation.

### 4.1.3 Instream gravel mining

Figure 4 shows the distribution of gravel mining through the period 1974-2015. The number of requested extractions presented a significant negative trend for this period ($\tau$ = -0.46, p-value = <0.001). Additionally, a significant breakpoint is obtained in 1990 (Figure 4), although the trends of the periods defined by the breakpoint are not significant. The first period (1974-1990) was characterized by a large number of requests. The number of requests generally exceeds the average value for the whole period (10.1 requests/year). The largest number of requests was in 1975 with 34. The second period (1991-2015) shows a clear decrease in the number of requests per year; no years exceeded the average value. The largest value was observed in 2010 (i.e. 10 requests/year). These two periods were related to the wetter and drier periods observed in terms of the annual runoff (specifically described in section 4.2), indicating that the CHE received more applications or requests to extract gravels from the river channel in the wetter period than in the drier period, and also a brief increase in requests after floods. Furthermore, these differences may be also related to different socio-economic needs or rules in river channel managing for this period.

Data on total requested volume per year were only available for the period 1990-2015. In this case there were no statistically significant trends identified, despite that is possible to observe two distinct periods: (i) between 1989 to 2000 when all volumes were below the average value for the whole period (i.e. 80,919 $m^3$/year); and (ii) between 2000 and 2015 when volumes increased with a mean value (i.e. 136,767 $m^3$/year), clearly larger than the average for the whole period, with marked peaks. The largest value of 350,000 $m^3$ was requested in 2003, corresponding to the 18% of the total volume requested in this period. The volume requested in the years 2001, 2003 and 2008, exceed 250,000 $m^3$, represents 48% of the total requested for the whole period (21 years; Figure 4). Our results show a positive relation between gravel mining and flood magnitude, i.e. the CHE received more requests to extract gravels after large floods (e.g. 1982 and 1987; Figure 4). This increase was mainly due to the high quantity of sediment mobilized after large floods. Currently, instream gravel mining works are only approved in projects aimed at improving channel conditions with the objective to prevent, for instance, channel erosion and flooding.

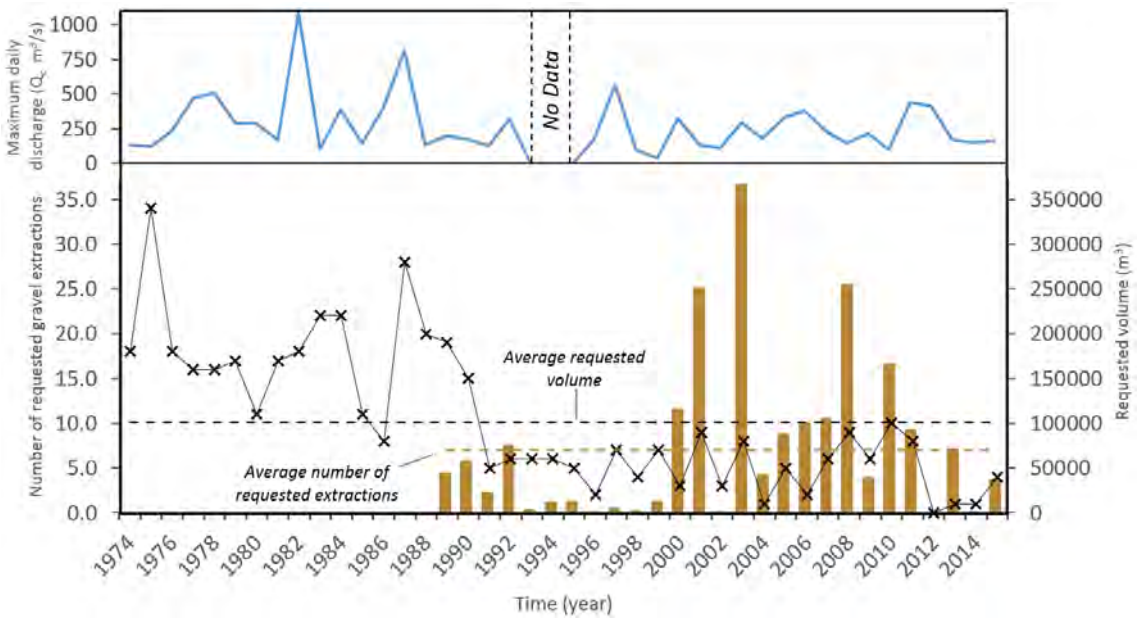


**Figure 4**. Number of requested gravel mining extractions (black crosses in the bottom axis); requested volume to extract (brown bars in bottom axis); and annual maximum daily discharge ($Q_c$, blue line in top axis) for the period 1974-2011. All data were supplied from the Ebro Water Authorities (CHE). The gravel mining data correspond to the total requested extractions made in all the study reach.

#### 4.1.4. Channel embankments

The majority of the lateral embankments (Figure 1) were constructed during the period 1984-1987. This fact was mainly attributed to the damages caused by the flood registered in 1982 ($Q_c$ = 1085 m$^3$/s, $Q_{ci}$= 1647 m$^3$/s; $T_{>100}$). After this flood, the CHE together with local governments decided to construct such channel-infrastructure aiming to prevent lateral bank erosion preserving floodplains for agricultural and other human-related uses and to reduce the possible damages caused by future floods (Hernández, 1991; Rubio, 1994). Within this context, by looking at the aerial photography covering the study reach before and after this period (i.e. 1982-1985), we have quantified that 5.3 and 3 km of embankments were constructed on the left and right banks respectively. As discussed in the following sections, these constructions had a direct effect on channel geometry, decreasing sinuosity significantly, concentrating flows (thereby increasing flow velocity and competence), and decreasing lateral connectivity. These conditions also increase constraining via incision and vegetation encroachment.

### 4.2. Process changes: water and sediment fluxes

Figure 5A shows the evolution of the annual runoff in the Upper Cinca for the period 1959 to 2015. Mean runoff for the whole period was 789 hm$^3$; however, it is highly variable between years, ranging from 216 hm$^3$ in 2010 to 1528 hm$^3$ in 1963. Despite this high variability, the Mann-Kendall test for the whole period (1959-2015) yields a significant downward trend ($\tau$ = -0.49, *p*-value = <0.001). Runoff series were split into two periods according to a significant breakpoint detected in 1978 by the use of the Change Point Model. The first period (i.e. 1959-1978) showed a slight negative trend although it is not considered significant ($\tau$ = -0.15, *p*-value = >0.5); while a more pronounced and significant negative trend ($\tau$ = -0.37, *p*-value = 0.001) is obtained for the period 1978-2015. Figure 5B represents the relative runoff contribution of each year in relation to the mean annual runoff for the whole study period. The average runoff was subtracted from each annual runoff and the results were accumulated. The Mann-Kendall test for all period (1959-2015) show a clear significant negative trend ($\tau$ = -0.57, *p*-value = <0.001),

while the Change Point Model for the entire data identifies a breakpoint in 1983. In that way, two distinct periods can be statistically identified: a wetter (1959-1983) and a drier period (1983-2015). Mann-Kendall test indicates that both periods are characterised by significant negative trends, although the wetter period, with an average runoff of 987 $hm^3$, presented a stronger negative trend ($\tau$ = -0.47, *p*-value = <0.001) in comparison to the drier period ($\tau$ = -0.35, *p*-value = 0.004), which presented an average runoff of 638 $hm^3$. In this way, our results indicate that the annual runoff has decreased around 50% in 58 years, a value very similar to the reported by Gallart and Llorens (2004) for the whole Ebro catchment, and by Bu et al. (2018) in mountainous catchment of the River Juma (NW China). Ruiz-Flaño et al. (1992) and Ruiz-Flaño (1993) also reported the presence of a wet period between 1959 and 1985 in the Aísa Valley (Southern Pyrenees), mainly attributed to land abandonment. This abandonment initially caused an increase of erosion and runoff until the vegetation was stablished, protecting soils, decreasing erosion, thus sediment transport, and interfering on runoff generation. Our results are in agreement with that in the sense that the beginning of the dry period (i.e. 1984-2015) matches with the period of most intense afforestation (e.g. 1977-2015). In terms of flood frequency and magnitude, although our results do not show any statically-based trend, data evidenced as the magnitude and frequency of floods has decreased in the dry period. This observation is also reported for other Pyrenean catchments such as the Aragón (López-Moreno et al., 2014) and the Llobregat and Ter (Gallart et al., 2011).

Figure 5C shows the recurrence interval curves calculated by means of both the average annual maximum daily discharge ($Q_c$) and the instantaneous maximum annual discharges ($Q_{ci}$). We used the $Q_c$ data instead of $Q_{ci}$ in order to avoid uncertainties associated to the reconstruction of the $Q_{ci}$ when data were not available. Based on $Q_c$ curves, a reference recurrence interval value (i.e. $T_5$ = 418 $m^3/s$) was extracted to classify them. Following the method used by the CHE, when the $Q_c$ of registered floods was lower than that associated with a recurrence interval of 5 years we considered these to be 'Ordinary Floods'; while when $Q_c$ values were higher than the $T_5$ value, these are considered 'Extraordinary Floods'. Henceforth only extraordinary floods will be considered, which will be simply called 'floods'. Figure 5D shows both the $Q_c$ and $Q_{ci}$ values for the entire period and the reference water discharge value associated to a $T_5$ ($Q_c$ based). $Q_{ci}$ values (both registered and estimated) are indicated to show the difference between both daily and instantaneous maximum values that in some occasions are significant; such differences ultimately determine the maximum competence of the river.

A total of eight floods occurred during the entire period (i-viii in Figure 5D). The first flood occurred in 1967 with a peak discharge of 637 $m^3/s$ and a return period of 48 years (i in Figure 5D). During the 1970 there was a flood with a $Q_c$ around 608 $m^3/s$ and a return period of 33 years ($T_{33}$; ii in Figure 3D). The next two floods occurred in 1977 and 1978 with daily peak discharges of 472 $m^3/s$ ($T_7$) and 506 $m^3/s$ ($T_{10}$) respectively (iii and iv in Figure 5D). Despite the low magnitudes compared with the other floods, the short interval between these floods may have a direct impact on channel morphology. The largest flood of the whole study period was recorded in November 1982 (v in Figure 5D). This flood had a daily peak flow ($Q_c$) of 1085 $m^3/s$ with a return period of >100 years. This flood is considered, along with the flood of 1907 (see specific paper analysing this flood event in e.g. Balasch et al., 2000; Batalla et al., 2007), one of the highest magnitude flood events of the twentieth century in the Central Pyrenees, causing significant geomorphological and socio-economic impacts. The second highest flood was registered in October 1987 (vi in Figure 5D), with a daily peak flow around 810 $m^3/s$ ($T_{84}$). Finally, two more floods of smaller magnitude were registered in 1997 (562 $m^3/s$; $T_{12}$; vii in Figure 5D) and 2011 (438 $m^3/s$; $T_{5.5}$; viii in Figure 5D).

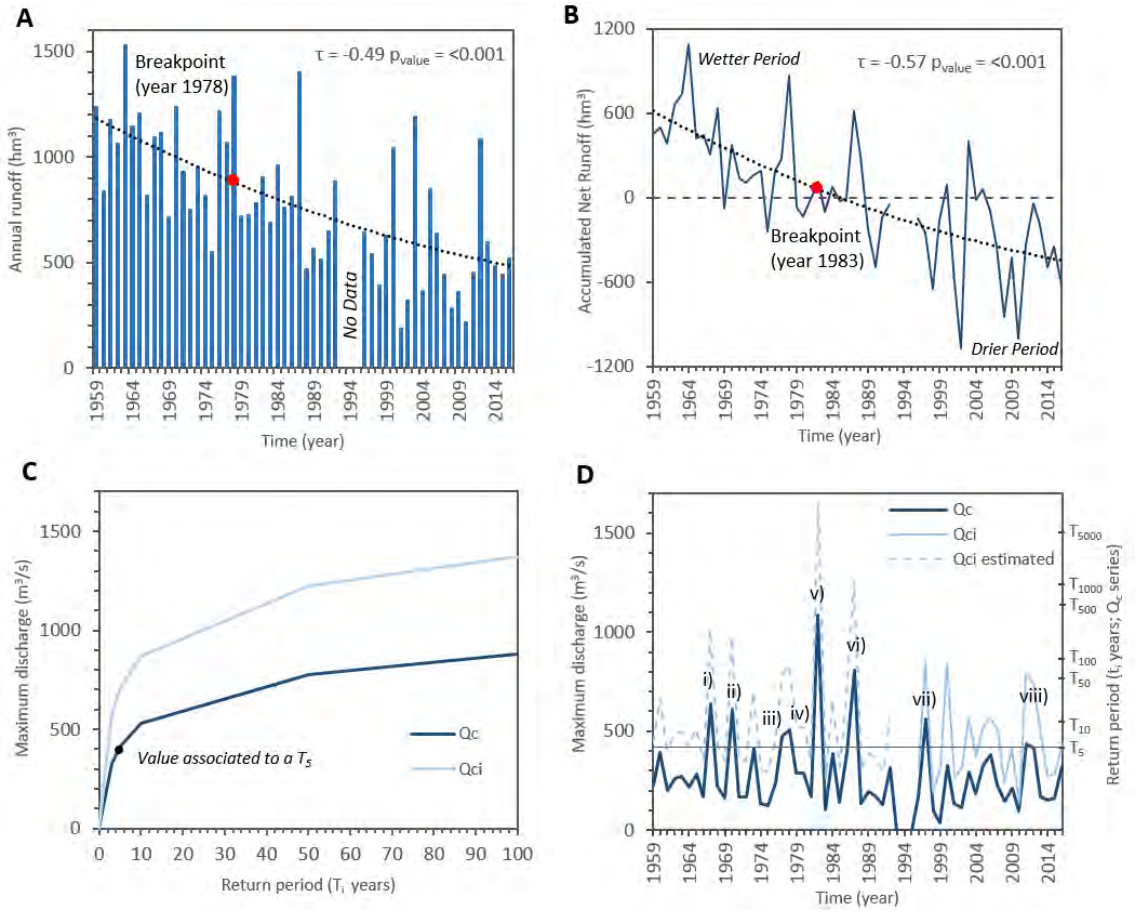


**Figure 5. A.** Annual runoff evolution with the corresponding general trend line, the position of the breakpoint in this and the results of the Mann-Kendall test (Kendall's τ and $p_{value}$). **B.** Accumulated Annual Net Runoff through the study period calculated as the accumulated value of the difference between the annual runoff and the average runoff for the entire period (1959-2016). Note that the general trend line, the position of the breakpoint in this and the results of the Mann-Kendall test (Kendall's τ and $p_{value}$) are also presented. Dry and wet periods were considered when values are below and above 0 respectively. **C.** Relationship between recurrence interval $T_i$ and maximum flow assessed by means of the Gumbell method and using both the annual maximum daily flows ($Q_c$) and annual maximum instantaneous flows ($Q_{ci}$). **D.** $Q_c$ and $Q_{ci}$ data during the study period. Note that the registered and estimated $Q_{ci}$ were differentiated (see text for more details), and that the floods are numbered. Labels (i-viii) mark the floods discussed in the text.

Results of the Mann-Kendall test for the whole maximum discharge data set (1959-2015, Figure 5D) show that there is no statistically significant breakpoint in the data (τ = -0.11, *p*-value = >0.5). Additionally, results indicate as any breakpoint is found to be significant. Despite the non-significant trends, data do point out as largest floods were concentrated in the period 1959-1983 (wetter period), while the period 1983-2015 (drier period) was characterised by fewer floods and, in general, the magnitude of these was smaller.

The increase of forest cover and climate change (e.g. changes on runoff and flood frequency and magnitude) have a direct effect on the hydrological and sediment transport regimes of many Mediterranean mountain catchments (e.g. McDonald et al., 2000; Beguería et al., 2003; Lasanta-Martínez et al., 2005; Bussi et al., 2014; Buendia et al., 2016). The significance and magnitude of these impacts are highly variable due to the inherent variability of rainfall together with the characteristics of the catchments (e.g. land cover and use, geology). Climate shifts have a direct

impact on the magnitude and amount of rainfall that ultimately will have a direct effect on runoff. Despite climate variables were not analysed in the present study for the period analysed, some previous studies near to the study area showed evidence of such changes and its relation with runoff. For instance, Gallart and Llorens (2004) reported a reduction of the mean annual flow of the River Ebro (large catchment, 104 $km^2$) of around 40% in 50 years. They found that this reduction was driven in equal parts by the increase of irrigation, shifting climate and afforestation. In contrast, although Buendia et al. (2016) found an upward trend for temperature and a general but not significant downward trend for precipitation in the Ribera Salada catchment (Southern Pyrenees), the downward trend observed for the annual runoff was less intense when afforestation was not considered in their modelling scenarios. Despite sediment transport data are not available, as discussed, all disturbances in the catchment indicate a clear negative trend (i.e. reduction of sediment fluxes). Reduction of water yield and sediment supply have a direct effect on the evolution of the reach scale morphology, which due to the deficit of sediment will tend to the constraining and incision process.

## 4.3. Geomorphic responses

### 4.3.1. Active channel width

The area occupied by the active channel in the focal reach was reduced during the study period (from 3.48 $km^2$ in 1957 to 2.59 $km^2$ in 2015). The active channel width was reduced by 33% on average (1927-2015; Figure 6A). This reduction was spatially variable as indicated by the ranges on the boxplot presented in Figure 6A. Results from the Mann-Kendall test indicate a significant decrease trend ($\tau$ = -0.93, p-value = 0.002) of the active channel width. In the same way, a significant breakpoint in the general trend is obtained in 1984. The trend in the first period (1927-1984) shows a decrease of the average active channel width through time although not significant ($\tau$ = -0.67, p-value = 0.3), while a negative and significant trend is obtained for the period 1984-2015 ($\tau$ = -0.91, p-value = 0.03). Figure 6B shows the active width along the entire study reach in 1957 and 2015. Note that all distances are stated as downstream of the upper end of the study reach. The maximum change was a width decrease of 80%, observed around 2.5 km downstream, while in absolute terms, the highest reduction was observed at around 10.5 km where the width changed from more than 600 m to almost 200 m (see Figure 7A for an example of such changes). Some sections in the study reach where minimum changes were observed are due to bedrock outcrops (e.g. at 1 km) or due to the natural confinement of the channel (e.g. between 7.5 and 8.5 km).

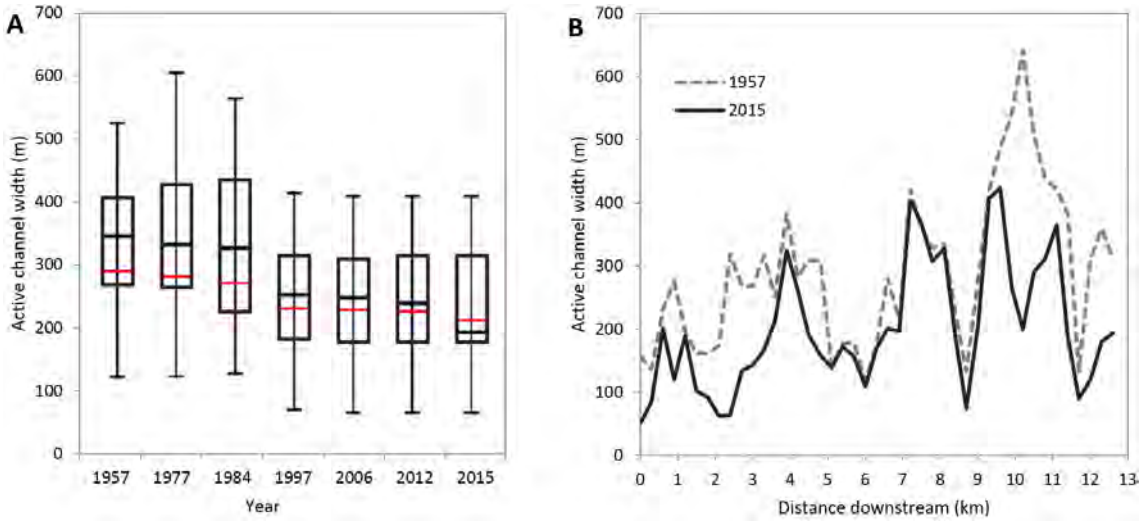


**Figure 6**. **A.** Box-plot of the active channel width during the study period. The central black line represents the median value, the red line represents the mean, the top and bottom ends of the box are the 75th and 25th percentiles respectively; and the upper and lower bars are the maximum and minimum values respectively. **B.** Spatial evolution of the active channel width during the years 1957 and 2015.

Figure 7B shows the spatial evolution of the active channel width through time as a heatmap (the standard deviation of the active width for the whole study period is also presented in Figure 7C). The figure reinforces the two periods statistically found in terms of changes on the mean active width. During the first period (1927-1984) the active width did not exhibit significant variations (Figure 7B), though it increased in specific locations mainly driven by local erosional processes due to the high magnitude floods of 1967 and 1971 (Figure 7B). During the second period (1984-2015), a generalized reduction of the active channel width is observed. Specifically, the most significant changes occurred between 1984 and 1997 (Figure 7B) mainly due to the construction of lateral embankments (as stated above) that reduced lateral connectivity (i.e. structural and functional water and sediment disconnection) increasing channel erosion and vegetation encroachment and constraining. Between 1997 and 2015 the active channel width did not change significantly (Figure 6A). The reduction of the median value between 2012 and 2015 observed in Figure 6A was attributed to the constraining of some of the lateral bars and the localised gravel mining extractions due to flood protection works. The impacts of lateral embankments on the reduction of active geomorphic units have been observed in several studies (e.g. Surian and Rinaldi 2003; Surian et al., 2009; Comiti et al., 2011; Downs et al., 2013; Ibisate et al., 2013; Latapie et al., 2014; Arnaud et al., 2015). Of particular interest is the study by Arnaud et al. (2015) in which the impact caused by the embankments and by-passing actions in the River Rhine (Germany) during the nineteenth century was demonstrated as a main factor for the decrease of the active channel area of around 45% between 1828 and 1872. Similarly in the Santa Clara River in California (USA), Downs et al. (2013) found that the construction of lateral embankments together with other human disturbances or influences (e.g. reservoirs, gravel mining) reduced the mean channel width almost 50% during the second hand of the 20$^{th}$ century.

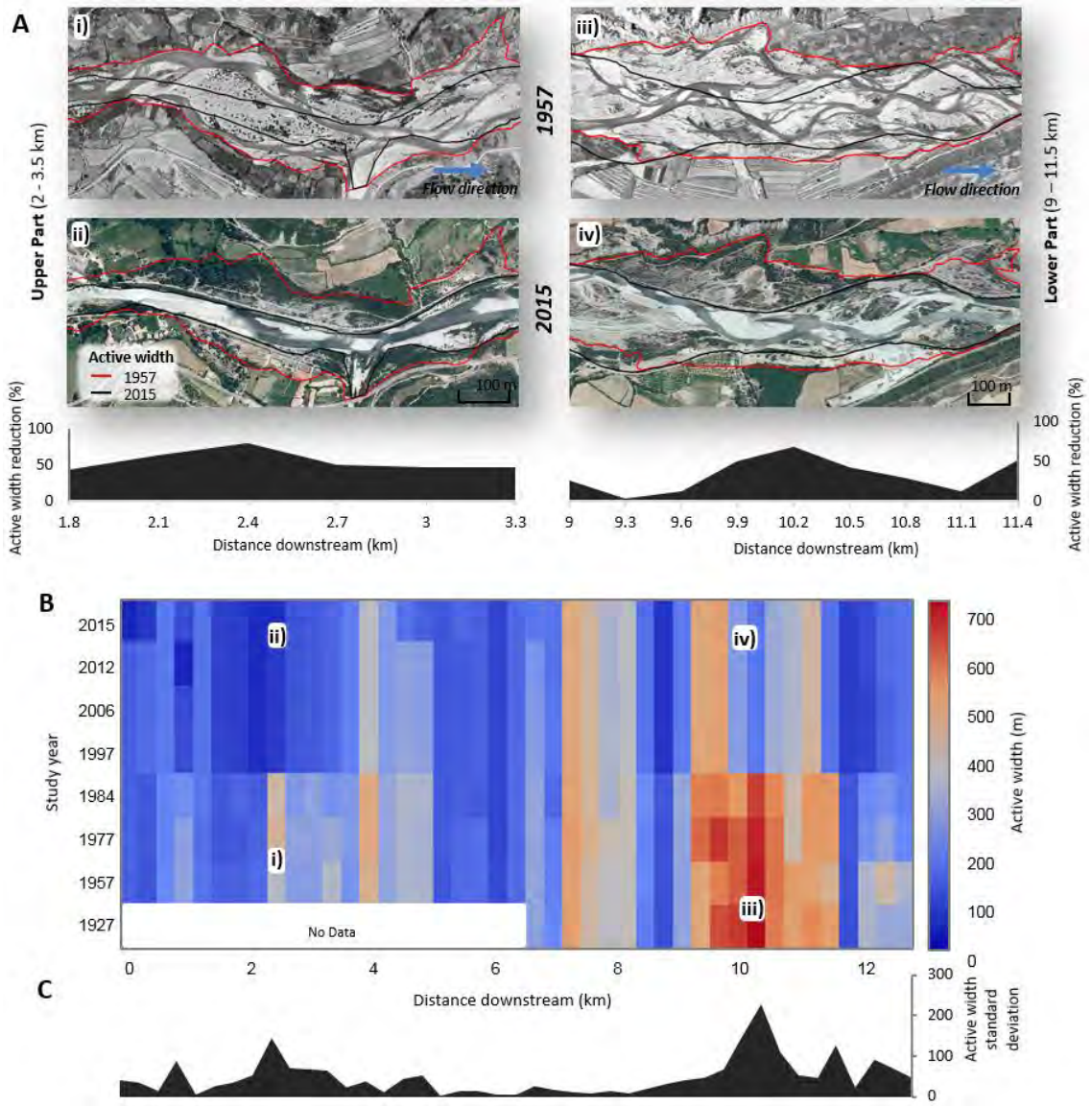


**Figure 7. A.** Orthomosaics of the upper (left) and lower (right) parts of the study reach for 1957 and 2015 years with the corresponding active channel boundaries plotted. Note that the reduction (%) of the active with between both periods is also presented below the othomosaics. **B.** Heatmap of the active channel width for each study year. Note that the lowercase letters (i.e. i, ii, iii, iv) indicate the location of the reaches presented in A. **C.** Standard deviation of the active channel width values for all the time series.

### 4.3.2. Geomorphic units

Figure 8A shows the evolution of the main geomorphic units. Two contrasted periods can be identified following the same statistical breakpoint obtained for the active width. In the first period (1927-1984), although no major changes on the extent of the geomorphic units were observed, results indicated that the average vegetation cover in the geomorphic units increased from 6% to 28%, being mainly concentrated in the period 1977-1984 (Figure 8C). This process has already observed by Beguería et al. (2006) in different rivers of the central Pyrenees, including the study reach, in which the surface occupied by active bars was reduced from 70% in 1929 to 30% in 1981. In the River Ijuez (Central Pyrenees), Sanjuán et al. (2016) observed how the increase of riparian vegetation caused a reduction of the active areas and a decrease of

connectivity between slopes and channels, which triggered channel incision and narrowing. In the case of the Cinca, the increase of vegetation was commensurate with the transformation of some of the central and lateral bars to islands and levees respectively (Figure 8A and 8B). In the second period, between 1984 and 2015, more changes in the number and extent of the geomorphic units were observed. The number and size of the longitudinal and diagonal bars was reduced meaningfully (Figure 8A and 8B). These changes were accompanied by a large reduction in the active area and width as presented above. After 1984, there was only a small increase in vegetation cover in the units until 2015 (from 28% to 33%; Figure 8C). The extent of the confluence bars was also reduced (Figure 8B), probably due to the decrease of the sediment supply from lateral tributaries caused by the reduced erosion rates attributed to an increase of the vegetation cover at the catchment (see section 4.1.1). For instance, in the central right part of Figure 8A, the confluence of the River Forcaz shows a progressive reduction of the extension of the confluence bar until its complete removal by 1984.

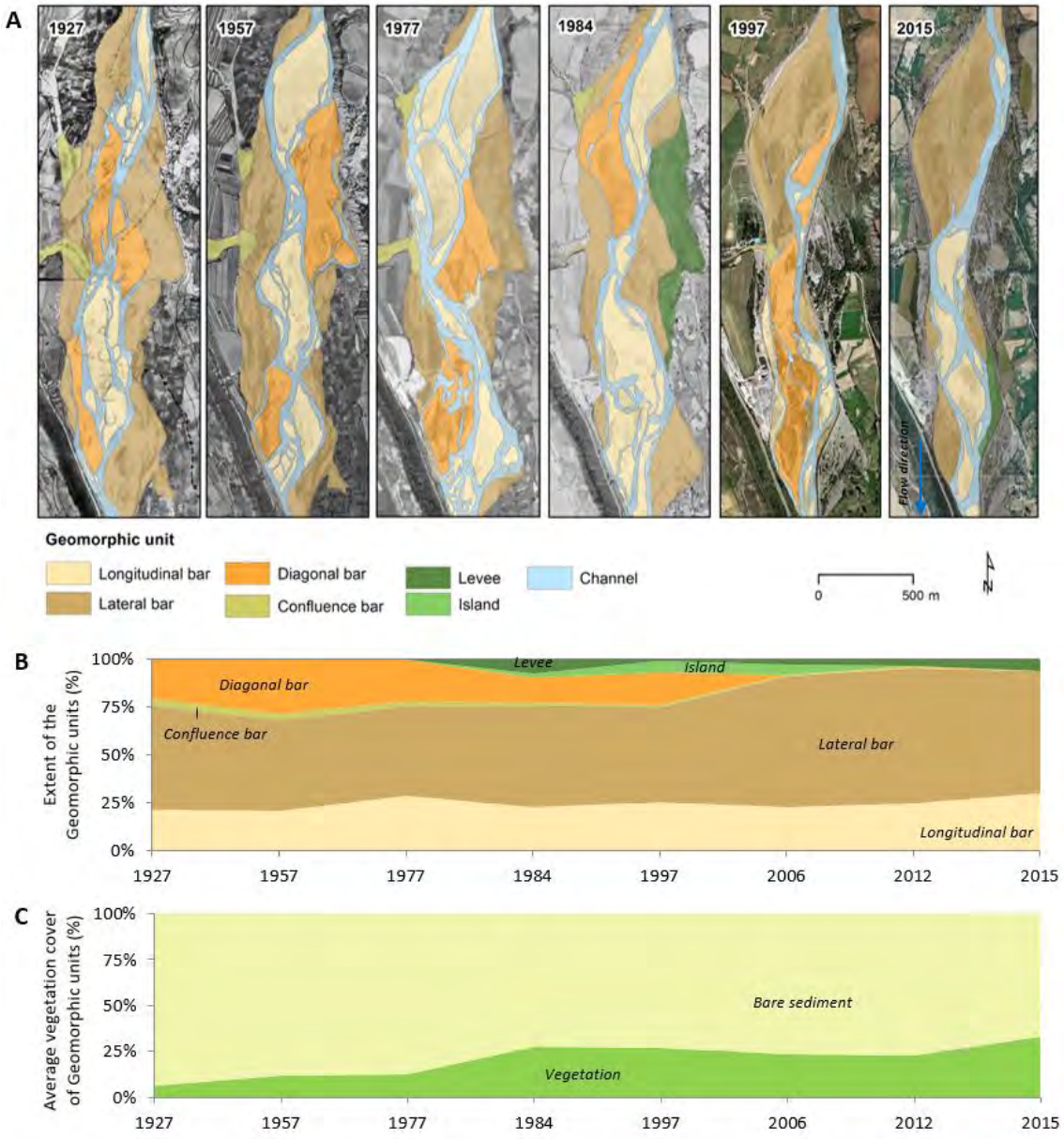


**Figure 8. A.** Evolution of the morphological units in a representative reach (Figure 2) of the Upper River Cinca (1927-2015). **B.** Evolution of the surface occupied per each geomorphic unit in relation to the total active area. **C.** Average vegetation cover in the geomorphic units.

### 4.3.3. Complexity of the channel pattern

A general trend towards a reduction of all the braiding complexity indices was observed during the whole study period (Figure 9). Although the reduction in mean and median values was not pronounced, it is evident that the variability of the values of these indices was reduced through time. A statistical significant negative trend is obtained when these indices are integrated in the Braided Complexity Index (BCI; $\tau$ = -0.57, p-value = 0.06). The Change Point Model identifies a breakpoint in the BCI data in 1977, slightly different the one observed for the active width. The first period (i.e. 1927-1977) shows a positive trend but without statistical significance ($\tau$ = 0.67, p-value = >0.5), exhibiting generally high values and variability (e.g. 1977). After 1977, braided complexity turn down, presenting a negative trend through time, although not being significant ($\tau$ = -0.6, p-value = 0.13; Figure 9C). This reduction is in agreement with the results of Surian (2006), which, in a compilation of morphological response to management in braided rivers in north Italy, reported a significant decrease in the braiding indices and a reduction of the active width. They attributed both decreases to the effects of gravel mining and the construction of embankments during the second half of the twentieth century.

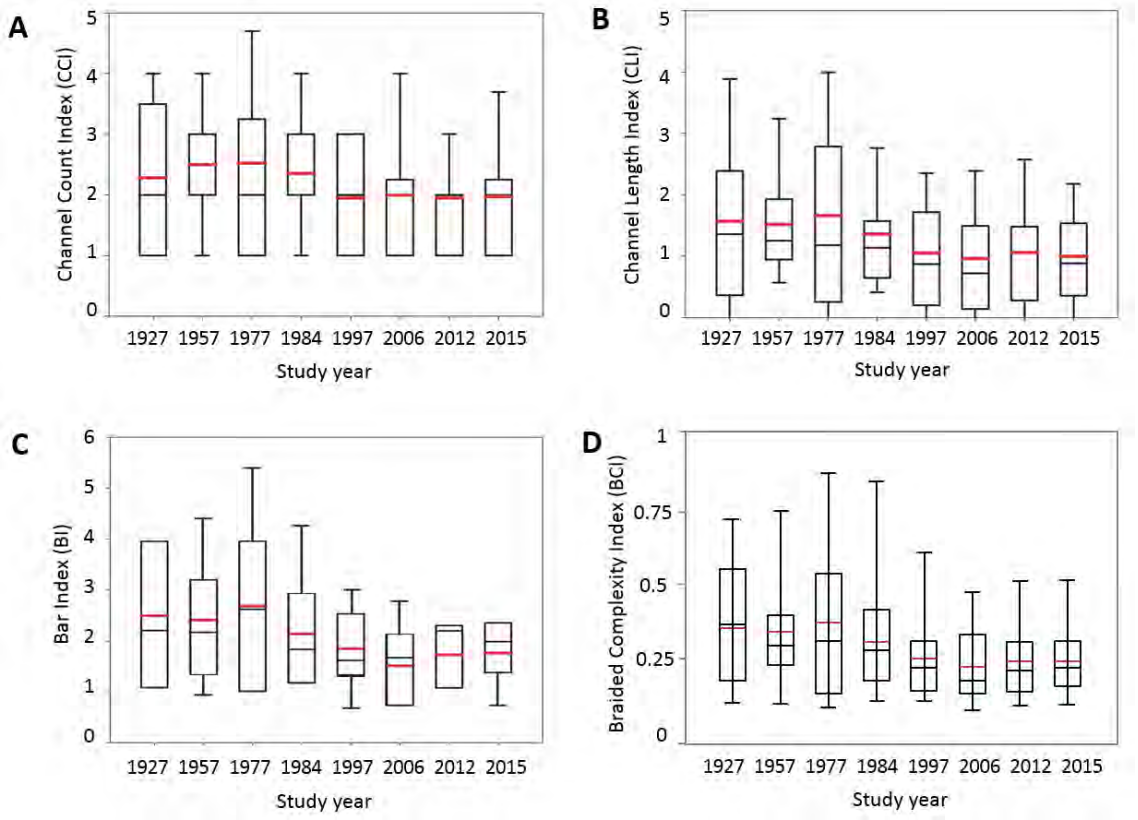


**Figure 91.** Box-plot of the (**A**) Channel Count Index (CCI), (**B**) Channel Length Index (CLI),(**C**) Bar Index (BI), and (**D**) Braided Complexity Index (BCI) during the study period. The central black line represents the median value, the red line represents the mean, the top and bottom ends of the box are the 75$^{th}$ and 25$^{th}$ percentiles respectively; and the upper and lower bars are the maximum and minimum values respectively.

Figure 10A shows the spatial and temporal evolution of the BCI through a heatmap, while Figure 10B shows the standard deviation of the BCI. Two distinct river reaches can be identified by looking at the patterns observed in Figure 10B. The first reach starts at the upstream end of the study reach and has an approximate length of 8 km. This reach presents very low and stable standard deviation values. Although the changes in the BCI are minimum, they can be observed in areas in which there was a minor local increase in complexity in 2015 (Figure 10A). In this case, the increase is due to the punctual direct effect of the gravel mining extraction on channel morphology, as can be seen in i of Figure 10C. The standard deviation of the BCI increased downstream (i.e. 8 to 12 km downstream), what indicates that channel complexity exhibited strong changes in this reach. The highest values of BCI were observed in this downstream reach during the period 1927-1977 (Figure 10A). The maximum value was observed in 1977 (i.e. a BCI of 0.8), at around 11 km downstream. This value was conditioned by local changes driven by the floods and also by gravel mining (see evidence in ii of Figure 10C). A clear trend towards a reduction of the BCI is observed since 1977 as stated by the results of the Mann-Kendall test.

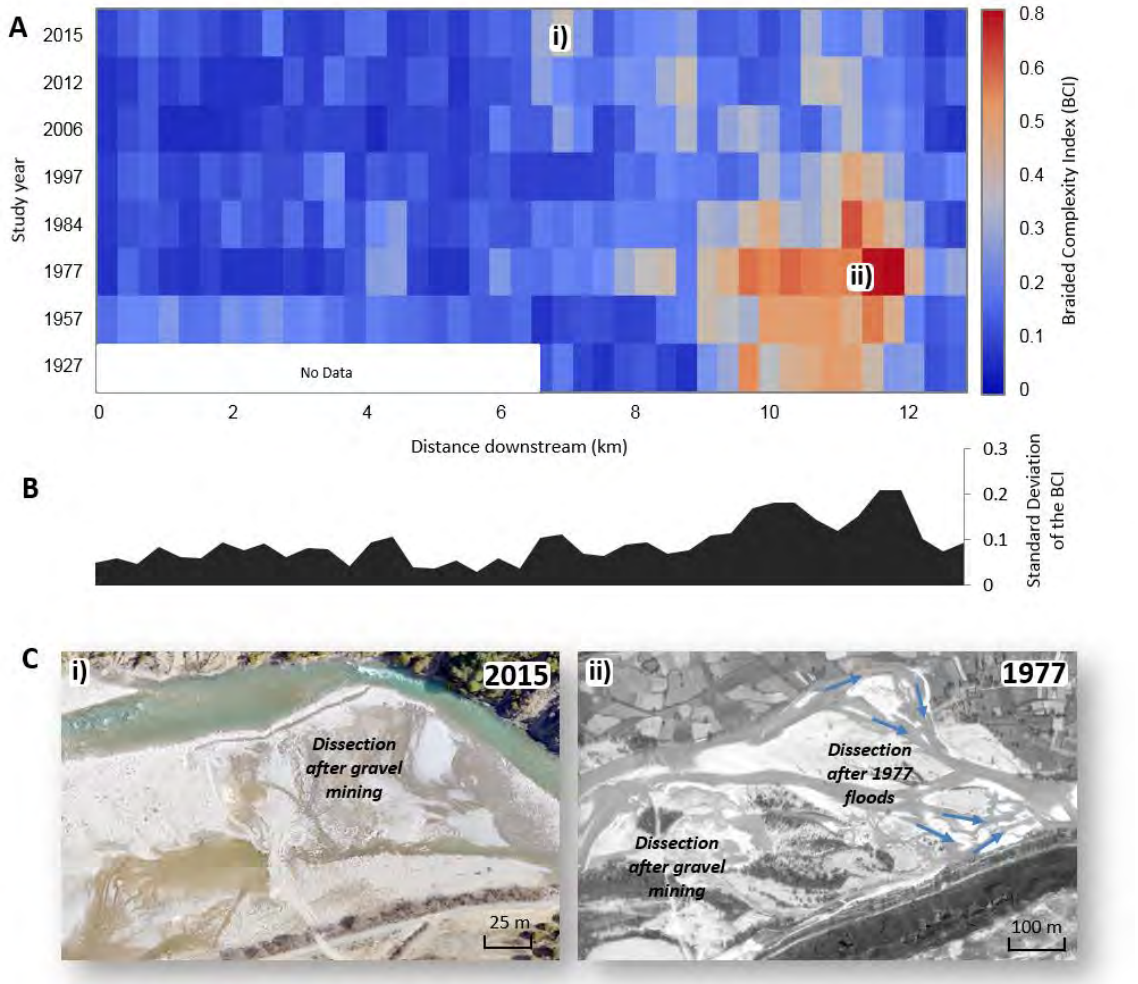


**Figure 10. A.** Heatmap of the Braided Complexity Index (BCI) for each study year (see text for further details in terms of the assessment of the BCI. Note that the lowercase letters (i.e. i and ii) indicate the locations of the reaches presented in C. **B.** Standard deviation of the BCI for all the time series. **C.** Ortomosaics of the middle (left) and lower (right) parts of the study reach in 2015 and 1957 showing an increase of braiding complexity due to the effects of floods and gravel mining.

### 4.3.4. Process-based changes and channel constraining

Figure 11A shows the percentage of each process for the 1927-1984 and 1984-2015 periods, while Figure 11B presents a map of the main acting processes. The periods were stablished based on the results of the Mann-Kendall test for the active width. During the first period the extent of lateral erosion (8% of the total) was similar to constraining (12%), indicating a balance in the active area of the study reach. Almost half of the reach was considered active (i.e. bars with no vegetation cover; Figure 11A). Although the extent of sedimentation and in-channel erosion processes remain similar in the second period (1984-2015), constraining increased 2.5 times, while lateral erosion was not observed in the whole study reach mainly attributed to the construction of embankments (Figure 11B). The proportion of the area with no change, considered that remained active (i.e. open bar), decreased to 38%. Figure 11B shows that in-channel erosion processes concentrate in a few but large channels during the period 1984-2015. This process was more spatially variable in the period 1927-1984 and was spread over the whole active floodplain. This trend is also observed in the case of sedimentation, altogether indicating channel staticity and simplification (reduction of braiding complexity), and reduction of lateral connectivity due to embankments and vegetation encroachment.

Figure 11C analyses the staticity of the wet channel by means of a simple probability map looking at the variation of the position of this unit through time. Two maps representing the probability of channel for the same periods than for the process-based changes are presented in Figure 11C. During the first period, the percentage of the area occupied by low probabilities (25%) was double (i.e. 60% of total surface) that for the second period (30%). In contrast, the area attributed to high probabilities (i.e. 100%) increased from 1% (1927-1984) to 10% (1984-2015). These results indicate that, between 1927 and 1984 the position of the wet channel was highly variable while channel staticity increased after 1984. This constraint occurs alongside the reduction of braided pattern, as can be observed in Figure 11B and 11C.

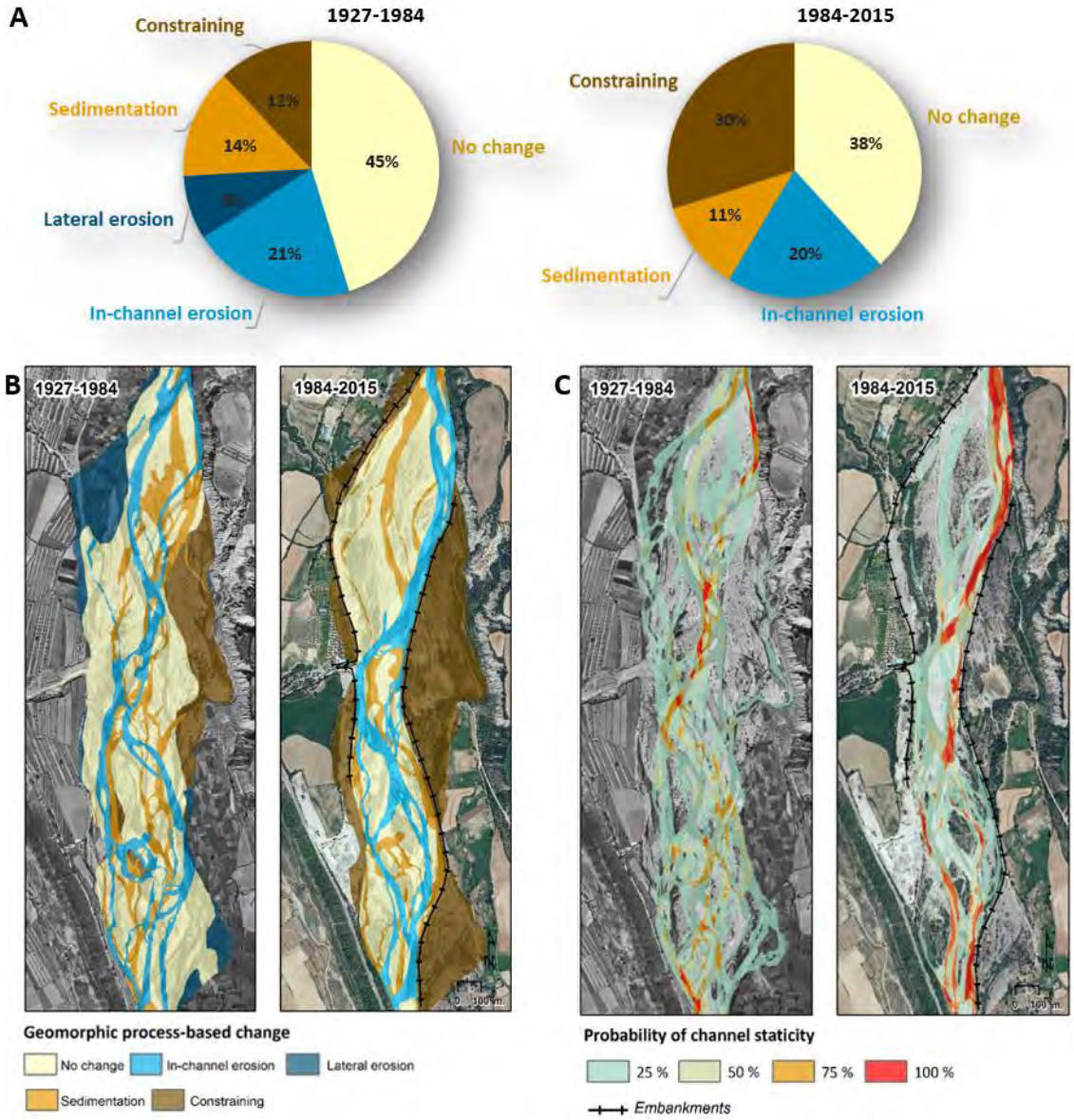


**Figure 11. A.** Contribution (expressed in %) of each process to the observed morphological changes between the period 1927-1984 and 1984-2015. **B.** Process-based channel change maps obtained by the intersection of morphological units between the periods: 1927-1984 and 1984-2015 (see text for more details). **C.** Maps representing the probability of channel staticity for the period 1927-1984 and 1984-2015 (see text for more details). Note that the location of lateral embankments is also presented in B and C.

### 4.3.5. Topographic changes

Figure 12A shows the longitudinal profiles of the time series 1957, 1977, 1984 and 2015, and the difference between the 1957 and 2015 profiles (i.e. long term evolution). In general, the evolution of the profiles shows a clear incision process through time and in virtually all of the study reach. The average channel incision (calculated as the mean of the changes in the cross-sections) for the period 1957-2015 was 1.7 m. Figure 12B shows 3D views of selected reaches along the profile where representative differences between the 1957 and 2015 profiles were observed. A maximum incision up to 4 m was observed between km 9 and 10 (iii in Figure 12), corresponding to an area where recurrent gravel mining activities were performed, together

with the construction of lateral embankments on the left bank side. In contrast, there were some areas where differences were minor or even positive (aggradation; Figure 12B). A series of bedrock outcrops preventing erosional processes are observed at 1 km. Local changes were non-existent due to the control exercised by the bedrock (i in Figure 12). Further downstream at 6 km, the channel exhibits a natural confinement on the left bank side and an artificial confinement on the right bank determined by the lateral embankment. In this case, aggradation appears to be a result of competence loss due to velocity decrease after the increase of channel width (i.e. after natural confinement) together with the effects of the lateral embankments constructed during the beginning of the 21th Century (ii in Figure 12). Finally, a large value of aggradation (almost 1 m) is located at the end of the reach (i.e. 12 km). In this case, the high aggradation is mainly due to the constraining of the confluence bar created between the Cinca and the Ara rivers, and also by the sedimentation caused by the Mediano reservoir (tail), constructed in 1959 (iv in Figure 12).

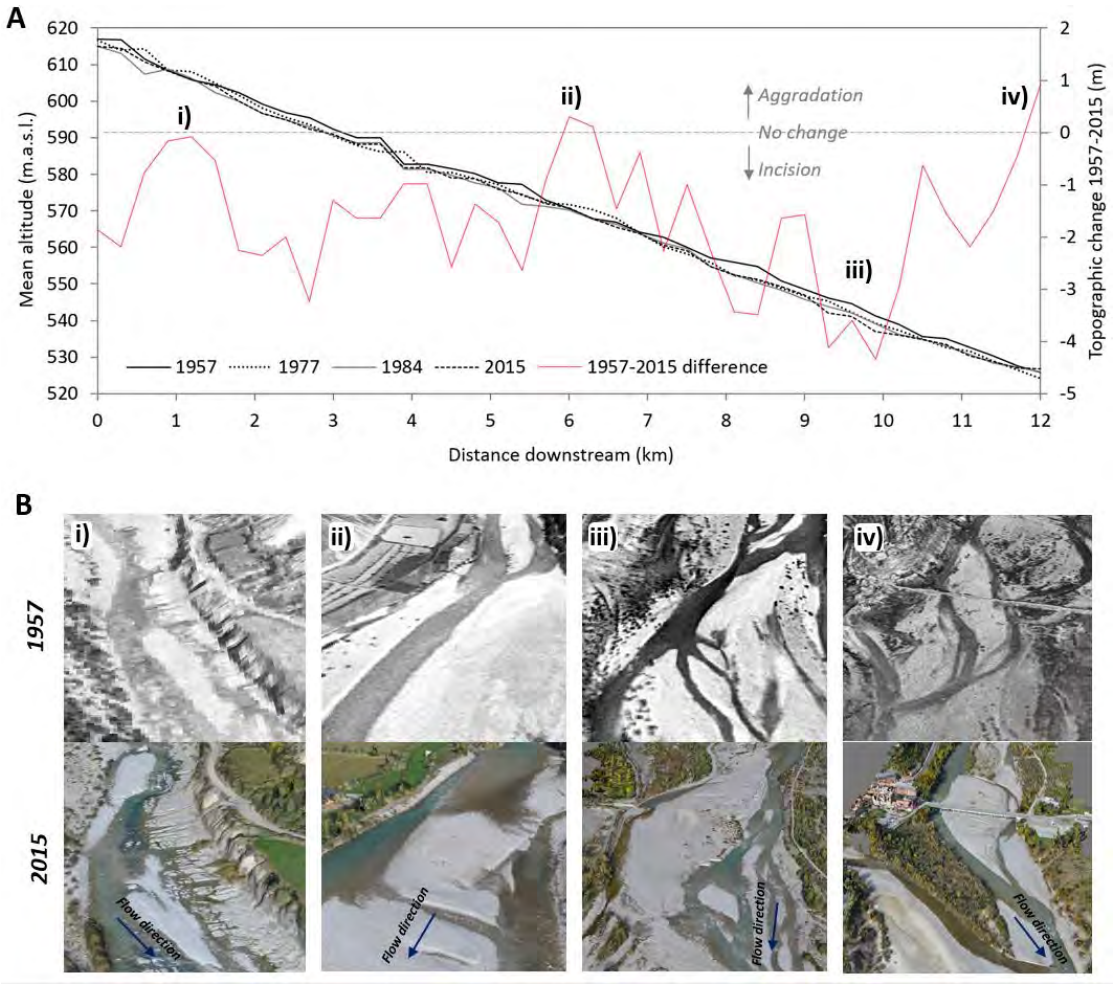


**Figure 12. A.** Longitudinal profiles of the study reach for the years 1957, 1977, 1984 and 2015. Note that the difference between the 1957 and 2015 longitudinal profiles is also presented. The lowercase letters (i.e. i, ii, iii, iv) indicated the locations of the examples presented in B. **B.** 3D photorendered point clouds of representative sections in 1957 and 2015.

In the case of the Upper Cinca we have observed a clear positive relation between channel incision and gravel mining activity. In this way, the periods in which there were more requested gravel mining operations (i.e. 1970s) were contemporaneous with those when more incision was observed (i.e. 1.9 m of average incision for the 1957-1977 period). Gravel mining activity decreased after 1984. Even so, clear erosional trends (i.e. incision) remained present in the longitudinal profile of the river (e.g. 0.3 m between the period 1984-2015). This fact indicates that the river kept adjusting to the new situation given by the water flow and sediment regimes, but also those imposed by the new channel morphology (e.g. reduced channel widths), configuration (e.g. single straighter channels), and confinements (e.g. embankments).

Several studies in gravel bed rivers in Mediterranean areas show that incision is the main cause of channel constraining, being the consequence of local impacts caused by gravel mining and the subsequent adjustment of the longitudinal profiles to the sediment deficit (e.g. Kondolf, 1997; Rinaldi et al., 2005; Surian et al., 2009; Comiti et al., 2011; Moretto et al., 2014; Sanchis-Ibor et al., 2017). The average values of channel incision registered in the Upper Cinca are in agreement with those reported by several other authors in Mediterranean mountain rivers. For instance, Landon and Piégay (1999) describe an average incision of 1.5 m up to maximum 5 m during the period 1931-1985 mainly caused by embankment construction and gravel mining activities in the Eygues basin (Southern French Pre-Alps). In the case of several Italian rivers subjected to in-channel gravel mining during the twentieth century, Surian and Rinaldi (2003) described average incisions between 3 to 4 m. Similarly, Rovira et al. (2005) observed an average incision of around 2 m for the period between 1956 and 1987 in the case of the Tordera River (Northeast Iberian Peninsula), indicating that the volume extracted was 14 times higher than the annual sediment supply from upstream. In the case of the River Gallego (Southern Pyrenees), Martin-Vide et al. (2010) observed how the incision (around 4-5 m in some sections) caused by intense gravel mining changed the magnitude of the shear stresses on the channel bed due to that the deeper and uniform channels accommodating higher discharges without overbank flooding. Finally, Calle et al. (2017) also observed an average incision between 3 and 5 m in an ephemeral stream in the east of the Iberian Peninsula during the 1946-2012 period, also caused by instream gravel mining.

DEMs of difference (DoDs) give us distributed maps of topographic changes. In this way, Figure 13A shows the comparison of the 1957 and 2015 DEMs; negative cells (i.e. red) indicate erosion while positive cells (i.e. blue) indicate sedimentation. Results show a generalized erosion process through the entire study reach (78% of the surface). Even so, sedimentation was observed in around the 12% of the reach. On one hand, in the case of the lower part of the study reach, incisions that can reach up to 5-7 m are observed in the current active channel. On the other hand, in the areas in which the main channel is laterally disconnected due to the embankments, high values of sedimentation were observed (see examples in Figure 13A and B, specifically in (i) for those areas where sedimentation was observed, and (ii) areas with high values of incision). Additionally, the establishment of a gravel mining plant on the right bank side has also led to significant topographic changes in the floodplain, in this case in the form of surface raising due to the storage of aggregates and gravels (see iv in Figure 13A and B).

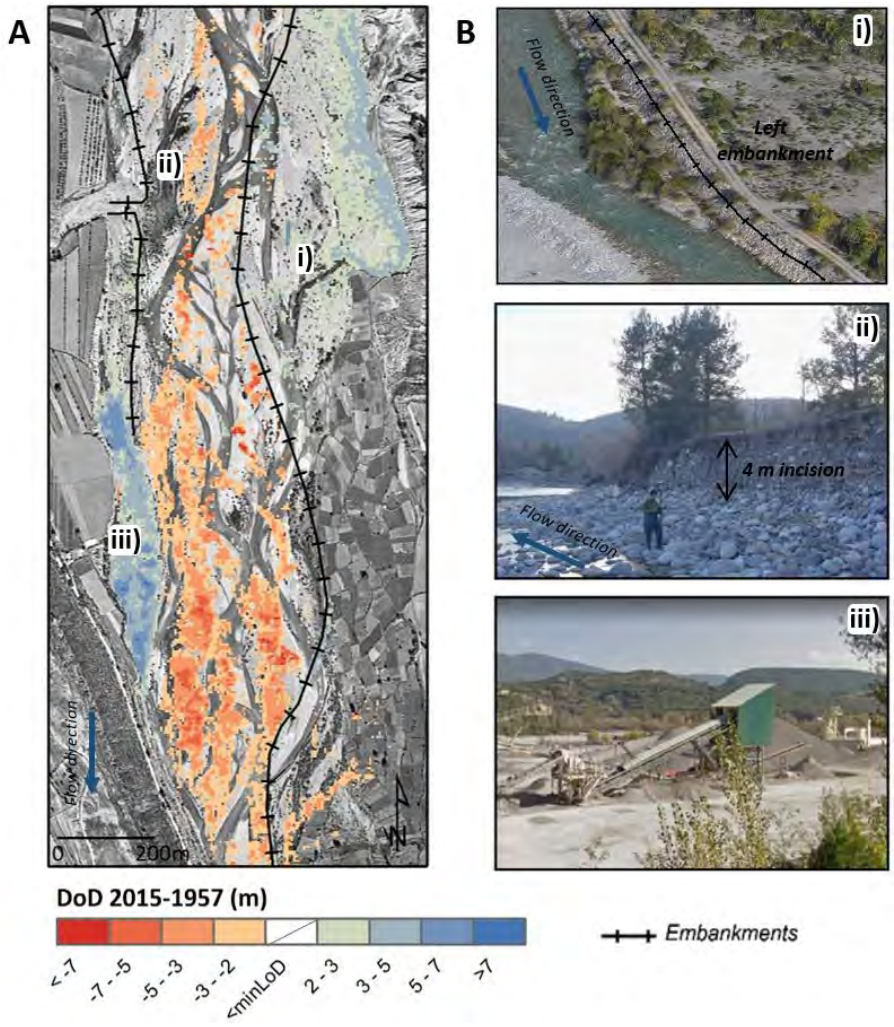


**Figure 13. A.** DEM of Difference (DoD) calculated using the 1957 and 2015 Digital Elevation Models (DEMs. The 1957 orthomosaic is presented as a base map. Negative values indicate erosion, while positive sedimentation. It should be noted that those changes between ± 2 m have been considered uncertain, below the minimum level of detection, which means that they have not been represented in the map of changes. The lowercase letters (i.e. i, ii, iii, iv) indicated the locations of the examples presented in B. Note that the location of lateral embankments is also presented. **B.** Examples of topographic changes observed in the field. Note that the location of these examples is presented by the lowercase letters in A.

## 4.4. Synthesis

Our results show the existence of significant trends and breakpoints in the time series of disturbances or influences, process changes and geomorphic descriptors (1927-2015). Figure 14 conceptually summarises main findings in this regard. In terms of disturbances during the overall study period, the Upper Cinca has suffered catchment-scale human-driven influences such as the associated to afforestation and climate change; and more localised or reach-scale disturbances associated mainly to the construction of dams, gravel mining and embankments. These disturbances have caused important process changes, mainly attributed to a reduction of discharge and sediment supply from upstream. At the same time, these changes have produced some geomorphic responses, mainly by reducing active channel width and braided complexity together with an increase of channel incision. Although this is the general trend, our analysis also pointed out the existence of significant breakpoints in this. These breakpoints are localised between 1977 and 1984, with the exception of the breakpoint in 1990 in the case of gravel

mining, being this later influenced by the 1982 flood and probably also by the limited data available in terms of gravel mining. Broadly, before 1984, the active channel width remained stable and the Braided Complexity Index was high. Main processes re-shaping channel morphology were those related to in-channel erosion, lateral erosion, sedimentation and constraining, the latter being compensated with lateral erosion caused by the high frequency floods occurred during the 1970s and early 1980s. The majority of the geomorphic units were active, and the relatively high values of channel incision were probably controlled by the large gravel mining activity in the 1970s together with the sediment deficit caused by the construction of the dams. This pattern reverses after 1984, when constraining and a significant reduction of the braided complexity were observed. The river still incising adjusting to the new situation given by the water and sediment regimes, both altered by catchment-scale disturbances, but also controlled by reach-scale disturbances. This is the period considered dry in terms of runoff. Locally, embankments (built in 1984-1985) have a direct impact on lateral connectivity and channel constraining. Further, the largest requests of gravel extraction were registered after the 1984 high magnitude flood event, decreasing sediment availability and changing channel geometry. We hypothesise that the reaction time after gravel mining activity, dam construction and embankments is different depending on the geomorphic descriptor used to analyse the channel response. In this way, topographic adjustments (e.g. channel incision) may have a relatively fast response, while planform adjustments (e.g. channel width) may have a slower response if these are associated to a reduction of flood magnitude and sediment fluxes, or they may have a faster response if are influenced by the construction of lateral embankments.

Our results point out to a fluvial metamorphosis following catchment and reach-scale disturbances, moving from a braided pattern to a more stable system towards a wandering river. Geomorphic responses observed in the Upper Cinca are in agreement with the hypothetical trajectory of fluvial metamorphosis presented by Petts and Gurnell (2005) associated to damming. They suggested that after the closure of a dam the river will change its regime state (i.e. equilibrium; Regime State 1) through a transient state (Figure 14). This transient state is controlled by a relaxation period, the time that the river needs to react and adjust to the new imposed conditions after the disturbance, i.e. to a new regime state (i.e. equilibrium; Regime State 2). Back to the Upper Cinca, as already discussed, we hypothesise that before 1927 the river was in a natural regime state, in an equilibrium state controlled mainly by floods (i.e. Regime State 1). After 1927, the river started to be in disequilibrium due to the mentioned disturbances. Around this year can be considered the start of the transient state, a period characterised by two changed channel states. The first one ended in 1984 and mainly characterised by channel incision. After 1984, in the second channel state, all geomorphic descriptors tended to be significantly reduced, pointing at channel simplification and constraining. Finally, between 2012 and 2015, all geomorphic descriptors appeared to be more static or stable (less changes). This relaxation in the adjustment of the channel allows us to hypothesise that the river may be reaching again a new regime state (i.e. Regime State 2), adjusting to the imposed water and sediment fluxes and channel configuration (Figure 14).

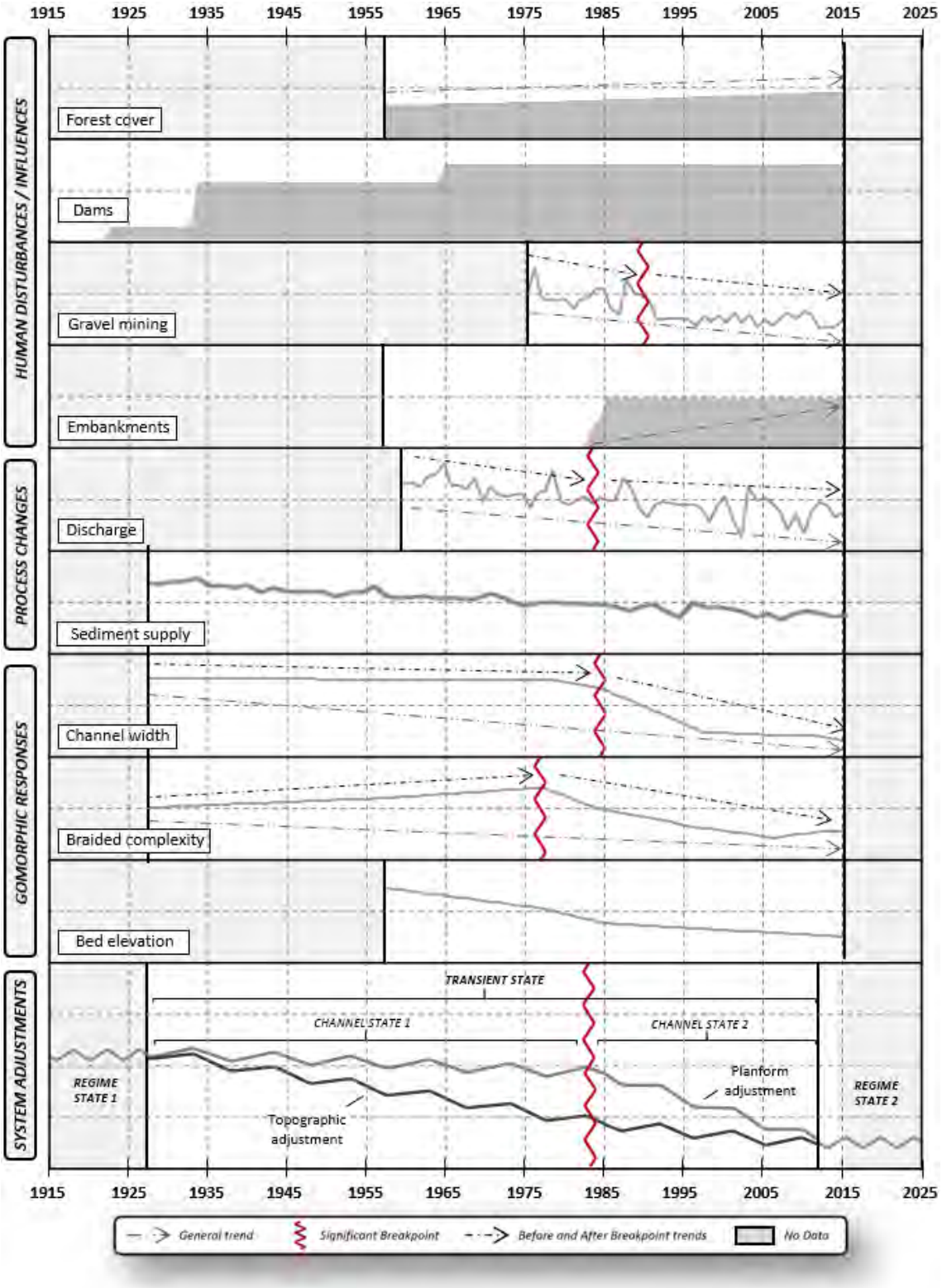


**Figure 14.** Trends and breakpoints on the human disturbances or influences, process changes, geomorphic responses and system adjustments. Note that sediment supply band is inferred from the data extracted from the literature cited in the manuscript (see section 4.2 for further information).

The present paper represents an original contribution from a methodological point of view. The quite novelty application of Structure from Motion (SfM) to historical imagery allows to estimate the geomorphic descriptors (i.e. planform and topography) for the study periods in which aerial photos with overlapping were available. More notably, the use of statistical trends and breakpoints analysis, allows identifying the different phases of change of the river system state after determined human disturbances or influences. Channel constraining through incision and lateral disconnectivity is a widely observed process in many mountain rivers such as the Upper Cinca, affecting multiple physical and ecological processes, and the conveyance and dissipation of floods that may have socio-economic impacts due to the increase of the human exposure in former active areas. Therefore, the morpho-sedimentary diagnosis of such rivers may be relevant for a better management practises and to assist objective-based rehabilitation measures of rivers subjected to multiple human influences or disturbances.

## 6. CONCLUSIONS

This paper links geomorphic adjustments to multi-scale disturbances or disturbances using a data set encompassing almost a century. The paper has analysed main channel adjustments inferring on the existence of significant trends and breakpoints in the temporal evolution of the geomorphic descriptors, process changes and disturbances. We conclude that:

- Afforestation was the main land use change exhibited between 1957 and 2015, being mainly concentrated in the period 1977 to 2015. Broadly, afforestation reduced water and sediment yields.
- Total annual runoff showed a clear significant negative trend. Two statistical significant hydrological periods are observed: (i) a wetter period between 1959 and 1983, and (ii) a drier period between 1983 and 2015. The frequency and magnitude of floods exhibits a decrease in the dry period when compared to the earlier wet period, although not statistically significant.
- The extraordinary flood registered in 1982 caused severe channel changes. Extensive gravel mining occurs after flood events, together with channel engineering works as the construction of embankments. These disturbances had a direct impact on lateral connectivity by confining and constraining channels and concentrating flows resulting in channel incision and constraining. The floodplain of the Upper Cinca is now totally disconnected to the contemporary flood regime.
- Three phases in the changes of the river channel during the last century were observed. First, a Regime State 1 (before 1927), where the river was potentially in equilibrium. Second, a Transient State (1927-2012) in which the river adjusted to the disequilibrium imposed by multiple human disturbances acting at different temporal and spatial scales. Finally, a Regime State 2 (after 2012), a period in which we hypothesise that the river may be reaching again a new equilibrium, adjusting to the imposed water and sediment fluxes and channel configuration.
- The Transient State (1927-2012) corresponded to the relaxation time and it was divided in two changed channel states, driven by the magnitude of changes observed in the geomorphic descriptors. The period 1927-1984 was characterised by having high geomorphic activity and channel incision. The period 1984-2012 was characterised, however, by having a low geomorphic activity, when channel constraining was the dominant process, mainly controlled by the decrease of flood frequency and magnitude and sediment supply, together with the impacts associated with channel embankment construction and the continuation of gravel

mining activities. Channel complexity was reduced together with channel width. Vegetation stabilised former active areas and flows concentrated in few and dominant river channels.

- Channel incision together with the reduction of the active channel, accentuated by the confinement effect caused by the lateral embankments, resulted in a trend toward a stable morphology with an increasingly simple pattern. The Upper River Cinca has changed from a braided active pattern to a more stable pattern towards wandering in the last century, a metamorphosis typical of many mountain river subjected to similar disturbances.
- Overall, we hypothesise the river has reached a new equilibrium imposed by the conditions led by the catchment and reach-scale disturbances. According to our observations, the relaxation time, the period needed to reach a new regime state was around 85 years.

The results of the Upper Cinca offer an interesting example of mountain fluvial landscape suitable to examine the effects of multi-scale disturbances on channel morphology, inferring in how the river changed channel states and the time the needed to adjust to the imposed water and sediment fluxes due to multiple disturbances acting at different temporal scales. Results may be also relevant to infer in future fluvial metamorphosis associated to the effects of global change on water and sediment fluxes in mountain catchments.

## 7. ACKNOWLEDGMENTS

This research was carried out within the framework of two research projects funded by the Spanish Ministry of Economy and Competitiveness and the European FEDER funds: MORPHSED (CGL2012-36394) and MORPHPEAK (CGL2016-78874-R). The first author has a grant funded by the Spanish Ministry of Education Culture and Sports (FPU016/01687). The second author is a Serra Húnter Fellow at the University of Lleida. The first and second authors are part of the Fluvial Dynamics Research Group-RIUS, which is a Consolidated Group recognized by the Generalitat de Catalunya (2017 SGR 459645). We also acknowledge the support of the CERCA Program of the Generalitat de Catalunya.

## 8. REFERENCES

Aguiar FC, Martins MJ, Silva PC. 2016. Riverscapes downstream of hydropower dams: Effects of altered flows and historical land-use change. *Landscape and urban Planning* 153: 83-98.

Arnaud F, Piégay H, Schmitt L, Rollet AJ, Ferrier V, Béal D. 2015. Historical geomorphic analysis (1932–2011) of a by-passed river reach in process-based restoration perspectives: The Old Rhine downstream of the Kembs diversion dam (France, Germany). *Geomorphology* 236: 163–177.

Baker VR, Kochel RC, Patton PC. 1988. *Flood geomorphology*. Wiley interscience. New York. 503 pp.

Bakker M, Lane SN. 2017. Archival photogrammetric analysis of river-floodplain systems using Structure from Motion (SfM) methods. *Earth Surface Processes and Landforms* 42: 1274–1286.

Balasch JC, Remacha R, Esteve J. 2000. *Las avenidas en la cuenca del río Segre. Descripción y análisis de algunos ejemplos recientes*. Actas del I Simposi Llatí sobre Geologia, Medi Ambient i Societat.

Batalla RJ, Gomez CM, Kondolf GM. 2004. Reservoir-induced hydrological changes in the Ebro River basin (Northeastern Spain). *Journal of Hydrology* 290(1- 2): 117-136.

Batalla RJ, Vericat D, Martínez T. 2006. River-channel changes downstream from dams in the lower Ebro River. *Zeitschrift für Geomorphologie* 143: 1-14.

Batalla RJ, Balasch JC, Carbayo A, Ferrer C, Novoa M, Werritty A, Vericat D, Llasat MC, Gómez C M, Palau A. 2007. *Les riuades: del desastre natural a la regeneració ambiental*. Actas del ciclo de conferencias organizado conjuntamente entre el Instituto de Estudios Ilerdenques y la Universidad de Lleida. Institut Estudis Ierdencs, Lleida. 56 pp.

Batalla RJ, Iroumé A, Hernández M, Llena M, Mazzorana B, Vericat D. 2018. Recent geomorphological evolution of a natural river channel in a Mediterranean Chilean basin. *Geomorphology* 303: 322-337.

Beguería S, López-Moreno JI, Lorente A, Seeger M, García-Ruiz JM. 2003. Assessing the Effect of Climate Oscillations and Land-use Changes on Streamflow in the Central Spanish Pyrenees. *Ambio* 32(4): 283-286.

Beguería S, López-Moreno JI, Gómez-Villar A, Rubio V, Lana-Renault N, García-Ruiz JM. 2006 Fluvial adjustments to soil erosion and plant cover changes in the Central Spanish Pyrenees. *Swedish Society for Antropology and Geography* 88: 177–186.

Belletti, B., Dufour, S., Piégay, H., 2013. What is the relative effect of space and time to explain the braided river width and island patters at regional scale? River Research Application 1–15.

Bollati IM, Pellegrini L, Rinaldi M, Duci G, Pelfini M. 2014. Reach-scalemorphological adjustments and stages of channel evolution: the case of the Trebbia River (northern Italy). *Geomorphology* 221: 176–186.

Brasington J, Rumsby BT, Mcvey RA. 2000. Monitoring and modelling morphological change in a braided gravel-bed river using high resolution GPS-based survey. *Earth Surface Processes and Landforms* 25: 973-990.

Brasington J, Vericat D, Rychkov I. 2012. Modeling river bed morphology, roughness, and surface sedimentology using high resolution terrestrial laser scanning. *Water Resources Research* 48: 1-18.

Bravard JP, Amoros C, Pautou G. 1986. Impact of civil engineering Works on the successions of communities in a fluvial system. A methodological and predictive approach applied to a section of the Upper Rhone River, France. *Oikos* 47: 92-111.

Béjar M, Gibbins CN, Vericat D, Batalla R. 2017. Effects of susoended sediment transport on invertebrate drift. *River Research and Applications* 33: 1655-1666.

Béjar M, Vericat D, Batalla R, Gibbins CN. 2018. Variation in flow and suspended sediment ransport in a montane river affected by hydropeaking and instream mining. *Geomorphology* 310: 69-83.

Bu J, Lu C, Niu J, Gao Y. 2018. Attribution of Runoff Reduction in the Juma River Basin to Climate Variation, Direct Human Intervention, and Land Use Change. *Water* 10(12): 1-26.

Buendia C, Batalla RJ, Sabater S, Palau A, Marcé R. 2015. Runoff trends driven by climate and afforestation in a Pyrenean basin. *Land Degradation and Development* 27: 823-838.

Buendia C, Bussi G, Tuset J, Vericat D, Sabater S, Palau A, Batalla RJ. 2016. Effects of afforestation on runoff and sediment load in an upland Mediterranean catchment. *Science of Total Environment* 540: 144-157.

Bussi G, Francés F, Horel E, López-Tarazón JA, Batalla RJ. 2014. Modelling the impact of climate change on sediment yield in a highly erodible Mediterranean catchment. *Journal of Soils and Sediments* 14(12): 1921-1937.

Calle M, Alho P, Benito G. 2017. Channel dynamics and geomorphic resilience in an ephemeral Mediterranean river affected by gravel mining. *Geomorphology* 285: 333-346.

Comiti F, Da Canal M, Surian N, Mao L, Picco L, Lenzi MA. 2011. Channel adjustments and vegetation cover dynamics in a large gravel bed river over the last 200 years. *Geomorphology* 125(1): 147–159.

Church MA. 1972. *Baffin Island sandar: a study of Artic fluvial environments*. Geological Survey of Canada. Canada. 208 pp.

Church MA, Jones D. 1982. Chanel bars in gravel bed rivers. In: *Gravel bed rivers* (Hey, R.D., Bayhurst, J.C. and Thorne, C.R. eds.). John Wiley. 291-324.

Church M. 2006. Bed Material Transport and the Morphology of Alluvial River Channels. *Annual Review of Earth and Planetary Sciences* 34: 325-354.

Chuvieco E. 2016. *Fundamentals of Satellite Remote Sensing: An Environmental Approach*. Second edition. Taylor and Francis, USA. 468 pp.

Downs PW, Dusterhoff SR, Sears WA. 2013. Reach-scale channel sensitivity to multiple human activities and natural events: Lower Santa Clara River, California, USA. *Geomorphology* 189: 121–134.

Downs PW, Piégay H. 2019. Catchment-sclae cumulative impact of human activities on river channels in the late Anthropocene: implications, limitations, prospect. *Geomorphology* 338: 88-104.

Egozi E, Ashmore P. 2008. Defining and measuring braiding intensity. *Earth Surface Processes and Landforms*. 33: 2121–2138.

Fryirs KA, Brierley GJ. 2013. *Geomorphic Analysis of River Systems: An Approach to Reading the Landscape*. Wiley-Blackwell. 360 pp.

Galán F. 2012. *Centrales hidroeléctricas y presas del Alto Aragón*. Fundación ESTEYCO. Madrid. 177 pp.

Gallart F, Llorens P, Latron J, Rabadà D. 1997. Hydrological functioning of Mediterranean mountain basins in Vallcebre, Catalonia: Some challenges for hydrological modeling. *Hydrological Processes* 11: 1263-1272.

Gallart F, Llorens P. 2004. Observations on land cover changes and water resources in the headwaters of the Ebro catchment, Iberian Peninsula. *Physics and Chemistry of the Earth* 29: 769-773.

Gallart F, Delgado J, Beatson SJV, Posner H, Llorens P, Marcé R. 2011. Analysing the effect of global change on the historical trends of water resources in the headwaters of the Llobregat and Ter river basins (Catalonia, Spain). *Physics and Chemistry of the Earth* 36: 655-661.

García-Ruiz JM, Ortigosa LM. 1988. Algunos efectos geomorfológicos de las repoblaciones forestales. Cambios en la dinámica del cauce en pequeñas cuencas del Pirineo Central español. *Cuaternario y Geomorfología* 2(1-4): 33-41.

Garcia-Ruiz JM, Lasanta T, Ruiz-Flano P, Ortigosa L, White S, Gonzalez C, Martí C. 1996. Land-use changes and sustainable development in mountain areas: a case study in the Spanish Pyrenees. *Landscape Ecology* 11: 267–277.

García-Ruiz JM, López-Bermúdez F. 2009. *La erosión del suelo en España*. Sociedad Española de Geomorfología, Zaragoza, 441 pp.

García-Ruiz JM, Lana-Renault N, Beguería S, Lasanta T, Regüés D, Nadal-Romero E, Serrano-Muela P, López-Moreno J, Alvera B, Martí-Bono C, Alatorre LC. 2010. From plot to regional scales: Interactions of slope and catchment hydrological and geomorphic processes in the Spanish Pyrenees. *Geomorphology* 120(3-4): 248–257.

García-Ruiz JM, Lana-Renault N. 2011. Hydrological and Erosive Consequences of Farmland Abandonment in Europe, with Special Reference to the Mediterranean Region—A Review. *Agriculture Ecosystems & Environment* 140(3): 317-338.

García-Ruiz JM, López-Moreno JI, Vicente-Serrano SM, Lasanta-Martínez T, Beguería S. 2011. Mediterranean water resources in a global change scenario. *Earth-Science Reviews* 105: 121-139.

Germanoski D, Schumm SA. 1993. Changes in braided river morphology resulting from aggradation and degradation. *Journal of Geology* 101: 451–466.

Gilvear DJ. 1999. Fluvial geomorphology and river engineering: future roles utilizing a fluvial hydrosystems framework. *Geomorphology* 31: 229-245.

González del Tánago M, Martínez-Fernandez V, García de Jalón D. 2016. Diagnosing problems produced by flow regulation and other disturbances in Southern European Rivers: the Porma and Curueño Rivers (Duero Basin, NW Spain). *Aquatic Sciences* 78: 121-133.

Ham D, Church M. 2012. Morphodynamics of an extended bar complex, Fraser River, British Columbia. *Earth Surface Processes and Landforms* 37: 1074-1089.

Hawkins DM, Qiu PH, Kang CW. 2003. The change point model for statistical process control. *Journal of Quality Technology* 35: 355–366.

Hawkins DM, Zamba KD, 2005. A change-point model for a shift in variance. *Journal of Quality Technology* 37: 21–31.

Hernández S. 1991. *Geomorfología del área de confluencia de los ríos Cinca y Ara (prov. de Huesca)*. University of Zaragoza. Spain. 311 pp.

Hicks DM, Duncan MJ, Lane ST, Tal M, Westway R. 2008. Contemporary morphological changes in braided gravel-bed rivers: new developments from field and laboratory studies, with particular references to the influence of riparian vegetation. In: Habersack, H.M., Piégay, H., Rinaldi, M. (Eds.), *Gravel-bed Rivers VI: From Processes Understanding to River Restoration*.

Hong LB, Davies TRH. 1979. A study of stream braiding. *Geological Society of America* 90: 1839–1859.

Hooke JM. 2006. Human impacts on fluvial systems in the Mediterranean region. *Geomorphology* 79: 311-335.

Hoyle J, Brooks A, Brierley G, Fryirs K, Lander J. 2008. Spatial variability in the timing, nature and extent of channel response to typical human disturbance along the upper Hunter River, New South Wales, Australia. *Earth Surface Processes and Landforms* 33 (6): 868–889.

Ibisate A, Díaz E, Ollero A, Acin V, Granado D. 2013. Channel response to multiple damming in a meandering river, middle and lower Aragon River (Spain). *Hydrobiologia,* 712, 5–23.

Keesstra SD, van Dam O, Verstraeten G, van Huissteden J. 2009. Changing sediment dynamics due to natural reforestation in the Dragonja catchment, SW Slovenia. *Catena* 78: 60-71.

Kendall MG. 1975. *Rank correlation measures*. CharlesGriffin: London; 202.

Kidová A, Lehotský M, Rusnák M. 2016. Geomorphic diversity in the braided-wandering Belá River, Slovak Carpathians, as a response to flood variability and environmental changes. *Geomorphology* 272: 137-149.

Kondolf GM. 1994. Geomorphic and environmental effects of instream gravel mining. *Landscape and urban Planning* 28: 225-243.

Kondolf GM. 1997. Hungry Water: Effects of Dams and Gravel Mining. *Environmental Management* 21: 533–551.

Lague D, Brodu N, Leroux J. 2013. Accurate 3D comparison of complex topography with terrestrial laser scanner : Application to the Rangitikei canyon (NZ). ISPRS Journal of Photogrammetry and Remote Sensing. 82: 10–26.

Landon N, Piégay H. 1999. *Mission d'expertise réalisée sur le bassin de l'Eygues pour le compte du Syndicat d'Aménagement Rural de la Drome et des Syndicats dromois et vauclusiens de l'Eygues, propositions pour une gestion physique équilibreé du lit de l'Eygues et de son bassin, Laboratoire environnementville-société* UMR5600 CNRS, 166 pp.

Lane EW. 1955. The importance of fluvial morphology in hydraulic engineering. *J. Hydraul. Div. ASCE*. 81: 1–17.

Lane SN, Tayefi V, Reid SC, Yu D, Hardy RJ. 2007. Interactions between sediment delivery, channel change, climate change and flood risk in a temperate upland environment. *Earth Surface Processes and Landforms* 32: 429-446.

Lasanta-Martínez T, Vicente-Serrano SM, Cuadrat-Prats JM. 2005. Mountain Mediterranean landscape evolution caused by the abandonment of traditional primary activities: a study of the Spanish Central Pyrenees. *Applied Geography* 25(1): 47-65.

Latapie A, Camenen B, Rodrigues S, Paquier A, Bouchard JP, Moatar F. 2014. Assessing channel response of a long river influenced by human disturbance. *Catena* 121: 1–12.

Liébault F, Hervé P. 2002. Causes of 20th century channel narrowing in mountain and Piedmont Rivers of southeastern France. *Earth Surface Processes and Landforms* 27: 425-444.

Liébault F, Clément P, Piégay H, Rogers CF, Kondolf GM, Landon N. 2002. Contemporary channel changes in the Eygues basin, southern French Prealps: the relationship of subbasin variability to watershed characteristics. *Geomorphology* 45: 53-66.

Liébault F, Gomez B, Page M, Marden M, Peacock D, Richard D, Trotter M. 2005. Land-use change, sediment production and channel response in upland regions. *River Research and Applications* 21: 739-756.

Livers B, Wohl E, Jackson KJ, Sutfin NA. 2018. Historical land use as a driver of alternative states for stream form and function in forested mountain watersheds of the Southern Rocky Mountains. *Earth Surface Processes and Landforms* 43: 669-684.

Llena M, Vericat D, Martínez-Casasnovas JA. 2016. Cambios geomorfológicos en el Alto Cinca (Periodo 1927–2014). In Comprendiendo el relieve: del pasado al futuro. *Actas de la XIV Reunión Nacional de Geomorfología*, Málaga, 2016, Durán JJ, Montes M, Robador

Llena M, Vericat D, Martínez-Casasnovas JA. 2018. Application of Structure from Motion (SfM) algorithms for the historical analysis of changes in fluvial geomorphology. *Cuaternario y Geomorfología* 32(1-2): 53-73.

Llena M, Vericat D, Cavalli M, Crema S, Smith MW. 2019. The effects of land use and topographic changes on sediment connectivity in mountain catchments. *Science of Total Environment* 660: 899-912.

Llorens P, Poch RM, Latron J, Gallart F. 1997. Rainfall interception by a Pinus sylvestris forest patch overgrown in a Mediterranean mountainous abandoned area. Monitoring design and results down to the event scale. *Journal of Hydrology* 199: 331-345.

López-Moreno JI, Beguería S, Valero-Garcés BL, García-Ruíz JM. 2009. Intensidad de las avenidas y aterramiento de embalses en el Pirineo Central español. *Ería. Revista Cuatrimestral de Geografía* 61: 159–167.

López-Moreno JI, Vicente-Serrano SM, Moran-Tejeda E, Zabalza J, Lorenzo-Lacruz J, García-Ruiz JM. 2011. Impact of climate evolution and land use changes on water yield in the ebro basin. *Hydrology and Earth System Sciences* 15: 311-322.

López-Moreno JI, Zabalza J, Vicente-Serrano SM, Revuelto J, Gilaberte M, Azorin-Molina C, Morán-Tejeda, García-Ruiz JM, Tague C. 2014. Impact of climate and land use change on water availability and reservoir management: Scenarios in the Upper Aragón River, Spanish Pyrenees. *Science of the Total Environment* 493: 1222-1231.

López-Vicente M, Poesen J, Navas A, Gaspar L. 2013. Predicting runoff and sediment connectivity and soil erosion by water for different land use scenarios in the Spanish PrePyrenees *Catena* 102: 62–73.

López-Vicente M, Nadal-Romero E, Cammeraat ELH. 2016. Hydrological Connectivity does change over 70 years of abandonment and afforestation in the Spanish Pyrenees. *Land Degradation and Development* 28(4): 1298-1310.

Martín-Vide JP, Ferrer-Boix C, Ollero A. 2010. Incision due to gravel mining: Modeling a case study from the Gállego River, Spain. *Geomorphology* 117(3-4): 261–271.

MacDonald D, Crabtree JR, Wiesinger G, Dax T, Stamou N, Fleury P, Gutierrez-Lazpita J, Gibon A. 2000. Agricultural abandonment in mountain areas of Europe: Environmental consequences and policy response. *Journal of Environmental Management* 59: 47-69.

Mann HB. 1945. Non-parametric tests against trend. *Econometrica* 13: 245–259.

Micheletti N, Lane SN, Chandler JH. 2015. Application of Archival Aerial Photogrammetry to Quantify Climate Forcing of Alpine Landscapes. *The Photogrammetric Record* 30: 143-165.

Moretto J, Rigon E, Mao L, Picco L, Delai F, Lenzi MA. 2014. Channel adjustments and island dynamics in the Brenta River (Italy) over the last 30 years. *River Research and Applications* 30: 719–732.

Mosley PM. 1981. Semi-determinate hydraulic geometry of river channels, South Island, New Zealand. *Earth Surface Processes and Landforms* 6: 127–137.

Mottet A, Ladet S, Coqué N, Gibon A. 2006. Agricultural land-use change and its drivers in mountain landscapes: A case study in the Pyrenees. *Agriculture Ecosystems & Environment* 114: 296-310.

Murgatroyd AL, Ternan JL. 1983. The impact of afforestation on stream bank erosion and channel form. *Earth Surface Processes and Landforms* 8(4): 357-369.

Nadal-Romero E, Lasanta T, García-Ruiz JM. 2013. Runoff and sediment yield from land under various uses in a Mediterranean mountain area: long-term results from an experimental station. *Earth Surface Processes and Landforms* 38: 346-355.

Newson M. 1980. The geomorphological effectiveness of floods—a contribution stimulated by two recent events in mid-wales. *Earth Surface Processes and Landforms* 5 (1): 1-16.

Picco L, Mao L, Rainato R, Lenzi MA. 2014. Medium-term fluvial island evolution in a disturbed gravel-bed river (Piave River, Northeastern Italian Alps). *Geografiska Annaler: Series A* 96: 83–97.

Picco L, Comiti F, Mao L, Tonon A, Lenzi MA. 2017. Mediumand short termriparian vegetation, island and channel evolution in response to human pressure in a regulated gravel bed river (Piave River, Italy). *Catena* 149: 760-769.

Pedraza J. 1996. *Geomorfología: principios, métodos y aplicaciones*. Rueda. Madrid. 414 pp.

Quiñonero-Rubio JM, Nadeu E, Boix-Fayos C, de Vente J. 2016. Evaluation of the effectiveness of forest restoration and check-dams to reduce catchment sediment yield. *Land Degradation & Development* 27: 1018-1031.

Richards K. 1982. *Rivers: form and process in alluvial channels*. Blackburn Press. London. 361 pp.

Rinaldi M, Wyzga B, Surian N. 2005. Sediment mining in alluvial channels: Physical effects and management perspectives. *River Research and Applications* 21(7): 805–828.

Rovira A, Batalla RJ, Sala M. 2005. Response of a river sediment budget after historical gravel mining (the Lower Tordera, NE Spain). *River Research and Applications* 21(7): 827–847.

Rubio V. 1995. *Dinámica Fluvial Del Rio Ara (Pirineo Aragonés)*. Universidad Autónoma de Madrid. 815 pp

Ruiz-Flaño P. 1993. *Procesos de erosión en campos abandonados del Pirineo*. Geoforma Ediciones, Logroño, 191 pp.

Ruiz-Flaño P, García-Ruiz JM, Ortigosa L. 1992. Geomorphological evolution of abandoned fields. A case study in the Central Pyrenees. *Catena* 19: 301-308.

Rychkov I, Brasington J, Vericat D. 2012. Computational and methodological aspects of terrestrial surface analysis based on point clouds. *Computers & Geosciences* 42: 64-70.

Sanchis-Ibor C, Segura-Beltrán F, Almonacid-Caballer J. 2017. Channel forms recovery in an ephemeral river after gravel mining (Palancia River, Eastern Spain). *Catena* 158: 357–370.

Sanjuán Y, Gómez-Villar A, Nadal-Romero E, Álvarez-Martínez J, Arnáez J, Serrano-Muela MP, Rubiales JM, González-Sampériz P, García-Ruiz JM. 2016. Linking land cover changes in the sub-alpine and montane belts to changes in a torrential river. *Land Degradation and Development* 27: 179-189.

Schumm SA, Lichty RW. 1965. Time, space, and causality in geomorphology. *American Journal of Science* 263: 110–119.

Scorpio V, Rosskopf CM. 2016. Channel adjustments in a Mediterranean river over the last 150 years in the context of antrophic and natural controls. *Geomorphology* 275: 90-104.

Smith ND. 1978. Some comments on terminology for bars in shallow rivers. In: *Fluvial Sedimentology*. Miall, A.D. Eds. Canadian Society Petroleum Geologist. 5:85-88.

Stover SC, Montgomery DR. 2001. Channel change and flooding, Skokomish River, Whashington. *Journal of Hydrology*. 243: 272-286.

Surian N, Ziliani L, Comiti F, Lenzi MA, Mao L. 2009. Channel adjustments and alteration of sediment fluxes in gravel-bed rivers of north-eastern Italy: potentials and limitations for channel recovery. *River Research and Applications* 25: 551-567.

Surian N, Rinaldi M. 2003. Morphological response to river engineering and management in alluvial channels in Italy. *Geomorphology* 50(4): 307–326.

Surian N. 2006. Effects of human impact on braided river morphology. In: *Braided Rivers: Process, Deposits, Ecology and Management*. Sambrook, G.H., Best, J.L., Bristow, C.S., Petts, G.E. Eds. IAS Spec. Publ. 36: 75–106.

Taillefumier F, Hervé P. 2003. Contemporary land use changes in prealpine Mediterranean mountains: a multivariate GIS-based approach applied to two municipalities in the Southern French Prealps. *Catena* 51: 267-296.

Tuset J, Vericat D, Batalla RJ. 2015. Evolución morfo-sedimentaria del tramo medio del río Segre. *Cuadernos de Investigación Geográfica* 41(1): 23-62

Ollero A, Ibisate A, Granado D, Real de Asua R. 2015. Channel Responses to Global Change and Local Impacts: Perspectives and Tools for Floodplain Management, Ebro River and Tributaries, NE Spain. In: *Geomorphic Approaches to Integrated Floodplain Management of Lowland Fluvial Systems in North America and Europe*. Hudson, P.F. Middelkoop H. Eds. Springer. New York. 351 pp.

Petts GE, Gurnell AM. 2005. Dams and geomorphology: Research progress and future directions. *Geomorphology* 71 (1–2): 27-47.

Piégay H, Walling DE, Landon N, He Q, Liébault F, Petiot R. 2004. Contemporary changes in sediment yield in an alpine mountain basin due to afforestation (the upper Drôme in France). *Catena* 55(2): 183–212.

Vericat D, Batalla RJ, Garcia C. 2006a. Breakup and reestablishment of the armour layer in a large gravel-bed river below dams: the lower Ebro. *Geomorphology* 76: 122-136.

Vericat D, Batalla RJ. 2006b. Sediment transport in a large impounded river: The lower Ebro, NE Iberian Peninsula. *Geomorphology* 79: 72-92.

Vericat D, Múñoz-Narciso E, Béjar M, Ramos-Madrona E. 2016. Case study: Multitemporal reach-scale topographic models in a wandering river – uncertainties and opportunities. In: *Structure from Motion in the Geosciencies. New Analytical Methods in the Earth Environmental Science* (J. L. Carrivick, M. W. Smith, D. J. Quincey, eds.). Willey, 194 pp.

Werritty A, Leys KF. 2001. The sensitivity of Scottish rivers and upland valley floors to recent environmental change. *Catena* 42(2-4): 251–273.

Wheaton JM, Fryirs KA, Brierley G, Bangen SG, Bouwes N, O'Brien G. 2015. Geomorphic mapping and taxonomy of fluvial landforms. *Geomorphology* 248: 273-295.

Williams GP, Wolman MG. 1985. *The Downstream Effects of Dams on Alluvial Rivers*. U.S. Geol. Surv., Prof. Pap. United States. 1286 pp.

Wohl E. 2006. Human impacts to mountain streams. *Geomorphology* 79: 217-248.

Ziliani L, Surian N. 2012. Evolutionary trajectory of channel morphology and controlling factors in a large gravel-bed river. *Geomorphology* 137-174: 104-117.

## 9. SUPPLEMENTARY MATERIALS

### 3.3. Aerial photos: orthomosaics, point clouds and land use maps

**Table 1**. Characteristics of aerial photographs used in the Upper Cinca River.

| Year | Type | Source | Nº photos** | Overlapping | Scale | Discharge ($m^3/s$) |
|---|---|---|---|---|---|---|
| 1927 | Panchromatic | CHE | - | No | 1/10,000 | - |
| 1957 | Panchromatic | CCFEA | 194 | Yes | 1/33,000 | 18.8 |
| 1977 | Panchromatic | CNIG | 284 | Yes | 1/18,000 | 14.5 - 57.4 |
| 1984 | Panchromatic | CNIG | 7 | Yes | 1/30,000 | 19.3 |
| 1997 | RGB | CINTA | - | No | 1/5,000 | 26.5 |
| 2006 | RGB | CNIG | - | No | 1/5,000 | 25.6 |
| 2012* | RGB | CNIG | - | No | 1/5,000 | 51.1 |
| 2015 | RGB | RIUS | 800 | Yes | | 16.4 |

CHE: Ebro basin Authorities (*Confederación Hidrográfica del Ebro*)
CECAF: Cartographic and Photographic Centre of the Spanish Air Force (*Centro Cartográfico y Fotográfico del Ejército del Aire*)
CNIG: Spanish National Centre of Geographic Information (*Centro Nacional de Información Geográfica*)
CINTA: Aragón Region Centre of Territorial Information (*Centro de Información Territorial de Aragón*)
RIUS: Fluvial Dynamics Research Group. University of Lleida
2012*: otrhomosaic already available
Nº photos**: Note that in 1957 and 1977 photos covered the totality of the Upper Cinca catchment.

#### *3.3.1. Extracting orthomosaics and point clouds*

Structure from Motion and Multi View Stereo Digital Photogrammetry (SfM-MVS) was applied to the aerial photographs in order to obtain georeferenced orthomosaics and point clouds. The method is fully explained in Llena et al. (2018), therefore, here we only provide a summary of the main steps of the workflow.

Data were processed using the Agisoft Photoscan Professional 1.2.2 software, with the exception of the 1927 series (details provided below). When using historical aerial photographs for 3D modelling there are some limiting factors that determine the achievable survey accuracy and precision. Image overlapping and quality are considered the most important (Micheletti et al., 2015; Bakker and Lane, 2017). Georeferencing and scaling were performed using Ground Control Points (GCPs). The selection of GCPs was based on the location of points in potentially unchanged locations (e.g. road crossings, field boundaries) in the case of the photos of 1957, 1977 and 1984. The x and y coordinates were extracted from the 2012 official CNIG orthomosaic already orthorectified with a Root Mean Square Error (RMSE; x and y) less than 1 m (Table 1 of supplementary materials). The elevation information (z) of the GCPs was obtained from the 2010

LiDAR survey (CNIG), which is characterized by a point cloud density of 0.5 pts/$m^2$ and an accuracy of ± 0.2 m. GCPs had a homogeneous spatially distribution and were projected using the UTM ETRS 1989 Zone 31 coordinate system. A total of 200 GCPs were established for the whole Upper Cinca Catchment, yielding an average density of 0.25 GCP/$km^2$. The RMSE of the SfM-MVS process was: 0.72 m for the aerials from 1957, 0.62 m (1977), and 0.66 m (1984). Although the RMSEs were relatively low, the areas farthest from the GCPs were subjected to larger errors. In order to minimize these errors, a co-registration of each point cloud with another reference point cloud was performed. In this study, the reference cloud was the available 2010 LiDAR survey, and the process was carried out using the tool Fine Registration (ICP) included in the software Cloud Compare 2.6.2 (Lague et al., 2013).

To analyse the accuracy of the point clouds after the co-registration, data on stable zones (i.e. rocky outcrops without vegetation cover) were compared with the reference point cloud (i.e. 2010 LiDAR), considering the latter as the real surface. The comparison of the point clouds was carried out by the M3C2 plugin included in Cloud Compare. The residuals in those areas were below 2 m in all the series, with a mean absolute value of 1.7 m and a standard deviation of 0.3 m. Finally, a dense point cloud (i.e. 0.5 pts/$m^2$) and an orthophotomosaic (i.e. 1 m/pixel resolution) were obtained for each of the study time series. In the case of the 2015 series, although the photos were also processed using Agisoft Photoscan Profesional 1.2.2, the quality and resolution of these were completely different and some of the limitations explained above were less restrictive. Photographs were taken from a piloted autogiro at a flying height of approximately 200 m. A total of 120 GCPs were established to post-process the data (i.e. around 20 GCPs/$km^2$). The result was a high resolution orthomosaic (i.e. 0.1 m), as well as high density point cloud (i.e. around 50 points/$m^2$) with a RMSE below 0.05 m (see more details in Vericat et al., 2016). Finally, the 1927 series were georeferenced using the ArcMap 10.5© Georeferencing Toolbox. A total of 12 GCPs were established and a $2^{nd}$ order polynomial model was used to create the final orthomosaic at 2 m resolution with a RMSE of 4.5 m.

*3.3.2. Extracting land use maps*

A supervised image classification of the orthomosaics of the entire Upper Cinca catchment for the 1957, 1977 and 2012 series was carried out to obtain land use maps. Due to the limited spectral response of the panchromatic historical aerial photos, only three different classes were identified for all periods: bare, meadow and forest. Nevertheless, these classes permit analysis of the general evolution of land use, mainly dominated by afforestation (Figure 1C). In the case of the 1977 survey, it was not possible to cover the entire catchment surface (85% of total cover) due to the lack of image overlap, especially in the north of the catchment. In order to avoid bias in comparing the different land uses between different periods, the total percentages for all periods were calculated from 85% of the basin limited in the 1977 series.

To estimate the accuracy of the classification, a confusion matrix for each year was calculated following the method described by Chuvieco (2016). In this way, 100 random points were distributed in the catchment to evaluate whether the results provided by the classification were in agreement with the real land use class. The percentage of agreement in the classifications was 75 % for the 1957 series, 84% (1977) and 87% (2012).

# CHAPTER 7

## DISCUSSION AND CONCLUSIONS

# CHAPTER 7: Discussion and conclusions

This chapter presents a general discussion and conclusions of the thesis based on the hypothesis and objectives formulated in Chapter 1. Additionally, specific and detailed discussions and conclusions can be also read in each of the focal chapters of the thesis (Chapters 3 to 6). Each one of the chapters, as already stated, is considered as a self-contained unit with an introduction section outlining the specific research context and objectives, the full details of the methods used, the results, discussion and conclusions. Finally, 3 additional research papers are also included in Chapter 2, methodological or technical notes providing new insights and being relevant for the focal chapters of the thesis.

## 1. GENERAL DISCUSSION

A river system can be divided in three zones according to the main acting hydro-sedimentary processes (Schumm, 1977). The headwaters are characterised as production zones, where most of the sediment and water is produced and transferred to the main channel networks. Transfer zones are areas where the main processes are related to conveying water and sediment fluxes downstream to the most distal zones, known as the deposition zones, ultimately reaching the deltas, seas and oceans. In this way, mainstream rivers can be seen as a conveyor belt transferring water and sediments from sources (i.e. production zones) to sinks (i.e. deposition zones; Kondolf, 1997). Rates of sediment supply from upstream and the ability to transport or store that sediment, the latter of which being influenced by the morpho-sedimentary characteristics of river channels linked to the imposed flow hydraulics, are key factors determining the sensitivity of a system to respond to a given disturbance.

The capacity of the conveyor belt of transferring the imposed water and sediment yield mediates the extent to which disturbances occurring in various parts of catchments at different temporal scales induce adjustments elsewhere (Fryirs, 2017). For instance, channel morphology of a given reach is in dynamic quasi-equilibrium when sediment exported from a specific reach is roughly equal to the supply from upstream reaches; however, when an inequity in this balance occurs, morpho-sedimentary changes are expected to follow (Williams and Wolman, 1984). The magnitude and frequency of disturbances dictate the reaction and relaxation time of the river systems to adjust to a new equilibrium, i.e. to a new system state that will be ultimately determined by the imposed conditions in the catchment. These conditions are not just those generated by proximal and recent disturbances, but also those imposed at multiple temporal scales and, eventually, located everywhere in the catchment. For instance, Church and Slaymaker (1989) reported that rivers in British Columbia (Canada) are still responding to the last glaciation, giving a landscape relaxation time greater than 10.000 years. Additionally, some systems may become more sensitive to disturbances, while others may become more resilient (Brunsden, 1993). In order to have an integrated vision of the river system functioning and its responses to certain disturbances, it is necessary to take into account a multi-temporal and multi-spatial approach, trying to cover all the compartments of the river system, as well as analyse its interaction for extended periods of time. In this way, the overall aim of this thesis is to assess the geomorphic responses to natural and human disturbances in a mountain catchment at multiple temporal and spatial scales, but specifically focused in the last century.

At the micro-catchment scale (Chapter 3), it has been proved that, in the case of sub-humid badlands developed on Eocene marls, geomorphic processes re-shaping such landscapes are

mainly controlled by meteorological variables (i.e. rainfall and air temperature), which cause topographic changes of different magnitude and direction (surface lowering or raising) depending on the morphometric properties of the landscape, including slope and aspect, but also connectivity and vegetation. Some studies have analysed the correlation between meteorological variables and geomorphological processes, both in terms of erosion and weathering (e.g. Cantón et al., 2001; Nadal-Romero et al., 2007). Several authors have also verified the correlation between erosion processes and the morphometric properties of the landscape (e.g. Cerdà and García-Fayos, 1997; Vericat et al., 2014). In the same way, there are some works in which the main geomorphic processes are inferred from DEMs and the models of change between them (e.g. Gude et al., 2002; Bartsch et al., 2002). As far as we know, however, there is not any previous attempt to integrate all three approaches in the same study and in two contrasted micro-catchments subjected to the same external forcing. Therefore, for the first time, quantitative analysis of geomorphic process signatures from the study of changes in form obtained from multi-temporal High Resolution Topography allows the identification of correlations between dominant processes, meteorological variables and the landscape morphometry. The results show, among others, that rainfall variables control surface flow-based processes, while those variables associated with low temperature exhibit a significant relationship with mass movement-based processes. At the same time, morphometric descriptors of slope, connectivity and vegetation cover have a direct impact in triggering geomorphic flow-based and mass movement-based processes. Specifically, dominant observed processes in relation to the magnitude of topographic change were *Cutting and Filling* in terms of surface lowering and *Mass Wasting* in terms of surface raising. In this way, the potential transfer of sediment from these well-known highly erodible landscapes or badlands to downstream will be determined by these interactions that vary spatially and temporally. But, do badlands always control catchment scale sediment yields?

Faulkner (2008) noted that some meso-catchments (i.e. $10^2$ $km^2$) may present a discontinuity between badlands (what may be known as a production zones as per Schumm, 1977) and the main drainage network (the transfer zones), depending on the landscape sensibility and connectivity. The Soto catchment (Chapter 4) differs from other studies analysing sediment yields in catchments with similar characteristics (e.g. López-Tarazón et al., 2011; Piqué et al., 2014; Buendia et al., 2015) in the way that annual sedimentary cycles and consequent sediment transfer, are not mainly controlled by the sediment supply from badlands. Sediment yield in catchments with constant base flow depends less on high magnitude pulses, as observed in intermittent streams (i.e. 'flashy' behaviour). Given its physiographic characteristics, the Soto basin represents a system with high structural connectivity, but with intermittent functional connectivity, mainly controlled by pulses of water and sediments. An example of this low level of functional connectivity, is the absence of a correlation between sediment production and export at the seasonal scale. In this way, our results have demonstrated that badlands do not always control the export of sediments due to, mainly, the fluctuation of the functional connectivity of the channel network caused by water and sediment pulses (e.g. flashy floods). The transfer of sediment through the channel network, once arrived, it is hydraulically limited. This is an important observation because differs to the results obtained in many Mediterranean catchments (mainly with perennial regimes) with a spatially extensive presence of badlands (e.g. Nadal and Regüés 2010; Gallart et al., 2013), which observed that sediment production in badlands control the overall catchments sediment yield. Our results obtained in a small intermittent stream are also important to understand future changes in fluvial systems, including aquatic ecosystems, given that some large permanent rivers are shifting to becoming intermittent systems because of climate changes and extraction of water (Acuña et al., 2014).

Increasing the temporal (i.e. from annual to decadal) and spatial (i.e. from sub-catchment to catchment) scales, Chapter 5 analysed the effect of land use changes and associated topographic changes on structural sediment connectivity, as a proxy of the changes in the (potential) sediment transfer in the Upper Cinca catchment. This catchment is considered representative catchment of many similar mountain reaches. Although, the reduction of sediment connectivity due to afforestation in Mediterranean mountain catchments has been reported previously by several other authors (e.g. Lizaga et al., 2016; López-Vicente et al., 2016), this chapter represents one of the first studies in which the effect of topographic changes associated to land use changes (e.g. terracing, road construction) on structural connectivity is analysed from a dynamic point of view. Chapter 5 demonstrates that sediment connectivity is affected to a larger degree by topographic changes than by land cover. Other authors have analysed the particular effects of the establishment of terraces on sediment connectivity (e.g. López-Vicente et al., 2013; Tarolli et al., 2014; Calsamiglia et al., 2018). Calsamiglia et al. (2018) observed how terraces caused: (i) general disconnectivity in sediment and water transfer; and (ii) water and sediment concentration in the areas where terraces were collapsed due to the land abandonment. Our results also indicate that during the second half of the 20$^{th}$ century, the Upper Cinca catchment, like most basins in the Mediterranean mountain area, exhibited a significant increase in forest cover due to rural abandonment causing a decrease in structural sedimentary connectivity, which is an indicator of the potential reduction of the sediment yield of these basins. Moreover, afforestation also has a direct impact on runoff generation and changes the magnitude of flows (e.g. López-Moreno et al., 2002). Our results, together with the data obtained in previous studies (e.g. García-Ruiz et al., 1996; MacDonald et al., 2000) can be coupled with hydrological and sediment transport models to improve our understanding of how changes in water and sediment production are propagated downstream to the channel network. In turn, this informs us as to which temporal and spatial scales are dominating channel adjustments that are observed in many mountain rivers that have experienced these type of disturbances in their headwaters during the 20$^{th}$ century (e.g. Sanjuán et al., 2016; Marchese et al., 2017).

Together with the reduction in water and sediment supply from upstream due to afforestation, the role of floods and other human-based disturbances or influences (e.g. instream gravel mining, hydroelectric infrastructures, dams, construction of lateral embankments) are also analysed in this thesis. The main objective of Chapter 6 is to understand the geomorphic responses of a 12 km river reach of the Upper Cinca during the last century. The segregation of these disturbances is limited because the feedbacks between these and the associated adjustments and the time required to the river to adjust to a new state after a given disturbance are variable (the later can be considered the relaxation period as per Petts and Gurnell, 2005). Recently, Lane et al. (2019) have analysed the role of human-induced climate change coupled with other human-based disturbances (such as land use changes, gravel mining and hydropower construction) on the sediment delivery in a catchment of the Alps during the Anthropocene (approximately last 200 years). They observed how these disturbances have counteracting effects on sediment supply at the catchment outlet; while climate change increases sediment supply due to the glacial melting, gravel mining and dam construction tends to decrease sediment supply or/and availability. In the case of the Pyrenees, the Upper Cinca catchment also experienced an important reduction in the sediment supply during the 20$^{th}$ century caused by catchment and reach-scale disturbances. This situation of structural sediment deficit, exaggerated locally by intense gravel extractions in the middle of the 20$^{th}$ century, led to a river metamorphosis, changing from a braided pattern to a more static channel towards a wandering pattern. In general, the channel incised and the active floodplain has been disconnected from the channel due to the incision or/and as a consequence of channel constriction caused by the embankments. Vegetation encroachment due to this disconnection helped the stability of the channel and reinforced channel incision. Studies of this type have been carried out in many

mountain rivers (e.g. Surian et al., 2009; Comiti et al., 2011; Arnaud et al., 2015; Batalla et al., 2018). The main novelty of this chapter is the use of statistical trends and breakpoints statistical analyses, allows identifying the different phases of change of the river system state after disturbances.. This approach permits a more informed interpretation of the cause-effect relations and the time required to the river to reach a new system state or equilibrium condition, governed by the imposed water and sediment fluxes. We hypothesise that the 12 km river reach adjusted to a new equilibrium 85 years after main human disturbances in the catchment were initiated (i.e. twenties of the 20$^{th}$ century). In this way, the mainstream reach works as a record of all the disturbances from upstream in form of morphologic and topographic changes to a new stable condition.

This thesis also presents some novel quantitative methods for the study of sediment production and transfer between the different compartments of fluvial catchments. The main transversal novelty in all the methods used in each chapter lies in the high resolution of the data obtained thorough the applications of different methods and used, both, spatially and temporally. Specifically, Chapter 3 presents the new developed Mapping Geomorphic Processes in the Environment (MaGPiE) algorithm, which allows inferring in the main geomorphic processes signatures from the analysis of High Resolution Terrain models (i.e. from the change in form). From the combination of the results of the DEMs of Difference (DoD) performed in two micro-catchments in badlands, and the water and sediment fluxes measured at the catchment outlet at high temporal resolution, Chapter 4 analyses the correlation between meteorological variables (external forcing), morphometric variables of the landscape, sediment production from badlands and sediment yield at the catchment outlet. Finally, the main novelty of the methods used in Chapters 5 and 6 lies in the use of Structure from Motion photogrammetry applied to historical photos that allows to obtain both planimmetric (i.e. orthomosaics) and topographic (i.e. 3D point clouds) data from multi-temporal data sets, which permits to characterize the geomorphic and morphometric characteristics of these periods, both at the catchment and reach scales, and their evolution through time and in relation to main disturbances acting at different spatial scales.

We believe that the results of each chapter of this thesis will be valuable for improving river system management strategies. Figure 1 graphically illustrates the main spatial scales addressed in this PhD together with some highlights and their interrelation. Observed correlations between meteorological and morphometric variables and geomorphic processes acting in badlands permits the development of predictive models of the potential magnitude and typology of geomorphic processes acting in such highly erodible landscapes while providing useful information for improving and parameterising landscape evolution models (e.g. Hancock et al., 2015). In the same way, integrating the measurement of sediment production in the main source areas (i.e. badlands) with sediment yield measures at the catchment outlet at different temporal scales, helps us to understand the role of sediment source areas and the drainage network on catchment-scale sediment budgets. This information can help inform the choice of different management measures (e.g. sediment trapping; Mekonmen et al., 2015), and help understand the link between physical and ecological processes. This link between physical and ecological processes was previously studied by Béjar et al. (2017) and Buendia et al. (2013) in relation to the impacts of suspended sediment concentrations on macroinvertebrate drift also in the Upper River Cinca, and in-channel sediment storage on benthic communities in the nearby Isábena catchment, respectively.

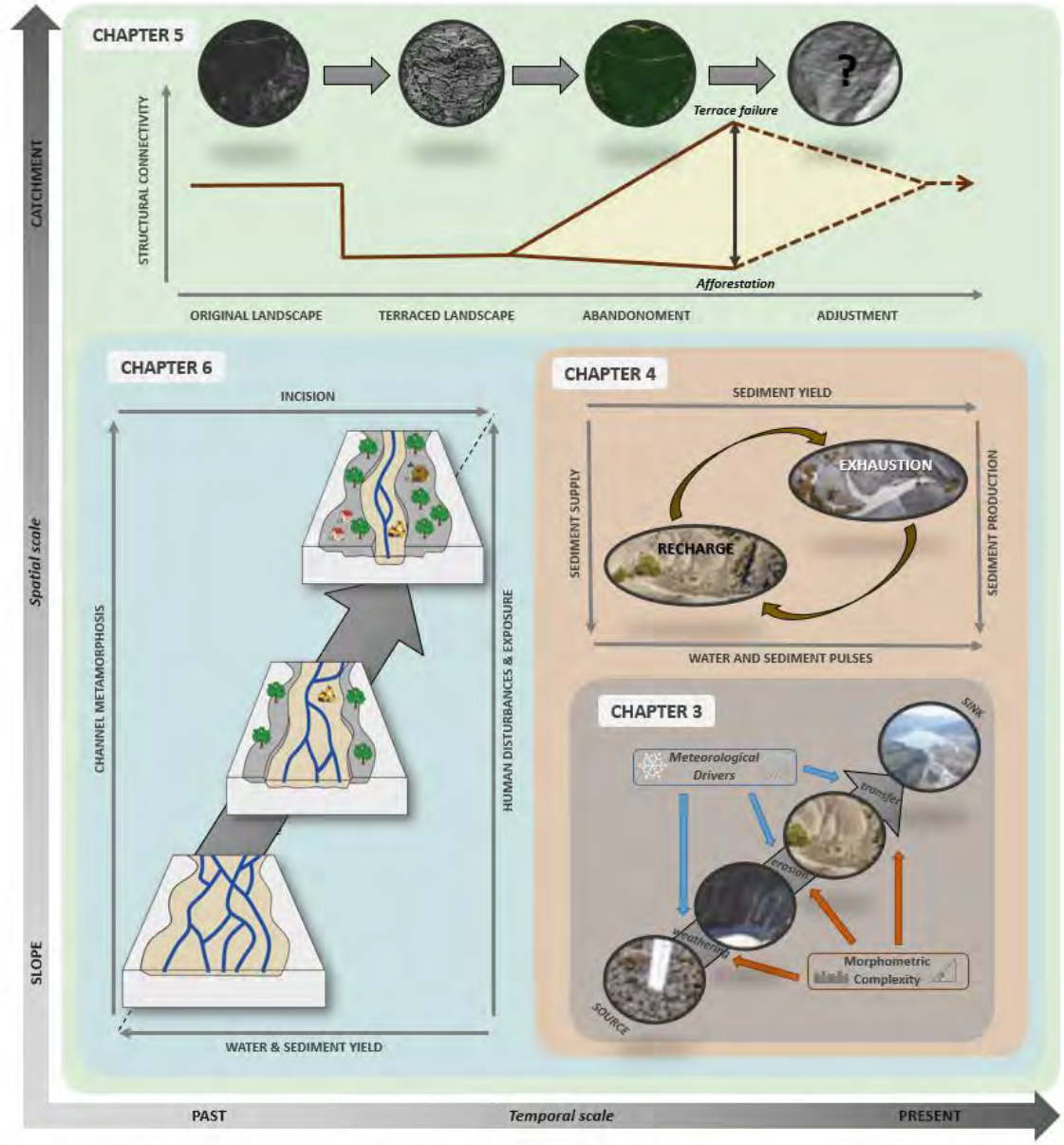


**Figure 1**. Graphically illustration of the main spatial scales addressed in this PhD together with some highlights and their interrelation.

Quantification of changes in the structural sediment connectivity through time associated with different disturbances can be a useful to help identify potential risks associated to planned morphological and land use changes, including, for instance, the construction or maintenance of road infrastructures (e.g. Kalantari et al., 2019), that have an important socio-economic value in mountain areas. Finally, many mountain river reaches are subjected to multiple stimuli affecting geomorphic responses and channel processes (e.g. Downs et al., 2013). Integrating geomorphic responses and their potential drivers at multiple spatial and temporal scales may be relevant to infer future fluvial metamorphosis associated with the effects of global change on changing water and sediment fluxes in mountain catchments. Additionally, the acquired knowledge about the river's evolutionary trajectory is also valuable to understand and support reach-scale management strategies (e.g. Arnaud et al., 2015; Mould and Fryirs, 2019), both objective based strategies or adaptive management strategies in dynamic natural systems such rivers.

## 2. LIMITATIONS AND FUTURE WORK

Although specific discussions in terms of data accuracy and precision are presented in each chapter, some limitations are also identified here. This section summarises some of these specific limitations, as well as proposing some possible future work or further research to improve all these aspects.

The inference of the main geomorphic processes re-shaping badlands (Chapter 3) was based on the interpretation of the changes in form by means of the MaGPiE algorithm. Despite the fact that the thresholds in the different inputs of the algorithm and the calibration of the specific signatures of each process were based on an expert-map procedure, there remains a degree of subjectivity at this stage, which results in a degree of uncertainty in the results. A more objective calibration of these variables would be possible using Machine Learning Software such as Weka (Witten et al., 2011). Smith and Warburton (2018) previously demonstrated this machine-learning approach to select the best roughness metrics for classifying peat surfaces. Regarding the analysis of processes, there are two key aspects that could contribute providing more information to the results already obtained in this thesis. On one hand, increasing of the frequency at which topographic surveys were performed (e.g. event-scale frequency) would help in depicting those specific processes masked during longer temporal scales due to change compensation. On the other hand, it would be very interesting to test if the results obtained in the contrasting but adjacent micro-catchments studied in this thesis remain similar in other badlands of the study area with similar characteristics. This would help to test if the trends observed in the two study badlands are reproducible and, therefore, validated, and also test the general calibration of the idea to completely different catchments.

As shown in Chapter 4, the production of sediment on surfaces covered by forest and agricultural fields was not directly measured in the field, although these land uses occupy almost the 50% of the Soto catchment. These values were extracted from the literature. Although a wide range of erosion rates were used, the results would benefit from some direct measures of sediment production in these areas, at least to validate the consulted values of the literature. In the same way, to prove the different formulated hypothesis in relation to the role of the drainage network as a sediment buffer, the use of tracers would improve future studies (e.g. Moreno-de las Heras et al., 2018). Additionally to these, the study of main topographic changes of the main channel (e.g. Jantzi et al., 2017) would also help in performing a better estimation of the specific role of the channel and the fluctuations of functional sediment connectivity, altogether improving the estimates of the residence time for those sediments produced in badlands, forest and agricultural fields transferred to the main channel network.

The assessment of changes in connectivity caused by land use changes (Chapter 5) was informed by the application of the Sediment Connectivity Index (IC; Cavalli et al., 2013). This index has some limitations, one of which is that the IC is dimensionless, which allows relative comparisons (e.g. of the same study area for different study periods), but does not permit absolute comparisons (e.g. of different study areas). One possible way to improve the representativeness of the IC would be its combination and comparison with other connectivity indices, such as the spatially distributed sediment delivery ratio presented by Heckman and Vericat (2018). By the assessment of both indices it would be possible to evaluate the changes of both structural and functional sediment connectivity. In the same way, the correlation between the results of the IC and the results of water and sediment transport modelling (e.g. Bussi et al., 2014; Buendia et al., 2016) may also help to study not just the relationships between structural and functional connectivity, but also changes through time and in relation to different disturbances.

Finally, although the results obtained in Chapter 6 proved that orthophotomosaics obtained from SfM applied to historical imagery have acceptable accuracy (i.e. around 1 m error), point clouds (i.e. 3D topographic data sets) presented relatively (very) low accuracies (i.e. around 2-3 m error) compared with the quality of SfM-based surveys applied to conventional digital photography. These associated errors determine the range of changes it is possible to measure by this method to only those for which the magnitude of change is above the minimum level of detection (considered the minimum magnitude of change required to be considered real based on the uncertainty of the data).

## 3. KEY CONCLUSIONS

This thesis is focused on the assessment of sediment transfer and geomorphic responses to natural and human disturbances in a mountain catchment at multiple temporal and spatial scales during the last century. The main findings corroborate the initial hypothesis of the thesis. Main conclusions can be drawn as follows:

**C1**. The application of the Mapping Geomorphic Processes in the Environment (MaGPiE) algorithm, developed in this thesis, permits inference of the main geomorphic process signatures from analysis of changes in form. Previously, bulk sediment yields have been correlated with meteorological or topographic variables and empirical relationships identified; however, MaGPiE allows us to make the link to geomorphic process much more explicitly. By identifying: (i) the dominant processes operating in each sub-catchment; and (ii) the relationship between each separate process and meteorological/topographic variables, we develop a richer understanding of the drivers of sediment production and export. Ultimately, this knowledge facilitates the development of much more generalizable/transferrable predictive models of sediment yield that would be missed without taking into account the process segregation. Specifically, process signatures determining surface lowering in the gentle-sloping south-facing badlands, characterised by lower connectivity and more vegetation cover, are driven by surface runoff-based processes, both diffuse, causing *Sheet Washing*, and concentrated, determining *Cutting and Filling* and *Rilling and Gullying*. The steeper and more connected north-facing slopes are re-shaped by means of gravitational processes, with *Mass Wasting* being dominant. In terms of processes determining surface raising, both *Mass Wasting* and *Cutting and Filling* are considered the main in both badlands. Any empirical model between meteorological variables and sediment export would only be appropriately applied to catchments with the same geomorphic process dominance.

**C2**. In small intermittent mountain catchments such the Soto (10 $km^2$), badlands, although are the main source of sediments, do not always control the export of sediments at the outlet of the catchment. This is mainly due to pronounced fluctuation of the functional connectivity of the channel network caused by the frequency and magnitude of water and sediment pulses during flashy floods, and the intermittent character of the stream. The channel drainage network acts as sediment source and sink and is key to understanding marked differences in the seasonal Sediment Delivery Ratio and differences between sediment production in badlands, forest and agricultural fields, and the export at the outlet of the catchment at the annual scale.

**C3**. Sediment connectivity in mountain catchments has been modified in the last century due to a series of human-based disturbances or influences. Changes in structural connectivity will have an impact on the transfer of sediments from sources to mainstream channels. Despite some sub-catchments experiencing a slight increase in sediment connectivity due to the establishment of new agricultural fields, most of the area of the Upper Cinca catchment has

undergone afforestation, which resulted in a decrease of structural sediment connectivity. Terracing affects connectivity much more than changes in land cover, generally reducing connectivity due to the establishment of flat areas between slopes, and locally increasing connectivity due the convergence produced by the structures or the collapse of terraces due to abandonment. Road construction, however, modifies slope and the drainage network, which leads to changes in connectivity that could affect erosional processes in the neighbouring areas with a direct impact on the stability of the road and on the transfer of sediments downstream.

**C4**. The evolution of the disturbances, process changes and geomorphic descriptors in a 12 km river reach indicated the existence of three phases in the changes of the river channel during the last century. First, a Regime State 1 (before 1927), where the river was potentially in equilibrium. Second, a Transient State (1927-2012) in which the river adjusted to the disequilibrium imposed by multi-scale disturbances by means of two contrasted channel states. The period 1927-1984 was characterised by having high geomorphic activity and channel incision. The period 1984-2012 was characterised, however, by having a low geomorphic activity, when channel constraining was the dominant process. Finally, a Regime State 2 (after 2012), a period in which we hypothesise that the river may be reaching again a new equilibrium, adjusting to the imposed water and sediment fluxes and channel configuration. Overall, we hypothesise the river has reached a new equilibrium imposed by the conditions led by the catchment and reach-scale disturbances. According to our observations, the relaxation time, the period needed to reach a new regime state, was around 85 years.

## 4. REFERENCES

Acuña V, Datry T, Marshall J, Barceló D, Dahm CN, Ginebreda A, McGregor G, Sabater S, Tockner K, Palmer A. 2014. Why Should We Care About Temporary Waterways?. *Science* 343: 1080-1081

Arnaud F, Piégay H, Schmitt L, Rollet AJ, Ferrier V, Béal D. 2015. Historical geomorphic analysis (1932–2011) of a by-passed river reach in process-based restoration perspectives: The Old Rhine downstream of the Kembs diversion dam (France, Germany). *Geomorphology* 236: 163–177.

Bartsch A, Gude M, Jonasson C, Scherer D. 2002. Identification of geomorphic process units in Kiirkevagge, northern Sweden, by remote sensing and digital terrain analysis. *Geografiska Annaler* 84(3-4): 171-178.

Batalla RJ, Iroumé A, Hernández M, Llena M, Mazzorana B, Vericat D. 2018. Recent geomorphological evolution of a natural river channel in a Mediterranean Chilean basin. *Geomorphology* 303: 322-337.

Béjar M, Gibbins CN, Vericat D, Batalla RJ. 2017. Effects of suspended sediment transport om invertebrate drift. *River Research and Applications* 33: 1655-1666.

Brunsden D. 1993. Barriers to geomorphological change. In *Landscape Sensitivity*, Thomas DSG, Allison RJ (eds). John Wiley & Sons: Chichester; 7–12.

Buendia C, Gibbins CN, Vericat D, Batalla RJ. Effects of flow and fine sediment dynamics on the turnover of stream invertebrate assemblages. *Ecohydrology* 7(4): 1105-1123.

Buendia C, Vericat D, Batalla RJ, Gibbins CN. 2016. Temporal dynamics of sediment transport and transient in-channel storage in a highly erodible catchment. *Land Degradation and Development* 27: 1045-1063.

Buendia C, Bussi G, Tuset J, Vericat D, Sabater S, Palau A, Batalla RJ. 2016. Effects of afforestation on runoff and sediment load in an upland Mediterranean catchment. *Science of Total Environment*. 540: 144-157.

Bussi G, Francés F, Horel E, López-Tarazón JA, Batalla RJ. 2014. Modelling the impact of climate change on sediment yield in a highly erodible Mediterranean catchment. *Journal of Soils and Sediments* 14: 1921-1937.

Calsamiglia A, Fortesa J, García-Comendador J, Lucas-Borja ME, Calvo-Cases A, Estrany J. 2018. Spatial patterns of sediment connectivity in terraced lands: Anthropogenic controls of catchment sensitivity. *Land Degradation and Development* 29: 1198-1210.

Canton Y, Domingo F, Solé-Benet, Puigdefábregas J. 2000. Hydrological and erosion response of a badlands system in semiarid SE Spain. *Journal of Hydrology* 252: 65-84.

Cavalli M, Trevisani S, Comiti F, Marchi L. 2013. Geomorphometric assessment of spatial sediment connectivity in small Alpine catchments. *Geomorphology*. 188, 31–41.

Cerdà A, García-Fayos P. 1997. The influence of slope angle on sediment, wáter and seed losses on badland landscapes. *Geomorphology* 18: 77-90.

Church C, Slaymaker O. 1989. Holocene disequilibrium of sediment yield in British Columbia. *Nature* 327: 452–454.

Comiti F, Da Canal M, Surian N, Mao L, Picco L, Lenzi MA. 2011. Channel adjustments and vegetation cover dynamics in a large gravel bed river over the last 200 years. *Geomorphology* 125(1): 147–159.

Downs PW, Dusterhoff SR, Sears WA. 2013. Reach-scale channel sensitivity to multiple human activities and natural events: Lower Santa Clara River, California, USA. *Geomorphology* 189: 121-134.

García-Ruiz JM, Lasanta T, Ruiz-Flano P, Ortigosa L, White S, González C, Martí C. 1996. Land-use changes and sustainable development in mountain areas: a case study in the Spanish Pyrenees. *Landscape Ecology* 11: 267-277.

Faukner H. 2008. Connectivity as a crucial determinant of badland morphology and evolution. *Geomorphology* 100: 91-103.

Fryirs, KA. 2017. River sensitivity: a lost foundation concept in fluvial geomorphology. *Earth Surface Processes and Landforms* 42: 55-70.

Gallart F, Marignani M, Pérez-Gallego N, Santi E, Maccherini S. 2013. Thirty years of studies on badlands, from physical to vegetational approaches. A succinct review. *Catena* 106: 4-11.

Gude M, Daut G, Dietrich S, Mäusbacher R, Jonasson C, Bartsch A, Scherer D. 2002. Towards an integration of process measurements, archive analysis and modelling in geomorphology – the Kärkevagge experimental site, Abisko area, northern Sweden. *Geografiska Annaler* 84(3–4): 205–212.

Hancock GR, Lowry JBC, Coulthard TJ. 2015. Catchment reconstruction – erosional stability at millennial time scales using landscape evolution models. *Geomorphology* 231: 15-27.

Heckmann T, Vericat D. 2018. Computing spatially distributed sediment delivery ratios: inferring functional sediment connectivity from repeat high-resolution digital elevation models. *Earth Surface Processes and Landforms* 43: 1547–1554.

Jantzi H, Liébault F, Klotz S. 2017. Sediment residence time in alluvial storage of black marl badlands. *Catena* 156: 82-91.

Kalantari Z, Cavalli M, Cantone C, Crema S, Destouni G. 2017. Flood probability quantification for road infrastructure: Data-driven spatial-statistical approach and case study Applications. *Science of the Total Environment* 581-582: 386-398.

Kondolf GM. 1997. Hungry Water: Effects of Dams and Gravel Mining. *Environmental Management* 21: 533–551.

Lane SN, Bakker M, Costa A, Girardclos S, Loizeau JL, Molnar P, Silva T, Stutenbecker L, Schlunegger F. 2019. Making stratigraphy in the Anthropocene: climate change impacts and economic conditions controlling the supply of sediment to Lake Geneva. *Scientific Reports* 9(1): 1-11.

Lizaga I, Quijano L, Palazón L, Gaspar L, Navas A. 2016. Enhancing Connectivity Index to Assess the Effects of Land Use Changes in a Mediterranean Catchment. *Land Degradation and Development* 29(3): 663-675.

López-Moreno JI, Beguería S, Valero-Garcés B, García-Ruiz JM. 2002. Intensidad de las avenidas y aterramiento de embalses en el Pirineo Central Español. *Ería* 61: 159-167.

López-Tarazón JA, Batalla RJ, Vericat D. 2011. In-channel sediment storage in a highly erodible catchment: the River Isábena (Ebro Basin, Southern Pyrenees). *Zeitschrift für Geomorphologie* 55(3): 365-382.

López-Vicente M, Poesen J, Navas A, Gaspar L. 2013. Predicting runoff and sediment connectivity and soil erosion by water for different land use scenarios in the Spanish PrePyrenees. *Catena* 102: 62–73.

López-Vicente M, Nadal-Romero E, Cammeraat EJH. 2016. Hydrological Connectivity Does Change Over 70 Years of Abandonment and Afforestation in the Spanish Pyrenees. *Land Degradation and Development* 28(4): 1298-1310.

MacDonald D, Crabtree JR, Wiesinger G, Dax T, Stamou N, Fleury P, Gutierrez-Lazpita J, Gibon A. 2000. Agricultural abandonment in mountain areas of Europe: Environmental consequences and policy response. *Journal of Environmental Management* 59: 47-69.

Marchese E, Scorpio V, Fuller I, McColl S, Comiti F. 2017. Morphological changes in Alpine rivers following the end of the Little Ice Age. *Geomorphology* 295: 811-826.

Mekonmen M, Keestra SD, Stroosnijder L, Baartman EM, Maroulis J. 2015. Soil conservation through sediment trapping: a review. *Land Degradation and Development* 26: 544-556.

Moreno-de las Heras M, Gallart F, Latron J, Martínez-Carreras N, Ferrer L, Estrany J. 2018. Testing the use of $^{210}Pb_{ex}$ to study sediment connectivity in a Mediterranean mountain basin with badlands. *Land Degradation and Development* 29: 676-689.

Mould S, Fryirs K. 2019. Contextualising the trajectory of geomorphic river recovery with environmental history to support river management. *Applied Geography* 94: 130-146.

Nadal-Romero E, Regüés D, Martí-Bono C, Serrano-Muela P. 2007. Badland dynamics in the Central Pyrenees: temporal and spatial patterns of weathering processes. *Earth Surface Processes and Landforms* 32: 888-904.

Nadal-Romero E, Regüés D. 2010. Geomorphological dynamics of sub-humid mountain badland areas: weathering, hydrological and suspended sediment transport processes. A case of study in the Araguás catchment (Central Pyrenees), and implications for altered hydro-climatic regimes. *Progress in Physical Geography* 34 (3): 123–150.

Piqué G, López-Tarazón JA, Batalla RJ. 2014. Variability of in-channel sediment storage in a river draining highly erodible areas (the Isábena, Ebro basin). *Journal Soils Sediments* 12: 2031-2044.

Schumm SA. 1977. *The fluvial system*. Wiley-Interscience, New York. 338 pp.

Smith MW, Warburton J. 2018. Microtopography of bare peat: a conceptual model and objective classification from high-resolution topographic survey data. *Earth Surface Processes and Landforms* 43: 1557-1574.

Sanjuán Y, Gómez-Villar A, Nadal-Romero E, Álvarez-Martínez J, Arnáez J, Serrano-Muela MP, Rubiales JM, González-Sampériz P, García-Ruiz JM. 2016. Linking land cover changes in the sub-alpine and montane belts to changes in a torrential river. *Land Degradation and Development* 27: 179-189.

Surian N, Ziliani L, Comiti F, Lenzi MA, Mao L. 2009. Channel adjustments and alteration of sediment fluxes in gravel-bed rivers of north-eastern Italy: potentials and limitations for channel recovery. *River Research and Applications* 25(5): 551-567.

Tarolli P, Preti F, Romano N. 2014. Terraced landscapes: From an old best practice to a potential hazard for soil degradation due to land abandonment. *Anthropocene* 6: 10-25.

Vericat D, Smith MW, Brasington J. 2014. Patterns of topographic change in sub-humid badlands determined by high resolution multi-temporal topographic surveys. *Catena* 120: 164–176.

Williams GP, Wolman MG. 1984. *Downstream Effrects of Dams on Alluvial Rivers*, US Geological Survey Profesional Paper. 90 pp.

Witten IH, Frank E, Hall MA. 2011. *Data Mining: Practical Machine Learning Tools and Techniques*, 3rd edn. Burlington USA: Morgan Kaufmann.

This thesis focusses on the study of water and sediment transfer from sources to sinks at multiple temporal and spatial scales and their implications for channel morphology in the Upper Cinca catchment, a mountain catchment located in the Southern Pyrenees. The thesis presents some novel quantitative methods for the study of sediment production and transfer between the different compartments of fluvial catchments. The main transversal novelty in all the methods used in each chapter lies in the high resolution of the data obtained. This comprehensive analysis aids at understanding the functioning of the river system and their evolution based on multiple-scale disturbances, which can help to support integrated watershed management practices or plans.